Genetic variation, pathogenicity, and pathophysiology of human channelopathies

By

Kevin Richard Bersell

Dissertation
Submitted to the Faculty of the
Graduate School of Vanderbilt University
in partial fulfillment of the requirements
for the degree of

DOCTOR OF PHILOSOPHY
in

Pharmacology
December, 2016
Nashville, Tennessee

Approved:

Dan M. Roden, MD

Charles C. Hong, MD, PhD

Björn C. Knollmann, MD, PhD

Katherine T. Murray, MD

P. Anthony Weil, PhD

To my loving wife, Liz, and our energetic son, Benjamin,

for being my biggest fans and my source of perspective

&

To my supportive family

for believing in me more than I believe in myself

ACKNOWLEDGEMENTS

Training in the laboratory of my dissertation mentor, Dan Roden, MD, has been an incredible and formative experience. Each day in the lab was inspiring as the energy, enthusiasm, and work ethic trickled down from the top. I hope to reflect many of Dr. Roden's professional characteristics to be a thorough scientist who is forward thinking in the pursuit of addressing clinically relevant questions. I was provided unlimited support to pursue ambitious projects within the lab with enough freedom to challenge myself in developing my approach to the scientific process and team management. With the aspiration to become a productive physician-scientist, Dr. Roden has been a terrific mentor for guiding my scientific training and will remain a valued friend and career mentor.

The scientific questions addressed were important and the projects completed during training benefitted from intellectual contributions provided by my dissertation committee: Charles Hong, MD/PhD, (chair), Björn Knollmann, MD/PhD, Kathy Murray, MD, and Tony Weil, PhD. Thank you for the critical evaluation, enthusiastic conversations about various topics, career advice, and encouragement throughout the process. I am also grateful for the institutional support provided by the Medical Scientist Training Program and the Department of Pharmacology that permitted me to focus on my training.

During my PhD training, I have come to appreciate the importance of constructing a talented team within a lab. The individuals within the Roden lab have taught me so much about science, functioning well as a team, and how to balance career

and personal life. Thank you to Tao Yang, PhD, for sharing his technical expertise in patch-clamp experimentation and enthusiasm for ion channel biology. I must also acknowledge the immensely generous and knowledgeable individuals who have contributed to my training as a budding physician-scientist including Quinn Wells, MD, (a valued clinical mentor and collaborator), Marcia Blair, Laura Short, Lynn Hall, Sara Van Driest, MD/PhD, Jonathan Mosely, MD/PhD, Tracy McGregor, MD, Wei Zhang, Andrew Glazer, PhD, Laura Daniel, PhD, Brett Kroncke, PhD, Dina Stroud, PhD, Christie Ingram, and Robin North. Without everyone's effort and contribution to my training, I would have not been as productive or efficient – certainly above and beyond expectations!

My dissertation work would not have been possible with fruitful collaborations with Jonathan Brown, MD, Prince Kannankeril, MD, Wenbiao Chen, PhD, Amanda Meyers, TK Feaster, PhD, Lili Wang, PhD, Shan Parikh, Kyungsoo Kim, PhD, Jay Montgomery, MD, Wendy Chung, MD, Courtney Campbell, MD/PhD, Benjamin Shoemaker, MD, Elijah Behr MD, and Ivan Moskowitz, MD/PhD. Thank you all for enthusiastically sharing your expertise, data generated, and providing career advice based on your experience.

The foundation of my electrophysiology training began in the laboratory of Al George, Jr, MD. During my "extended rotation" prior to Dr. George accepting the Chair of Pharmacology position at Northwestern University, the laboratory instilled exceptional practice in performing and designing experiments in electrophysiology. Many individuals, including Carlos Vanoye, PhD, Christopher Thompson, PhD, Rick Welch, Franck Potet, PhD, Jennifer Kunic, and Lisa Scudder, PhD, spent numerous hours

involved in my training and discussion of data. My time working in the George lab was foundational and I am grateful for the friendship and continued mentorship provided by Dr. George.

After college, I was fortunate to work for Dr. Bernhard Kühn, MD, who saw potential in me as a budding scientist. Dr. Kühn was the first physician-scientist that I encountered in my professional development. Working for him as a research assistant exposed me to the level of dedication and effort required to advance scientific understanding. Through his example I learned to aim high and work diligently to achieve my goals. Without the training and support provided by Dr. Kühn, I would have never made it to Vanderbilt University. Now as a collaborator and friend, I look forward to continuing a relationship with my first scientific mentor.

My family has always been important in my professional development. My journey as a scientist began in first grade during exploratory adventures in the creek behind our home with my grandmother, Jeanne Odom. We collected critters to observe their movements and water samples to look at under my microscope. This was my first lesson in observation, a trait that has benefited me throughout my academic career. I have watched the compassion that my mother, Linda, has for others and I hope to emulate that characteristic. My older sister, Karen, is a terrific example of discipline and work ethic required of a student striving to care for patients while my younger brother, Dave, inspires me to be thoughtful and have integrity in every aspect of life. There are many additional family members who I need to thank for showing me love, providing support, and sharing laughs during my PhD education. Thank you Doug, Ryan, Jack, Baby Charlie, Mark, and Charlie Odom. Also, thank you to my in-laws who have accepted me

so willingly (after proper vetting) into their family. Thank you, Anne, Michael, Katie, Jill, James, Gavin, Ryan, Mikey, Teddy, and Auntie Martha.

Most importantly, thank you to my wife and best friend, Liz. We met during our undergraduate studies at Saint Anselm College. During college if I wanted to spend time with Liz, it had to be in the library as she was a very dedicated student. Without this influence, I may have never made it to where I am today. Even though my dream of becoming a doctor seemed like a long shot after college, she supported me and believed in me. Once again, she was right. We made it to the MD/PhD program at Vanderbilt University because she wouldn't let me stop pursuing my career ambitions. She knew we would be here someday and for that, Liz, this PhD is as much yours as it is mine. We have grown and sacrificed together. Vanderbilt will always be important to us as we think fondly of our time here when we were newlyweds and later started our family together. We are blessed with a beautiful, smart, and kind little boy, Benjamin Francis. I must thank Ben and Liz for making every day in lab a little better by being able to end the day in a loving home.

Thank you everyone for helping me reach this achievement.

TABLE OF CONTENTS

LIST OF TABLES

LIST OF FIGURES

LIST OF ABBREVIATIONS

μm	micrometer
ACMG	American College of Medical Genetics and Genomics
ACTH	Adrenocorticotropic hormone
ANOVA	analysis of variance
ANP	atrial natriuretic peptide
APD	action potential duration
APD50	time to 50% repolarization of action potential duration
APD90	time to 90% repolarization of action potential duration
ATP	adenosine triphosphate
ATX-II	47 amino acid peptidyl sea anemone toxin
BrS	Brugada syndrome
Ca^{+2}	calcium
CaMK	Ca2+/calmodulin-dependent protein kinase II
Cas9	CRISPR-associated protein 9
Ca_V	voltage-gated calcium channel
CDG	congenital disorders of glycosylation
ChIP	chromatin immunoprecipitation
CHO cells	Chinese hamster ovarian cells
Cl^-	chloride
CNV	copy number variant
CRISPR	clustered regularly interspaced palindromic repeat

CSF	cerebrospinal fluid
DCM	dilated cardiomyopathy
de novo	from the beginning
DNA	deoxyribonucleic acid
ECG	electrocardiogram
EEG	electroencephalogram
EFP	electric field potential
EGTA	ethylene glycol-bis(β-aminoethyl ether)-N,N,N',N'-tetraacetic acid
EMSA	electrophoretic mobility shift assay
E_{rev}	reversal potential
ESC	embryonic stem cell
et. al.	and others
ExAC	exome aggregation consortium
FDA	Food and Drug Administration
FPD	field potential duration
FRET	fluorescence resonance energy transfer
GATA4	GATA binding protein 4
Gd^{+3}	gadolinium
GO	gene ontology
GTCS	generalized tonic-clonic seizures
GWAS	genome wide association studies
HCN	Hyperpolarization-activated Cyclic Nucleotide-gated
HDR	homology-directed repair

HEK	human embryonic kidney
HEPES	4-(2-hydroxyethyl)-1-piperazineethanesulfonic acid
hERG	human ether-a-go-go
HOS	Holt-Oram syndrome
ICD	internal cardiac defibrillator
I_f	funny current
I_{K1}	transient inward rectifying potassium current
I_{Kr}	rapid delayed rectifying potasisum current
I_{Ks}	slow delayed rectifying potassium current
I_{Kur}	ultrarapid delayed rectifying potassium current
in silico	by means of computer modeling
in vitro	in glass
$I_{Na\text{-}L}$	late sodium current
indel	inserton/deletion type variant
iPSC	induced pluripotent stem cell
iPSC-CM	induced pluripotent stem cell-derived cardiomyocyte
JLNS	Jervell and Lange-Nielsen syndrome
K	Kelvin
K^+	potassium
K_V	voltage-gated potassium channel
LQTS	long QT syndrome
LTV	long term variability
Mg^{+2}	magnesium

MMEJ	microdomain-mediated end joining
mol	moles
msec	milliseconds
Na^+	sodium
Na_V	voltage-gated sodium channel
NCL	neuronal ceroid lipofuscinosis
NGS	next-generation sequencing
NHEJ	non-homologous end joining
NHLBI	National Heart, Lung, and Blood Institute
NKX2.5	Homeobox transcription factor 2.5
$NMDG^+$	N-methyl-D-glucamine
PAM	protospacer adjacent motif
PCR	polymerase chain reaction
PI3K	phosphoinositol 3-kinase
PIP3	3,4,5-triphosphate
PKC	protein kinase C
QTc	heart rate corrected QT interval
Rb^+	Rubidium
RFLP	restriction fragment length polymorphisms
RNA-seq	RNA sequencing
S. pyogenes	Streptococcus pyogenes
SC-ADVISER	Scripps Genome Annotation and Distributed Variant Interpretation Server
SCD	sudden cardiac death

SEM	standard error of the mean
SINE	short interspersed elements
SNV	single nucleotide variant
SR	sarcoplasmic reticulum
STV	short term variability
TALEN	trascription activator-like effector nuclease
TBX3	T-box transcription factor 3
TBX5	T-box transcription factor 5
TF	transcription factor
TSD	target site duplication
VLCFA	very long chain fatty acid
VUS	variant of unknown significance
WES	whole exome sequencing
WGS	whole genome sequencing
ZFN	zinc-finger nuclease

CHAPTER I

INTRODUCTION

Basic principles in cardiac electrophysiology

The primary function of the heart is to distribute blood throughout the body for the delivery of oxygen, nutrients, and signaling molecules while contributing to waste removal. This seemingly simple pump function of the heart requires complex coordination through a process known as excitation-contraction coupling. The adult human heart is comprised of approximately 4 billion cardiomyocytes,[1] the functional cells of the heart, which work in harmony to propagate the electrical signal governing excitation and subsequent contraction. At rest a human ventricular cardiomyocyte has a membrane potential of -90 mV. When excited, the cardiomyocyte membrane becomes depolarized leading to a release of intracellular calcium stores from the sarcoplasmic reticulum, providing the signal for a cell to contract. Disruption of this coordinated process can have severe consequences on cardiac pump function and electrical rhythms. Therefore, it is critical to understand normal cardiac electrical activity at the tissue and cellular level in order to define the molecular mechanisms of disease.

The surface electrocardiogram (ECG) was invented in 1901 by Dr. Willem Einthoven to provide a timed record of the cardiac electrical activity in health and disease. Einthoven first identified and named the repeating rhythmic series of distinct waves now commonly known as the P wave, QRS complex, and the T wave (**Fig 1A**). The heart has automaticity, meaning that it is self-excitable, that originates from a specialized structure located in the upper right atrium called the sinoatrial node (**Fig 1B-1**). The signal is propagated through the right and left atria and

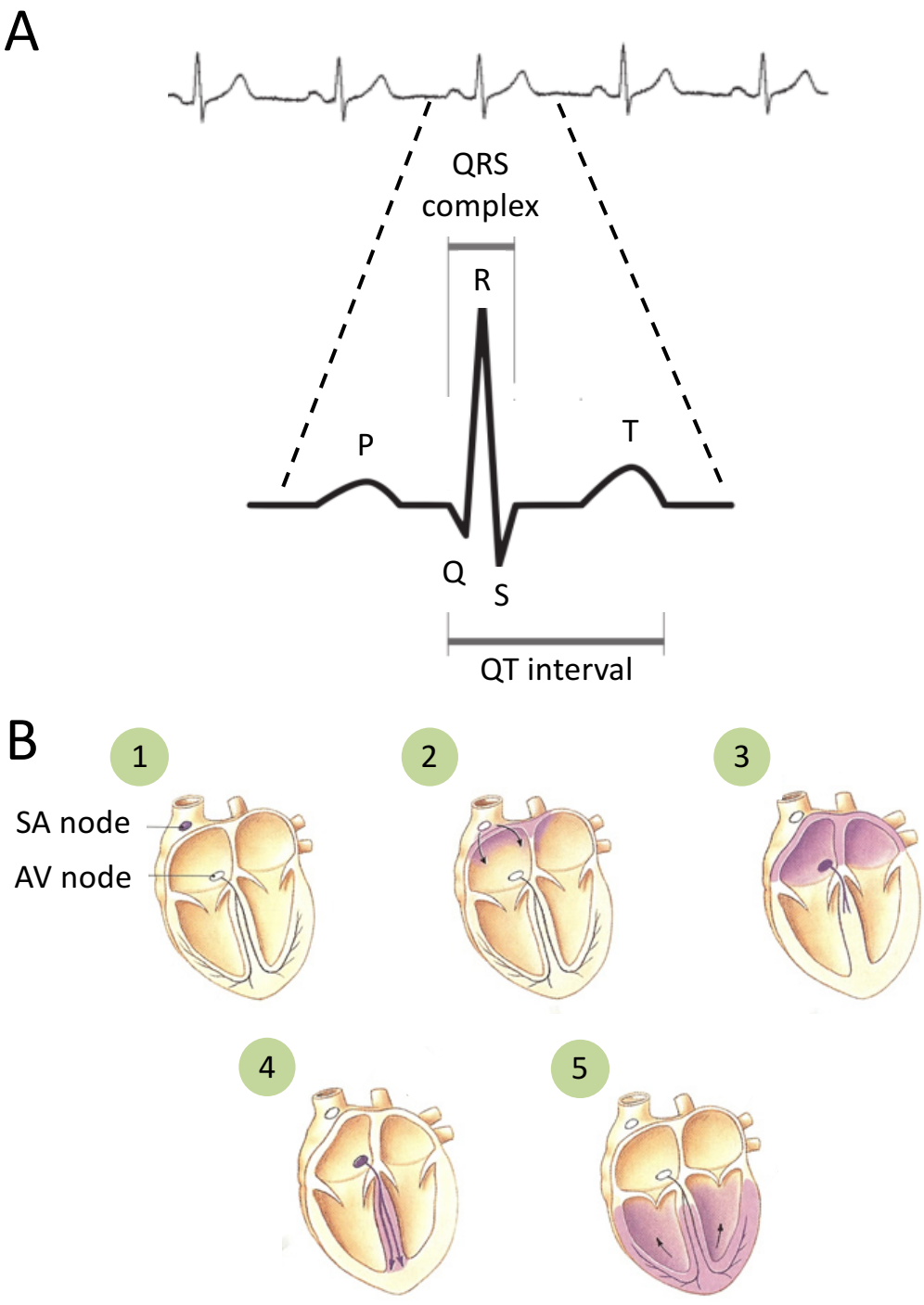

Figure 1. Electrical activity in the healthy human heart. (**A**) Representative electrocardiogram in normal sinus rhythm. The schematic drawing below illustrates the phases of the ECG. The P-wave represents depolarization of the atria, the QRS complex the depolarization of the ventricles, and the T-wave the repolarization of the ventricles. (**B**) Order of depolarization in the human heart. Purple shading represents depolarized tissue. Modified from From *Human Physiology: An Integrated Approach* (4th edition), San Francisco: Pearson/Benjamin Cummings.

this collective atrial activation/depolarization is observed as the P wave on surface ECG recordings (**Fig 1B-2/3**). Electrical communication between the atria and ventricles relays through the atrioventricular node at the base of the right atrium that delays the transmission before proceeding through the rapid His-Purkinje system to the ventricular myocardium (**Fig 1B-4**). The QRS complex represents ventricular activation/depolarization (**Fig 1B-5**). While the return to rest or repolarization of the atria cannot be observed on surfaced ECGs, ventricular repolarization is represented as the T wave.

The features on an ECG can be evaluated quantitatively to describe electrical conduction within the heart to identify individuals who are at increased risk of arrhythmia onset. The PR interval defines the conduction time from the sinoatrial node through the atrioventricular node and the normal range is between 120-200 msec. The QRS duration is normally 70-110 msec and represents the time required for the entire ventricle to depolarize. The entirety of excitation-contraction coupling within the ventricles occurs between the initiation of the QRS complex and the end of the T wave and is measured as the QT interval. The depolarization and repolarization of individual cardiomyocytes within both ventricles are additive events comprising the whole organ QT duration determined by ECG. Therefore, the QT interval is a representation of the duration of a single cell action potential (APD).

As the ECG allows one to record electrical activity in the entire heart, the electrical properties of a single cell can be evaluated using patch-clamp techniques. Electrical activity in excitable cells was first recorded and systematically analyzed by Hodgkin and Huxley in the 1940s for which they shared the Nobel Prize in Physiology or Medicine in 1963.[2,3] The patch clamp was developed during the late 1970s by Erwin Neher and Bert Sakmann and was awarded the Nobel Prize in 1991.[4] The patch clamp system uses a differential amplifier to define zero

current based on a reference electrode set in the extracellular solution while the recording electrode is housed within a fine tipped glass pipette (**Fig 2A**). The glass pipettes have a small 0.1-1 μm opening that, with a small amount of negative pressure, creates a tight seal (thereby isolating a "patch" of membrane) with >1GigaOhm resistance with the cell membrane. The GigaOhm seal essentially has infinite resistance that is impermeable to ion passage between the pipette and membrane. This seal allows for the study of a single or few ion channels present within the small opening of the pipette (**Fig 2B**). Alternatively, one can gain access to the intracellular environment of the cell in whole-cell patch-clamp experiments by applying additional negative pressure to rupture the underlying membrane or using perforating antifungal agents within the pipette to record ion currents resulting from the summative function of all channels contained within a cell (**Fig 2C**). Patch-clamp experiments either clamp or hold the voltage to study ion currents generated at a given test voltage or clamp the current and study the resulting changes in membrane potential, and both are important experimental designs contributing to the understanding of cardiac electrophysiology.

Decades of patch-clamp experiments have guided the understanding that the cardiac action potential duration and morphology is constructed by the summation of multiple ionic currents within a single cardiomyocyte.[5] There are many cellular features that contribute to the excitability of cardiomyocytes. The cell membrane is a lipid bilayer that is itself impermeable to ions but enables differences in intracellular and extracellular ionic composition and charge. These electrochemical gradients are generated and maintained by a collection of ion channels, ATP-consuming ion pumps, primarily the Na-K ATPase, and exchangers. Ionic gradients are utilized by a cell to translate stimuli received from the extracellular environment or neighboring cells to a secondary signal through ion channels.

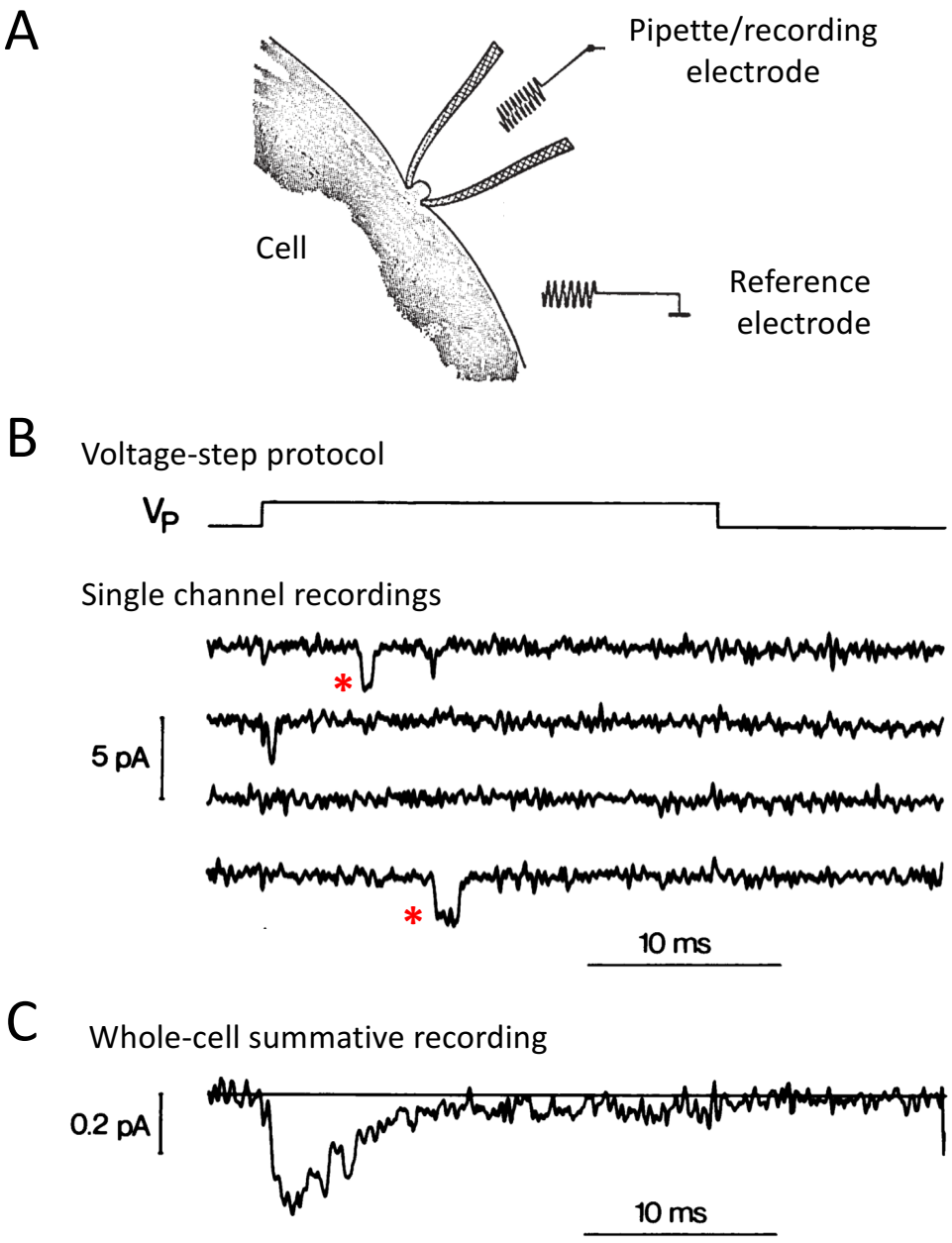

Figure 2. Application of patch clamp techniques to cellular electrophysiology. (**A**) Schematic of cellular patch clamp methodology. Fine-tipped glass pipette forms high resistance seal with the cell membrane. The recording electrode is contained within the pipette. A reference electrode is located in the extracellular space. (**B**) Representative single sodium channel recordings for a test voltage step protocol. Red asterisk indicated downward deflection resulting from single channel opening. (**C**) Representative whole-cell patch clamp sodium current recording. Sodium current is represented as a downward deflection by convention. The whole cell current is the product of the single channel current, the number of channels present, and the probability that a channel will be open at any given time. Modified from Sigworth and Neher. *Nature* 1980.

Ion channels are transmembrane proteins that selectively allow ions to travel through a central pore until the chemical driving force created by internal and external concentration differences are equal to the opposing electrical driving force or electric potential. The electric equilibrium potential in an idealized setting for an individual ionic species can be described by the Nernst equation:

$$V_{\text{Eq.}} = \frac{RT}{zF} \ln\left(\frac{[X]_{\text{out}}}{[X]_{\text{in}}}\right)$$

Where R is the gas constant (8.314 Joules K^{-1} mol^{-1}), T is temperature in Kelvin (K), F is Faraday's constant (9.648×10^4 C mol^{-1}), and x is the valence of the ion. While the Nernst equation provides understanding of the electrochemical force for an individual ion channel, its utility is best appreciated in experimental conditions that can isolate the function of one type of ion channel. During the cardiac action potential, changes in permeability of multiple ionic species occur throughout the action potential and the cumulative behavior of the channels can be described by the Goldman-Hodgkin-Katz equation:

$$V_{\text{m}} = \frac{RT}{F} \ln\left(\frac{p_{\text{K}}[\text{K}]_{\text{o}} + p_{\text{Na}}[\text{Na}]_{\text{o}} + p_{\text{Cl}}[\text{Cl}]_{\text{i}}}{p_{\text{K}}[\text{K}]_{\text{i}} + p_{\text{Na}}[\text{Na}]_{\text{i}} + p_{\text{Cl}}[\text{Cl}]_{\text{o}}}\right)$$

Where p_x represents the membrane permeability of a given ion, in this case either K^+, Na^+, or Cl^-, at a given voltage dependent upon ion concentrations inside (subscript i) and outside (subscript o) the cell. The unique time-dependent changes in cell permeability to different ions, often simultaneously, generate five distinct phases of the cardiac action potential (summarized in **Fig 3A**). To appreciate the complexity of this process, it is critical to understand the expression,

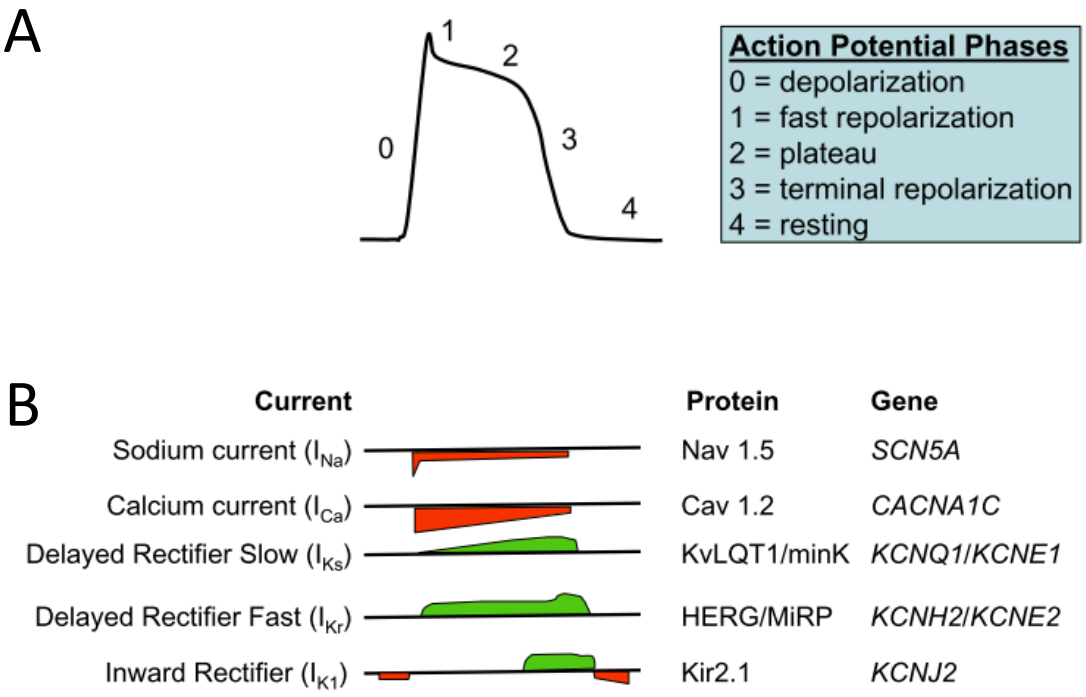

Figure 3. Ionic currents contributing to ventricular cardiac action potential morphology. (**A**) Schematic of ventricular action potential labeled with five distinct phases. (**B**) Ionic currents contributing to the phases of the action potential. Red indicates inward/depolarizing currents. Green indicates outward/repolarizing currents. Channel protein name and encoding gene provided for major ionic currents. Modified from Napolitano *et. al*. *Pharmacology and Therapeutics* 2006.

distribution, and characteristics of individual ion channels within a cardiomyocyte. For example, the regulation of ion channel function can vary from channels (*e.g.* Kir2.X family) where the pore is always open, to gated channels that must be activated by either a voltage change (*e.g.* $K_V1.X$, $Na_V1.X$) or ligand binding (*e.g.* K_{ATP}). The biophysical properties of select ion channels in relation to their role during unique phases of the cardiac action potential will be discussed further.

Excitation originates from the SA node due to the property of automaticity inherent to nodal cells (**Fig 1B**). A slowly activated inward cationic current, known as the "funny" current (I_f), depolarizes the membrane during phase 4 of the action potential.[6] I_f is conducted by the Hyperpolarization-activated Cyclic Nucleotide-gated (HCN) family of proteins.[7] As the name suggests, behavior of the HCN family is modified by the secondary messenger of adrenergic signaling, cyclic AMP, to modify heart rate. The upstroke of the action potential is triggered when I_f depolarizes the membrane potential to a voltage that activates voltage-gated sodium channels.

The initiation or upstroke of the cardiac action potential (phase 0) results from the opening of voltage-gated sodium channels, primarily $Na_V1.5$, in atrial, ventricular, and Purkinje cardiomyocytes (**Fig 3B**). Like other sodium channels, $Na_V1.5$ is comprised of the alpha pore-forming subunit of the channel as a single protein containing four structurally homologous domains (D1-D4) whose function can be modified by interactions with auxiliary beta subunits or other regulating proteins (**Fig 4A**). Each of the four domains contains six helical transmembrane segments (S1-S6) with S4 serving as the voltage sensor due to the distribution of positively-charged residues (lysine, arginine or occasionally histidine) every three amino acids. Upon local membrane depolarization, these positive changes cause the S4 helix to move outward relative to

the pore.[8,9] This structural change is propagated to other portions of the channel shifting it from the closed to the open state allowing sodium to enter the cell along its electrochemical gradient (I_{Na}). Segment five, segment six, and the S5-S6 pore loop of each domain face one another forming the central pore and the selectivity filter of the channel providing $Na_V1.5$ a preference for conducting sodium over other monovalent cations.[10] After opening, sodium channels are very rapidly inactivated, even if the membrane is still depolarized, when the inactivation gate present in the D3-D4 linker blocks the cytoplasmic face of the pore rendering the channel non-conductive (**Fig 4B**).[11,12] There are physiologic conditions and genetic variants in the sodium channel that prevent complete inactivation and generate what is known as a late sodium current with important implications to probability of experiencing sudden cardiac death; this will be discussed further later in this and subsequent chapters. The sodium channel remains in the inactivated state, unable to transition to open state again, until the process of recovery from inactivation occurs with membrane repolarization. This inability to be re-excited contributes importantly to the phenomenon of cellular and whole organ refractoriness.

The process of membrane repolarization begins early in the cardiac action potential as sodium channels inactivate and $K_V4.3$ potassium channels activate, generating a transient outward current (I_{TO}), to create a small notch during phase 1 (**Fig 3B**). The $K_V4.X$ family has similar topology to other K_V channels comprised of six transmembranous segmented subunits interacting as a tetramer to form a functional channel. All K^+-selective channels share a S5-S6 linker that contains a conserved selectivity filter (containing a required GxG motif, where x is usually T or Y).[13,14] However, there are significant differences in the accessory beta subunits that modify function of each voltage-gated K^+ channel. $K_V4.3$ has an obligatory beta subunit (KChIP2) that enhances I_{TO}.[15] While Kv4.3 is uniformly expressed across the ventricular wall,

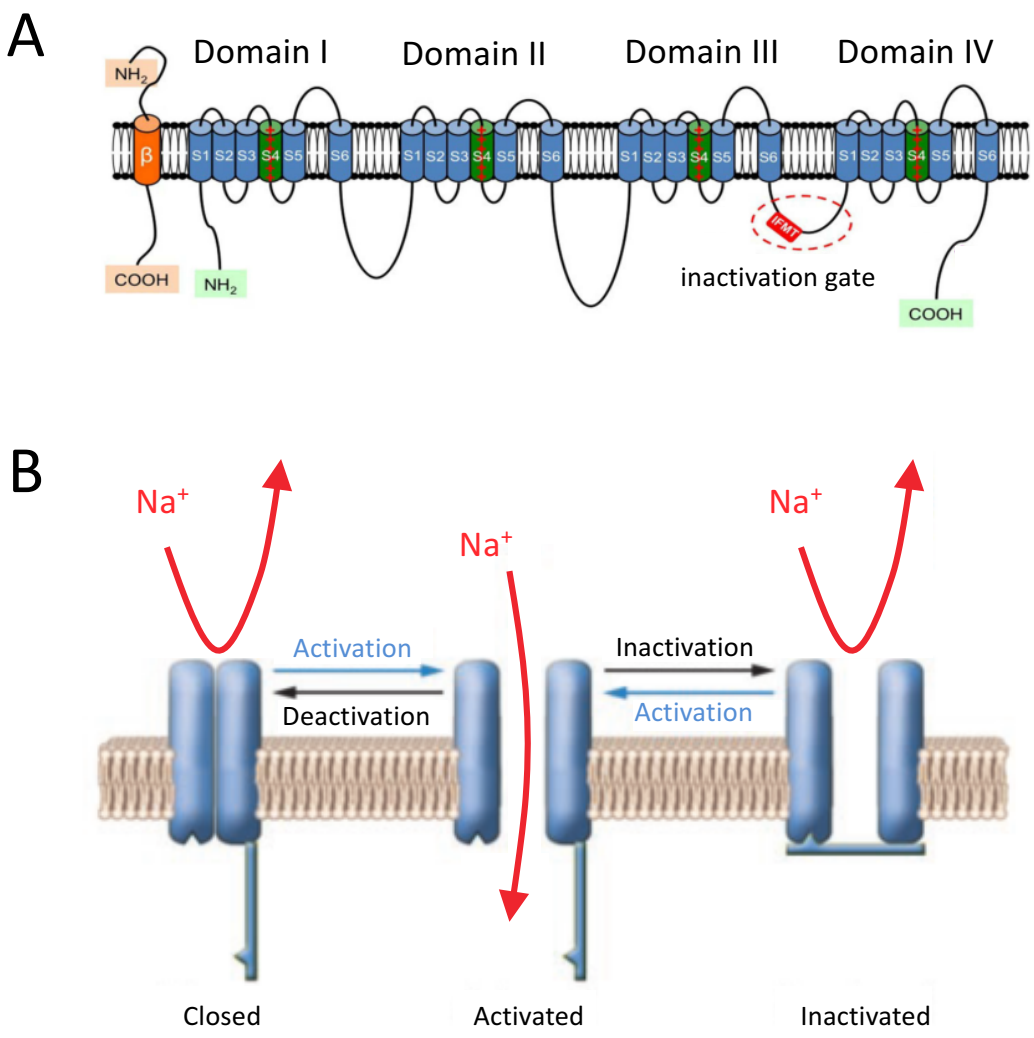

Figure 4. Cardiac sodium channel structure and functional states. (**A**) Topologic view of NaV1.5 demonstrating four domains comprised of six transmembranous domains. The inactivation gate in intracellular DIII-DIV linker is highlighted. Figure modified from Savio-Galimberti *et. al*. 2012 (**B**) Schematic demonstrating the three major gating states of NaV1.5. Figure modified from George. *JCI*. 2005.

there is a gradient of I_{TO} due to decreasing expression of the KChIP2 beta subunit within cardiomyocytes from to epicardial surface to the endocardium.[16,17] Genetic variants that cause a decrease or increase in I_{TO} are associated with inherited arrhythmia syndromes, highlighting the significance of maintaining proper ion transport during an action potential.

Voltage-gated ion channels that open during phase 2 of the action potential activate more slowly than those involved in phase 0 ($Na_V1.5$) and phase 1 ($K_V4.3$). During phase 2 there is a concurrent depolarizing Ca^{+2} influx and repolarizing K^+ efflux to create a plateau where the membrane voltage is relatively stable (**Fig 3B**). The former is a result of calcium entering the cell from the extracellular environment through the voltage gated L-type calcium channel, $Ca_V1.2$. $Ca_V1.2$ is localized primarily in the t-tubule system, a perfect position that overlies the sarcoplasmic reticulum to serve the primary function of stimulating calcium-induced calcium release. Calcium release from the sarcoplasmic reticulum provides the chemical signal to elicit heart muscle contraction.

During the plateau of the action potential, outward potassium currents are generated by three predominant outward currents, the ultrarapid (I_{Kur}), rapid (I_{Kr}), and delayed (I_{Ks}) rectifiers. These channels are critical to initial repolarization that occurs during phase 3 of the action potential. At rest, I_{Kr} is a main driver of repolarization as it is activated more rapidly than I_{Ks} but does inactivate with prolonged depolarization. This current is conducted by hERG alpha subunits (also called $K_V11.1$; encoded by *KCNH2*) and an accessory beta subunit, either KCNE1 or KCNE2. Inhibition of this channel is a common cause of medication-induced arrhythmias. I_{Ks} contributes little to repolarization except for during times of sympathetic stimulation *e.g.* during the fight or flight response; it has been described as providing "repolarization reserve" within the myocardium.[18] This current is conducted through a tetramer of KCNQ1 (also called $K_V7.1$) alpha

subunits with the KCNE1 beta subunit that activate slowly, hence the name slow rectifying potassium current. I_{Ks} has little to no inactivation but remains open until the membrane potential is more negative than -40 mV. The remainder of repolarization is carried out by the potassium-conducting transient inward rectifying currents (I_{K1}) by the $K_{ir}2.X$ family of proteins, mainly $K_{ir}2.1$ in ventricular cardiomyocytes.

Inward rectification means these channels have preference for conducting K^+ into the cardiomyocyte through a mechanism of magnesium (or polyamine) block of outward current. At more depolarized potentials, the electrochemical gradient for Mg^{+2} is outward and this drives Mg^{+2} into the vestibule of $K_{ir}2.1$ only allowing K^+ to enter the cell along its electrochemical gradient. In addition to completing repolarization, I_{K1} is largely responsible for setting and maintaining the resting membrane potential during phase 4 of the action potential. At rest, the cardiomyocyte membrane is most permeable to K^+, consistent with the resting membrane potential being at or near the equilibrium potential predicted by the Nernst equation of -90 mV at physiologic concentrations of K^+. The maintenance of the hyperpolarized state allows inactivated sodium and calcium channels to return to the closed state in order to repeat the excitation process.

Ion channel dysfunction in arrhythmia syndromes

The magnitude of individual ion currents increases or decreases after opening as a function of modulators such as transmembrane voltage, ligand concentration (if ligand gated) and time after opening. Heart rate and rhythm are governed by complex coordination of multiple ion channels in cells, and the transmission of electrical activity from cell to cell. Environmental factors or genetic variation that alters ion channel function can have devastating outcomes. In the United States, sudden cardiac death (SCD) accounts for 8-18% of all deaths and is commonly

associated with structural heart disease.[19] Ischemia-induced ventricular fibrillation is a common cause of SCD shortly after ischemic insult due to combined effects of mild membrane depolarization, intracellular acidosis, elevated intracellular concentrations of calcium and sodium.[20] Medication exposure is another environmental factor that can lead to arrhythmia onset through a multitude of mechanisms. One of the most prominent mechanisms of drug arrhythmogenesis is inhibition of I_{Kr}, leading to prolongation of the QT interval and increased risk of the morphologically distinctive polymorphic ventricular tachyarrhythmia torsades de pointes (TdP). Evaluation of the effect of any new drug candidate on I_{Kr} function is now a required part of drug development prior to receiving FDA approval.[21] An additional mechanism of drug-induced arrhythmias is a reduction in sodium current. In patients, exposure to sodium channel blocking drugs, such as flecainide, was associated with increased mortality after myocardial infarction in the landmark Cardiac Arrhythmia Suppression Trial.[22] Similarly, genetic variants that reduce the same ion currents (I_{Kr} or I_{Na}) affected by medications increases an individual's risk of experiencing SCD. Approximately 5-10% of cases of sudden death result from high-penetrance genetic conditions altering ion channel function predisposing to ventricular arrhythmias, including the Long QT (LQTS) and the Brugada (BrS) syndromes.

Genetic variants that alter cardiac repolarization result in a prolonged QT interval on ECG. The diagnosis of LQTS is made in individuals with a QTc (corrected for heart rate) longer than 480 msec and has a prevalence of 1:3,000.[23-25] The delayed repolarization increases an individual's risk of TdP, syncope, and sudden cardiac death.[26] Activities or experiences that increase sympathetic nervous system activity, such as exercise, emotional state, or arousing sounds, are arrhythmogenic triggers for LQTS.[27,28] Therefore, the mainstay of pharmacologic therapy is to dampen sympathetic tone through beta-adrenergic receptor blockade with propranolol and nodalol being more effective

that other beta blockers at preventing cardiac events of syncope or cardiac arrest.[29,30] However, approximately 20% of patients on beta blocker therapy still experience syncopal episodes and require alternative or complementary therapies of permanent cardiac pacing or internal cardiac defibrillator placement.[24,31] The severity and significance of properly identifying individuals at risk for this syndrome is highlighted by the fact that 10-15% of affected individuals present clinically for the first time with sudden death.[28,32]

This genetic condition is inherited in an autosomal dominant fashion. To date, variants in at least 15 genes are known to be causal for LQTS by multiple mechanisms that prolong the action potential duration in individual cardiomyocytes.[33] Single nucleotide variants (SNVs), very short insertions/deletions (indels), altered splicing, and occasionally large deletions (e.g. entire exons) that contribute to the underlying mechanism of delayed repolarization in cardiomyocytes through either reduced repolarizing potassium current or enhanced depolarizing current through calcium or sodium channels have been reported.[34] In 1991, Keating *et. al*. identified the first genetic locus associated with the syndrome on the short arm of chromosome 11 using linkage analysis in a large family pedigree affected by LQTS later recognized to contain the gene *KCNQ1*.[35] *KCNQ1* encodes the pore forming subunit of a voltage gated potassium channel, that along with an accessory subunit encoded by *KCNE1*, generates I_{Ks}.[36,37] Heterozygous loss of function variants in *KCNQ1* causes type 1 LQTS (LQT1), the most common form, accounting for >50% of all cases. Homozygous or compound heterozygous variants in *KCNQ1* or *KCNE1* cause a particularly severe form of LQTS known as the Jervell and Lange-Nielsen Syndrome (JLNS).[38,39] Patients with JLNS have severely prolonged QT intervals and congenital deafness as I_{Ks} is required for generating and maintaining the endolymph balance in the cochlea of the inner ear.[40] LQTS type 2 (LQTS2) is caused by reduced I_{Kr} due to loss of function variants in *KCNH2* and is the second most common form of this condition.

Even though the majority of LQTS cases are due to decreased repolarizing currents, approximately 10% are a result of genetic variants that enhance depolarizing currents, primarily due to gain of function variants in *SCN5A*, the gene encoding the cardiac sodium channel.[39,41]

Through the study of LQTS-associated *SCN5A* variants using patch-clamp methods, several alterations in sodium channel function have been described that result in a "gain of function" to prolong a cardiac action potential. The most common biophysical alteration is impaired inactivation that results in either sustained late sodium current (I_{Na-L}) or a severely slowed rate of inactivation.[42] Both of these parameters are influenced by interactions with auxiliary subunits.[43-45] Alternative and less common mechanisms include shifts in voltage-dependence of activation/inactivation and faster recovery from inactivation.[46] Unlike LQT1 that typically responds well to beta blockade, this pharmacologic therapy had variable efficacy on preventing the occurrence of cardiac events in patients with LQT3.[47] Further, in a mouse model of LQT3, adrenergic stimulation had a protective effect with a shortening of the action potential duration after isoproterenol injections, presumably through enhanced I_{Ks}.[48] The differential responses to beta blocker therapy have motivated genetic variant class specific interventions. The scientific community rationalized that since LQT3 is a result of increased sodium current, a logical therapy would be to treat with sodium channel blockers. Mexiletine, a class IB antiarrhythmic, showed variable efficacy in a small trial of five patients with the greatest effect in variants that resulted in a hyperpolarizing shift in $V_{1/2}$ of inactivation but long-term studies investigating the effect on patient survival are yet to be completed.[49,50] More recently, ranolazine, a medication that specifically blocks the late sodium current gained by many *SCN5A* variants, shortened the QTc specifically in a LQT3 patient population.[51] Larger, multi-center studies investigating the efficacy of ranolazine are currently ongoing (Clinical trial NCT01648205). The example of LQT3 demonstrates the power of understanding the genetic basis and mechanisms

driving disease in order to tailor therapy unique to the patient. Fortunately, the genetic basis of LQTS is relatively well understood as the causative variant is identified in 80% of cases.[34] However, a subset of patients with LQTS has undefined genetic etiology either due to limitations of current methodology or contributions of yet to be discovered causal genes. Chapter II describes identification of a novel variant in one such case.

The problem of undefined genetic contributions to an inherited condition is even more significant in another arrhythmia condition, the Brugada Syndrome. The Brugada Syndrome (BrS) was first described in 1992 as an inherited arrhythmia condition that increases risk of ventricular tachyarrhythmias and sudden cardiac death .[52] Patients with BrS are typically diagnosed based on a structurally normal heart and a characteristic ECG pattern (ST segment elevation in the precordial leads often with prolonged duration of the QRS complex, an index of conduction velocity within the ventricle). This rare condition has a prevalence of 0.4-1% of the population but is thought to cause 20% of sudden death events in individuals with a structurally normal heart.[53] Typically, patients come to medical attention because the ECG pattern is noted incidentally, or during evaluation for syncope or cardiac arrest, or after sudden death in a family member. The current first line of care for patients with BrS is placement of an implantable cardiac defibrillator based an initial clinical trial involving 63 patients diagnosed with BrS. This trial looked at the efficacy of ICD placement, pharmacologic therapy with beta-blockers and/or amiodarone, or no treatment. While the incidence of arrhythmic events was similar in the three groups, only ICD placement reduced mortality due to sudden cardiac death.[54] Additional reports support the finding that currently available pharmacologic therapies have been largely ineffective in reducing total mortality in BrS patients.[55,56]

The clinical picture for BrS is highly variable and can range from overt basal presence of the Brugada ECG pattern or only appearing after drug challenge with sodium channel blockers such as flecainide or procainamide.[57] Further, patients with baseline Brugada ECG pattern can experience symptoms of syncope or polymorphic ventricular tachycardia, often presented as palpitations, or can be completely asymptomatic. While many individual with BrS do not develop arrhythmias under normal conditions, stressors such as medication and fever are known to trigger arrhythmic events.[58-61] The exact tissue and cellular mechanisms causing BrS remain debated in the field complicating full understanding of the heterogeneity in clinical presentation. There are two major competing pathophysiologic theories that underlie the Brugada ECG pattern: the repolarization hypothesis and the depolarization hypothesis.

The repolarization hypothesis is based on experimental evidence collected from canine wedge preparations studying transmural (from epicardium to endocardium) repolarization dispersion.[62] Medication or genetic variants that accentuate a gradient in repolarization by decreasing depolarizing currents (I_{Na} or I_{Ca}) or enhance repolarizing currents (I_K) generate a transmural dispersion that is vulnerable to ventricular tachycardia through a phase 2 reentry mechanism.[63] The repolarization hypothesis has received criticism after clinical observations constructed the counter depolarization hypothesis.

The depolarization hypothesis is formulated on clinical and genetic evidence of slowed right ventricular conduction and theoretical involvement of mild structural abnormalities. Sodium channel blocking drugs that are used to unmask the Brugada ECG pattern cause conduction slowing and make the tissue susceptible to late potentials, a feature associated with arrhythmia onset.[64] Sodium channel blockade produces the same acute effect on slowed conduction as loss of function variants in *SCN5A*, the most common type of variant identified in this syndrome. The depolarization hypothesis

contends that decreased sodium current is required but perhaps not sufficient to cause the Brugada phenotype. Microscopic structural abnormalities have been observed in explanted hearts with Brugada Syndrome.[65] Perhaps the structural remodeling that takes place during the natural aging process is the final stressor necessary to unveil the BrS, consistent with the average age of onset to be in the early 40s.[66] More recent evidence using contact electrode methods in BrS patients or control volunteers, demonstrated slowed kinetics of action potential duration restitution (supporting the repolarization hypothesis) and conduction delay (supporting the depolarization hypothesis).[67] It is possible that a spectrum of the two mechanisms contributes to the phenotype of BrS and may depend on the particular genetics of the individual. Technologic and genetic advances are beginning to reveal the complexity of BrS pathophysiology.

Genotype-phenotype studies have identified the cellular electrophysiologic hallmark of BrS as decreased peak sodium current due to abnormal gating or reduced cell surface expression.[68,69] Over 300 loss of function mutations have been identified in *SCN5A*, the gene encoding the cardiac sodium channel $Na_V1.5$, in patients with BrS, contributing to the understanding that BrS is a monogenic disease with autosomal dominant inheritance.[46,70-72] Importantly, however, *SCN5A* mutations are identified in only ~20% of probands.[68] *Scn5a* heterozygous knockout mice have many of the features seen in patients with BrS including localized ST elevation, disordered QRS complexes, and increased susceptibility to ventricular tachyarrhythmias.[73,74] An additional 10% of BrS cases can be explained by rare loss of function variants distributed among 15 other genes, many of which encode ion channels or ion channel-associated proteins (**Table 1**). The remaining 70% of BrS cases are a result of unknown genetic etiology. It is conceivable that a portion of those cases are monogenic and driven by rare, large effect variants and others are polygenic resulting from a cumulative risk from multiple small effect variants.

Table 1. Proposed mechanisms of Brugada syndrome associated genes. Modified from Nielsen *et. al.* 2013.

Brugada syndrome subtype	Associated gene	Proposed mechanism
BrS1	*SCN5A*	Decreased sodium current[75]
BrS2	*GPD1L*	Decreased sodium current[76]
BrS3	*CACNA1C*	Decreased L-type calcium current[77,78]
BrS4	*CACNB2*	Decreased L-type calcium current[77-79]
BrS5	*SCN1B*	Decreased sodium current[79-81]
BrS6	*KCNE3*	Increased potassium current[82]
BrS7	*SCN3B*	Decreased sodium current[83]
BrS8	*KCNH2*	Increased potassium current[84]
BrS9	*KCNJ8*	Increased potassium current[85]
BrS10	*CACNA2D1*	Undefined mechanism[78]
BrS11	*RANGRF*	Decreased sodium current[86]
BrS12	*KCNE5*	Increased potassium current[87]
BrS13	*KCND3*	Increased potassium current [88]
BrS14	*HCN4*	Undefined mechanism[79]
BrS15	*SNMAP*	Decreased sodium current[89]
BrS16	*TRPM4*	Increased or decreased calcium current[90]
BrS17	*SCN2B*	Decreased sodium current[91]

Genetic approaches to the study of inherited arrhythmia syndromes

The first arrhythmia locus was identified in 1991 using linkage analysis in a large family with long QT syndrome.[35] Traditionally, linkage analysis utilized differences in restriction endonuclease target sites within the genome due to genetic variation. Restriction enzymes are bacterially derived and evolved to cut DNA at specific sequences. Therefore, an assay termed restriction fragment length polymorphisms (RFLP) was developed to correlate a clinical phenotype to patterns of DNA digestion by restriction enzymes. Current approaches perform genotyping with genome sequencing in place of RFLP. Statistical analysis determines a logarithm of odds score that represents the likelihood that a genotype is linked to a particular phenotype. Linkage analysis isolated the short arm of chromosome 11 as a genetic locus causing the long QT syndrome but it took an additional five years of positional cloning to identify the gene responsible, *KCNQ1*.[92] The study of human genetics using solely linkage analysis is restrictive based on two major limitations: (1) it requires large family pedigrees and therefore cannot be applied to small families or *de novo* variant identification and (2) it is too labor intensive to be applied to large datasets used in studying population genetics. Fortunately, major technologic and computational advances have developed alternative methods to identify the contributing common and rare polymorphisms.

The human genome project, a 13-year effort completed in 2003, provided the entire sequence of a human genome.[93] Having a defined human genome was critical for the development of next-generation sequencing (NGS), a technique that maps short reads to a reference genomic sequence and has emerged as a powerful tool for identifying genetic variation. Rapid technologic improvements in NGS now allow affordable and scalable massively parallel sequencing to identify both rare and common genetic variants. Rare variants in the coding region

of a gene that segregate with the presence of disease within a family are generally considered to have a large effect on protein function and to be potentially causative of Mendelian diseases. Alternatively, common genetic variants associated with disease are considered small effect variants that are modifiers rather than major drivers of disease susceptibility (**Fig 5**). Genome-wide association studies (GWAS) utilize advanced chip-based genotyping approaches in large population-based studies to determine if the presence or absence of common single nucleotide variants (SNVs) associates to a defined trait/disease compared to a control group. The SNVs identified contribute to the understanding of disease pathology by either identifying modifiers of health and disease that may provide more accurate risk stratification or discover novel molecular pathways that are potential therapeutic targets.

A genetic contribution to electrocardiographic variability was first established through twin studies. The exact variation underlying this heritability could not be determined due to small sample sizes between 73-350 twin pairs.[94-97] The genetic contribution to variation of heart rate, PR interval, QRS duration, and QT interval within the general population has been studied using GWAS approaches. Some of the signals detected in these GWAS are not surprising based on the biologic plausibility of the genes in which the SNVs occur in or near, such as ion channel or ion channel associated proteins. The sensitivity of GWAS approaches to identify genetic loci contributing a small to moderate effect on a phenotype increases with the number of individuals included in the analysis. The first QT interval GWAS studied only 200 subjects with extreme QT values drawn from a normal population of 3,966 subjects, and identified variants near *NOS1AP* as QT modulators.[98] Subsequent studies, enabled by cheaper and denser genotyping, included larger numbers of subjects.[99,100] A meta-analysis of QT interval GWAS combined more than 100,000 individuals to validate many previous GWAS loci and to identify 22 new associations in

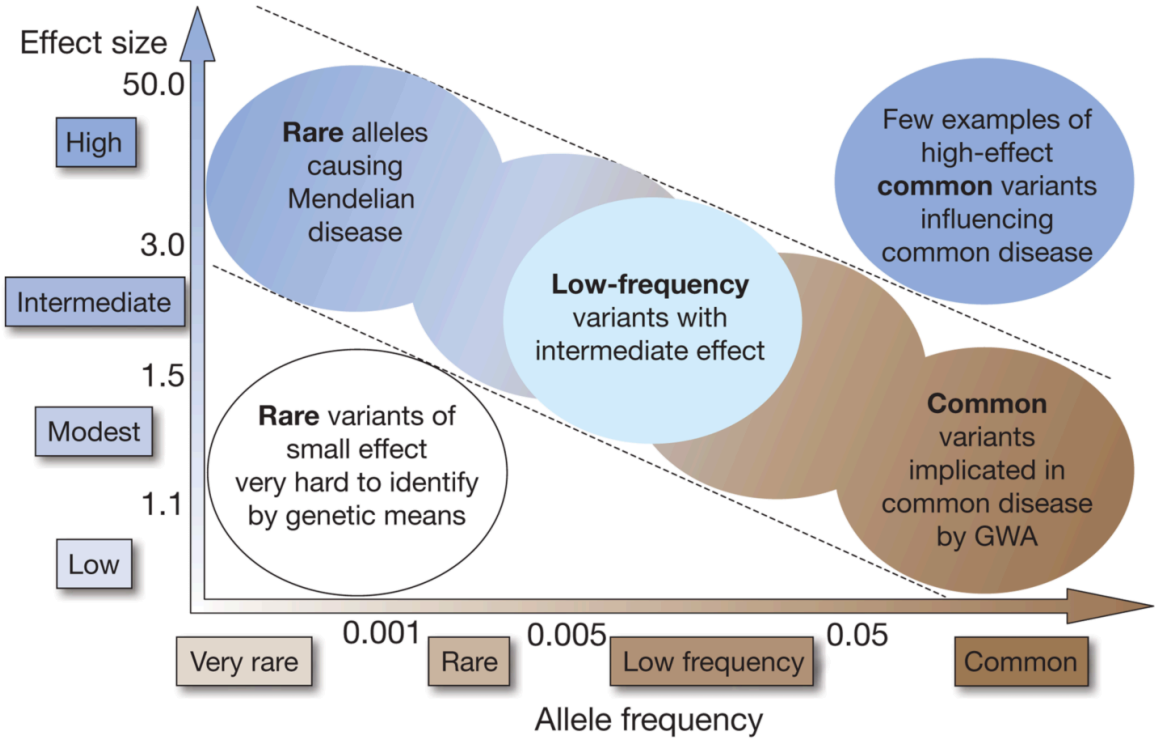

Figure 5. Schematic representation of the theory of mean allele frequency on impact of disease risk. Modified from Manolio *et. al*. *Nature* 2009.[101]

genes with unknown biologic contributions to the physiology governing QT interval.[102] QT interval GWAS data found common variants in or near five genes known to cause monogenic LQTS leading to the hypothesis that other QT interval GWAS loci may occur near previously unrecognized Mendelian LQTS genes. Therefore, large effect rare variants in these genes may explain a portion of the 20% of genetically undefined cases of inherited LQTS. Mutational screening of the coding region of a subset of these genes in 298 genetically undefined congenital long QT cases found missense variants or frameshifting single nucleotide insertions in multiple individuals in four genes, *ATP2A2*, *SLC8A1*, *SLR*, and *TRPM7*. While the rare variants identified in the four genes may contribute to the pathogenesis of LQTS in these individuals, the causative relationship of these variants require further functional or statistical evidence.

GWAS has also been applied to many disease states. A GWAS comparing 312 patients with BrS to 1,115 population controls identified three significant association signals, two in sodium channel genes, *SCN5A* (rs11708996) and *SCN10A* (rs10428132), and a third near the gene encoding the HEY2 transcription factor (rs9388451).[103] A mouse model of *Hey2* homozygous genetic deletion demonstrated that in an adult mouse the absence of Hey2 transcription factor results in moderate alteration in isolated myocyte action potential upstroke velocity and reduced expression of *Scn5a*, *Kcnj2,* and *Cacna1c* but did not promote spontaneous arrhythmias.[104] A report using a mouse model of *Hey2* heterozygous genetic deletion found contradicting impact on action potential upstroke velocity as mice lacking one copy of *Hey2* had increased upstroke velocity resulting in enhanced conduction velocity across the ventricular myocardium.[103] While mouse model data needs further investigation to understand the role of Hey2 in cardiac conduction, SNVs near *HEY2* still may contribute to BrS susceptibility.

Individual SNVs identified as GWAS signals actually detect large "neighborhoods" of DNA containing multiple variants inherited together (in linkage disequilibrium) that associate to the phenotype. A significant challenge is isolating which SNV located in linkage disequilibrium is the "functional" SNV. An important example of functional SNV identification is the *SCN10A* signal identified as a modifier of QRS duration[105] and in BrS susceptibility.[103] rs10428132 is in strong LD with 14 other SNVs, including one in the coding region of *SCN10A* (rs6801957).[106] It was originally hypothesized that this coding variant accounted for the association but functional assessment using heterologous expression found the hypothesized risk allele increased sodium current by 40% and if anything one would speculate may protect against BrS.[107] However, the contribution of *SCN10A* to cardiac function is highly debated and evidence supports little to no expression of this gene within cardiac myocytes.[108] Closer examination of this BrS risk region identified another SNV (rs6801957) that was located within a presumed enhancer region based on overlap with binding sites for transcription factors (TBX5, NKX2.5, and GATA4) and transcriptional co-activators (p300 and RNA Polymerase III). Utilization of chromosome conformation sequencing, a method utilizing NGS, specifically defined the enhancer that contains rs6801957 interacts with the *SCN5A* promoter to participate in the regulation of *SCN5A* expression (**Fig 6A**).[109] Multiple lines of evidence, including zebrafish models, mouse models, and association to human tissue samples, show the risk allele rs6801957 causes reduced *SCN5A* expression, consistent with the known pathophysiology of BrS. The mechanism is thought to be disruption of the binding site of cardiac transcription factors TBX3 and TBX5 (**Fig 6B**). This example highlights that SNVs can contribute to the pathogenesis of inherited conditions, adding complexity to the previous view of BrS as a Mendelian disease.

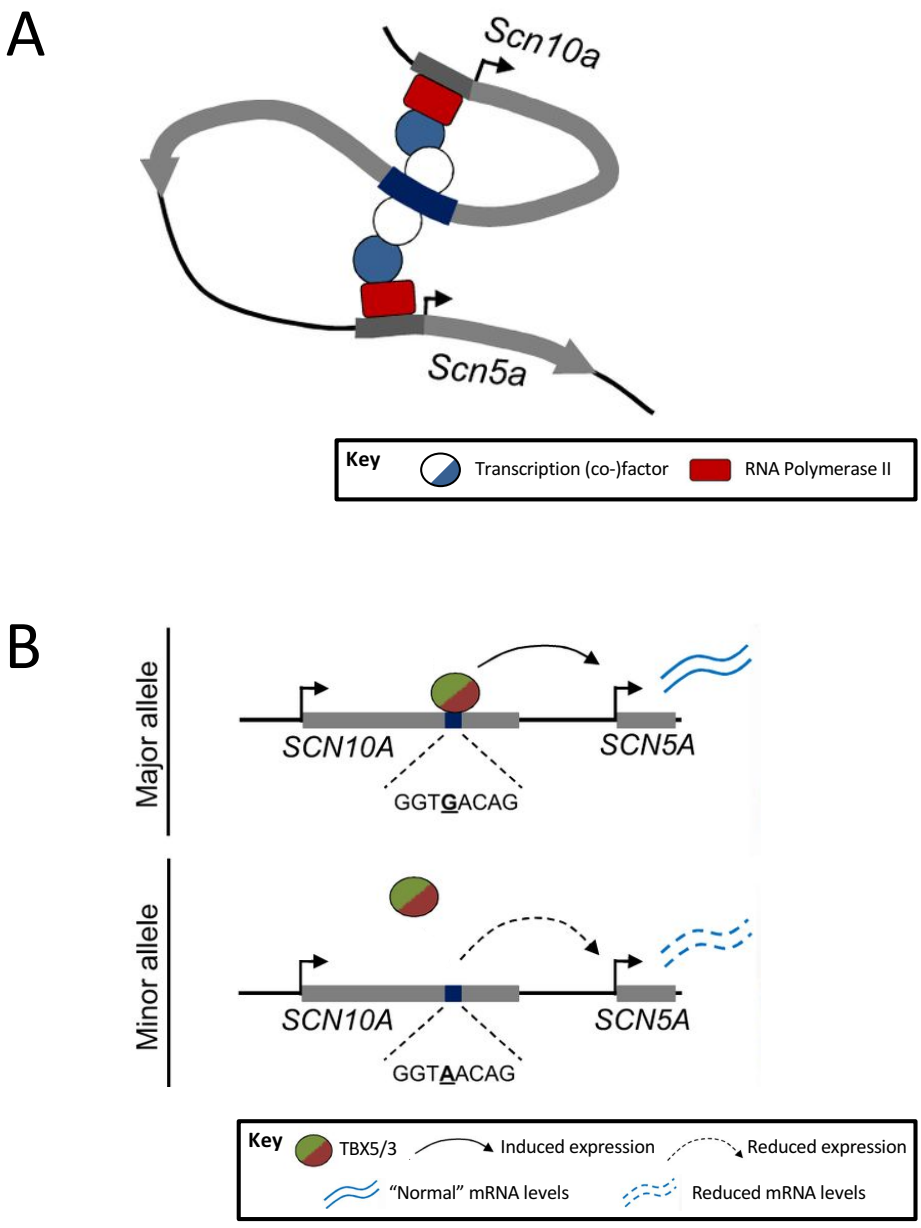

Figure 6. Shared cis-regulatory enhancer of *SCN5A-SCN10A* is disrupted by common single nucleotide variant. (**A**) The enhancer in *Scn10a* physically contacts the promoters of both *Scn5a* and *Scn10a* to mediate their expression. (**B**) The variant in *Scn10a* alters *Scn5a* expression. The major allele harbors a T-box binding element that is occupied by Tbx5 to drive *Scn5a* expression in the heart (indicated by black arrowheads). The variant alters a base in the minor allele, disrupting the T-box binding element and causing a strongly decreased affinity for Tbx5. Modified from Hendrik van Weerd and Christoffels. *Development*. 2016.

When considering just the three SNVs associated with BrS, each person could carry as many as six risk alleles (each genome contains two copies of each chromosome) within his or her genome. The total genetic contribution of BrS susceptibility is cumulative based on the number of inherited BrS risk alleles. The initial analysis of the BrS GWAS indicated that an individual with ≥5 BrS risk alleles has an odds ratio of 21.5 to be diagnosed with BrS compared to those with 0-1 risk alleles.[103] Based on the cumulative risk of just these 3 SNVs, some have postulated that BrS, and perhaps other diseases, can result in some cases from a combination of many common SNVs making BrS a polygenic disease. Rare examples of individuals in a family in which a loss of function variant in *SCN5A* has been identified have the BrS phenotype in the absence of the *SCN5A* variant.[110] Alternatively, cases exist of fully and variably penetrant *SCN5A* variants within family pedigrees. The variable penetrance of some *SCN5A* variants in BrS may be explained by the genetic background of the individuals containing common SNVs that act as modifiers of disease risk.

While combinations of common variants may explain a fraction of the 70% of genetically undefined BrS cases, there are still efforts to identify rare variants in genes not currently associated with BrS. In efforts to identify these novel Mendelian BrS genes, sequencing of the coding region and flanking intronic regions of a list of seven candidate genes was performed in 156 individuals diagnosed with BrS who do not harbor coding variants in *SCN5A*. The candidate gene list was constructed based on genes implicated by GWAS as playing a role in variability in PR intervals or QRS duration.[107] This approach identified rare non-synonymous SNVs in five genes (but could not further establish causality), including G145R in *TBX5*, the gene encoding the cardiac transcription factor TBX5, a known regulator of *SCN5A* expression.

TBX5 as a Brugada Syndrome Candidate Gene

Altered gene expression is in fact an appreciated causative or modulatory mechanism in inherited arrhythmia syndromes. In patients diagnosed with BrS that carry heterozygous loss of function *SCN5A* mutations, the presence of common variants in the *SCN5A* promoter is associated with a more severe phenotype.[111-113] TBX5 is implicated in BrS pathogenesis through a previously described BrS-associated common *SCN10A* variant (rs6801957) that is located in a putative TBX5 binding motif of an *SCN5A* enhancer, causing lower levels of *SCN5A* expression in human myocardium.[103,109] Common variants located near TBX5 are associated with prolonged QRS duration, a feature observed in BrS.[114] Missense variants in TBX5 (gain of function mutation),[115] and other transcription factors GATA4 (loss of function mutations)[116-118] and NKX2.5 (loss of function mutations)[119] have been identified in cases of familial atrial fibrillation, supporting transcriptional misregulation as a mechanism of arrhythmia conditions. Therefore, TBX5-G145R is an intriguing causal candidate variant in familial BrS.[107] This is variant is not reported in the Exome Aggregation Server, indicating it is very rare.

TBX5 is a T-box containing transcription factor critical to mammalian tissue patterning and cellular differentiation during development of the upper extremities and the heart. *TBX5* variants that result in TBX5 haploinsufficiency (nonsense, frameshifting indels, and splice site variants) or severe alterations in DNA binding (missense and intragenic duplications) cause the human condition Holt-Oram syndrome (HOS).[120] HOS is a rare developmental syndrome affecting 1:100,000 live births with abnormal development of the upper limbs and the heart. The severity of developmental defects can range from mild to severe. Mild hand involvement includes hypoplastic thenar musculature and short radius while the severe types have gross hypoplasia of the thumb or radius. In the heart, isolated atrial septal defects and arrhythmia risk are the mild presentations.[121]

The most severe cases can result in complex cardiac anomalies such as tetralogy of Fallot or ventricular septal defects.

The *TBX5* gene contains 9 exons that encode 518 amino acids with the first 237 amino acids comprising the conserved T-box family DNA binding domain.[122] TBX5 binds a variable octamer sequence (A/G)GGTGT(C/G/T)(A/G) with the TGT sequence being most conserved among TBX5 regulated genes (**Fig 7A**).[122] However, TBX5 can bind somewhat promiscuously as exemplified by its interaction with the EnhancerA of *SCN5A* GGTGACAG sequence within the *SCN10A* gene.[123] TBX5 binds the major groove of its DNA targets through hydrogen bonds with an ab-loop structure of TBX5. This ab-loop contains a glycine at amino acid position 80 that is mutated to an arginine in one form of HOS, disrupting TBX5-DNA interactions (**Fig 7B** and **7C**).[124] The terminal alpha helix of the DNA binding domain of TBX5 is structured by a salt bridge occurring between glutamate at position 228 and arginine at position 237 (**Fig 7B** and **7C**). This helix binds the minor groove of TBX5 DNA targets. HOS mutations R237W and R237G alter TBX5 interactions with the minor groove due to an unstructured terminal.[120] Comparison of the amino acid position mutated in TBX5 and the severity of hand or heart involvement generated the hypothesis that disruption of major groove binding causes more severe cardiac defects and minor groove disruption is associated with more severe upper limb anomalies.[120] Missense variants in the DNA binding domain of TBX5 can alter DNA binding affinity of specific target sequences, resulting in increased DNA binding capacity[115] or, more typically, decreased DNA binding.[122,125] Interestingly, some missense variants increased affinity for non-specific DNA target sites, either preventing appropriate TBX5 chromatin localization or perhaps influences expression of genes not typically regulated by TBX5.[126] Further evaluation is required to elucidate the functional implications of aberrant mutant TBX5-DNA interactions.

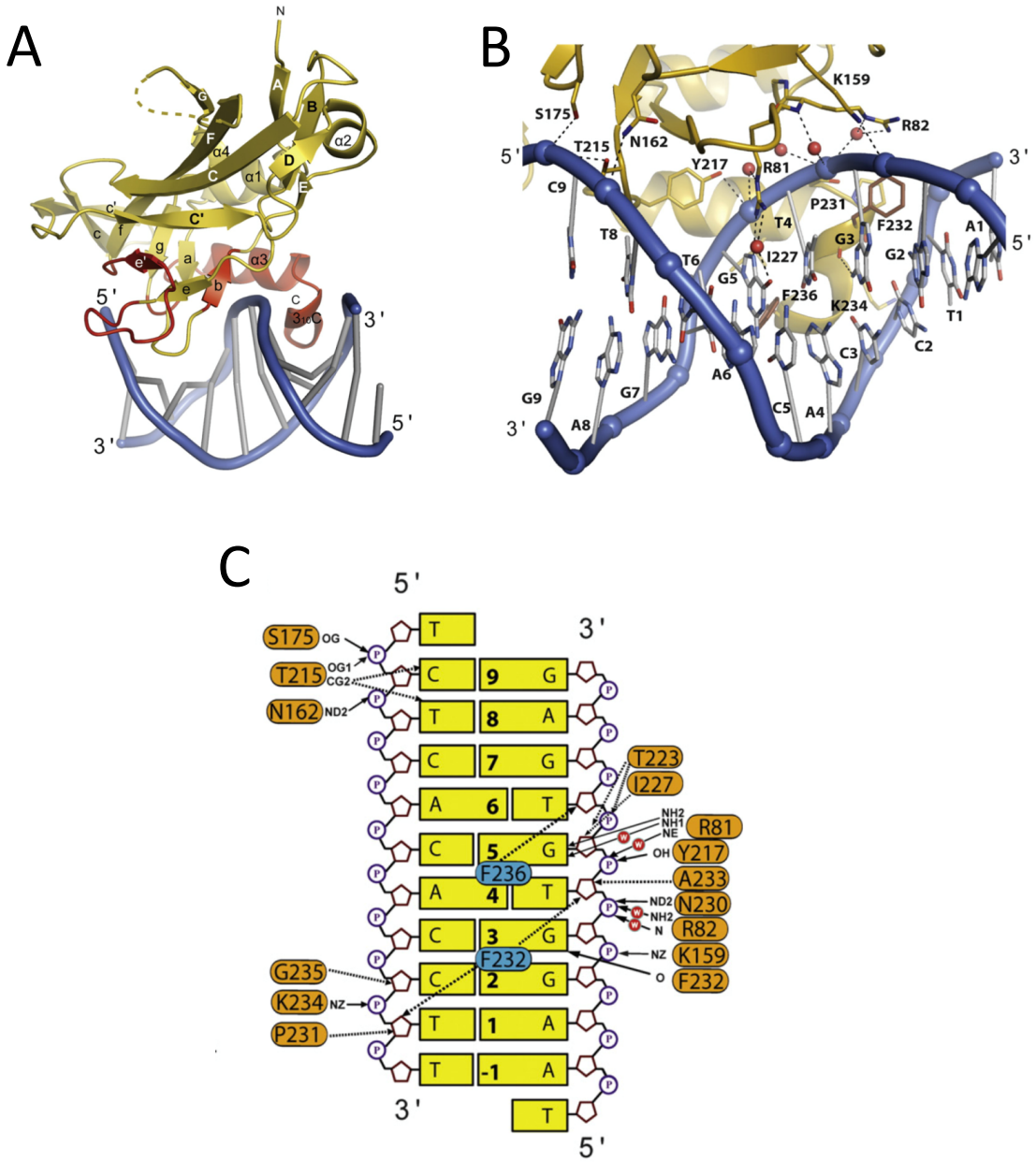

Figure 7. Structural features of the TBX5–DNA interaction. (**A**) Overview of the TBX5–*NPPA* promoter (5' – AGGTGTGAGA – 3') complex. TBX5 is depicted in yellow, parts interacting with DNA are in red, and the DNA is in marine and gray. The unstructured loop is depicted as yellow broken line. β-Strands involved in the β-barrel are labeled with capital letters (A–G), and β-strands from the β- pleated sheets are in lowercase letters (a–g). (**B**) Close-up view of the interaction between TBX5 (yellow) and the DNA (blue-gray). Hydrogen bonds are depicted as black broken lines, and water molecules mediating hydrogen bonds are depicted as red spheres. (**C**) Interaction diagram of the TBX5–DNA interactions. Polar interactions are indicated by black dashed arrows; hydrophobic interactions are in solid black. Modified from Stirnimann *et. al*. *Journal of Molecular Biology* 2010.

Transcriptional activators and repressors work in concert to regulate gene expression and influence cellular differentiation. TBX3 is a transcriptional repressor that competes with TBX5 to bind DNA targets required in cardiac conduction system precursors. In the absence of TBX3, the precursors differentiate into working myocardium instead of the specialized tissue of the conduction system. TBX5 is a crucial positive regulator of TBX3 expression[127] but also auto-regulates its own expression. The TBX5 promoter region contains two auto-regulatory T-box binding elements critical for TBX5 expression.[128] Regulation of TBX5 can occur through modulation of expression levels or through interactions with other proteins. MicroRNAs are involved in cardiac development through posttranscriptional regulation of gene expression.[129] Specifically, miR-10a and miR-10b bind the 3'-untranslated region of TBX5 transcripts to decrease translation.[130] At the protein level, TBX5 is degraded by the ubiquitin-proteasome system via the Fbxo25-mediated E3 ubiquitin ligase complex.[131] A primary mode of TBX5 regulation is nuclear availability through protein interactions with the two nuclear localization sequences (NLS)[132] and one nuclear export sequence (NES).[133] LMP4 interacts with the NLS located in the C-terminal half of TBX5 to mediate the dynamic shuttling of TBX5 between the cytoplasm and the nuclear. The export protein CRM1 binds the NES within TBX5 promoting nuclear export.[134]

Protein function can be modulated by post-translational modifications and synergistic protein-protein interactions. Histone deacetylase 3 (Hdac3) lacks a DNA binding domain but locates to chromatin in translational machinery complexes through interactions with transcription factors. Hdac3 is a negative regulator of Tbx5 function that directly binds and modulates the acetylation state of Tbx5. In a mouse model that lacks Hdac3, enhanced acetylation of Tbx5 increased expression of Tbx5-regulated genes and caused hypoplastic ventricular myocardium.[135]

Loss of Hdac3 induces aberrant cardiomyocyte differentiation from progenitor cells, similar findings were observed in progenitor cells in which Tbx5 was overexpressed or contained the gain of function TBX5-G125R mutant.[115,136] TBX5 physically interacts with other transcription factors/co-factors critical to cardiogenesis, including NKX2.5, GATA4, myocardin, and MEF2C, through interactions in the DNA binding domain (amino acids 54-237) to synergistically activate gene targets.[137-140] Interestingly, some TBX5 missense variants completely abolish synergistic activation of gene targets and others have no impact on target gene expression. TXB5 associates with NKX2.5 to synergistically activated *NPPA* expression. TBX5-G80R fails to bind the *NPPA* promoter or show synergistic activation in the presence of NKX2.5, likely due to the complete loss of DNA binding. In contrast, TBX5-R237Q similarly activates *NPPA* expression compared to wild-type protein and has synergy with NKX2.5.[137] Recently, a crystal structure of TBX5 and NKX2.5 bound to the *NPPA* promoter identified residues important for the intermolecular interactions.[124] Several hydrogen bonds occur between the two molecules with the highly conserved amino acids D140, P142, and R150 contributing to these hydrogen bonds. The D140 and P142 amino acids are part of a highly conserved loop (amino acids 137-143) that creates a small acidic domain that interacts with basic amino acid side chains of NKX2.5.[124] It is presumed that GATA4 interacts with the same acidic patch as mutant TBX5-A143T prevents complex formation and synergistic activation of *NPPA* expression in the presence of GATA4.[141]

Animal models have provided mechanistic insight into the role of TBX5 on cardiac development. In zebrafish, reduced Tbx5 levels dampen cardiomyocyte progenitor proliferation and epicardial cell migration.[142] Germline haploinsufficiency of *Tbx5* in murine models phenocopies many human HOS features and results in diminished cardiac expression of gap junction proteins, atrial natriuretic peptide, and the cardiac sodium channel. Surface ECGs

recorded from *Tbx5* heterozygous knockout mice demonstrate localized ST elevation and disordered QRS complexes.[143-145] Expression patterns of Tbx5 in the developing mouse heart show an anteroposterior gradient of expression with higher expression in the left ventricle compared to the right side. This pattern of Tbx5 expression is maintained within the adult mouse heart with highest expression of Tbx5 within the atria and conduction system. In the developing human heart, TBX5 is expressed with a similar pattern as the developing mouse with atrial levels being greater than ventricular and a transmyocardial gradient (epicardium higher than endocardium) present in all four chambers.[146,147] In contrast to the adult mouse heart, TBX5 expression is present in all four chambers of the adult human heart without a gradient present across the myocardium.[147] Based the uniform expression of TBX5, it is reasonable to hypothesize that TBX5 is critical to heart maintenance and variants in *TBX5* may have implications beyond cardiac development.

Conditional deletion of Tbx5 from the mature mouse ventricular conduction system (VCS) demonstrates Tbx5 serves an important role in the maintenance of the cardiac conduction system. Induced deletion of Tbx5 in the adult VCS results in loss of fast conduction, arrhythmias, and sudden death.[148] Tbx5 regulates expression of *Scn5a* and *Cx40*, encoding the sodium channel and a major gap junction protein, the main mediators of fast conduction, through interactions with local and distant cis-regulatory elements.[109] The significance of TBX5 in the maintenance of electrical and contractile function of the ventricular myocardium remains to be elucidated.

Clinical evidence supports the notion that TBX5 is critical to maintenance of heart function. Adult victims of sudden unexplained death syndrome have been attributed to structural heart disease and arrhythmia conditions. Genetic analysis of unexplained sudden death in 25 cases aged 19-50 years identified rare variants in *TBX5* (D18P and D43P) in unrelated 27-year

old female and 36-year old male.[149] Histologic analysis of the explanted hearts found conduction system fibrosis that was not observed in the other 23 hearts without *TBX5* variants examined. Other missense mutations located in the DNA binding domain have been described in other cardiac diseases that may present in adulthood, including cardiomyopathy and Brugada.[107,141,150] Two independent efforts identified rare missense variants in *TBX5* in cases of dilated cardiomyopathy (DCM). TBX5-S154A completely segregated in familial DCM[150] and TBX5-A143T was found in a case of sporadic DCM.[141] Both reports looked at the functional implications of mutant TBX5 using a single *NPPA* promoter-driven luciferase reporter assay; the authors demonstrated that these variant results in reduced, but not null, transcriptional activity. To date, the *NPPA* gene or its product atrial natriuretic peptide (ANP) have not been implicated in the pathogenesis of DCM but ANP is a biomarker of disease progression[151] and *NPPA* mutations have been reported in familial atrial fibrillation.[152] Assessing the functional and transcriptional effects of TBX5-A143T or TBX5-S154A in cardiomyocytes may provide further insight into causality and pathogenesis. In a single case of BrS, the novel TBX5-G145R variant (studied in Chapter IV) was identified and classified as likely pathogenic based on the criteria of being a nonsynonymous variant, not present in 8,600 control alleles, and predicted pathogenic by at least three *in silico* prediction tools.[107] For each of these examples, while the variants were uniformly predicted to be deleterious to protein function and likely pathogenic, conclusive functional evidence that these variants cause the disease is still lacking.

Modern tools in molecular cardiology

NGS is used clinically to confirm diagnoses, screen family members of effected individuals, and to guide therapeutic approaches. Commercial and academic genetic testing is provided by laboratories certified by the Clinical Laboratory Improvement Amendments program. As part of genetic testing, the company or institution evaluates the genome for lesions

and interprets the findings for potential contribution to the disease state. For identified variants there are three possible designations: pathogenic, benign, and variant of unknown clinical significance (VUS). VUS pose a significant hurdle to understand mechanistic and causative contributions to disease. Multiple efforts have attempted to provide accurate and useful predictive modeling of VUS pathogenicity leading to the standard and guidelines for the interpretation of missense variants by the American College of Medical Genetics and Genomics (ACMG).[153-155] A recent report tested these ACMG standards to evaluate the efficacy of predictive modeling to assign pathogenicity to incidentally identified rare variants in the Mendelian disease genes *SCN5A* and *KCNH2*.[156] In a large prospective cohort study of 2,022 individuals, 63 individuals carried at least one variant in these two genes. Three expert laboratories evaluated the incidentally identified *SCN5A* and *KCNH2* variants designating 42 as potentially pathogenic with poor concordance across laboratories as only 33% were classified as potentially pathogenic by multiple locations. Review of the medical records of the variant carriers found only 35% had evidence of arrhythmia or ECG phenotypes highlighting the need for more accurate evaluation of the functional implications of identified genetic variants. One approach to augment predictive modeling is to use functional assessment as an additional factor used in determining variant pathogenicity (see Chapters III and IV).

The majority of inherited arrhythmia syndromes are result of genetic variants affecting ion channel function. Classically, ion channel variants have been studied in heterologous expression systems. Cloning of ion channel cDNA, such as *SCN5A*,[157] permits transient expression of wild-type or mutant proteins in standard laboratory cells lines for functional assessment. However, there are limitations to this approach as exemplified by $Na_V1.5$-D1275N. In heterologous expression systems, $Na_V1.5$-D1275N has identical function as wild-type protein

even though there is strong clinical evidence this mutant results in conduction disease.[158] Watanabe and colleagues generated a transgenic mouse model harboring this variant to study the functional implications within a cardiomyocyte. Within a mouse cardiomyocyte, $Na_V1.5$-D1275N resulted in a dose-dependent reduction in peak sodium current and channel abundance at the membrane demonstrating that some genetic variants must be studied in the correct cellular context to evaluate pathogenicity. Animal models provide an *in vivo* assessment of genetic variation but, as is true with all disease models, has limitations. Transgenic animal generation and colony maintenance is costly and labor intensive. There are also physiologic species differences that may complicate interpretation of results. For example, the adult mouse is more resistant to arrhythmic triggers compared to humans in part because of differential ion channel expression required to maintain the mouse resting heart rate of 350-600 beats per minute compared to a human rate of 60-100. Recent advances in molecular and human stem cell biology have extended the types of models that are now utilized in understanding the genetics and mechanisms of cardiac disease.

Embryonic stem cells (ESCs) are totipotent cells derived from an early embryo capable in infinite self-renewal and the ability to differentiate into any cell type. The first isolation of ESCs from a mouse embryo was performed in 1981 and the potential as it relates to science and medicine was immediately realized.[159] Efforts began to isolate and culture human ESCs and were achieved in 1998.[160] Human ESCs were employed to advance understanding of developmental biology and pursued for future transplantation therapeutics. For ethical concerns, the US government has restricted the use of public funding to support human ESC research, limiting the utility of these cell lines.[161] Fortunately, the next breakthrough for stem cell biology occurred in 2006 when Yamanaka (who went on to share the Nobel Prize in 2012) showed that somatic cells

from an adult mouse could be reprogrammed back to a stem cell like state to generate induced pluripotent stem cells (iPSCs).[162] This same approach was reproduced using human fibroblasts just a year later.[163] Transient expression of the four pluripotency factors OCT4, MYC, KFL4 and SOX2, a combination now known as the Yamanaka factors, efficiently return human fibroblasts, mononuclear blood cells, and keratinocytes to iPSCs.[163-165] iPSCs, like ESCs, are self-renewing and capable of differentiation to cells derived of the three germ layers: endoderm, mesoderm, and ectoderm. Decades of cardiac development pathway dissection allows directed differentiation of stem cells to cardiomyocyte lineages, permitting mechanistic studies in human cardiomyocytes.

Reprogramming of somatic cells to a stem cell-like phenotype and subsequent differentiation to a cardiomyocyte fate provides a renewable resource for biologic discovery. Early protocols utilized embryoid bodies, clusters of stem cells, to mimic normal development. In the presence of growth factors, iPSC-derived embryoid bodies differentiate to all three germ lineages, producing cardiomyocytes with an efficiency of 1-10%.[166] An improved method of differentiating a monolayer of iPSCs with chemical modulation of Wnt-pathway signaling increased the efficiency and purity of cardiomyocytes to over 85%.[167] Human iPSC-CMs have the advantage of containing the human genomic architecture, making genomic insights possible, but also contain an inherent limitation of being functionally immature cardiomyocytes.[168] For example, iPSC-CMs display slower action potential upstroke and a more depolarized resting membrane potential compared to adult human ventricular cardiomyocytes. Further, there has been significant inter-laboratory variation in these key parameters creating a challenge in comparing results. Even though the cells have an immature phenotype, multiple studies in iPSC-derived cardiomyocytes verify that this approach can recapitulate inherited heart disease

phenotypes within a petri dish, including cardiomyopathy and arrhythmia syndromes.[169] Through mid-2016, iPSC-CM models of seven inherited arrhythmia syndromes have produced the individual ion channel and action potential lesions anticipated in genetic arrhythmia syndromes.[170-172] Current arrhythmia models have established iPSC-CMs as a usable model in studying electrical phenotypes and have set the framework for evaluating genetic variant causality and advancing mechanistic insight.

Genome editing

Manipulation of the human genome with the programmable zinc-finger nucleases (ZFNs), transcription activator-like effector nucleases (TALENs), and RNA guided Cas9 expand the scientific questions one can address. These approaches generate a double-strand break in DNA that ultimately results in gene disruption or specific editing. ZFNs and TALENs are protein guided nucleases constructed of a DNA binding domain, either a zinc finger protein (ZFP) or a transcription activator-like effector (TALE), tethered to a FokI restriction enzyme. FokI is a non-specific DNA cleavage enzyme so the specificity of target cleavage is governed by the binding site of ZFP and TALE domains.[173] Even though ZFPs bind GC-rich 3-bp DNA sites, the need of ZFNs to function as adjacently bound dimers, within 5-7 base pairs, results in an available target site present on average every 100 bases within the genome.[174] Alternatively, TALENs target repetitive DNA sequences and can be designed to target almost any sequence of DNA. Because of the nature of TALEN DNA targeting using complementary binding to repetitive structures, these proteins are more difficult to synthesize due the inappropriate annealing of synthetic oligomers within the repetitive DNA binding domain.[175] RNA-guided nucleases use a common nuclease that exerts its nuclease activity after interacting with a guide RNA bound to complementary DNA. The limitation of RNA-guide nuclease targeting is requirement of a

defined three nucleotide sequence specific to each version of nuclease, at the end of the target sequence. Cas9, the first and most extensively studied RNA guided nuclease, scans the genome using a NGG sequence, known as the protospacer adjacent motif (PAM site), where N can be any nucleotide and the GG dinucleotide occurs approximately every 8 bases in the double stranded genome. An alternative RNA-guided nuclease, Cpf1, was recently identified that uses different PAM sequences of NTT that generates more targeting options in T-rich intronic regions of the genome.[176] The major advantage of RNA-guide nucleases is the simple cloning required to modify the guide RNA sequences and by using RNA targeting, multiplex editing is easily achievable.

The three discussed approaches target specific DNA sequences to induce double-strand breaks. The preferred mode of double-strand break repair in eukaryotic cells is error prone non-homologous end joining (NHEJ) that creates insertion/deletion mutations.[177] NHEJ can be used to disrupt a gene in order to generate knockout models through random generation of frameshifting insertions/deletions. Concurrent delivery of the nuclease with a repair template leads to homology-directed repair (HDR) to specifically edit the genome to modify single nucleotides or insert larger sections of DNA.[178,179] The HDR approach in patient-specific iPSCs is a tractable approach to study the functional implications of singe nucleotide variants.

Genome editing of patient-specific cells generates isogenic control lines that are genetically identical except for the edited site. Even though the utilization of these techniques has become increasingly commonplace since 2013, few studies generate isogenic controls to isolate effects driven by genetic variations. Since 2010, more than 60 publications have studied inherited arrhythmia conditions using iPSC-CM models.[180] In the majority of those publications, the disease lines are compared to control lines generated from healthy control volunteers from

the general population, and therefore failing to appreciate the effect of genetic variation on the phenotype of interest. Less than 12% of iPSC-CM arrhythmia models use isogenic controls. Genome editing in patient-derived iPSCs provides definitive testing of the pathogenicity of rare variants identified in congenital arrhythmia syndromes.

Objective

The purpose of this dissertation is to advance the understanding and utilization of genome science for the application to inherited heart disease. First, in order to utilize next-generation sequencing to guide clinical practice, it is imperative to understand the limitations of this technology. Using a Long QT syndrome phenotype that is very suggestive of an underlying genetic cause of compound heterozygous *KCNQ1* variants, we sought to identify a genetic lesion not identified by NGS (see Chapter II). Second, while the ability to sequence large portions of the genome exists, a significant challenge remaining is how to best interpret the data in order to understand the implications of the findings on disease risk. Each person's genome has 300-600 rare coding variants.[181] While many of the variants identified using NGS and GWAS approaches can be rationalized based on the known or associated biology, statistical or functional evidence is required to establish causality. Presented here are two approaches to functionally establish causation and define the molecular and transcriptional mechanisms of novel variants identified in human channelopathies: heterologous expression and stem cell-derived cardiomyocyte models. In Chapter III, I characterized the biophysical properties of rare variants in a voltage-gated potassium channel identified in epileptic encephalopathy compared to wild-type protein. In Chapter IV, genome editing in patient-specific stem cell-derived cardiomyocytes was used to study a rare variant in a cardiac transcription factor identified in the Brugada Syndrome.

CHAPTER II

IDENTIFICATION OF GENETIC VARIATION: A PARTIAL DUPLICATION AND POLY(A) INSERTION IN *KCNQ1* NOT DETECTED BY NEXT-GENERATION SEQUENCING IN JERVELL AND LANGE-NIELSEN SYNDROME*

ABSTRACT

Purpose: The Jervell and Lange-Nielsen syndrome (JLNS) is an autosomal recessive disease (caused by loss of function variants in *KCNQ1* or *KCNE1*) defined by congenital deafness, markedly prolonged QT interval, and high risk for sudden cardiac death. Variant negative cases provide an opportunity to define new types of causative lesions.

Methods and results: Next generation sequencing (NGS) was undertaken in a woman with congenital deafness, severe QT prolongation, and polymorphic ventricular tachycardia. However, only a single heterozygous mutation in *KCNQ1* resulting in a premature stop codon, R518X, was identified. Convinced by the clinical phenotype that a second variant was present, Sanger sequencing was used to identify a 52-base pair (bp) insertion comprised of a 36-bp poly-adenine tract and partial exonic duplication, consistent with a truncated Alu element. The two variants were present in trans, establishing *KCNQ1* compound heterozygosity as the etiology for JLNS in this case.

Conclusion: Short reads used by NGS can miss complex genetic variations including intermediate size indels which have not previously been reported in the congenital long QT syndromes. Thus, this result raises the possibility that other cases of genotype-negative congenital long QT syndrome can be caused by this kind of genetic variant.

INTRODUCTION

Genetic information has become increasingly important to the practice of medicine and the effort to understand mechanisms of disease through basic science. Next generation sequencing (NGS), a technique that maps short reads to a reference sequence, has emerged as a powerful tool for identifying genetic variation. While current NGS algorithms detect single nucleotide variants (SNVs) with high confidence, insertion/deletion variants (indels) are not as sensitively detected.[182] Detection of indels by NGS is inconsistent. Small indels (2-10 bases) and large indels (exonic or larger) are readily identified, but intermediate sized indels (10-200 bases) are still a significant challenge, and insertions are more challenging to detect than deletions.[183,184]

Prolongation of the rate-corrected QT interval (QTc) on the surface electrocardiogram (ECG) is a key feature of the congenital long QT syndromes (LQTS). This family of inherited syndromes predisposes to the morphologically distinctive polymorphic ventricular tachyarrhythmia torsades de pointes, syncope, and sudden cardiac death. The underlying mechanism is delayed repolarization in cardiomyocytes through either reduced repolarizing potassium current or enhanced depolarizing current through calcium or sodium channels.[34] Genetic evaluation of affected individuals and families has associated variants in at least 15 genes with the syndrome;[33] SNVs, very short indels, altered splicing, and occasionally large deletions (e.g. entire exons) have been reported. Type 1 LQTS (LQT1), the most common form, accounts for >50% of cases and is caused by heterozygous loss of function variants in *KCNQ1*, the gene encoding the pore forming subunit that, with an accessory subunit encoded by *KCNE1*, generates the slow delayed rectifying repolarizing potassium current (I_{Ks}).[36,37] Heterozygous loss of function variants in *KCNE1* result in type 5 LQTS.[185]

Most LQTS is inherited in an autosomal dominant fashion. However, an especially severe form is the Jervell and Lange-Nielsen Syndrome (JLNS), an autosomal recessive form of the disease defined by a markedly prolonged QT interval and congenital sensorineural deafness. Homozygous or compound heterozygous variants in *KCNQ1* or *KCNE1* cause JLNS.[38,40] Sympathetic activation by emotional or exertional stress is a common trigger for arrhythmia in LQT1 and in JLNS.

We present a clinical case of JLNS with high susceptibility to exercise-induced arrhythmia. However, evaluation by NGS only identified a single loss of function variant in *KCNQ1*. Because the clinical presentation and the known genetics of JLNS strongly suggested that a second mutation must be present, we used conventional Sanger sequencing to identify a complex ~50 bp indel undetected by NGS. This report not only describes a new type of variant causing LQTS but also highlights current limitations in the use of short NGS reads for diagnosis of genetic diseases.

MATERIALS AND METHODS

Patient Enrollment: This study was reviewed and approved by the Institutional Review Board at Vanderbilt University Medical Center (Nashville, TN). All participants provided written informed consent.

Genomic DNA Acquisition: After informed consent, DNA was extracted from peripheral blood using Puregene Chemistry on the Autopure LS robotic system according to manufacturer's recommendations (Qiagen, product number 9001340).

GeneDx Next-generation Sequencing: Using genomic DNA from the submitted specimen, the coding regions and splice junctions of 12 arrhythmia-associated genes were enriched using a proprietary targeted capture system developed by GeneDx (Gaithersburg, Maryland). These targeted regions (read length ~50 bp) were sequenced simultaneously by massively parallel (NextGen) sequencing on an Illumina platform with paired-end reads. Bi-directional sequence was assembled, aligned to reference gene sequences based on human genome build GRCh37/UCSC hg19, and analyzed for sequence variants. Capillary sequencing was used to confirm all potentially pathogenic variants and to obtain sequence for regions where fewer than 15 reads were achieved by NextGen sequencing.

GeneDx Exon Array Evaluation: Concurrent deletion/duplication testing was performed for the genes in the panel using exon-level oligo array CGH (ExonArrayDx). Data analysis was performed using gene-specific filtering. Probe sequences and locations were based on human

genome build GRCh37/UCSC hg19. Sequence and array CGH alterations were reported according to the Human Genome Variation Society (HGVS) or International System for Human Cytogenetic Nomenclature (ISCN) guidelines, respectively.

***KCNQ1* Sanger Sequencing Evaluation**: Amplicons of each exon of *KCNQ1* were generated by RT-PCR using the primer sets listed in table 2. The amplification was performed using Applied Biosystems Veriti 96-well thermal cycler with a melting temperature of 95^{o}C, annealing temp listed next to each primer set in table S1, and extended at 72^{o}C. Each reaction used 30 cycles for amplification.

***KCNQ1* Allele-specific Analysis**: PCR amplicons were placed in an expression vector using polyA cloning according to manufacturer's protocol (Promega, catalog # A1360). DH5α competent E. coli were transformed and 10 individual clones were expanded for plasmid isolation and subsequent Sanger sequencing.

RESULTS

Case Report

A 47 year old female with a history of congenital deafness and severe QT prolongation was referred for management. She had her first episode of syncope at 6 years of age, was reported to have marked QT prolongation, and was placed on beta-blocker therapy at that time. Shortly thereafter, she was lost to follow-up. She had no siblings and further family history was not available. At age 40, she had an episode of syncope while working outdoors in the heat, and beta-blocker (propranolol at that time) was continued although she admitted to incomplete compliance due to fatigue. At age 46, she had another syncopal episode. She was switched to metoprolol 100 mg daily and referred for further evaluation. Her baseline ECG (**Fig 8A**) showed broad symmetric T waves with a rate-corrected QT (QTc) of 580 msec (normal <480), and a Holter monitor showed QT intervals after an ectopic atrial beat as long as 800 msec (**Fig 8B**). An implantable cardioverter-defibrillator was recommended but she declined. An exercise test was performed to assess the adequacy of beta-blockade. At a heart rate of 101 at 5 minutes, 50 seconds of exercise on a standard Bruce Protocol, she developed marked T wave lability followed by a 40-second, self-terminating episode of torsades de pointes, during which she transiently lost consciousness (**Fig 9A-F**).

Causative Mutation Identification

Proband DNA was submitted for commercial (GeneDx Inc, Gaithersburg, Maryland) next-generation sequencing (NGS). A single heterozygous nonsense variant (R518X) was identified in exon 12 of *KCNQ1*, and array testing revealed no large deletions or insertions in the

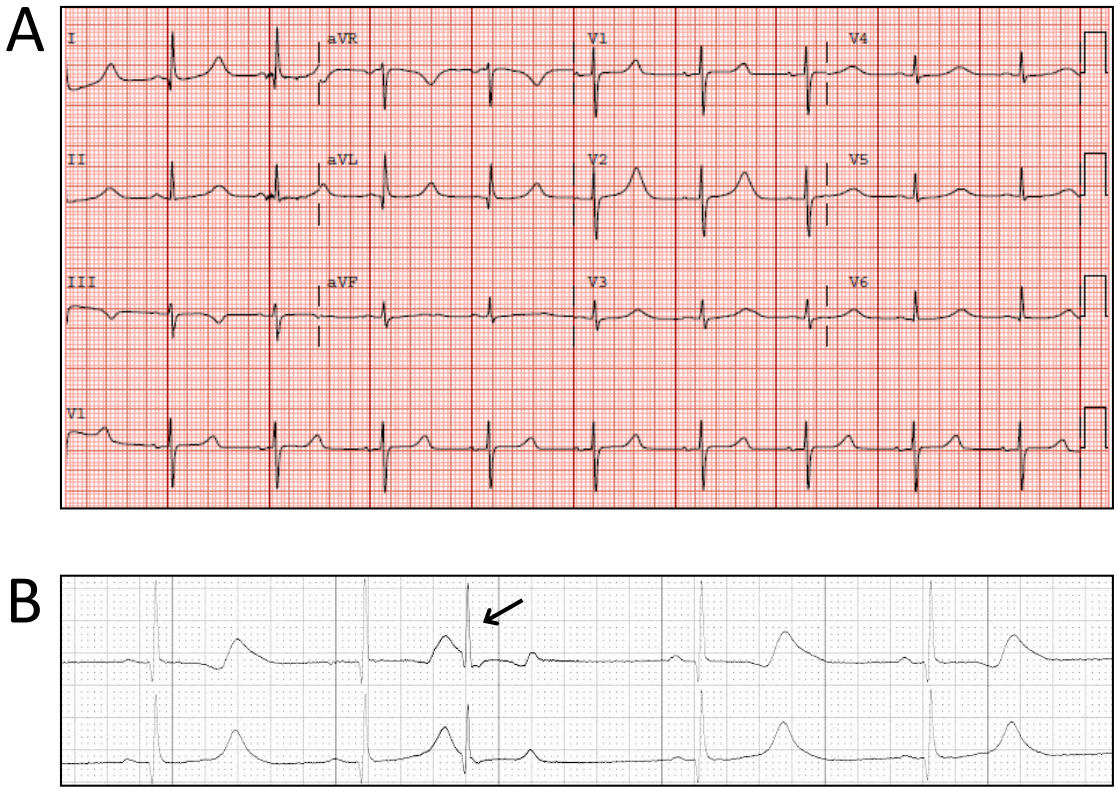

Figure 8. Marked QT prolongation at baseline. (A) Resting 12-lead ECG showed a baseline QT interval of 600msec (QTc 580msec). **(B)** Holter monitoring revealed a QT interval of 800msec on a post-PAC complex (indicated by black arrow). PAC: premature atrial contraction.

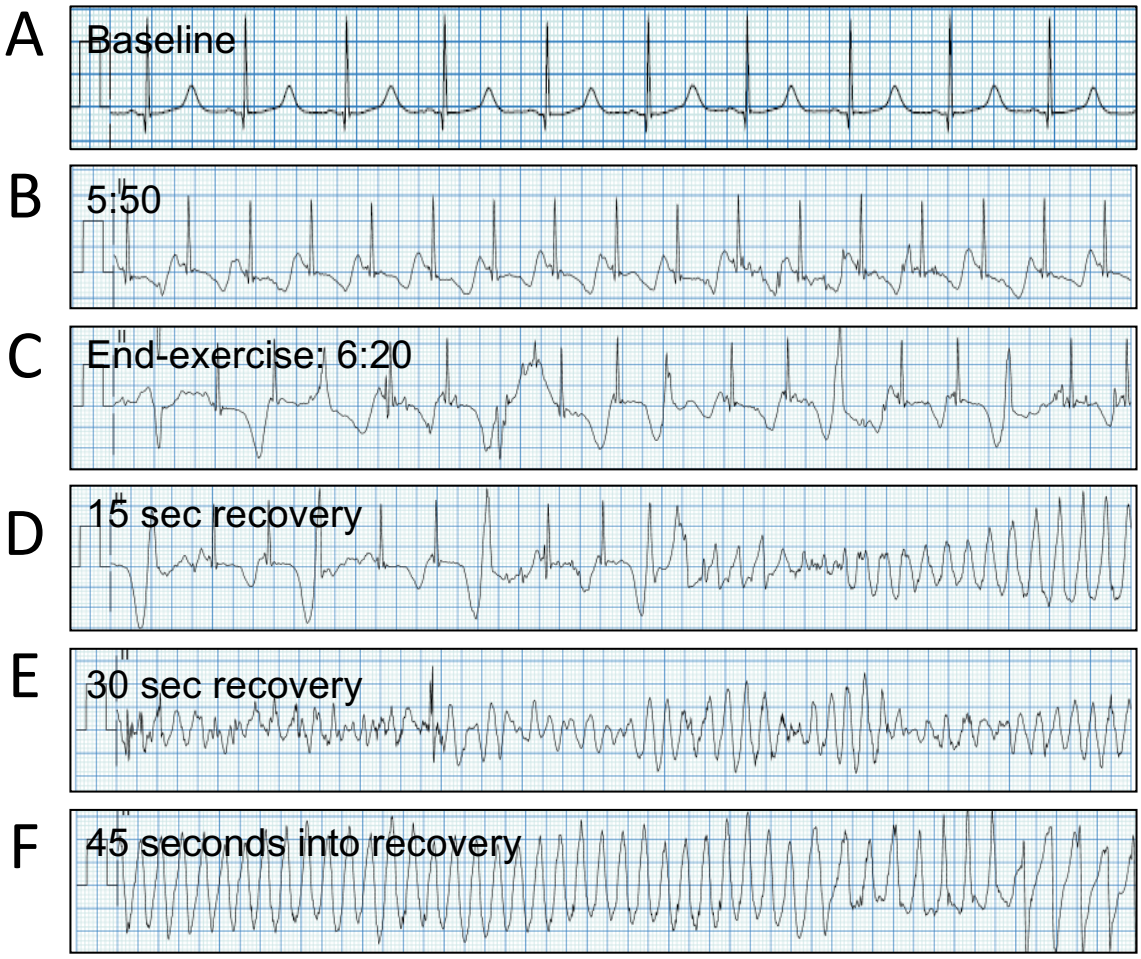

Figure 9. Exercise stress test. (**A**) Pre-exercise rhythm strip showed normal sinus rhythm with broad, symmetric T waves with corrected QT interval (QTc) 580 msec. (**B**) At 5 minutes, 50 seconds of exercise, the ECG exhibited a heart rate of 101 bpm with biphasic T waves and corrected QT interval (QTc) 908 msec. (**C**) Thirty seconds later, the patient felt lightheaded, and exercise was stopped. The ECG showed deep T wave inversions with periodic T wave accentuation (in a non-alternans fashion) and ventricular trigeminy. Torsades de Pointes then developed (**D**), persisting for 40 seconds (**E**) before self-terminating (**F**).

gene. KCNQ1-R518X has been reported in LQTS previously, and functional testing has shown absent potassium current when KCNQ1-R518X is expressed in oocytes.[186] The clinical picture of severe QT prolongation and torsades de pointes, onset at an early age, and congenital deafness, strongly suggested that a second *KCNQ1* variant was present but undetected by NGS. To test this hypothesis, we performed PCR amplification of each exon and approximately 50 base pairs (bp) of flanking intronic sequence for Sanger sequencing analysis (primer sets are presented in **Table 2**). Sanger sequencing of exon 12 confirmed the heterozygous nonsense variant R518X in the JLNS proband (**Fig 10A**), and analysis of parental DNA showed the R518X allele was paternally inherited. PCR amplification of exon 15 in the proband produced two products, one at the anticipated size of 500 bp and a second larger product, ~550 bp (**Fig 10B**). Sequencing of the 500 bp product showed no variation compared to the reference sequence (NM_000218; **Fig 10C**). Sequencing of the larger product identified a frame-shifting 52-bp insertion comprised of a partial duplication of the 5' end of exon 15 and an insertion of 36 adenines followed by uninterrupted exon 15 sequence (**Fig 10D**). The indel is predicted to change the coding sequence beginning at amino acid 583 with a truncation occurring after amino acid 667 (**Fig 11**). The unique 52-bp insertion was a *de novo* event as targeted sequencing of exon 15 in parental DNA did not detect the insertion. There were no indels or non-synonymous SNPs identified in exons 1-4, 6-14, and 16. Parental relationships were confirmed by genetic fingerprinting.

The Two *KCNQ1* Variants are Located in Trans

For the two identified mutations to be the genetic cause of JLNS in this patient, the two variants must be located in trans (on separate alleles) to one another. Since R518X was located on the paternal allele and the 52-bp insertion was a *de novo* event, we sought to establish that the insertion was on the maternal allele. To test this idea, we used common SNVs (rs163149,

Table 2. KCNQ1 primers used for Sanger sequencing

Exon	Primer direction	5' -> 3' sequence	Annealing temperature (^{o}C)
1	Forward	TCGCCTTCGCTGCAGCTC	60
	Reverse	TCCCCCACACCAGCTCTCAG	
2	Forward	ATGGGCAGAGGCCGTGATGCTGAC	60
	Reverse	ATCCAGCCATGCCCTCAGATGC	
3	Forward	GTTCAAACAGGTTGCAGGGTCTGA	62
	Reverse	CTTCCTGGTCTGGAAACCTGG	
4	Forward	CCCTTCCCCAGACGAGAGCA	58
	Reverse	CTCCACCCATCCCAGCACAT	
5	Forward	TCTGGGGACTGAGGGAATCTGGAGGTA	60
	Reverse	CCGGGTCCTTGATTTGCCTGGGTTTTT	
6	Forward	TCGCTGGGACTCGCTGCCTT	64
	Reverse	TGTCCTGCCCACTCCTCAGCCT	
7	Forward	TGGCTGACCACTGTCCCTCT	60
	Reverse	CCCCAGGACCCCAGCTGTCCAA	
8	Forward	GCTGGCAGTGGCCTGTGTGGA	58
	Reverse	AACAGTGACCAAAATGACAGTGAC	
9	Forward	TGGCTCAGCAGGTGACAGC	58
	Reverse	TGGTGGCAGGTGGGCTACT	

Table 2 continued. KCNQ1 primers used for Sanger sequencing.

10	Forward	GCCTGGCAGACGATGTCCA	58
	Reverse	CAACTGCCTGAGGGGTTCT	
11	Forward	CTGTCCCCACACTTTCTCCT	60
	Reverse	TGAGCTCCAGTCCCCTCCAG	
12	Forward	TGGCCACTCACAATCTCCT	58
	Reverse	GCCTTGACACCCTCCACTA	
13	Forward	GGCACAGGGAGGAGAAGTG	60
	Reverse	CGGCACCGCTGATCATGCA	
14	Forward	CGGGCACGTCAAGCTGTCTGTC	58
	Reverse	CTCCCCTTACTCCCTGGCTTTCA	
15	Forward	GGCCCTGATTTGGGTGTTTTA	58
	Reverse	CACAGGGAGGTGCCTGCT	
16	Forward	CGACCGAGGGCCTTGCAGACATAG	60
	Reverse	CCCCCACACCGGCCAGGAAGAGG	

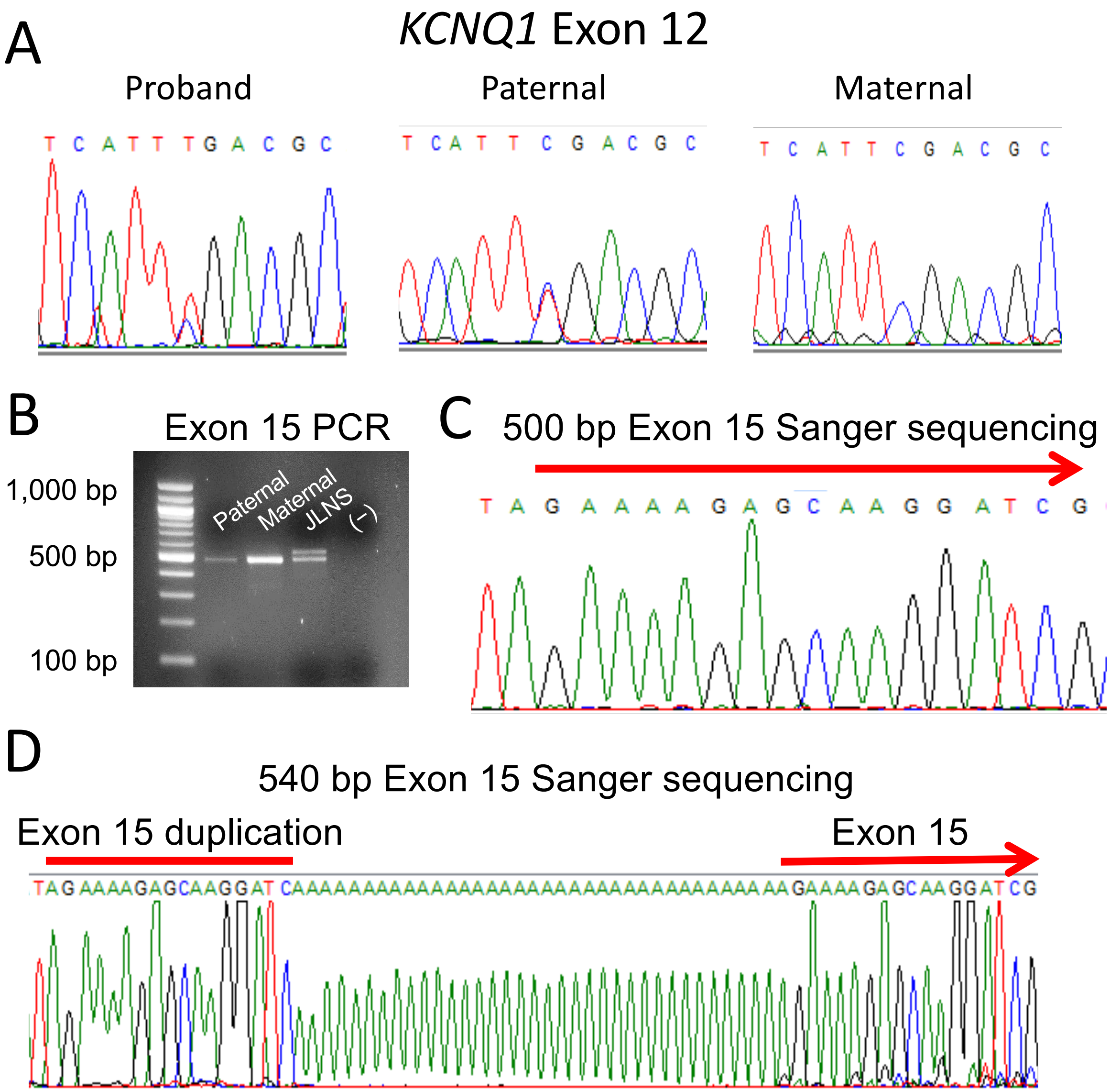

Figure 10. Compound heterozygous variation in KCNQ1 identified by Sanger sequencing. **(A)** *KCNQ1* p.R518X is present in exon 12 of proband and paternal DNA and is absent in maternal DNA. (**B**) PCR amplification of exon 15 visualized with ethidium bromide results in two distinct products in the proband that is absent in parental DNA. **(C)** Allele specific Sanger sequencing of smaller product, which shows normal (reference) sequence. **(D)** Allele-specific Sanger sequencing of larger PCR product identifies a 52-bp insertion comprised of a 15-bp partial duplication of exon 15 and insertion of a 36-adenine tract.

```
1   MAAASSPPRA ERKRWGWGRL PGARRGSAGL AKKCPFSLEL AEGGPAGGAL YAPIAPGAPG
    MAAASSPPRA ERKRWGWGRL PGARRGSAGL AKKCPFSLEL AEGGPAGGAL YAPIAPGAPG

61  PAPPASPAAP AAPPVASDLG PRPPVSLDPR VSIYSTRRPV LARTHVQGRV YNFLERPTGW
    PAPPASPAAP AAPPVASDLG PRPPVSLDPR VSIYSTRRPV LARTHVQGRV YNFLERPTGW

121 KCFVYHFAVF LIVLVCLIFS VLSTIEQYAA LATGTLFWME IVLVVFFGTE YVVRLWSAGC
    KCFVYHFAVF LIVLVCLIFS VLSTIEQYAA LATGTLFWME IVLVVFFGTE YVVRLWSAGC

181 RSKYVGLWGR LRFARKPISI IDLIVVVASM VVLCVGSKGQ VFATSAIRGI RFLQILRMLH
    RSKYVGLWGR LRFARKPISI IDLIVVVASM VVLCVGSKGQ VFATSAIRGI RFLQILRMLH

241 VDRQGGTWRL LGSVVFIHRQ ELITTLYIGF LGLIFSSYFV YLAEKDAVNE SGRVEFGSYA
    VDRQGGTWRL LGSVVFIHRQ ELITTLYIGF LGLIFSSYFV YLAEKDAVNE SGRVEFGSYA

301 DALWWGVVTV TTIGYGDKVP QTWVGKTIAS CFSVFAISFF ALPAGILGSG FALKVQQKQR
    DALWWGVVTV TTIGYGDKVP QTWVGKTIAS CFSVFAISFF ALPAGILGSG FALKVQQKQR

361 QKHFNRQIPA AASLIQTAWR CYAAENPDSS TWKIYIRKAP RSHTLLSPSP KPKKSVVVKK
    QKHFNRQIPA AASLIQTAWR CYAAENPDSS TWKIYIRKAP RSHTLLSPSP KPKKSVVVKK

421 KKFKLDKDNG VTPGEKMLTV PHITCDPPEE RRLDHFSVDG YDSSVRKSPT LLEVSMPHFM
    KKFKLDKDNG VTPGEKMLTV PHITCDPPEE RRLDHFSVDG YDSSVRKSPT LLEVSMPHFM

481 RTNSFAEDLD LEGETLLTPI THISQLREHH RATIKVIRRM QYFVAKKKFQ QARKPYDVRD
    RTNSFAEDLD LEGETLLTPI THISQLREHH RATIKVIRRM QYFVAKKKFQ QARKPYDVRD

541 VIEQYSQGHL NLMVRIKELQ RRLDQSIGKP SLFISVSEKS KDRGSNTIGA RLNRVEDKVT
    VIEQYSQGHL NLMVRIKELQ RRLDQSIGKP SLFISVSEKS KDQKKKKKKK KKKKRKEQGS

601 QLDQRLALIT DMLHQLLSLH GGSTPGSGGP PREGGAHITQ PCGSGGSVDP ELFLPSNTLP
    RQQHDRRPPE PSRRQGDAAG PEAGTHHRHA SPAALLARWQ HPRQRRPPQR GRGPHHPALR

661 TYEQLTVPRR GPDEGS
    QWRLRRP
```

Figure 11. Predicted KCNQ1 amino acid sequence resulting from frameshifting exon 15 insertion. Black text indicates the wild-type KCNQ1 amino acid sequence. Red text indicates insertion sequence. Underlined text highlights the amino acid changes resulting from the frameshifting insertion.

rs163150, and rs1057128; **Fig 12**) located within 2,500 nucleotides upstream of exon 15 at which the father's genotype was homozygous for the reference allele and the genotype in the mother and the proband were heterozygous for the SNVs (**Fig 13A** and **Table 3**). Allele-specific sequencing demonstrated that the maternal common CNVs were on the same allele as the duplication/insertion (**Fig 13B** rs163149 shown as an example). Thus, the proband inherited the variant encoding KCNQ1-R518X from the father and the poly(A) insertion-partial exon 15 duplication is a *de novo* event that occurred on the maternally-inherited allele (**Fig 13C**).

Re-evaluation of NGS Data

After we identified the unique 52-bp insertion, the original reads were re-examined at GeneDx. During the original assessment using 50-bp reads and repeat attempts using 2X100-bp reads, a small number of reads that contained the poly-adenine signal at the 5' or 3' edge (meaning only one copy of 5' exon 15 sequence) mapped to the reference sequence. Intermediate-sized indels are known to be challenging to identify by NGS.[184] There was a drop-off in read depth at the insertion site, supporting the idea that the algorithm analyzing the NGS clipped and then discarded reads containing the insertion near their center due to misalignment with the reference sequence. When the 52-bp duplication-insertion was included in a modified reference sequence, the insertion-containing variant reads mapped with high confidence to the modified reference while reads from the paternal allele failed to map leading to a drop off in read depth (**Fig 14**).

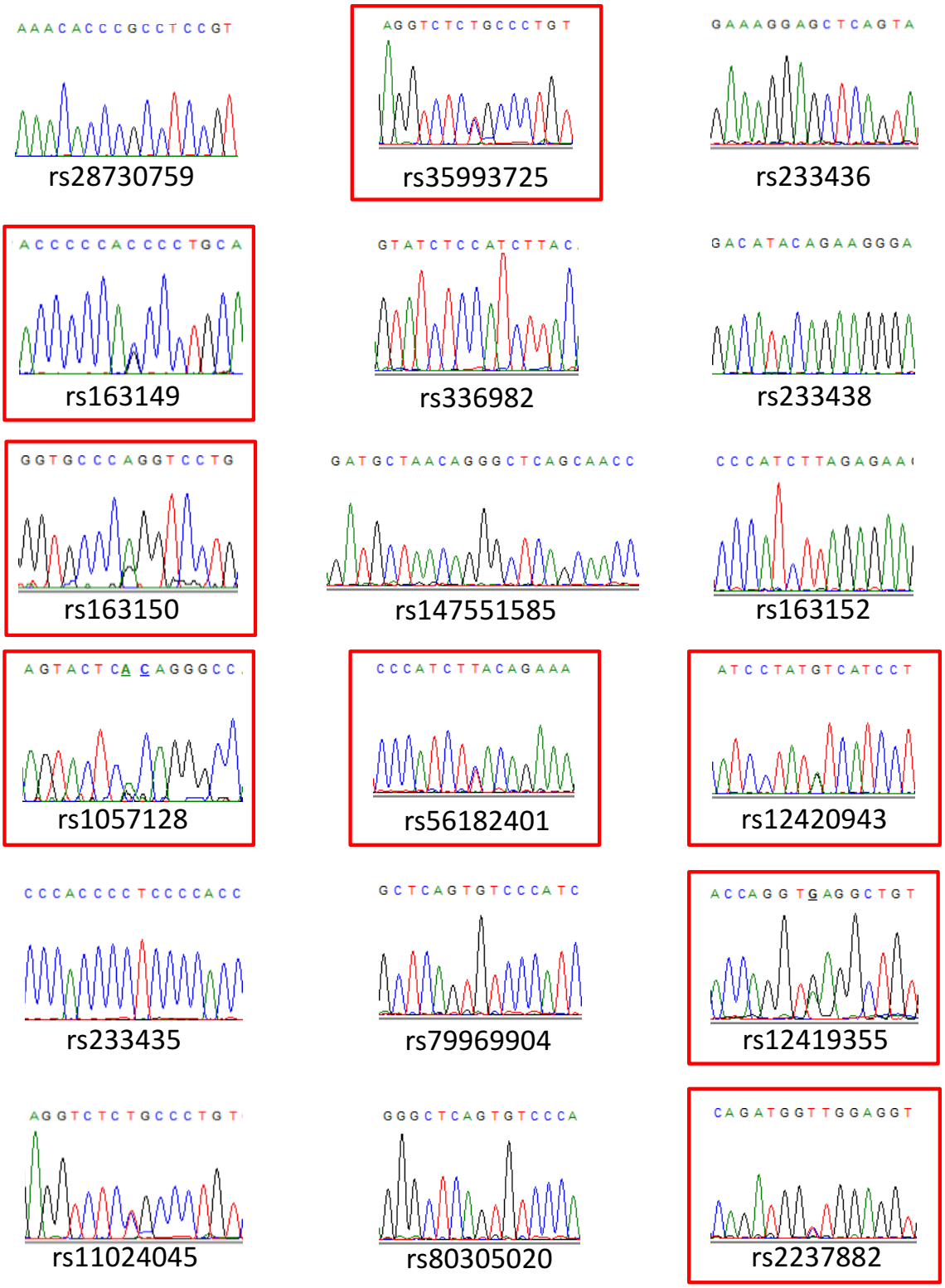

Figure 12. Screening of the proband for common SNVs located between exons 12 and 15. Sanger sequencing results for SNVs with a MAF >10%. Red boxes indicate CNVs found to be heterozygous in the proband.

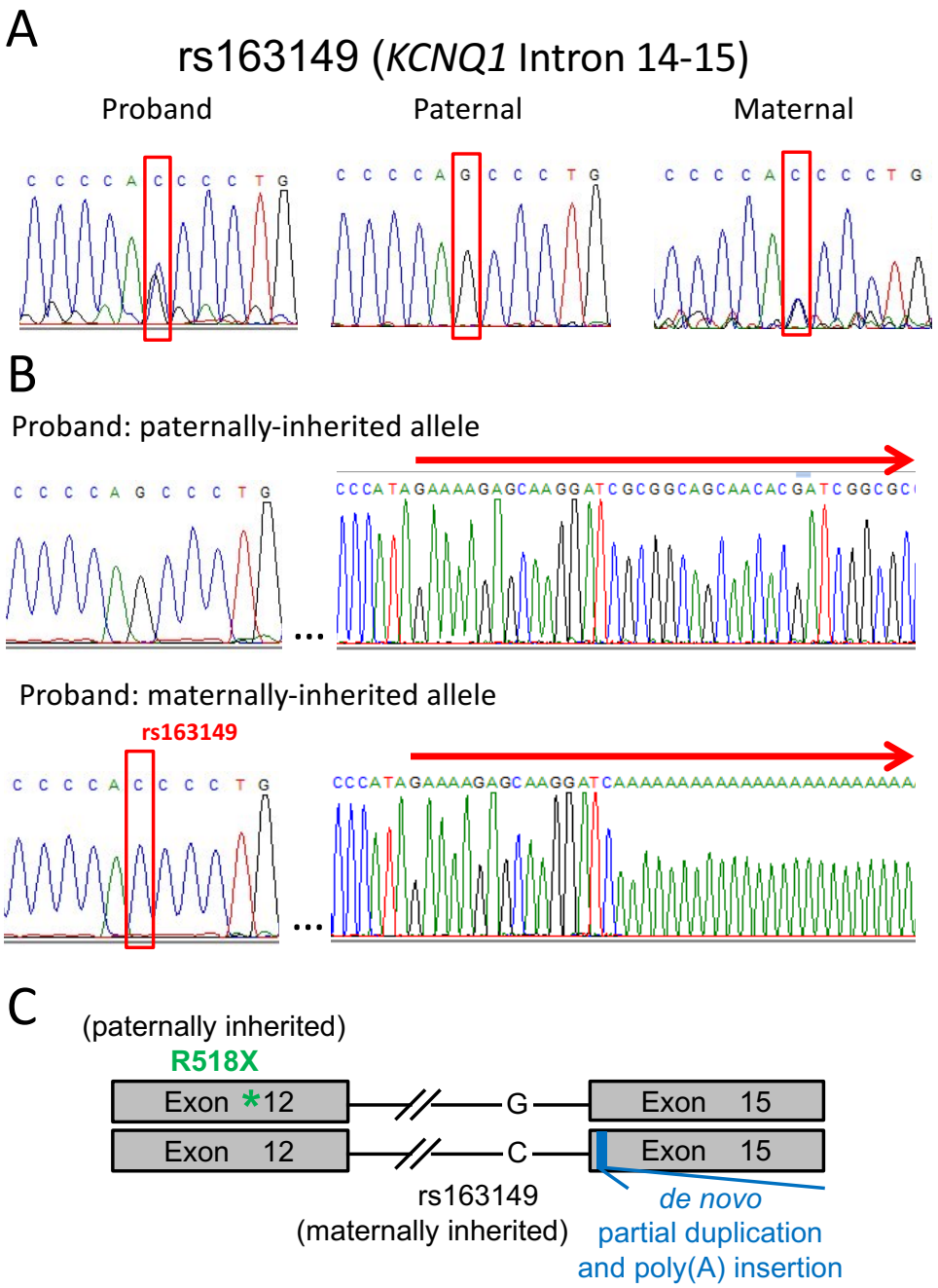

Figure 13. Compound heterozygous variants in *KCNQ1* located on separate alleles.
(**A**) Proband and maternal DNA possess common SNV rs163149 located 1,772 bp upstream of exon 15. PCR amplification was performed using Roche expand long template PCR system with forward primer 5'-CGTGTCTTTTTGTCCCGCAG-3' and reverse primer 5'-CACAGGGAGGTGCCTGCT -3' (**B**) Allele specific sequencing demonstrates the *de novo* insertion is present on the maternally inherited allele. (**C**) Schematic representation of the compound heterozygous variants being located in trans to one another. SNV: single nucleotide variant.

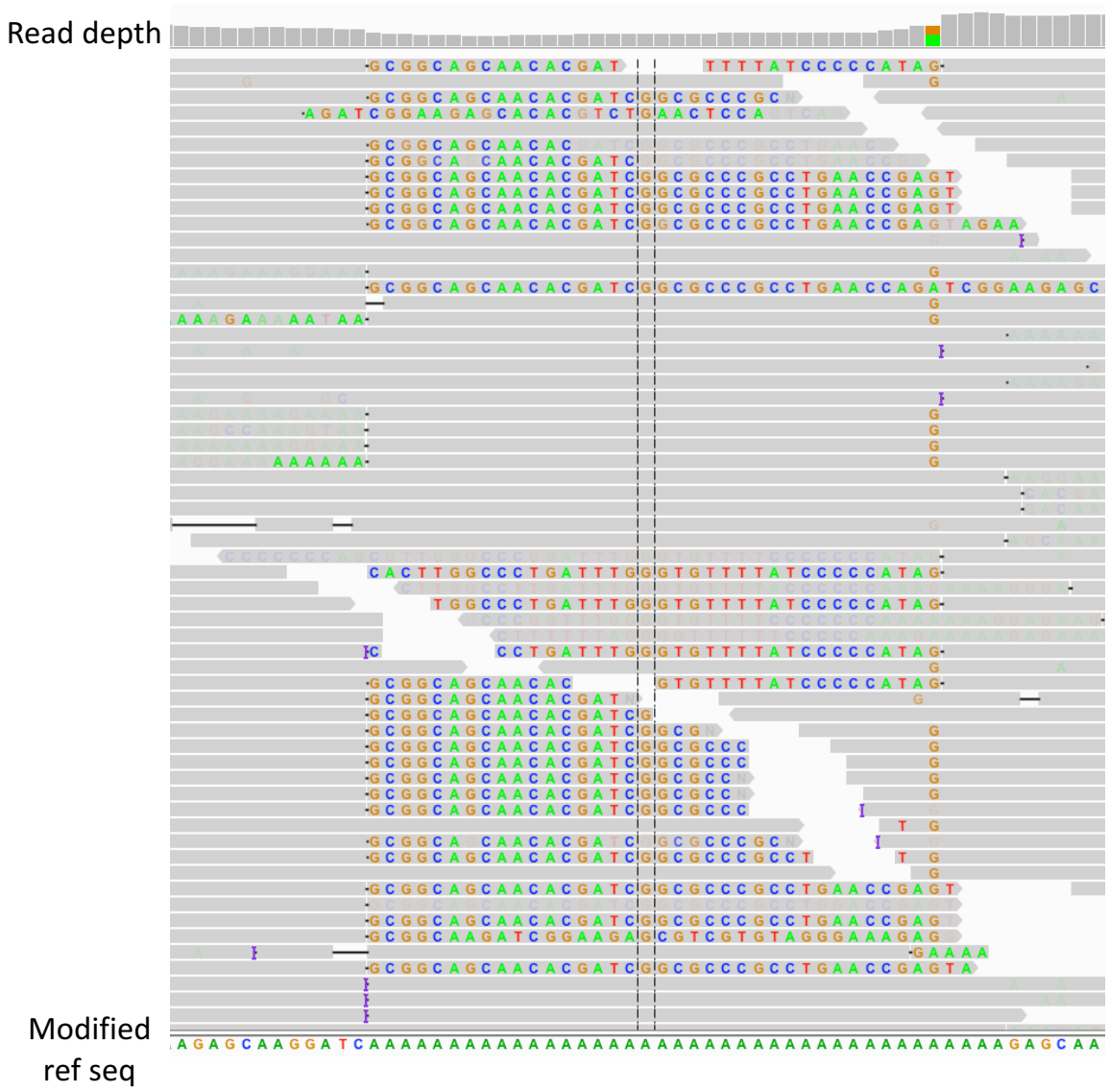

Figure 14. Next generating sequencing confirms complex 52-bp insertion by ad hoc alignment. Alignment of the next generation sequencing reads to a reference sequence modified to include the identified insertion (modified ref seq) confirms its presence. Grey horizontal bars indicate perfect sequence alignment. Note the decrease in read depth (top) at the insertion site, consistent with the rejection of reads that include the paternal allele.

Table 3. Common SNVs in *KCNQ1* used to determine maternally-inherited allele.

SNP rs#	position GRCh38	Reference Allele	Alternate Allele	MAF	Genotype		
					Proband	Maternal	Paternal
rs163149	11:2776200	C	G	0.459	C/G	C/G	G/G
rs163150	11:2776090	G	A	0.333	G/A	G/A	A/A
rs1057128	11:2776007	G	A	0.200	G/A	G/A	A/A

MAF = minor allele frequency.

DISCUSSION

We report here compound heterozygous variants in *KCNQ1* resulting in a severe clinical presentation of JLNS with exercise-induced arrhythmias despite beta-blocker therapy. Next-generation sequencing identified a previously reported LQT1-associated *KCNQ1* mutation (R518X) but failed to recognize an unusual and complex 52-bp duplication-insertion.[187] This type of variant has not been previously reported in LQTS. While NGS is currently the most commonly used method for genetic diagnosis in this disease, initial studies for 15+ years after the first disease genes were identified in 1995 did not report this type of variant, either because it is rare or not recognized in conventional testing.

JLNS is a severe autosomal recessive form of long QT syndrome that has the additional clinical feature of congenital sensorineural deafness, thought to arise because of altered endolymph maintenance in the developing cochlea. This results in collapse of Reissner's membrane, a critical cochlear structure, and loss of hair cells.[188] JLNS has only two known genetic associations, compound heterozygous or homozygous variation in *KCNQ1* (JLNS1) or *KCNE1* (JLNS2) resulting in near-total loss of I_{Ks}. Patients with JLNS typically have a markedly prolonged QT interval and have a high incidence of sudden cardiac death in childhood.[189] Cardiac events in JLNS, like LQT1, arise during times of sympathetic activation such as exercise or emotional stress.[190]

There are several especially unusual features in this case. First, the patient exhibited marked T wave instability but in a trigeminal and then a non-alternans fashion during exercise. This less common variant of T wave instability has been described previously as an unusual manifestation of LQTS thought to reflect temporal variability in repolarization with sympathetic

activation.[189,191,192] Another unusual feature is that the patient has survived to age 47 with only intermittent medical therapy and without experiencing sudden death. While her survival could be attributed to a milder phenotype of disease, the extremely long QT intervals and T wave instability during exercise would seem to contradict this.

Missense variants account for the majority of LQTS1 genetic associations but pathogenicity may be difficult to predict.[191,192] In heterologous expression systems, KCNQ1-R518X is a complete loss of function variant that does not traffic to the membrane and is trapped in the ER.[186,193] Additionally, like other variants that result in a truncated C-terminus, R518X does not interact with wild-type KCNQ1, consistent with the non-dominant effect of this mutant protein.[190] These truncating variants terminate the protein prior to a proposed coil-coil domain in the C-terminus; evidence that this domain mediates assembly and cell surface expression includes extensive mutagenesis experiments[194] and the inability of KCNQ1-R594Q to interact with wild-type protein.[195,196] The same mechanism is speculated to occur in frameshifting variants, such as the novel 52-bp insertion identified in this report and a previously reported 1008delC.[195,197]

The severe clinical features of this case provided robust evidence for the diagnosis; having identified a single variant in *KCNQ1* (R518X), we performed additional genetic evaluation to find what we were convinced was a second variant in *KCNQ1*. Genetic testing in cases with clear LQTS identifies a likely causative variant in 80% of cases.[34] In LQT1 single nucleotide variants, short indels, and large deletions (exonic or larger) have all been described.[198,199] It is possible that a portion of the remaining 20% of cases without known genetic causes could result from intermediate sized indels like the one described here. Alternatively,

undiscovered JLNS-associated genes or deep intronic or regulatory variants that disrupt KCNQ1 expression or transcript processing may also contribute.

Clinical re-sequencing in LQTS has turned increasingly toward NGS approaches to aid in diagnostics and patient/family counseling. NGS has evolved as a low cost, efficient method to generate data on a large number of genes in parallel to screen a targeted panel of arrhythmia susceptibility genes in patients diagnosed with LQTS. The current NGS algorithms align short reads to a reference sequence and have successfully identified SNVs, copy number variants, and large exonic deletions in LQT1.[199] Algorithms have been designed to better detect indels in NGS data sets by utilizing split read and dropped read depth signatures. These approaches have a validation rate between 56-80% of indels reported in the 1,000 genomes project.[183,200-202] While there is a low false negative rate in most approaches, there is discordance between algorithms suggesting a high false positive rate.[182,184,203] Speaking specifically to the insertion identified in this study, it is likely that the 15-bp duplication complicated indel detection by NGS alignment approaches that allow for split read alignment such as PINDEL and PRISM.[200,204] In addition to improvements to NGS analysis algorithms, increasing read length beyond the current 2X100 approach is another method that may increase the sensitivity of detection for intermediate-sized indels. Inclusion of a drop in read depth as an indel signature used by the program inGAP-sv is not an approach commonly utilized due to false discovery resulting from poor quality of read amplicon generation.[205] *De novo* sequence assembly can be generated and subsequently compared to a reference sequence as a complement to mapping based approaches to improve indel detection.

The partial duplication and poly(A) insertion is an unusual *de novo* variant. The poly(A) portion on this variant could result from DNA polymerase slippage.[206] However, we consider

DNA polymerase slippage unlikely to be the mechanism of the insertion identified because it cannot account for the partial duplication. Rather, this variant is most likely a 5'-truncated Alu element. Insertions of these short interspersed elements (SINEs) result from DNA nicking by L1 endonuclease activity at defined target sequences that opens the genome for insertion of an RNA intermediate Alu element, a poly(A) insertion, and a DNA target site duplication (TSD).[207] The duplicated portion of exon 15 in *KCNQ1* contains a 5' GAAAAG target sequence making it likely to be the resultant TSD.[208] Approximately 85% of Alu elements found in the human genome are full length containing the ~290 bps encoding the Alu plus a variable length poly(A) tail.[209] Significantly truncated versions of Alu elements have been observed throughout the genome and comprise ~8% of Alu elements identified.[209,210] Truncation of the Alu can result from microdomain-mediated end joining (MMEJ) where the Alu RNA sequence can align with the 3' overhang of the cut genomic DNA.[210] The 3' end of the TSD in this case has a microdomain of TC, the terminal 3' nucleotides of all five modern human Alu subfamilies.[211] The single stranded template is then filled by DNA polymerases and joined by DNA ligase as part of a DNA repair process.

Alu elements have been implicated in other diseases through inducing large deletions, misregulating transcription when inserted in introns, or disrupting the coding sequence when inserted within exons.[212] The first described *de novo* Alu element insertion resulting in disease was described in *NF1* in 1998 causing neurofibromatosis.[213] Since then more than 36 identified diseases have been associated with Alu element-mediated variation due to a multitude of mechanisms.[214] In 2007, two families affected by cystic fibrosis with no identified variation in *CFTR* were found to contain considerably truncated Alu elements located within the gene.[210] *NF1* appears to be an Alu insert hotspot as 18 additional cases of neurofibromatosis have been

explained by Alu element insertions, including one proposed 5'-truncated element comprised of a 120-bp poly(T) flanked by TSDs, very similar to the insertion we identified.[215] This is the first report of Alu element insertion in an ion channel gene associated with a cardiac arrhythmia susceptibility syndrome.

CONCLUSION

This chapter highlights that current NGS approaches to variant identification is limited for complex insertions. Approaches that provide precise and sensitive interrogation of the genome are a necessity as molecular diagnostics increasingly influence clinical practice. Algorithms that specifically search for Alu elements, such as Mobster, could be run in patients in which genetic evaluation has returned "no variants identified."[216] Additionally, methods to identify intermediate-sized indels, such as Sanger sequencing or *de novo* construction of an individual's genetic code, should be included when the clinical picture strongly implicates known disease-associated genes. Further, complex insertions like the truncated Alu element described here may comprise a portion of LQT1 cases.

CHAPTER III

DE NOVO KCNB1 VARIANTS IN EPILEPTIC ENCEPHALOPATHY*

ABSTRACT

Background: Numerous studies have demonstrated increased load of *de novo* copy number variants (CNVs) or single nucleotide variants (SNVs) in individuals with neurodevelopmental disorders, including epileptic encephalopathies, intellectual disability and autism.

Materials and Methods: We searched for *de novo* mutations in a family quartet with a sporadic case of epileptic encephalopathy with no known etiology to determine the underlying cause using high coverage whole exome sequencing (WES) and lower coverage whole genome sequencing (WGS). Mutations in additional patients were identified by WES. The effect of mutations on protein function was assessed in a heterologous expression system.

Results: We identified a *de novo* missense mutation in *KCNB1* that encodes the $K_V2.1$ voltage-gated potassium channel. Functional studies demonstrated a deleterious effect of the mutation on $K_V2.1$ function leading to a loss of ion selectivity and gain of a depolarizing inward cation conductance. Subsequently, we identified two additional patients with epileptic encephalopathy and *de novo KCNB1* missense mutations that cause a similar pattern of $K_V2.1$ dysfunction.

* Modified from Torkamani, Bersell, and Jorge et. al. Annals of Neurology. (2014).

Conclusion: Our genetic and functional evidence demonstrate that *KCNB1* mutation can result in early onset epileptic encephalopathy. This expands the locus heterogeneity associated with epileptic encephalopathies and suggests that clinical WES may be useful for diagnosis of epileptic encephalopathies of unknown etiology.

INTRODUCTION

Epileptic encephalopathies are a heterogeneous group of severe childhood-onset epilepsies characterized by refractory seizures, neurodevelopmental impairment, and poor prognosis.[217] The developmental trajectory is normal prior to seizure onset, after which cognitive and motor delays become apparent. Ongoing epileptiform activity adversely affects development and contributes to functional decline. Therefore, early diagnosis and intervention may improve long term outcomes.[218-220]

Recently, there has been significant progress in identifying genes responsible for epileptic encephalopathies and *de novo* mutations have been reported in approximately a dozen genes, including *SCN1A*, *SCN2A*, *SCN8A*, *KCNQ2*, *HCN1, GABRA1*, *GABRB3*, *STXBP1*, *CDKL5*, *CHD2*, *SYNGAP1*, and *ALG13*.[221-225] The majority of mutations reported are in genes encoding voltage-gated ion channels, neurotransmitter receptors and synaptic proteins. There is significant phenotype heterogeneity, with mutations in the same gene resulting in different clinical presentations, as well as locus heterogeneity, with mutations in different genes resulting in the same syndrome. Further, epileptic encephalopathy genes have substantial overlap with genes responsible for other neurodevelopmental disorders, including autism and intellectual disability.[226-228]

Due to the considerable phenotype and locus heterogeneity, it is difficult to predict appropriate candidate genes for testing in a particular patient. Therefore hypothesis-free approaches such as whole exome sequencing (WES) or whole genome sequencing (WGS) may be useful for uncovering causative variations in epileptic encephalopathies of unknown etiology.

We aimed to identify the underlying genetic cause of epileptic encephalopathy in the proband by WES and WGS of a family quartet.

MATERIALS AND METHODS

Study Subjects. Study participants included ID9, parents ID9F and ID9M, and an unaffected sister ID9S. Adults provided written informed consent, with additional assent by ID9 and ID9S, under a protocol approved by the Scripps institutional review board. Consent for release of medical information for individual 2 was obtained from the parents. Clinical details are below and summarized in Table 7.

Individual ID9 is a 9-year-old female with epileptic encephalopathy, hypotonia, developmental delays, cognitive impairment, and intermittent agitation. Pre- and perinatal histories were unremarkable, although hypotonia and excessive somnolence were noted early. Motor milestones were delayed, with sitting at 9 months, walking at 20 months, and persistent clumsiness. Language acquisition was delayed with regression at age 18 months. Motor, language and behavior have fluctuated but overall there has been forward developmental progress. Onset of generalized tonic-clonic seizures (GTCS) was at 4·75 years of age, although behavioral manifestations likely representing other seizure types were present earlier. Multiple seizure semiologies were reported including rare GTCS, head drops, and more common facial twitching with drooling, eye fluttering, gagging, vomiting and stiffening. Rare GTCS are controlled with levetiracetam and clonazepam, but other seizure types have been poorly controlled with multiple therapies that were ineffective or limited by side effects (**Table 7**). In addition, the patient experiences sumatriptan-responsive migrainous episodes consisting of headache, abdominal discomfort, photophobia and lethargy.

Brain MRI showed subtle asymmetric volume loss in left hippocampus. Seven day video-EEG monitoring revealed mild diffuse slowing and abundant bi-hemispheric multifocal epileptiform discharges more prominent in right temporal and midparietal regions. Electroclinical seizures began in the left hemisphere, with two in centro-parietal areas and one without clear localization. Magnetoencephalography showed frequent epileptiform spikes during sleep (648 spikes observed over 50 minutes), with frequent trains of spikes. Source modeling showed epileptiform spike activity arising from bilateral posterior perisylvian regions. The first cluster of spikes (~55%) originated from the anterior-inferior aspect of the left parietal lobe, extending to the left superior temporal gyrus. The second cluster of spikes (~45%) originated from the right temporal-parietal junction. No propagations were observed.

Muscle biopsy showed type 1 fiber predominance with mild generalized hypertrophy. There was slight elevation of plasma guanidinoacetate 2·5 (0.3-2.1 μM) but not in the range typically associated with disease. There was mild elevation of cerebrospinal fluid (CSF) pyruvate with normal lactate [2.06 (0.5-2.2 mM)/147 (0-75 μM)]. CSF 5-methyltetrahydrofolate was mildly reduced 36 (40-128 nM). Folinic acid therapy has had unclear impact. Extensive additional work-up was normal and included: karyotype, fragile X and Angelman syndrome testing, CGH Oligo-SNP Array, mitochondrial DNA Southern blot and mitochondrial DNA sequencing, plasma acylcarnitine, CPK, uric acid, biotinidase, ammonia, Vitamin B12, folate, homocysteine, folate receptor antibodies, lymphocyte pyruvate dehydrogenase activity, urine organic acids, urine creatine and guanidinoacetate, CSF glucose, protein, amino acids, neurotransmitter metabolite levels and pterins, muscle carnitine, CoQ10, and electron transport chain complex analysis.

Individual 2 presented as a 2-yr-10-month male with poor seizure control, developmental delay, absent speech, stereotyped handwringing movements, and progressive in-turning of feet requiring orthotic support. Prenatal and perinatal histories were normal. Development plateaued at 6 months and seizures began at 8 months of age, with hypoarrythmic EEG for which he was treated with ACTH. Although seizures were resistant to conventional treatment (**Table 7**), a gluten/casein/sugar/starch-free diet begun at 2.5 years of age resulted in seizure reduction to 3/day despite marked spike activity demonstrable on EEG. At 4 years of age, seizures worsened and L-carnitine was added with subsequent amelioration. At 5 years of age, EEG was persistently abnormal with epileptiform discharges of multifocal origin including bursts of diffuse polyspikes, diffuse polyspike-wave, right temporal spike and wave, left occipital spikes and diffuse polyspike bursts lasting up to 4 minutes. Brain MRI studies at 9 months did not show structural, neuronal migration, or white matter abnormalities. He began walking at 2.5 years, and became interactive socially, though nonverbal. Extensive additional work-up was normal (**Table 7**). Genetic testing for mutations associated with *SCN1A*, *MECP2*, *CDKL5*, *FOXG1*, *ARX*, Fragile X, Pitt-Hopkins and Angelman syndromes were negative. Tests for plasma and cerebrospinal fluid (CSF) amino acid concentrations, urine organic acid levels, CSF neurotransmitter levels, lysosomal enzymes, very long chain fatty acids (VLCFA), neuronal ceroid lipofuscinosis (NCL) 1 & 2, urine sulfocysteine, congenital disorders of glycosylation (CDG), and oligo array were all normal. Clinical WES was performed by GeneDx (Gaithersburg, MD) and reported variants were confirmed by Sanger sequencing.

Individual 3 (Coriell ND27062) was ascertained by the Epilepsy Phenome/Genome Project[229] as part of a patient cohort with infantile spasms and/or Lennox-Gastaut syndrome.[5] Seizure onset

occurred during the first year of life and seizure types include tonic-clonic, atypical absence, atonic, infantile spasms and focal dyscognitive (**Table 7**). EEG findings were unspecified, while imaging studies were reported as normal.

Whole Exome, Whole Genome Sequencing, Variant Calling, and Filtration. Genomic DNA was extracted from blood using the QiaAmp system (Qiagen, Valencia, CA). Enriched exome libraries were prepared using the SureSelect XT enrichment system (Agilent, Santa Clara, CA). WES was performed on an Illumina HiSeq2500 instrument with indexed, 100-bp, paired-end sequencing. Reads were mapped to the hg19 reference genome using BWA,[230] variant calling and quality filtration was performed using GATK best practices variant quality score recalibration.[202,231,232] Mean coverage of 97 to 124-fold was achieved for each subject with 94-95% of the target exome covered by >10 reads (**Table 4**). Libraries for low-pass WGS were prepared using the NEBNext DNA Library Prep System (New England Biolabs, Ipswich, MA). WGS was performed on an Illumina HiSeq2500 with 100-bp indexed, paired-end sequencing. Mean coverage of 4 to 7-fold was achieved for each subject with ~64.3% of the genome covered by >5 reads (**Table 4**). Copy number variants (CNVs) were identified by CNVNator.[233]

Variant annotation was performed using the Scripps Genome Annotation and Distributed Variant Interpretation Server (SG-ADVISER) (http://genomics.scripps.edu/ADVISER/) as previously described.[234] A series of filters were applied to derive a set of candidate disease-causing variants (**Table 5**): (1) population-based filtration removed variants present at >1% allele frequency in the HapMap[235] or 1,000 Genomes,[236] NHLBI Exome Sequencing Project (http://evs.gs.washington.edu/EVS/), or Scripps Wellderly populations (individuals over the age of 80 with no common chronic conditions sequenced on the Complete Genomics platform); (2)

annotation-based filtration removed variants in segmental duplication regions that are prone to produce false positive variant calls due to mapping errors;[237] (3) functional impact-based filtration retained only variants that are non-synonymous, frameshift, nonsense, or affect canonical splice-site donor/acceptor sites, and (4) inheritance-based filters removed variants not present in the trio in a manner consistent with affectation status. Following filtering, retained variants were confirmed by Sanger sequencing.

Locus Specific Mutation Rate Estimate. The *KCNB1* locus specific mutation rate was determined as described.[238] Human and chimpanzee alignments of the protein coding portion of exons and intronic essential splice sites were considered. The *KCNB1* mutation rate per site is 2.71×10^{-3} differences per bp of aligned sequence. Assuming a divergence time of 12 million years between chimpanzee and human and a 25 year average generation time, the *KCNB1* locus specific mutation rate per site per generation is 5.65×10^{-9}. The probability of observing *de novo* mutation events was estimated using the Poisson distribution:

$$P(X;\ \mu) = \ [(e^{-\mu})(\mu^{X})]/X!$$

where X is the number of *de novo* events observed and μ is the average number of *de novo* events based on the locus specific mutation rate.

Plasmids and Cell Transfection. Mutations were introduced into full-length human $K_V2.1$ cDNA engineered in plasmid pIRES2-Ds-Red-MST[24] by QuikChange mutagenesis (Agilent). Wildtype human $K_V2.1$ cDNA was subcloned into the pIRES2-smGFP expression vector. Expression of wildtype and mutant $K_V2.1$ in CHO-K1 cells was achieved by transient transfection using FUGENE-6 (Roche) and 0.5 μg of total cDNA (1:1 mass ratio). Expression of

wildtype alone was achieved by transfection with pIRES2-smGFP-WT-K_V2.1 plus empty pIRES2-DsRed-MST, while expression of mutant alone was performed with pIRES2-DsRed-MST-mutant-K_V2.1 and empty pIRES2-smGFP. Co-expression of mutant and wildtype was achieved by co-transfection with pIRES2-smGFP-WT-K_V2.1 and pIRES2-DsRed-MST-mutant-K_V2.1 or pIRES2-dsRed-MST-WT-K_V2.1. Following transfection cells were incubated for 48 hours before use in experiments.

Cell Surface Biotinylation. Proteins on the surface of CHO-K1 cells transfected with wildtype and/or mutant K_V2.1 were labeled with cell membrane-impermeable Sulfo-NHS-Biotin (Thermo Scientific). Following quenching with 100 mM glycine, cells were lysed and centrifuged. Supernatant was collected and an aliquot was retained as the total protein fraction. Biotinylated surface proteins (100 µg per sample) were recovered from the remaining supernatant by incubation with streptavidin-agarose beads (ThermoScientific) and eluted in Laemmli sample buffer. Total (1 µg per lane) and surface fractions were analyzed by Western blotting using mouse anti-K_V2.1 (1:500; NeuroMab, clone K89/34), mouse anti-transferrin receptor (1:500; Invitrogen, #13-6800), rabbit anti-calnexin (H70)(1:250; Santa Cruz, sc-11397) primary antibodies, and peroxidase-conjugated mouse anti-rabbit IgG (1:100,000 Jackson ImmunoResearch) and goat anti-mouse IgG (1:50,000, Jackson ImmunoResearch) secondary antibodies. Blots were probed for each protein in succession, stripping in between with Restore Western Blot Stripping Buffer (Pierce). Western blot analysis was performed in triplicate on samples from three independent transfections. The order of anti-Kv2.1 and anti-transferrin receptor antibodies was alternated, with transferrin receptor probed first in two of three experiments. Selectivity of biotin labeling for cell surface was confirmed by probing with

calnexin following detection of $K_V2.1$ and transferrin receptor. Calnexin signal was consistently present in total protein lanes and absent in surface fraction lanes. Densitometry was performed using NIH ImageJ software. To control for protein loading, $K_V2.1$ bands were normalized to the corresponding transferrin receptor band. For each genotype, the normalized values were then expressed as a ratio of surface:total expression. Normalized total, surface and surface:total ratios were compared between genotypes using one-way ANOVA.

Electrophysiology. Whole cell patch-clamp recordings were performed as described,[239] except recording solutions were altered to achieve appropriate voltage-control. The external solution contained (in mM): 132 XCl [where X is Na^+ except when molar substitution for K^+, Rb^+ or N-methyl-D-glucamine ($NMDG^+$) is indicated in the figure], 4.8 KCl, 1.2 $MgCl_2$, 2 $CaCl_2$, 10 glucose, and 10 HEPES, pH 7.4. The internal solution contained (in mM): 20 K-aspartate, 90 NMDG-Cl, 1 $MgCl_2$, 1 $CaCl_2$, 11 EGTA, 10 HEPES, and 5 K_2ATP, pH 7·3. When cells expressing mutant channels alone or co-expressed with wildtype Kv2.1 (Kv2.1-WT) were held at -80 mV, they exhibited large currents that prevented adequate voltage control. Therefore, a holding potential of -30 mV was used for experiments. Whole cell currents were measured from -80 to +60 mV (in 10 mV, 500 msec long steps) from a holding potential of -30 mV followed by a 500 msec step to 0 mV (tail currents). Voltage-dependence of activation was evaluated from tail currents measured 10 msec after stepping to 0 mV from -40mV to +30mV and fit to the Boltzmann equation. Kinetic analysis of activation rate was performed by exponential fit of the first 50 msec of current induced after a voltage step from the holding potential.

For cation selectivity experiments, recording solutions were altered as follows: sucrose dilution was performed by adding 300 mM sucrose solution 10:1 (v/v) to the external solution

described above. For determining permeability ratios, the internal solution was modified to contain (in mM): 110 K-aspartate, 1 $MgCl_2$, 1 $CaCl_2$, 11 EGTA, 10 HEPES, and 5 K_2ATP, pH 7.3 and equimolar replacement of extracellular sodium with the monovalent cations K^+, Rb^+ and $NMDG^+$. The permeability ratio (P_X/P_{Na}) was calculated from measured reversal potentials (E_{rev}) according to the following equation:[240]

$$E_{rev} = (RT/F)\ \ln(P_x[X^+]_o / PK^+[Na^+]_i$$

where R is the gas constant, T is absolute temperature, F is Faraday's constant, X^+ is the monovalent cation in the extracellular solution, and P_X is permeability of the X^+ cation.

Data for each experimental condition were collected from ≥3 transient transfections, and analyzed and plotted using Clampfit (Molecular Devices) and Graphpad Prism5 (Graphpad Software). Currents were normalized for membrane capacitance and shown as mean ± SEM, and number of cells used for each experimental condition is listed in Table 8. Statistical significance was determined using unpaired Student's *t* test (Graphpad). *P* values are provided in the figures or figure legends.

RESULTS

Genome-wide evaluation identifies *de novo* variants in a case of epileptic encephalopathy

We employed WES (~100X coverage) and WGS (~5X coverage) of the proband (ID9), unaffected father (ID9F), unaffected mother (ID9M), and unaffected sister (ID9S) to identify the molecular cause of an epileptic encephalopathy. Filtering of WES variants was done under the assumption that disease in ID9 was the result of a heterozygous *de novo* mutation, but we also considered simple and compound recessive models. Variants discovered by WES were processed through a series of population-, variant annotation-, functional-impact-, and inheritance-based filters, to identify a set of candidate disease-causing variants (**Table 4**). Sequence coverage and detailed variant data are presented in Table 5. CNVs were also interrogated by WGS, however, no CNVs consistent with disease segregation were identified. This process identified *de novo* missense variants in 2 candidate genes, *KCNB1* and *MLST8* (**Table 5**). Under other genetic models, we identified a homozygous missense variant in *HRNBP3* and compound heterozygous variants in *NLRP1* and *BAHCC1*. Of all the identified variants, the *KCNB1* variant was deemed the most likely candidate based on the *de novo* inheritance pattern, the function of *KCNB1* and its relationship to other epilepsy genes, and the predicted deleterious consequence on protein function by multiple algorithms (**Table 6**). *KCNB1* encodes the alpha subunit of the $K_V2.1$ voltage-gated potassium channel, a delayed rectifier potassium channel that is an important regulator of neuronal excitability. The S347R variant is located in the pore domain that is necessary for ion selectivity and gating (**Fig 15**).

Table 4. **Whole exome sequencing variant filtration for individual ID9**

Variant Type	# in Family
Total Variants	101,797
Rare Variants (<1% allele frequency)	18,475
Not in Segmental Duplication	13,463
Nonsynonymous, Truncating, or Splice Site	1,053
De Novo Inheritance	2
Homozygous or Compound Heterozygous Inheritance	3

Table 5. **Whole exome and whole genome sequencing coverage**

Sample	Whole Exome Sequencing		Whole Genome Sequencing	
	Coverage (Mean)	% Target Exome with at least 10 Reads	Coverage (Mean)	% Genome Redundancy of 5 Reads
ID9 – Proband	109	94.5%	4.1	37.9%
ID9F – Father	109	94.6%	6.0	66.7%
ID9M – Mother	124	94.9%	6.9	75.2%
ID9M – Sister	97	94.2%	7.2	77.4%

Table 6. **Inheritance of validated candidate variants in individual ID9.**

Gene	ID1 Status	Amino Acid Change	WES Genotype				Predicted Consequence		
			ID9	ID9F	ID9M	ID9S	Provean	SIFT	Polyphen 2
KCNB1	*de-novo*	S347R	01	00	00	00	deleterious (-4.996)	damaging (0.003)	probably damaging (0.995)
MLST8	*de-novo*	Q302R	01	00	00	00	neutral (-2.12)	tolerated (0.203)	benign (0.114)
HRNBP3	homozygous	Y5H	11	01	01	00	deleterious (-3.54)	damaging (0.000)	benign (0.446)
NLRP1	compound heterozygous	V939M	01	00	01	01	neutral (-2.08)	damaging (0.006)	probably damaging (0.982)
		R834C	10	01	00	00	neutral (-0.46)	tolerated (0.216)	benign (0.000)
BAHCC1	compound heterozygous	A941T	01	00	01	01	neutral (-1.38)	tolerated (0.215)	benign (0.009)
		E1990K	10	01	00	00	neutral (-0.91)	tolerated (0.168)	possibly damaging (0.900)

Genotypes: 0 – reference allele, 1 – alternate allele

Additional unrelated cases with rare missense *KCNB1* variants

We identified two additional unrelated patients with epileptic encephalopathy and *de novo* missense variants in *KCNB1* discovered by WES. Individual 2 presented with a sporadic epileptic encephalopathy of unknown cause (**Table 7**). After a series of negative genetic and metabolic tests, he was referred for clinical WES. From that analysis it was determined that he had a single *de novo* missense variant in *KCNB1*. The variant G379R, located in the selectivity filter of $K_V2.1$, was predicted to be deleterious by functional impact algorithms (**Fig 15**; **Table 7**). Additional inherited variants included a heterozygous splice site mutation in the *NPC2* gene (IVS4+1 G>A) inherited from his unaffected father and a variant of unknown significance in *GRIN2A* (A1276G) inherited from his unaffected mother. Neither of these transmitted variants was thought to be causative for principal phenotypes of individual 2, although they may contribute by modifying overall expression the clinical phenotype. Inheritance of NPC type 2 is generally recessive and the clinical phenotype of individual 2 was not consistent with NPC type 2. The *GRIN2A* A1276G variant is a known SNV that was inherited from the unaffected mother and exists in the general population (0.1% MAF in European Americans). A1276G is a conservative substitution in an alternatively spliced portion of the *GRIN2A* gene at a position that does not show a high degree of evolutionary conservation and was predicted to be benign by multiple functional impact algorithms (Provean: neutral (-0.78); SIFT: tolerated (0.284; Polyphen2: benign (0.376)).

Individual 3 was recently reported as part of an epileptic encephalopathy exome sequencing study by the Epi4K consortium.[5] She presented with early-onset epileptic encephalopathy and cerebral palsy (**Table 7**). A *de novo* missense variant in *KCNB1* was reported for individual 3, with no additional *de novo* variants reported.[5] The variant T374I is

located in the pore domain of KV2.1 and was predicted to be deleterious by functional impact algorithms (**Fig 15**; **Table 7**). Given the locus-specific mutation rate of KCNB1 ($5.65x10^{-9}$ mutation rate/base/generation), the probability of identifying three independent mutations is low (P<1·1x10-13), providing statistical evidence that these variants may be pathogenic. The altered residues show a very high degree of evolutionary conservation (**Fig 15A**), with T374 and G379 being invariant through the ancestral KcsA bacterial potassium channel. Further, all three *KCNB1* variants are located in the functionally important pore domain of the $K_V2.1$ channel protein. Serine 347 is located in the pre-pore transmembrane segment and threonine 374 is located in the pore helix. Glycine 379 is part of the critical "GYG" motif that defines the potassium selectivity filter (**Fig 15A** and **15B**).

Missense variants in pore region of $K_V2.1$ alter channel function

Effects of the *KCNB1* variants on $K_V2.1$ channel function were evaluated following transient expression in CHO-K1 cells. Expression of each mutant in CHO-K1 cells resulted in total and cell surface expression similar to the wildtype channel, with no significant genotype-dependent differences in total ($F_{3,8}$=1.767, p=0.213), surface ($F_{3,8}$=0.017, p=0.997) and surface:total ($F_{3,8}$=0.266, p=0.848) expression of Kv2.1. This indicates that the mutations do not interfere with protein expression or trafficking of channels to the cell surface (**Fig 15C**). Expression of $K_V2.1$-WT resulted in large voltage-dependent potassium currents with characteristic outward rectification and late inactivation (**Fig 16B** and **16C**). In contrast, expression of each of the three mutants yielded small currents with linear current-voltage relationships (**Fig 16B** and **16C**). These aberrant currents were blocked by gadolinium (Gd^{3+}),

Table 7. Clinical features in three individuals with epileptic encephalopathy and *KCNB1* missense mutations.

Individual	Age of onset	Seizure types	Seizure control with anti-epileptics? (treatments)	Developmental Delay	Brain MRI	EEG	Other	Presumed causal variant	Amino Acid Change	Predicted Consequence: Provean (score) SIFT (score) Polyphen2 (score)
ID9	4 yrs	Tonic-clonic; Tonic; Atonic; Focal; Focal with secondary generalization	No (Topiramate, clobazam, levetiracetam, Depakote, carbamazepine, trileptal, lacosamide, clonazepam, oxcarbazepine)	Yes (motor and language)	Subtle volume loss in left hippocampus	Mild diffuse slowing and abundant bi-hemispheric multifocal epileptiform discharges	Hypotonia; Strabismus; Migraine;	Chr20: 47991056 G/T	S347R	Deleterious (-4.996) Damaging (0.003) Probably Damaging (0.995)
2	8 months	Tonic-clonic; Atonic; Focal; Infantile spasms	No (ACTH, Topiramate, Depakote, pyridoxine; ketogenic diet)	Yes (motor and language)	normal	Hypsarrhythmia; diffuse polyspikes, diffuse polyspike-wave, right temporal spike and wave, left occipital spikes and series of bursts of diffuse polyspikes	Hypotonia Strabismus; Tremulousness; Non-verbal; Stereotyped handwringing movements; In-turning of feet	Chr20: 47990962 C/T	G379R	Deleterious (-7.926) Damaging (0.000) Probably Damaging (1.000)
3 (Coriell ND27062)	0 years	Tonic-clonic; Atonic; Focal dyscognitive Atypical absence; Infantile spasms;	unknown	Yes (unspecified)	normal	unspecified	Cerebral palsy	Chr20: 47990976 G/A	T374I	Deleterious (-5.945) Damaging (0.000) Probably Damaging (0.999)

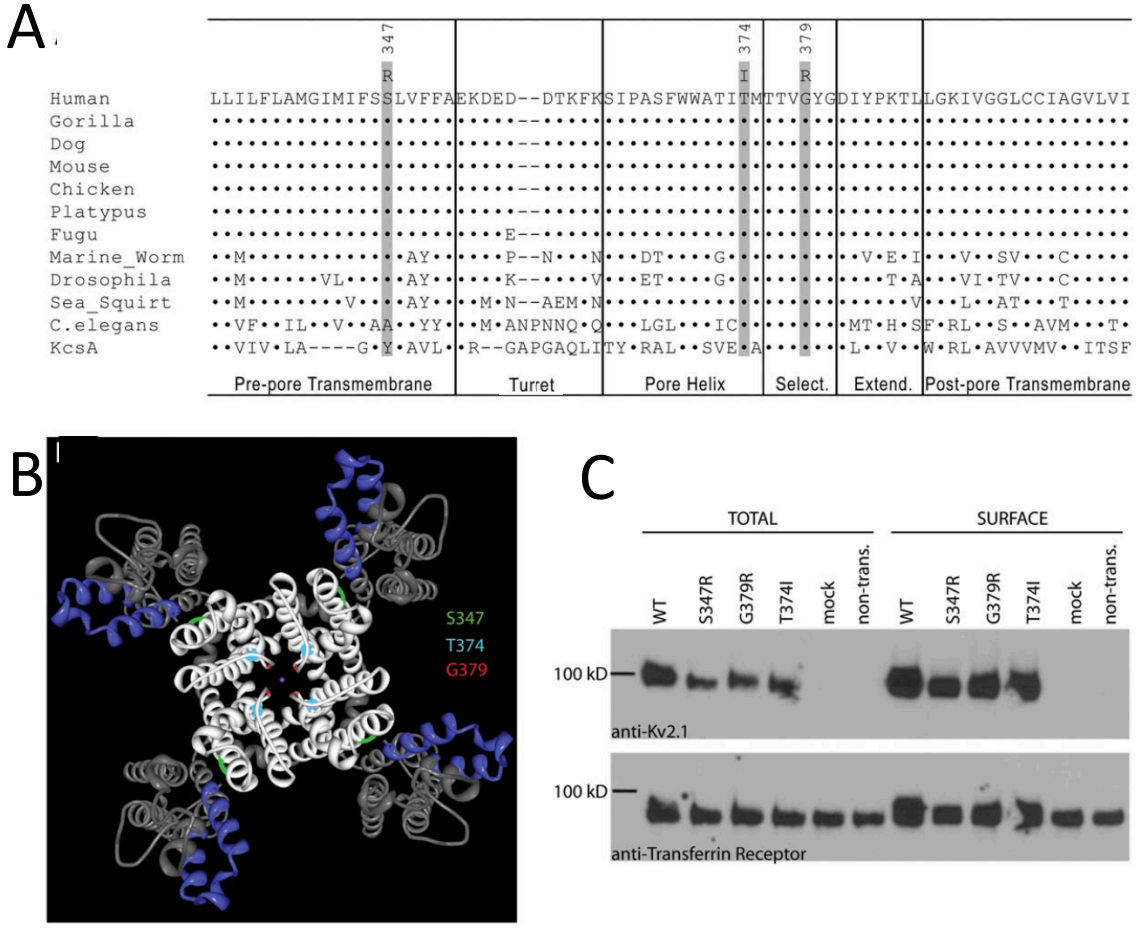

Figure 15. K_V2.1 mutations identified in three individuals with epileptic encephalopathy. (**A**) Evolutionary conservation of K_V2.1. Multiple alignment of K_V2.1 species orthologs (Clustal Omega[241]). Mutated amino acids are shaded and functional sub-domains of the pore region are indicated. (**B**) Location of mutations mapped onto the crystal structure of a K_V2.1/K_V1.2 chimera (PDB 29R9).[242] The left panel shows a channel tetramer from the extracellular side. S347 (green) lies at the interface between the voltage sensor (blue) and pore (white) domains. T374 (teal) lies adjacent to the selectivity filter, while G379 (red) lies in the selectivity filter. (**C**) Mutant K_V2.1 proteins are expressed and trafficked to the cell surface. Cell surface expression was measured using cell surface biotinylation of CHO-K1 cells transfected with wildtype or mutant K_V2.1. Total and surface fractions of K_V2.1 were detected with anti-K_V2.1 antibody. Endogenous transferrin receptor levels were measured as a loading control.

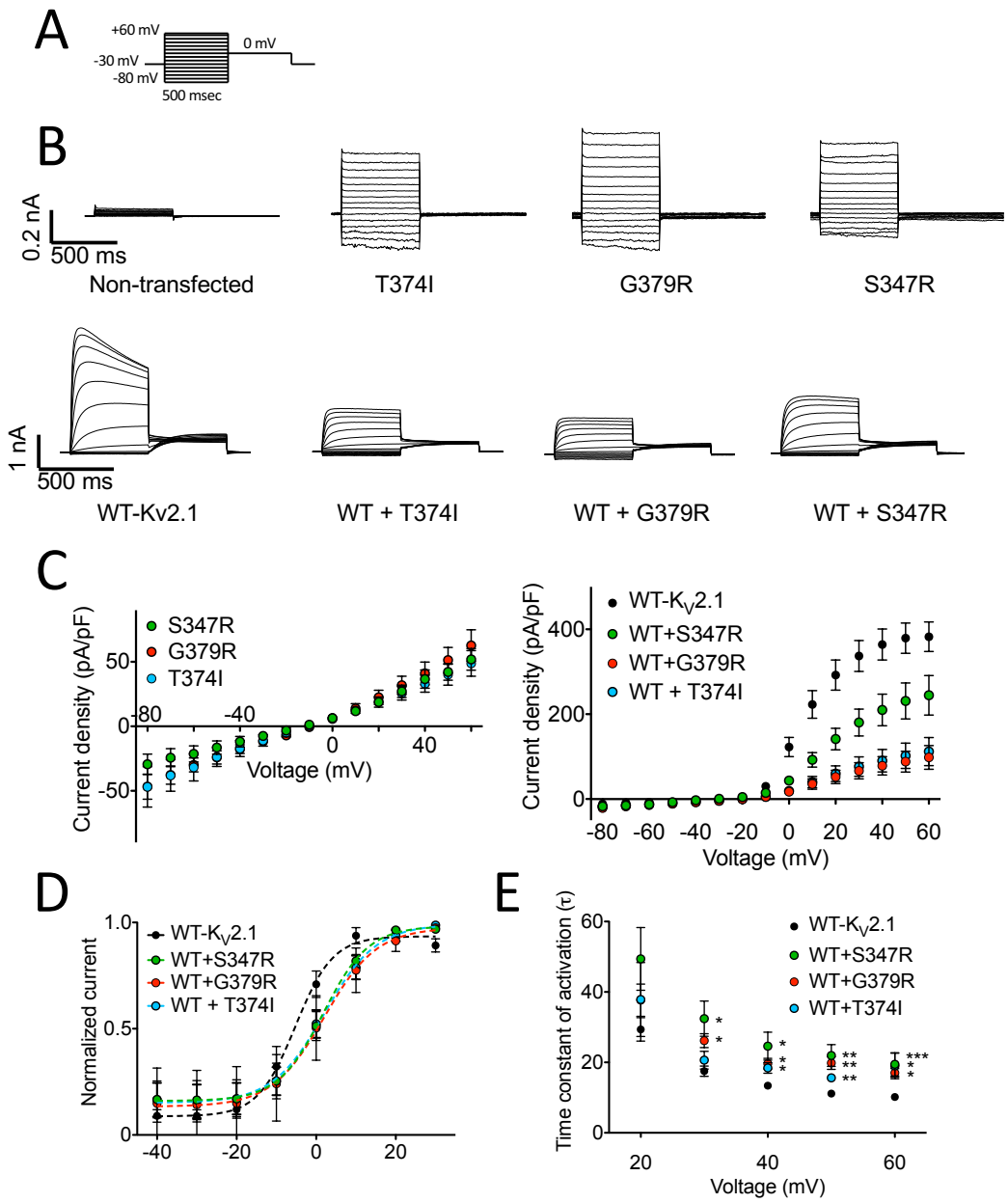

Figure 16. Functional consequence of K_V2.1 mutations. (**a**) CHO-K1 cells were held at -30mV and whole cell currents were recorded from -80 to +60 mV in 10 mV steps for 500 msec followed by a 500ms step to 0mV to record tail currents. (**b**) Average whole-cell current traces recorded from non-transfected CHO-K1 cells and CHO-K1 cells transiently expressing wild-type or mutant (G379R, S347R, T374I) K_V2.1 channels, or co-expressing wild-type plus mutant channels. (**c**) Current density–voltage relationships measured from CHO-K1 cells expressing mutant, wild-type, or co-expressing wild-type and mutant K_V2.1 channels. Currents were normalized to cell capacitance (pF). (**d**) Voltage dependence of steady-state activation. Tail currents were normalized to peak amplitude and fit with Boltzmann function. Biophysical parameters of voltage-dependence are detailed in Table 8. (**e**) The time constant of activation was determined from exponential fit of individual current traces.

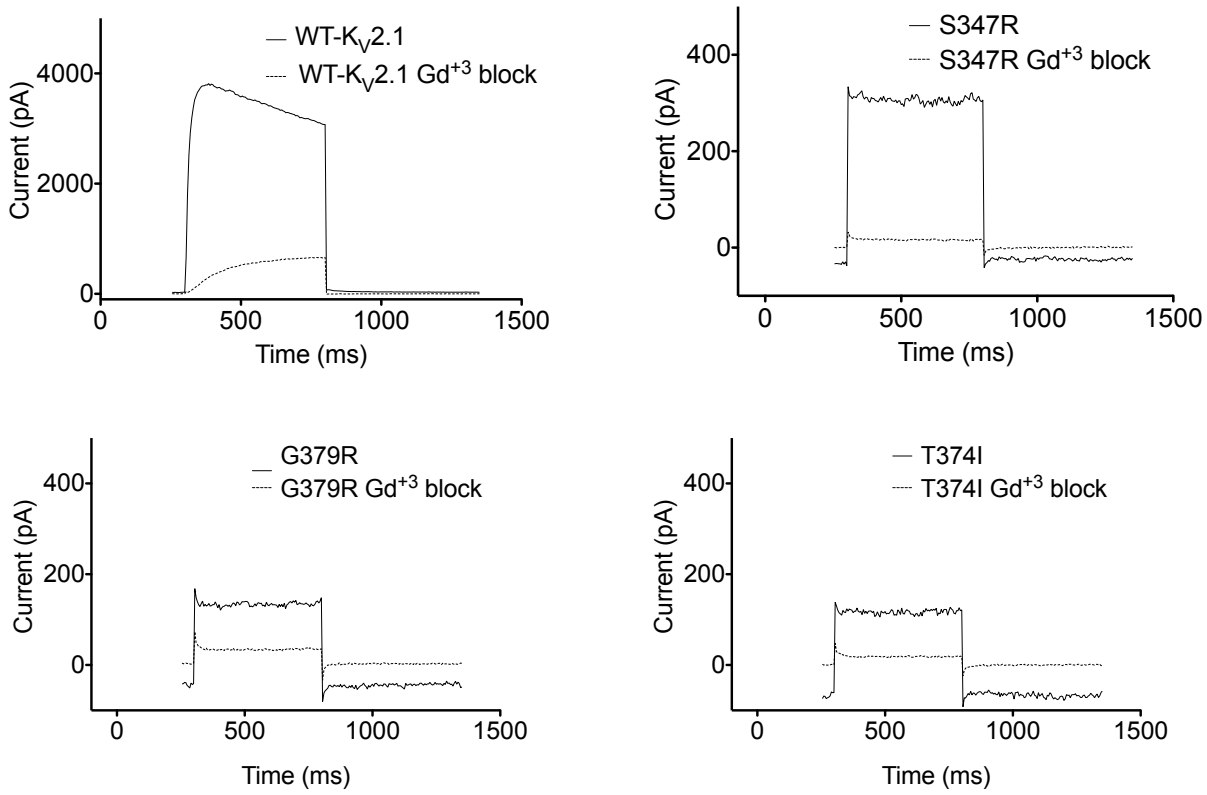

Figure 17. $GdCl_3$ block of mutant KV2.1 channels. Representative traces of control and Gd^{+3} block at +60 mV of wild-type (86±2.1%, n=5) or mutant channels (S347R (94±3.7%, n=3), G379R (79±4.2%, n=4), T374I (94±2.5%, n=3)).

strongly suggesting that the currents are pore-mediated (**Fig 17**). Based upon the external and internal K^+ concentrations used in these experiments, the theoretical reversal potential (E_{rev}) for K^+-selective currents is -47 mV. Expression of the mutant channels produced currents with depolarized E_{rev} (S347R: -23·2±4·8 mV; G379R -14·0±4·5 mV; T374I -16·5±5·5 mV) indicating that the mutations affect ion selectivity. To test ion selectivity, the external solution was diluted 1:10 with 300 mM sucrose. Under these conditions, a depolarizing shift in E_{rev} would indicate anion selectivity, while a hyperpolarizing shift would indicate cation selectivity. Dilution of the extracellular solution produced a hyperpolarizing shift in E_{rev} confirming the current conducted was cation-selective (**Fig 18**). Changes in cation selectivity were determined by measuring changes in E_{rev} following molar replacement of extracellular sodium with monovalent cations. All three mutants exhibited loss of K^+ selectivity, with K^+/Na^+ permeability ratios of 0.9 (**Fig 18**; **Table 8**) compared to the reported 14:1 ratio for Kv2.1-WT.[243]

To investigate the effects of the mutant channels in a heterozygous background, we co-expressed each mutant with Kv2.1-WT channel and compared to the wildtype channel expressed alone. Co-expression of K_V2.1-WT with T374I, S347R, or G379R resulted in reduced current measured at test potentials ranging from 0 to +60 mV (**Fig 14C**), depolarizing shifts in the voltage-dependence of steady-state activation (**Fig 16D** and **20**; **Table 8**), and greater time constants of activation (τ) measured from +30 to +60 mV test potentials (**Fig 16E** and **20**). The observed changes in kinetic parameters suggest that the mutant and wild-type subunits can form heterotetrameric channels.

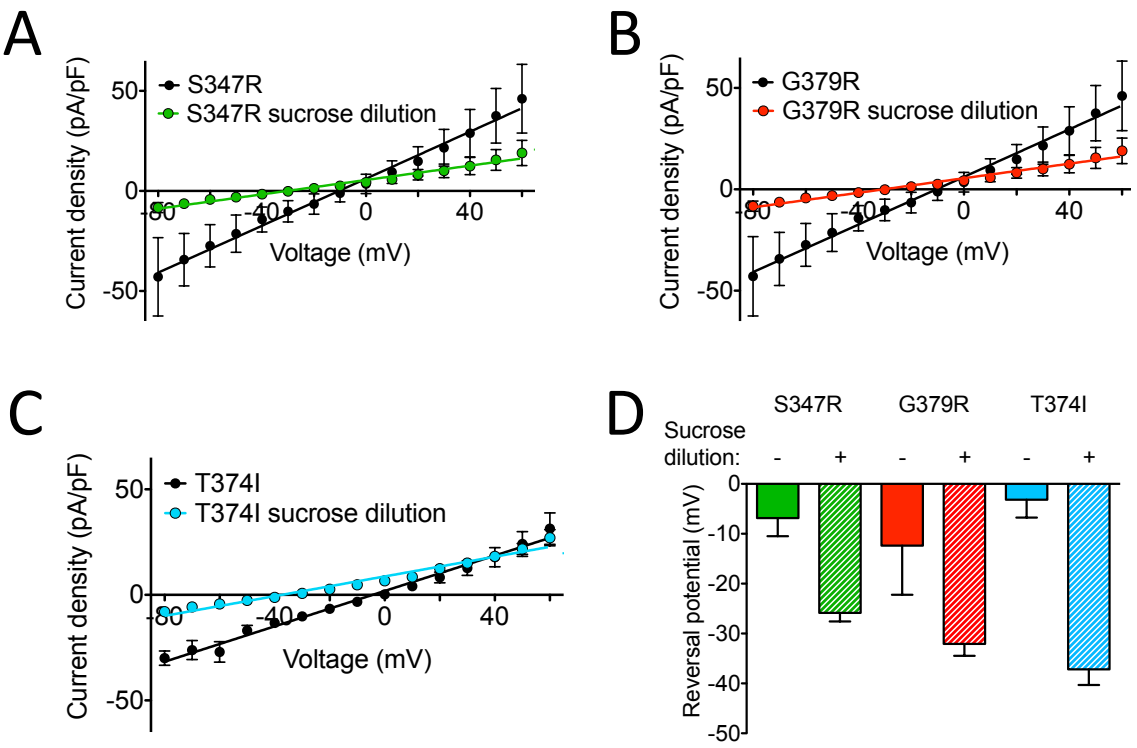

Figure 18. Extracellular cations are conducted through mutant K_V2.1 channels. Current-voltage plots in control bath and after bath was diluted 10-fold in 300mM sucrose solution in (**a**) K_V2.1-S347R (**b**) K_V2.1-G379R and (**c**) K_V2.1-T374I. (**d**) Reversal potentials were determined by linear fit to y=mx+b in control bath and after bath was diluted 10-fold in 300mM sucrose solution.

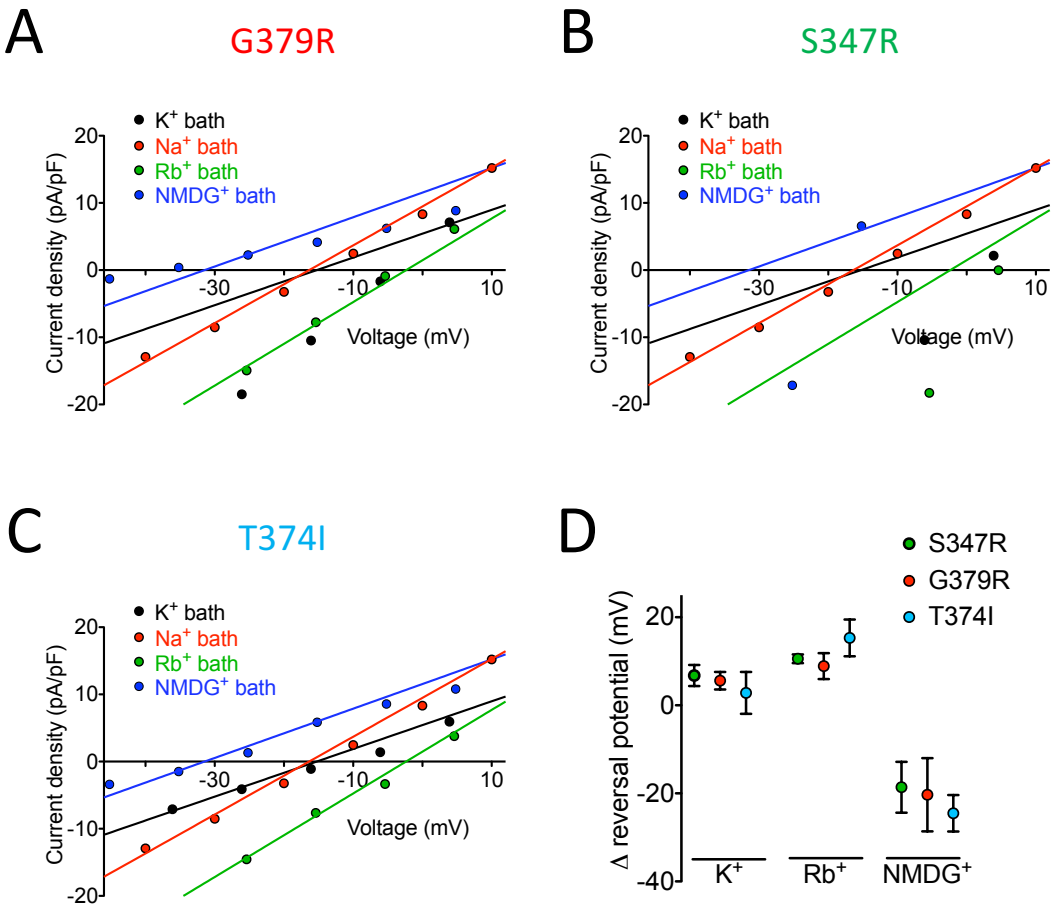

Figure 19. Ion selectivity of mutant K_V2.1 channels. Reversal potentials were determined by linear fit to y=mx+b in control bath and after bath solution change with equimolar substitution of extracellular monovalent Na^+ in (**a**) K_V2.1-S347R (**b**) K_V2.1-G379R and (**c**) K_V2.1-T374I. (**d**) Change in reversal potential after equimolar substitution of extracellular monovalent Na^+.

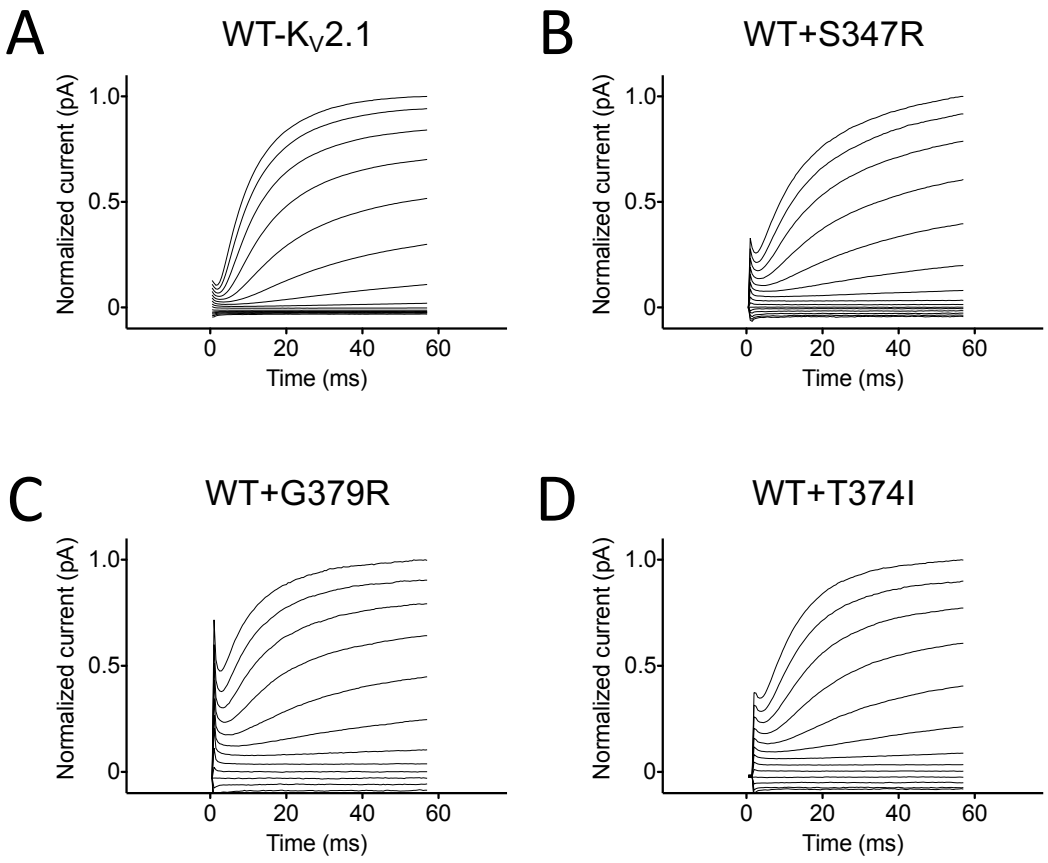

Figure 20. **Expanded view of whole-cell current traces for evaluation of activation kinetics of wild-type K_V2.1 channel alone or co-expressed with mutant channels**. Expanded view of the first 50 msec of whole-cell currents following voltage change from -80mV to +60mV and normalized to peak current recorded from CHO-K1 cells transiently expressing K_V2.1-WT (**a**) or co-expressing wild-type and mutant K_V2.1 channels ((**b**) G379R, (**c**) S347R, (**d**) T374I).

Table 8. **Biophysical properties of voltage-dependence of activation for wild-type and mutant K_V2.1 channels.**

	Mean $V_{1/2}$ ± S.E.M.	Slope factor ± S.E.M.	*n*
Kv2.1-WT	-4·1 ± 1·5	4·4 ± 0·4	12
Kv2.1-WT + G379R	1·3 ± 2·0 *	5·2 ± 0·6	8
Kv2.1-WT + S347R	2·8 ± 1·6 *	5·9 ± 0·5	8
Kv2.1-WT + T374I	1·9 ± 1·5 *	5·7 ± 0·2	7

* $P < 0.05$

DISCUSSION

Co-occurrence of *de novo* variants in *KCNB1* in three independent patients with overlapping clinical phenotypes that include epileptic encephalopathy with associated cognitive and motor dysfunction provides strong genetic evidence that the *KCNB1* variants are likely pathogenic. Further evidence for a pathogenic effect of the *KCNB1* mutations comes from functional studies of mutant $K_V2.1$ channels. All three mutations, located within the pore domain of $K_V2.1$, resulted in channels with similar dysfunctional features.

Previous studies demonstrated that mutations in the pore region can result in altered ion selectivity.[244-247] Consistent with this, each $K_V2.1$ mutant exhibited voltage-independent, non-selective cation currents. When co-expressed with wildtype channels, all Kv2.1 mutants induced depolarizing shifts in the voltage-dependence of activation and reduced current density at more depolarized voltages. Further, co-expression of the Kv2.1 mutants with wildtype channels resulted in inward currents in the voltage range where $K_V2.1$ channels are normally closed, as evidenced by large inward currents observed when using a holding potential of -80 mV. These gain-of-function and dominant-negative functional defects are predicted to result in depolarized resting membrane potential and impaired membrane repolarization, with increased cellular excitability as a net consequence.

$K_V2.1$ is the main contributor to delayed rectifier potassium current in pyramidal neurons of the hippocampus and cortex.[248-252] Delayed rectifier potassium current is critical for membrane repolarization under conditions of repetitive stimulation and acts to dampen high frequency firing. Reduction of delayed rectifier potassium current by *Kcnb1* deletion in mice results in reduced thresholds to induced seizures, but not spontaneous seizures.[253] This suggests that loss of $K_V2.1$ function predisposes neuronal networks to hyperactivity, resulting in a modest

increase in seizure risk. In contrast, our results demonstrate that gain-of-function and dominant-negative effects result in epileptic encephalopathy. A similar phenomenon is observed with *KCNQ2* wherein heterozygous loss-of-function mutations result in benign familial neonatal seizures, while mutations with dominant-negative effects result in epileptic encephalopathy.[254] This suggests that variable functional defects resulting from different mutations in the same gene contribute to the pleiotropic effects observed for genes associated with neurodevelopmental disorders.

In summary, our genetic and functional evidence identify mutation of *KCNB1* as a cause of epileptic encephalopathy. This expands the considerable locus heterogeneity associated with epileptic encephalopathies, suggesting that clinical exome sequencing may be useful for molecular diagnosis. Rapid genetic diagnosis is beneficial for appropriate disease management and may improve long-term outcomes in epileptic encephalopathies.

CONCLUSIONS

Based on the data presented here, *KCNB1* is a novel genetic cause of epileptic encephalopathy. Heterologous expression studies that I performed of wild-type or mutant $K_V2.1$ elucidated a combined loss- and gain-of-function mechanism associated with epileptic encephalopathy. Disruption of the selectivity filter in this neuronal voltage-gated potassium channel not only loses the repolarizing outward potassium current, but also renders the channel insensitive to voltage control and allows passage of large monovalent cations through the pore. These biophysical changes suggest the variants described here result in enhanced neuronal excitability through combined loss- and gain-of-function mechanisms.

CHAPTER IV

FUNCTIONAL AND TRANSCRIPTIONAL MECHANISMS OF RARE MISSENSE *TBX5* VARIANT CAUSING THE BRUGADA SYNDROME

ABSTRACT

Background. Loss of function variants in SCN5A, the gene encoding the cardiac sodium channel, are the only major monogenic cause of the Brugada Syndrome (BrS) but account for only 20% of cases. Rare, predicted protein altering variants in multiple other genes have been implicated, but evidence supporting their role in BrS pathogenesis has been weak. Our laboratory identified a rare variant, resulting in the substitution of glycine (G) for arginine (R) at amino acid position 145 (G145R), in the cardiac transcription factor TBX5 in an *SCN5A*-negative BrS family. *TBX5* is a candidate BrS gene because it is known to modulate *SCN5A* expression and a common BrS-associated variant disrupts a putative TBX5 binding site in an *SCN5A* enhancer. However, approaches to establish that variants in transcription factor genes cause congenital arrhythmia syndromes have not been developed.

Materials and Methods. We compared *in vitro* DNA binding and transcriptional activity of wild-type TBX5, BrS-identified G145R, and Holt-Oram syndrome-associated G80R as a control loss-of-function mutation. We generated induced pluripotent stem cells (iPSCs) from family members with BrS and from population controls. Using CRISPR/Cas9, we generated other *TBX5*

variants, and also corrected the G145R variant to create isogenic control lines. We differentiated the iPSCs to cardiomyocytes (iPSC-CMs) for functional and transcriptional assessments, including electrophysiologic studies and RNA sequencing.

Results. *In vitro*, TBX5-G145R displayed markedly reduced (-63%) transcriptional activity and (-97%) binding to TBX5 target sequences compared to wild-type. *SCN5A* expression and peak sodium current were reduced ~50% in $TBX5^{G145R/WT}$ iPSC-CMs. Correction of the TBX5 variant restored SCN5A expression to levels detected in population control lines. Unexpectedly, TBX5-G145R also caused increased late sodium current and action potential duration lability. The heterogeneity in action potential duration was inhibited with pharmacologic blockade of the late sodium current and with genome editing to correct the missense variant. Genes with altered expression in TBX5-G145R relative to *TBX5* heterozygous knockout and wild-type myocytes included members of the PI3 kinase pathway, a known modulator of late sodium current.

Conclusion. Using genome editing in patient-derived cardiomyocytes, we were able to demonstrate that TBX5-G145R reduces cardiac sodium current, the hallmark of BrS. Missense variants in transcription factors can result in discrete alterations in gene expression resulting in pleiotropic or variable expressivity of clinical presentations due to unique variants in a common gene. Genome editing in patient-derived cells is a powerful approach to directly establish the role of DNA variants in human disease.

INTRODUCTION

The Brugada syndrome (BrS) is an inherited arrhythmia condition that increases risk of ventricular tachyarrhythmia and sudden cardiac death.[52,255] The most common genetic cause of BrS, accounting for 20% of cases, is loss of function variants in *SCN5A*[46,75] but approximately 70% of cases of BrS are due to genetically undefined etiology. Genotype-phenotype studies have identified decreased peak sodium current due to abnormal gating or reduced cell surface expression as the cellular electrophysiologic hallmark of BrS.[68,69] We have recently described a missense variant in the cardiac transcription factor TBX5 that is predicted to be deleterious to protein function in a case of BrS.[107] This is variant is not reported in the Exome Aggregation Server, indicating that it is very rare.

Altered gene expression is an appreciated causative or modulatory mechanism in inherited arrhythmia syndromes. Missense variants in TBX5 (gain of function mutation),[115] and other transcription factors GATA4 (loss of function mutations)[116-118] and NKX2.5 (loss of function mutations)[119] have been identified in cases of familial atrial fibrillation, supporting transcriptional misregulation as a mechanism of arrhythmia conditions.[107] Common variants located near TBX5 are associated with prolonged QRS duration, a feature observed in BrS.[114] TBX5 is implicated in BrS pathogenesis through a previously described BrS-associated common *SCN10A* variant (rs6801957) that is located in a putative TBX5 binding motif of an *SCN5A* enhancer, causing lower levels of *SCN5A* expression in human myocardium.[103,109] Therefore, TBX5-G145R is a reasonable causal candidate variant in familial BrS. The conventional approach to functionally characterizing candidate variants in ion channelopathies is to compare electrophysiologic properties of reference and mutant sequences using electrophysiologic assays in heterologous expression systems.

However, this approach cannot be used to assess the functional properties of variants in upstream pathways such as regulators of transcription.

TBX5 is a T-box containing transcription factor critical to mammalian tissue patterning and cellular differentiation during development of the upper extremities and the heart. *TBX5* variants that result in TBX5 haploinsufficiency (nonsense, frameshifting indels, and splice site variants) or severe alterations in DNA binding (missense and intragenic duplications) cause the human condition Holt-Oram syndrome (HOS).[120] HOS is a rare developmental syndrome affecting 1:100,000 live births with abnormal development of the upper limbs and the heart. In the heart, common pathology includes isolated septal defects and conduction defects.[121] Haploinsufficiency of *Tbx5* in murine models results in diminished cardiac expression of gap junction proteins, atrial natriuretic peptide, and the cardiac sodium channel.[140,143] Models (animal or cellular) of specific missense variants in *TBX5* under endogenous expression have not been studied in order to define the resultant transcriptional mechanism underlying disease.

Differentiation of cardiomyocytes from stem cells derived from somatic cell origin has provided a human model of heart disease. Inherited[256-263] and drug-induced[264,265] arrhythmia conditions have been recapitulated in induced pluripotent stem cell-derived cardiomyocytes (iPSC-CMs). Accurate models of sodium channel dysfunction have been established in human iPSC-CMs containing genetic lesions in *SCN5A* that cause BrS and Long QT syndrome (LQTS).[172,266] Integrating genome editing approaches (TALENs, ZFNs, and CRISPR/Cas9) with iPSC-CMs provides an advanced model for testing causation of genetic variants on cellular phenotypes and a way to account for the confounding effect of genetic background. This approach has been validated by editing variants in known Mendelian disease genes, such as

KCNH2 in LQTS[267] and phospholamban in dilated cardiomyopathy,[268] and is primed for the application of test the causality of novel genetic associations.

We generated iPSC-CMs from patients carrying TBX5-G145R, and demonstrated decreased sodium channel expression and current, consistent with the BrS phenotype. However, this experiment did not establish the contribution of the G145R variant to the phenotype. Generation of isogenic control iPSC-CMs through RNA-guided nuclease-mediated homology-directed repair reversed the functional defect, thereby proving that TBX5-G145R causes BrS in this family. By generating this human model, we also identified a previously unappreciated role for TBX5 in modulating late sodium current and action potential duration lability leading to arrhythmia activity. Treatment of TBX5-G145R containing iPSC-CMs with the late sodium channel blocker ranolazine prevented the observed arrhythmogenic features. Our findings advance molecular diagnostics to progress from variant identification to causation with mechanistic understanding of disease pathogenesis.

MATERIALS AND METHODS

Patient enrollment: This study was reviewed and approved by the Institutional Review Board at Vanderbilt University Medical Center (Nashville, TN). All participants provided written informed consent.

Genotyping: After informed consent, DNA was extracted from peripheral blood using Puregene Chemistry on the Autopure LS robotic system according to manufacturer's recommendations (Qiagen, product number 9001340). Amplicons of containing each SNV of interest were generated by RT-PCR using the primer sets listed in **table 9**. The amplification was performed using Applied Biosystems Veriti 96-well thermal cycler with a melting temperature of 95^{o}C, annealing temp listed next to each primer set in table 9, and extended at 72^{o}C. Each reaction used 30 cycles for amplification.

TBX5 structural modeling: The G145R variant of TBX5 was modeled into the Tbx5-DNA complex (PDBID: 2X6V) using PyMOL (Schrodinger; NY, NY). Energy minimized analysis of 10 iterative side-chain repacking and gradient-based minimization with a ramping repulsive potential (relax) was performed on 1,000 models. Wild-type structures were also subjected to this minimization protocol to generate a total of 100 structures. The best scoring 10 models of WT and G145R were compared by Rosetta energy score to estimate energy well depth.

Human TBX5 expression vectors: An expression vector containing full-length human TBX5 cDNA under control of the CMV promoter was purchased from Origene (catalog # RC216520).

Table 9. Primers for Sanger sequencing to genotype rare and common BrS SNVs.

Target	Primer direction	5' -> 3' sequence	Annealing temperature (^{o}C)
TBX5 c.G433A	Forward	TCCCAGCTACTACTCAACAACCC	58
	Reverse	GCGACGAAAGTGGGGGAAAATG	
rs6801957	Forward	CTCAGGGCATTCACCTCTGC	60
	Reverse	GTAGGGAACTTGGCCACCTG	
rs9388451	Forward	TGAACGGAGTTGGGCCACTA	60
	Reverse	AGGGAGCGAGGAGAATACCA	
rs10428132	Forward	ATTCAGATGGTTATAAACAAATG	58
	Reverse	GTAGGGTACACAGTTTATATCTG	

Site-direct mutagenesis introduced single missense variants c.433G>A (p.Gly145Arg) or c.238G>A (p.Gly80Arg, a known HOS-associated mutation) into the expression vector using the QuikChange system (Stratagene).

In vitro transcription/translation: TBX5 (reference or mutant) was synthesized using *in vitro* transcription/translation with rabbit reticulocyte lysate using the T7 RNA polymerase TNT system (Promega).

Electrophoretic mobility shift assays: A well described TBX5 binding site in the *NPPA* promoter was generated by annealing the 22-mer oligonucleotide 5'–TTACTCTTCTCACACCTTTGAAGTGG – 3' to the complementary sequence. After annealing, the DNA target was radiolabeled with γ-^{32}ATP using T4 polynucleotide kinase (NEB) and purified with a Sephadex G-50 gravity column. In vitro translated TBX5 was incubated with radiolabeled DNA target site in binding buffer (20 mM HEPES, 20% glycerol, 50 mM NaCl, 5 mM $MgCl_2$, 0.5 mM EDTA, 2 mM DTT, 1 μg/mL BSA, and 1 μg dI-dC) at room temperature for 20 min. DNA-TBX5 complex was separated from unbound DNA by electrophoresis. Afterwards the gel was dried for 45 mins onto DE-81 paper and visualized using overnight exposure to a K-screen.

Luciferase assay: The *NPPA* promoter (-337 to 0 position from the transcription start site as previously reported[138]) was inserted into the pGL3 basic reporter construct multiple cloning site using SacI and NheI. Human embryonic kidney cells (HEKs) were grown and maintained in Dulbecco's minimum essential medium supplemented with 10 fetal bovine serum, 1%

penicillin/streptomycin, and 1X non-essential amino acids. 20,000 cells per well were plated in a 96 well plate and transfected 24-hours later using FuGene6. Each well received 4 ng of renilla, 30 ng of NPPA-luciferase reporter construct, and 30 ng of TBX5 construct. Luciferase assays were performed according to Promega Dual Luciferase Assay Kit. The renilla signal was used to normalize for transfection efficiency among wells. Experiments were performed in triplicate for each condition and results presented are averages from three independent experiments.

Human induced pluripotent stem cell (iPSC) reprograming: Dermal fibroblasts were isolated from a 2-mm dermal punch biopsy from consented participants. Fibroblasts from the second passage were reprogrammed into iPSCs using electroporation delivery (Neon system) of non-integrating episomal vectors (Epi5™ Episomal iPSC Reprogramming Kit (ThermoFisher)). After episomal delivery, fibroblasts were plated on a standard cell culture grade 10-cm plate. iPSC-like colonies were manually moved to hES-grade matrigel (Corning) coated 24-well plates between day 14-30 post-electroporation. Individual colonies were expanded for validation and line maintenance.

Human iPSC "stemness" validation: Human iPSC were validated for the presence of stem cell associated markers via immunofluorescent detection of OCT4 (Cell Signaling, #2750), SSEA4 (DSHB, MC-813-70), SSEA3 (Millipore, MAB4303), Tra-1-60 (Millipore, MAB4360). The presence of stem cell-associated alkaline phosphatase were detected by commercially available colorimetric assay (Stemgent, 00-0055).

Human iPSC pluripotency validation: Human iPSCs were grown in suspension on low adherence plates in DMEM/F12 w/ GlutamaX (Invitrogen, 10565) supplemented with 20% knockout serum replacement (Invitrogen , 10828-028), 1% non-essential amino acids (Sigma, M7145), 1% penicillin/streptomycin (MediaTech,15140122). The media was supplemented with 10 μM Rho kinase inhibitor (Y-27632 , CalBiochem) on day 0 to promote the formation of embryoid bodies (EBs). EBs were pelleted by gravity for 10 minutes and media were exchanged every 2 days. On day 7 of differentiation, individual EBs were replated on growth factor reduced matrigel (Corning) coated glass coverslips for 7-14 days in media listed above. The presence of cells in the endoderm, mesoderm, and ectoderm lineages was visualized by immunofluorescent detection of proteins associated with each of the three germ layers: GATA4 (Abcam, ab84593) for endoderm, α-smooth muscle actin (Abcam, ab7817) for mesoderm, and βIII-tubulin (Millipore, MAB1637f) for ectoderm.

Human iPSC chromosomal assessment: Twenty iPSCs were screened for large chromosomal abnormalities by commercial karyotype analysis (Genetics Associates, Nashville, TN).

Human iPSC maintenance: Human iPSCs were maintained on growth factor-reduced Matrigel (Corning) coated plates (1:200 dilution, DMEM/F12) in mTeSR1 medium (Stemcell Technologies). Cells were passaged every 4-5 days using 0.5 mM EDTA (Life Technologies) in D-PBS without $CaCl_2$ or $MgCl_2$ (Life Technologies). 10 μM Rho kinase inhibitor (Y-27632, CalBiochem) was added for the first 24 hours after passaging. Cells were maintained at 37^{o}C, with 5 % CO_2 and 20% O_2.

CRISPR/Cas9 expression vector construction: Guide RNAs (gRNA) were designed using the Zhang lab CRISPR design tool (http://crispr.mit.edu/). gRNAs 20 nucleotides in length with a low number of predicted coding region off-target sites were selected for insertion into Px459[269] expression system (Addgene). Px459 is an expression vector containing a U6 promoter driven gRNA (crRNA tethered to a tracrRNA sequence) and a CMV promoter driven human optimized *S. pyogenes* Cas9. Elements for specific genomic targeting were constructed by the following methods. A 25mer oligonucleotide containing the gRNA targeting exon 5 of *TBX5* and BbsI compatible 5' overhangs (Forward sequence 5' – CACCGCCACCCGGGGCGATTGGATG – 3'; Reverse sequence 5- AAACCATCCAATGCGCCCCGGTGGCC – 3') was annealed and subsequently phosphorylated with T4 polynucleotide kinase. Px459 was linearized using BbsI and ligated to the phosphoannealed oligomers in a single reaction. The plasmid was transformed in competent cells lines and isolated from bacterial cultures using MAXI preparations. The gRNA insertion was confirmed by Sanger sequencing.

Genome modification in patient-derived iPSCs: iPSCs were singularized using 0.5 mM EDTA in PBS without $CaCl_2$ and $MgCl_2$ and passed through a 30 micron filter. Ten micrograms of gRNA inserted Px459 plasmid and 10 μmoles of 150 base pair single-stranded repair template were delivered to $2X10^6$ iPSCs via electroporation (Neon system, ThermoFisher). Post-delivery iPSCs were plated on matrigel GFR coated 10-cm plates for expansion of individual clones. Clonal colonies were manually passaged to matrigel-coated 24-well plates for expansion. Each colony was passaged using 0.5 mM EDTA for line maintenance and DNA extraction. DNA was isolated using QuickExtract solution (EpiCentre) for PCR amplification of exon 5 of *TBX5*. Screening of the specific edit was done by NciI digestion as wild-type sequence is selectively cut

by this enzyme and *TBX5 c.G433A* is not. The editing event in all clones that were screened positive by restriction digest was confirmed by Sanger sequencing.

Cas9 off-target analysis: Predicted off-target sites (determined by http://crispr.mit.edu/) were amplified by PCR and evaluated by Sanger sequencing. The genomic location, nearest gene, and primers used for amplification are presented in Table 10.

Cardiomyocyte differentiation: Human iPSCs were cultured in mTeSR media and split at 1:12-20 ratios. Cells were grown for 4-5 days to achieve ~80% confluency. This is referred to as day 0 of differentiation and media was change to cardiac differentiation media supplemented with 6 μM CHIR99021 (LC Laboratories) for day 0 to day 2. Cardiac differentiation media is comprised of RPMI 1640 (11875, Life Technologies), 2% B-27 minus insulin supplement (A1895601, Life Technologies), and 1% Pen-Strep (Life Technologies). On day 2 medium was changed to cardiac differentiation medium. On day 3 medium was changed to cardiac differentiation medium supplemented with 5 μM IWR-1 (Sigma). Cardiac differentiation media was replenished every other day. On days 13, 15, and 17 the medium was switch to metabolic selection medium consisting of RPMI1640 without glucose (11879, Life Technologies), 2% B-27 minus insulin supplement (A1895601, Life Technologies), and 1% Pen-Strep (Life Technologies). On day 19, the media was switched to cardiomyocyte media consisting of RPMI 1640 (11875, Life Technologies), 2% B-27 supplement (17504, Life Technologies), and 1% Pen-Strep (Life Technologies). Cardiomyocyte medium was exchanged every other day until dissociation, generally at day 30-35 in these experiments.

Cardiomyocyte dissociation: Human iPSC-derived cardiomyocytes (iPSC-CMs) were incubated with TrypLE Express (Life Technologies) for 13 min at room temperature to dissociate cells. Cardiomyocytes were passed through a 100 micron filter to remove non-dissociated aggregates and either used immediately for experiments or cryopreserved in 10% DMSO, 90% FBS and stored in liquid nitrogen. Human iPSC-CMs were thawed and plated at high density on Matrigel growth factor-reduced coated dishes in cardiomyocyte media. Human iPSC-CMs were maintained at 5% CO_2 and 21% O_2 for 4-5 days prior to performing experiments.

mRNA Quantification: Total RNA was isolated from iPSC-CM on day 32-35 of differentiation using the RNAeasy Mini Kit with DNAse treatment (Qiagen). cDNA was synthesized from 2 μg of the RNA by use of the Transcriptor First Strand cDNA Synthesis Kit with random hexamer primers (Roche Applied Science, Indianapolis, IL) and used as a template. To generate a standard curve for absolute quantification, *SCN5A* subcloned into the pGEM-T vector (Clontech, Mountain View, CA) was used. cDNA and 5 different dilutions of the SCN5A vector were prepared with predesigned 6-carboxyfluorescein-labeled fluorogenic TaqMan probe and primers (Applied Biosystems) for *SCN5A* (Hs00165693.m1), *TBX5* (Hs01052562) or RPL19 (Hs02338565.qh) in triplicate in the same 96-well plate for real-time polymerase chain reaction amplification. Real-time quantitative RT-PCR was conducted with a 7900HT Real-Time Instrument (Applied Biosystems). Data were collected with instrument spectral compensation and analyzed by use of absolute quantification and a standard curve with SDS 2.2 software (Applied Biosystems). Each value was normalized to that for RPL19.

Cell Surface Biotinylation: On day 35 of differentiation iPSC-CMs were washed with room temperature PBS without calcium and magnesium and then treated with PBS containing 1.5 mg/ml sulfo-NHS-LC-biotin (Pierce) at 4 °C for 1 hour. Excess biotin was inactivated and removed by a 20-min incubation in 10 mM glycine/PBS at 4 °C and three washes in PBS. The cells were lysed in lysis buffer containing (in mM) 10 Tris (pH 7.3), 150 NaCl, 1 EDTA, 1% Triton X-100, and 1% sodium deoxycholate and a mixture of mammalian protease inhibitors (Roche). Cell lysates were spun at 13,000 × *g* for 20 min, and the supernatants were incubated with streptavidin-coated beads (Pierce) for 1 hour at room temperature. Beads were washed four times with lysis buffer and resuspended in Laemelli buffer, boiled, and analyzed by Western blot.

Western Blot Analysis: Whole-cell lysates or biotinylated membrane fractions were prepared from iPSC-CMs on day 35 of differentiation. Lysates were centrifuged at 10,000*g* for 5 min, and protein content was analyzed with a bicinchoninic acid assay (Pierce Biochemicals, Rockford, IL). Proteins (40 to 100 μg) were separated by running the sample on a NuPage 4-20% Tris-HCl gel (Invitrogen, Carlsbad, CA). The protein was transferred to PVDF membranes (BioRad, 0.45 um pore), blocked for 1 hour with 5% nonfat dry milk in 0.1% Tween-20 Tris-buffered saline (TTBS) plus at room temperature and then incubated overnight with antibodies targeting SCN5A (anti-pan Na_V polyclonal antibody, 1:250; Alomone Labs, Israel), βIII-tubulin (1:1,000; Abcam), or calnexin (polyclonal antibody, 1:1000, Stressgen Bioreagents, Belgium) at 4^{o}C. Membranes were washed 9 times with TTBS for 10-30 min each and incubated with secondary anti-mouse and anti-rabbit horseradish peroxidase-linked antibodies (Amersham Biosciences) in TTBS at

room temperature for 1hr. The blots were then washed 6 times for 10-30 min each in TTBS, and antibody interactions were visualized with the ECL system (Amersham Biosciences).

Whole cell voltage clamp sodium current measurements: Whole-cell voltage clamp experiments were conducted at room temperature (22-23°C). To record sodium currents, the external solution contained (in mM) NaCl 135, KCl 4.0, $MgCl_2$ 1.0, $CaCl_2$ 1.8, glucose 10, and HEPES 10; the pH was 7.4, adjusted with NaOH. The pipette (intracellular) solution contained (mM) NaF 5, CsF 110, CsCl 20, EGTA 10, and HEPES 10; the pH was 7.4, adjusted with CsOH. To eliminate L- and T-type inward calcium currents as well as outward potassium currents, 1 μmol/L nisoldipine, 200 μmol/L NiCl2, and 500 μmol/L 4-aminopyride (4-AP) were added into the bath solution. Glass microelectrodes were heat polished to tip resistances of 0.5-2 MΩ. To measure sodium current densities, cells were held at -100 mV, and sodium current was elicited with a single 50-ms pulse from -100 to +60 mV in 20 mV increments. To measure late sodium current, current was averaged in a 3 ms time window (195-198 ms after the pulse) before the capacity transient at the end of a 200 ms depolarizing pulse of -30mV from a resting voltage of -100 mV. Data acquisition was carried out using an Axopatch 200B patch-clamp amplifier and pCLAMP version 9.2 software (MDS Inc., Mississauga, Ontario, Canada). Currents were filtered at 5 kHz (−3 dB, four-pole Bessel filter) and digitized using an analog-to-digital interface (DigiData 1322A, MDS Inc.). To minimize capacitive transients, capacitance and series resistance were corrected ~80%. Current magnitudes were normalized to cell size, generated from the cell capacitance calculated by Membrane Test (OUT 0) in pClamp 9.2. Clamp protocols used are shown on the figures. Electrophysiological data were analyzed using pCLAMP version 9.2 software and the figures were prepared by using GraphPad Prism6.

Whole cell current clamp: In whole cell rupture patch current-clamp mode, action potentials from isolated human iPSC-CMs on day 30-35 of differentiation were elicited by injection of a brief stimulus current (1–2 nA, 2–6 ms, variable stimulation frequencies). The bath (extracellular) solution contained (in mM): NaCl 135, KCl 4.0 , $CaCl_2$ 1.8, and $MgCl_2$ 1, HEPES 5, glucose 10, with a pH of 7.4 (adjusted by NaOH). The pipette (intracellular) solution contained (in mM): 120 Aspartate-K, 25 KCl, 4 ATP-Na_2, 1 $MgCl_2$, 2 Phosphocreatine-Na2, 2 GTP-Na, 1 $CaCl_2$, 10 EGTA, and 5 HEPES, with a pH of 7.3 (adjusted by KOH). Microelectrodes with tip resistances of 3-5 mΩ were used. Twenty successive traces were averaged for analysis of action potential durations at 50 and 90% repolarization (APD_{50} and APD_{90}). The short term variability (STV) was calculated using $\sum(|APD_{i+1}-APD_i|)/[n_{beat}\sqrt{2}]$ and long term variability (LTV) using $\sum(|APD_{i+1}+APD_i - (2*APD_{mean})|)/[n_{beat}\sqrt{2}]$.[270] The scatter area of each cell was calculated assuming the shape of an ellipse using $\pi * STV * LTV$.[270]

Calcium handling: Human iPSC-CMs were incubated with 2 μM Fura-2 AM for 8 minutes at room temperature to load the indicator in the cytosol. CMs were washed twice for 10 minutes with Tyrode's solution containing 250 μM probenecid to retain the indicator in the cytosol. A minimum of 30 min were allowed for de-esterification before imaging the cells. Fura-2 AM loaded Ca transients were recorded during spontaneous beating or 0.2 Hz field stimulation in 2 mM Ca^{+2} Tyrode's solution. For experiments assessing sarcoplasmic reticulum calcium content, 10 mM caffeine was introduced for 5 seconds. Ca^{+2} transients were recorded and analyzed using commercially available data analysis software (IonOptix, IonWizardTM Milton, MA). For each cell and each experimental condition, tau (τ), amplitude and baseline values were averaged. All

experiments were conducted at room temperature. Tyrode's solution containing (in mM): $CaCl_2$ 5, NaCl 134, KCl 5.4, $MgCl_2$ 1, glucose 10, and HEPES 10, pH adjusted to 7.4 with NaOH.

Human iPSC-CM monolayer extracellular field potential: Day 30 iPSC-CMs were plated at 65,000 cells/well on 1:100 Matrigel coated 96-well plates. After 5 days of acclimation, plates were loaded on a CardioExcyte-96 (Nanion) for acquisition of extracellular field potential. Measurements were acquired at 37^0C, 80% humidity, and 5% CO_2 at a sampling rate of 1ms. Data were exported and converted to text files for compatibility on LabChart 6 (ADI). Utilizing the peak analysis tool, peak detection threshold was set to identify duration of beat rate as well as field potential duration (FPD_{max}). Beat rate was calculated by identifying duration of interspike intervals as defined by time between adjacent sodium spikes. FPD_{max} was calculated by measuring the duration between the most positive deflection of the sodium spike to the peak of the repolarization wave. Analyses were performed on 30 seconds of EFP recordings to produce ~40 measurements per well for both parameters. Measurements were averaged and denoted as FPD_{max}.

RNA-sequencing: Total RNA was isolated from iPSC-CM on day 32-35 of differentiation using the RNAeasy Mini Kit with DNAse treatment (Qiagen). Total RNA quality was assessed using the 2100 Bioanalyzer (Agilent). rRNA-depleted libraries were generated using TruSeq Total RNA sample kits with indexed adaptors (Illumina). Library quality was assessed using the 2100 Bioanalyzer (Agilent) and libraries were quantitated using KAPA Library Quantification Kits (KAPA Biosystems). Pooled libraries were subjected to 75 bp paired-end sequencing according to the manufacturer's protocol (Illumina HiSeq3000). Bcl2fastq2 Conversion Software (Illumina) was used to generate de-multiplexed Fastq files. The short-read sequence files generated by Illumina's CASAVA pipeline were processed by FastQC

(http://www.bioinformatics.babraham.ac.uk/projects/fastqc/). Low mean base-call quality scores well below pred-like values of 30 in the first 5 and last 4 positions of all samples prompted hard trimming of the reads. The sequence files were then aligned to human assembly build GRCh38 using the Tophat2 splice junction mapper (http://ccb.jhu.edu/software/tophat/index.shtml). Transcripts were assembled by and differential expression analysis was performed with Cufflinks (http://cole-trapnell-lab.github.io/cufflinks/) using the bias-correction. All non-coding RNA features were masked and RefSeq gene annotation was provided to the algorithm to allow for quantification of known transcript isoforms. Cuffdiff was run twice to test for pairwise differential expression between all individual samples as well as between sample groups. Gene level expression tests flagged as "NOTEST" or "HIDATA" were excluded from further analysis. Normalized expression values were databased and plotted using CummeRbund (http://compbio.mit.edu/cummeRbund/). For variant calling of RNA-seq data, short reads were aligned using the 2-pass method from the STAR RNA-seq aligner (http://bioinformatics.oxfordjournals.org/content/early/2012/10/25/bioinformatics.bts635).

Duplicate reads were flagged, and alignments with CIGAR strings containing "N" were split and trimmed of intronic overlaps. GATK was then used for base-call quality score recalibration, variant calling, and hard filtering using the following thresholds: 3^{+} SNP clusters in 35bp windows; FS>30; QD<2.0.

Statistical analyses: Data are mean ± SEM unless otherwise indicated. Statistical differences among two groups were tested with two-tailed Student's t test or Whitney Manning test for nonparametric comparisons. Statistical differences among more than two groups were assessed using one-way ANOVA followed by post-hoc Bonferroni correction. Results were considered

statistically significant if the p-value was less than 0.05. Statistical analysis was performed using GraphPad Prism 6. Please refer to RNA-seq methods for statistics related this experimental approach.

RESULTS

Clinical presentation of Brugada syndrome and *TBX5* genotyping

A male patient was diagnosed with Brugada syndrome during evaluation for a near syncopal episode at the age of 12 based on a characteristic ECG pattern of ST elevation in the right precordial leads (**Fig 21A**). Sequencing of the coding and flanking intronic regions of known BrS-associated genes failed to find rare non-synonymous variants. Through a collaborative effort, a novel and rare missense variant in the gene encoding the cardiac transcription factor TBX5 (c.G433A; p.G145R) was identified in the proband and predicted to be deleterious by the consensus classifier PredictSNP.[107,153] Subsequent genotyping and clinical screening for the Brugada syndrome identified multiple family members who harbor the *TBX5* variant and were later diagnosed with BrS due to a type I ECG patterns present at baseline or after flecainide challenge (**Fig 21B** and **21C**). All individuals in this pedigree diagnosed with BrS carry the *TBX5* variant while a single individual is a phenotypically-normal carrier. Accordingly, we hypothesized that $TBX5^{G145R/WT}$ causes BrS in this family.

TBX5-G145R decreases DNA binding and transcriptional activation

Modeling based on the crystal structure of wild-type TBX5 (TBX5-WT) bound to the *NPPA* promoter[126] predicts TBX5-G145R is a destabilizing variant likely to alter protein function (**Fig 22A**), consistent with the PredictSNP prediction.[153] To evaluate if the identified *TBX5* variant impacts protein function, we tested the impact of the glycine to arginine amino acid change at amino acid position 145 on DNA binding and transcriptional activation. Expression of TBX5 was not impacted by presence of missense variants as determined by Western blot

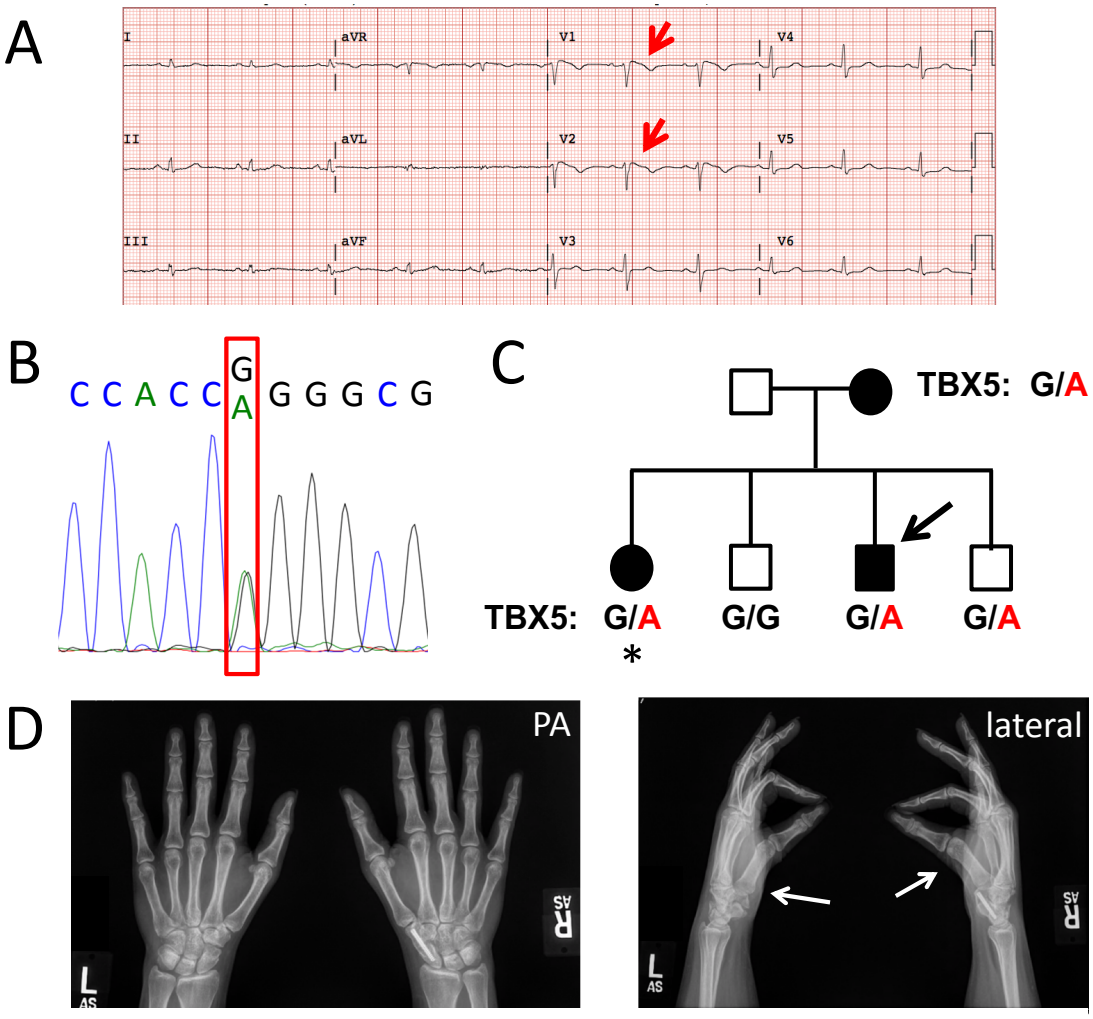

Figure 21 Familial Brugada syndrome-associated TBX5 variant. (**A**) Representative Type I Brugada syndrome ECG pattern of affected family member. Red arrows highlight ST segment elevation in right precordial leads. (**B**) Sanger sequencing confirmation of hypothesized risk allele *TBX5* c.G433A (**C**) Genotype of *TBX5* variant listed below individuals in pedigree. Red letters signify risk allele. Arrow indicates proband. Filled shapes indicate clinically diagnosed BrS. Asterisk indicates iPSC participant. (**D**) X-ray evaluation of hand pathology found hypoplastic thenar musculature. Prior surgical scaphotrapezial fusion of the right wrist was also evident. White arrows highlight hypoplastic musculature. PA = posteroanterior view.

approaches (**Fig 2B**). We performed an electrophoretic mobility shift assay (ESMA) to test DNA binding capacity using the previously described TBX5 binding site present in the *NPPA* promoter.[115,137,138] In EMSA experiments, incubation of *in vitro* translated TBX5-G145R from rabbit reticulocyte lysate with radiolabeled *NPPA* promoter sequence resulted in 2.3±0.4% (*n*=3 experiments) of the amount of shifted complex compared to wild-type protein (**Fig 22C**). TBX5-G80R is a known complete loss of function mutation at a position critical for TBX5 binding the major groove of DNA.[122,126,271] While TBX5-G145R maintained some capacity to bind specific DNA targets; TBX5-G80R generated no detectable complex formation in EMSAs (**Fig 22C**). We assessed the functional impact of TBX5-G145R on transcriptional activation using a NPPA-luciferase reporter assay. TBX5 (wild-type, G145R, or G80R) was co-transfected with the reporter construct in human embryonic kidney cells (HEKs). Cells transfected with TBX5-G145R had 37% the luciferase activity of wild-type TBX5 while TBX5-G80R had similar activity to a no TBX5 control condition (**Fig 22D**). Based on these biochemical assays of DNA binding and transcriptional activation, TBX5-G145R is a partial loss of function variant.

TBX5-G145R causes subtle features of Holt-Oram syndrome

Loss of function variants in TBX5 commonly cause the human condition Holt-Oram syndrome (HOS) defined by upper limb abnormalities and, in a subset of patients, heart pathology. While malformation of the upper extremities in the individual is required for the diagnosis of HOS, the heart involvement can either be present in the individual and/or through family history of heart malformations or cardiac conduction disease.[272] After determining TBX5-G145R is a partial loss of function variant, we evaluated the *TBX5 c.G433A* carriers for HOS clinical phenotypes of structural abnormalities of the hands and heart by X-ray and echocardiography, respectively. No evaluated family members had structural alterations in the

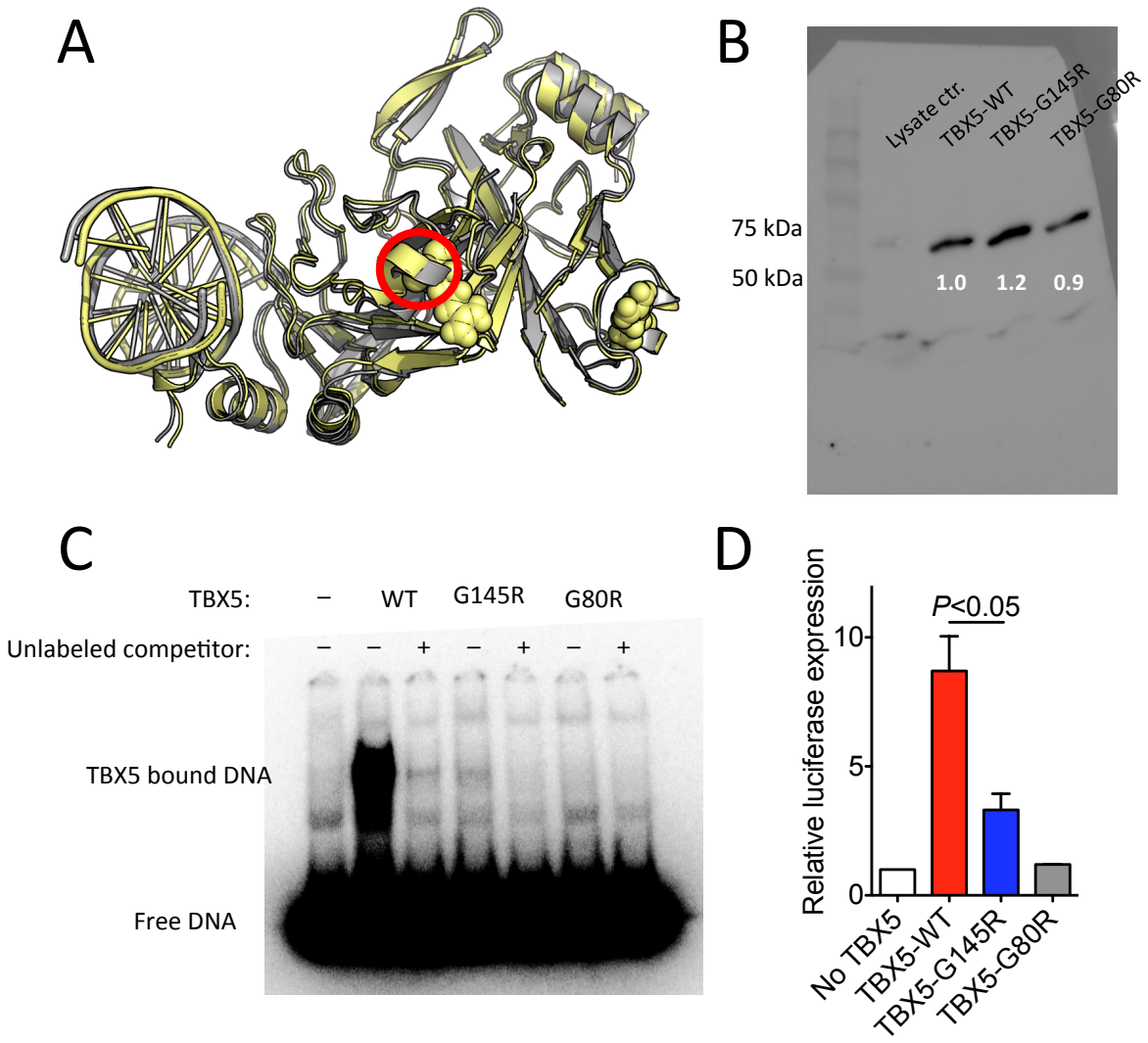

Figure 22. TBX5-G145R impairs DNA binding and transcriptional regulation. (**A**) Rosetta modeling predicted TBX5-G145R destabilizes protein-DNA interactions. Grey indicates published wild-type TBX5 bound to *NPPA* promoter. Yellow indicates predicted TBX5-G145R structure. Modeling done in collaboration with Brett Kroncke, PhD. (**B**) Wild-type and mutant TBX5 (65 kDa) are expressed at similar levels (n=3 experiments). kDa = kiloDaltons. (**C**) Electrophoretic mobility shift assay demonstrated TBX5-G145R has reduced DNA binding capacity compared to wild-type protein. TBX5-G80R included as loss of function control variant. (**D**) TBX5-G145R had reduced luciferase activity compared to WT.

heart, although the family reports atrial and ventricular septal defects in the extended family. X-ray analysis of one family member identified bilateral hypoplasia of the thenar musculature confirming a diagnosis of HOS. Also observed on X-ray was prior surgical fusion along the radial aspect of the right wrist, performed for treatment of scaphotrapezial arthritis, and all other bones of the hand were evaluated as normal (**Fig 21D**). It is unknown if the scaphotrapezial fusion was related to mal-development of the hand or an unrelated pathology. Thenar muscular hypoplasia has been reported as a variable manifestation of HOS.[273] The extent of reduced DNA binding and transcriptional activation of TBX5-G145R is consistent with other *TBX5* variants identified in HOS[274] but the family pedigree presented here is the first implication of *TBX5* in BrS pathogenesis.

Generation of a human iPSC-CM model of BrS

In order to study TBX5-G145R in the context of a human cardiomyocyte, dermal fibroblasts were isolated from a 26-year old woman from the described family diagnosed with BrS who carries the *TBX5* variant (asterisk in **Fig 21C**). Using non-integrating episomal expression vectors to transiently express reprogramming factors, we established multiple induced pluripotent stem cell (iPSC) clones. Each line expressed stem cell-associated proteins OCT4, SSEA3, and alkaline phosphatase (**Fig 23A**). Non-directed differentiation of iPSCs using embryoid body protocols generated cells of each of the three germ layers, establishing pluripotency characteristics (**Fig 23B**). All reprogrammed and validated lines tested were capable of differentiation through chemical modulation of Wnt signaling to cardiomyocyte lineage (**Fig 23C**). Lastly, the cells that acquired large chromosomal abnormalities during the process of reprograming from dermal fibroblasts to iPSCs were excluded from further studies (**Fig 23D** and

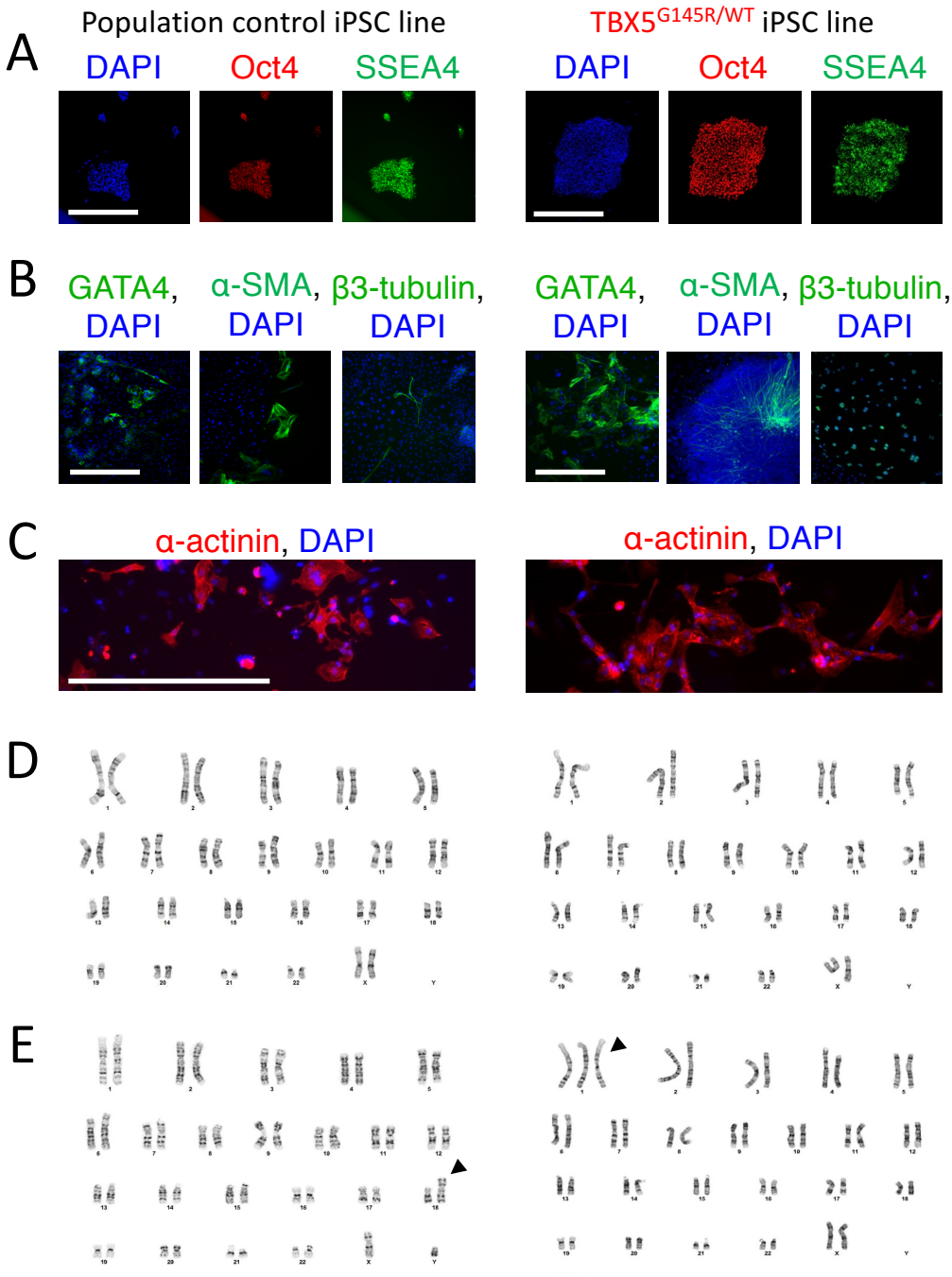

Figure 23. iPSC generation and validation. (**A**) iPSC colony express stem cell-associated proteins (**B**) Embryoid body differentiation to three germ layers demonstrates iPSC pluripotency: endoderm (GATA4), mesoderm (α-SMA), ectoderm (β3-tubulin). Scale bars = 50 microns. (**C**) All lines studied efficiently differentiate to cardiomyocytes (marked by α-actinin). (**D**) Multiple iPSC clones were identified that maintained a normal karyotype from each donor. (**E**) iPSC clones determined to have abnormal karyotypes were removed from the study. Black arrowheads indicate representative abnormalities.

23E). iPSCs were also generated and validated from somatic cells obtained from four population control donors.

TBX5 variant correction in patient-derived iPSCs

To directly test if TBX5-G145R caused the BrS phenotype, we edited the *TBX5 c.G433A* missense variant back to the reference sequence using the RNA-guided Cas9 nuclease system. Genome targeting occurs through gRNA binding through complementation to specific DNA sequences.[275] The Cas9 protein scans the genome by pausing at defined trinucleotide sequences, known as the PAM, and, when adjacent to gRNA-DNA, hybridizes to induce a conformation change in Cas9 exposing the active nuclease domains.[276,277] Cas9 derived from *S. pyogenes* uses a PAM sequence of NGG, where N can be any nucleotide. The Cas9 conformational change leads to the generation of a double strand break five base pairs away from the PAM site. Specific modifications to the genome can be achieved when active Cas9 is delivered in the presence of excess repair template to promote homology-directed repair (HDR; **Fig 24A**). This approach was carried out in patient-derived iPSCs and plated for clonal screening. PCR amplicons of genomic DNA containing the wild-type sequence of *TBX5* is selectively digested with the restriction enzyme NciI and this difference in restriction site between wildtype and G145R was utilized to screen for edited cells. Targeting exon5 of *TBX5* with CRISPR/Cas9 repaired the missense variant present in familial BrS with HDR efficiency of 30% (**Fig 24B**). Initial efforts used a template that attempted to generate a single nucleotide change to correct only *TBX5* c.G433A but all clones that screened positive by restriction digest contained secondary insertion/deletion (indel) variants due to repeat targeting of Cas9. As long as Cas9 is expressed and gRNA is present, the nuclease activity remains active due to the maintained presence of the PAM site.

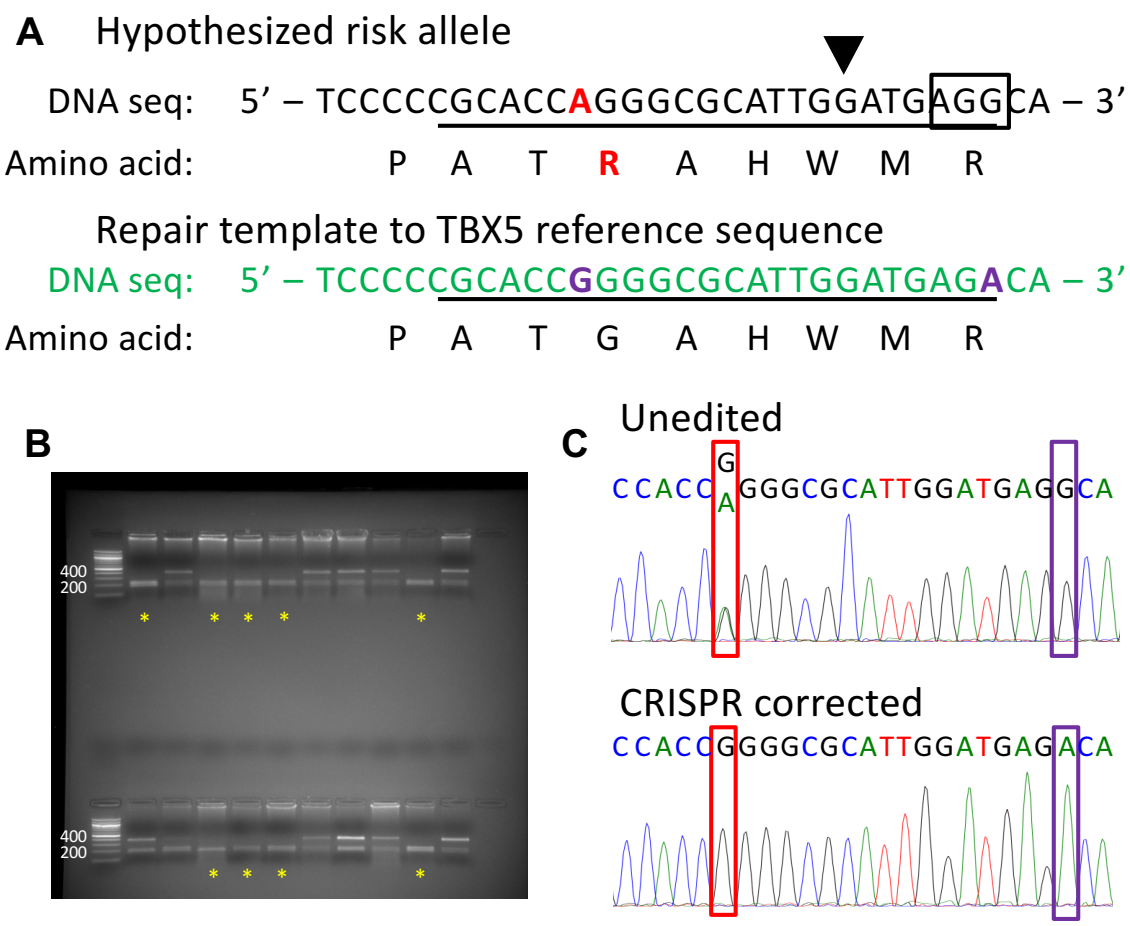

Figure 24. TBX5 variant correction in patient-derived iPSCs. (**A**) Schematic of genome editing approach using CRISPR/Cas9 in patient-derived iPSCs. Risk single nucleotide variant indicated as red text. Purple letters indicate nucleotide changes in repair template. Arrow head indicates cut site by Cas9. The black box indicates the protospacer adjacent motif (PAM). (**B**) NciI restriction digest of 400 bp TBX5 PCR product. The NciI cut site is present in wild-type sequence but not c.G433A. A yellow star indicates *TBX5* edited to homozygous wild-type sequence. Unlabeled lanes indicate iPSCs heterozygous for G145R. (**C**) Sanger sequencing of PCR amplified exon 5 of *TBX5* unedited (upper panel) and edited to reference sequence (lower panel). Red box indicates c.433 and the purple box indicates c.449.

Therefore, repeat efforts introduced two nucleotide alterations in the repair template, correction of the *TBX5* variant and a silent SNV that disrupted the PAM sequence. This approach successfully prevented retargeting by Cas9 to generate multiple subclones with the two nucleotide changes that repair *TBX5* c.G433A (p.G145R) and disrupt the PAM site (c.G449A; p.R150R) (**Fig 24A** and **24C**). Nonspecific genomic changes due to off-target Cas9 activity were evaluated by Sanger sequencing of *in silico* determined potential off-target sequences (**Table 10**).

TBX5-G145R containing iPSC-CMs recapitulate the BrS phenotype of reduced sodium channel expression and current

Reduced sodium current is the most common mechanism of inherited BrS due to reduced channel expression or loss of function variants in *SCN5A* or genes encoding $Na_V1.5$-associated proteins. We first tested the hypothesis that TBX5-G145R causes reduced sodium channel expression and thus the BrS phenotype in the study family. Population controls were used to define "normal" levels of sodium channel transcript and protein. Isogenic controls generated by genome editing with Cas9 directly tested the changes in sodium channel expression compared to $TBX5^{G145R/WT}$ iPSC-CMs. $TBX5^{G145R/WT}$ iPSC-CMs have significantly reduced levels of *SCN5A* transcript while expression of *TBX5* is unchanged compared to both population and isogenic controls ($P<0.05$; **Fig 25A**). Expression of *SCN5A* or *TBX5* is not significantly different between population and isogenic control groups. To confirm the mRNA quantification reflects the actual amount of sodium channel at the cell surface, we performed biotinylation experiments to semi-quantitatively compare the amount of voltage-gated sodium channel present in each group. Similar to the transcript level analysis, $TBX5^{G145R/WT}$ iPSC-CMs have approximately half of the amount of $Na_V1.5$ protein in whole-cell lysate and membrane-associated fraction (**Fig 25B).**

Table 10. *In silico* predicted CRISPR/Cas9 off-target sites.

Potential off-target complementation	Number of mismatches [variable nucleotide]	Genomic position	Forward sequencing primer	Reverse sequencing primer
CCACTGGTGCACATTGGATGCGG	3MMs [5:8:11]	chr16:-30100319	GAGGCCCGCTACTTGTTTCT	GGTGAGCTTGACACGATGGA
CCCCGGGGAGGCATTGGATGGGG	4MMs [3:5:9:10]	chr11:+119599131	CAGCTGACCTGGATCCTTCG	CAAGCCGTGACCCAACTTTT
CCACAGGCGCACCTTGGATGTGG	4MMs [5:8:11:13]	chr17:-72345473	AACGTCTCCTACCACATCGC	AAGGTGGGGTTGGGAAATCG
CCCCGGGGGCTCATGGGATGTGG	4MMs [3:5:11:15]	chr1:-203830934	TCAGGACTAGGAGGTTCGGG	GTCCATTCCTGCATTCCCCA
CCAAGGGCGCGCAGTGGATGAAG	4MMs [4:5:8:14]	chr22:+19751765	ACAGGGTGTCCAGTTCCTTG	TTCTACAGGCCTCTTAGGGACA
CCACTGGGGCCTATTGGATTTGG	4MMs [5:11:12:20]	chr2:-31412447	GCAGATGACCTAACCCGTCT	ACCCTGAGGACGAACTCTGA
CCGCCGGCGCTCATTGGCTGGGG	4MMs [3:8:11:18]	chr11:-134201815	CTGCAGGCGCGGAGC	AGCTCCCAGAAAGAAGCAGC
CCACAGGAGCCCACTGGATGCGG	4MMs [5:8:11:14]	chr17:+59544934	GGTGGGACCAGCAGCTATTT	CCCGGAGTGGATTCTCCCTA
CCACCGTAGCACATTGGTTGTAG	4MMs [7:8:11:18]	chr11:+14901717	TGGATTGGCATCCTGCCTTT	TATACTTGGCTGGCATCGCA
CCACGGGGGCACATTGGCAGGGG	4MMs [5:11:18:19]	chr16:-89265840	GGATGAAGGTTGGACCCTGG	AGGGTACTCACGAGCCAGAT
CCACCGGGGTGGCGTGGATGGGG	4MMs [10:12:13:14]	chr7:+134931463	GACTGGCAGCGGGATCATTA	CTGCACCTCCAACCTGCTAA
CCACCGTGGCACATGGGGTGAGG	4MMs [7:11:15:18]	chr7:+5519995	GACATCCTCCTGGCATCTGAG	GCAAGGAGCTGCTGAAAACC
CCACCTGGGCGCGCTGGGTGAGG	4MMs [6:13:14:18]	chr16:-30596717	TCTCCCGAGGAGTGGGAATG	ACGGGAGGGGAGAATGAGAC

To evaluate the effect of reduced sodium channel expression on the generation of sodium current, we performed whole cell voltage-clamp experiments after 35 days of differentiation. The result paralleled the mRNA result in that $TBX5^{G145R/WT}$ iPSC-CMs displayed ~50% reduced peak sodium current (-97±35 pA/pF) compared to the control groups (population: -211±36; isogenic: -213±38) for a test voltage of -30mV ($P<0.05$; **Fig 25C** and **25D**). TBX5-G145R cells demonstrate the electrophysiologic hallmark of BrS, reduced sodium current, and in this instance the reduction is attributable to reduced *SCN5A* expression without altering the kinetics of channel activation, consistent with murine heterozygous germline Scn5a knockout models (**Fig 25E**).[73,74] However, the comparison of population controls and TBX5-G145R cells did not establish that the mutation causes the phenotype. It is the result of the genomic editing experiment, showing reversal of the transcriptional and electrophysiologic defect, that proves that TBX5-G145R is the cause of the functional defect, and thus the BrS phenotype, in this family.

Unexpected arrhythmogenic late sodium current and APD lability in patient-derived iPSC-CMs are caused by TBX5-G145R

SCN5A-associated Long QT Syndrome mutations generate a persistent ("late") sodium current (I_{Na-L}) usually through defective fast inactivation.[46] Some *SCN5A* mutations, such as E1784K and 1795insD in the cytoplasmic c-terminus, result in overlap BrS and Long QT type 3 (LQT3) syndromes, characterized by both decreased peak current and increased late current.[278,279] Interestingly and unexpectedly, $TBX5^{G145R/WT}$ iPSC-CMs had increased I_{Na-L} measured at the end of a 200-msec test pulse (-30 mV) that was not appreciably measured in any of the population control lines studied (**Fig 26C** and **26D**). Treatment of $TBX5^{G145R/WT}$ iPSC-CMs with 3 μM ranolazine, the late sodium current blocker, completely eliminated I_{Na-L}

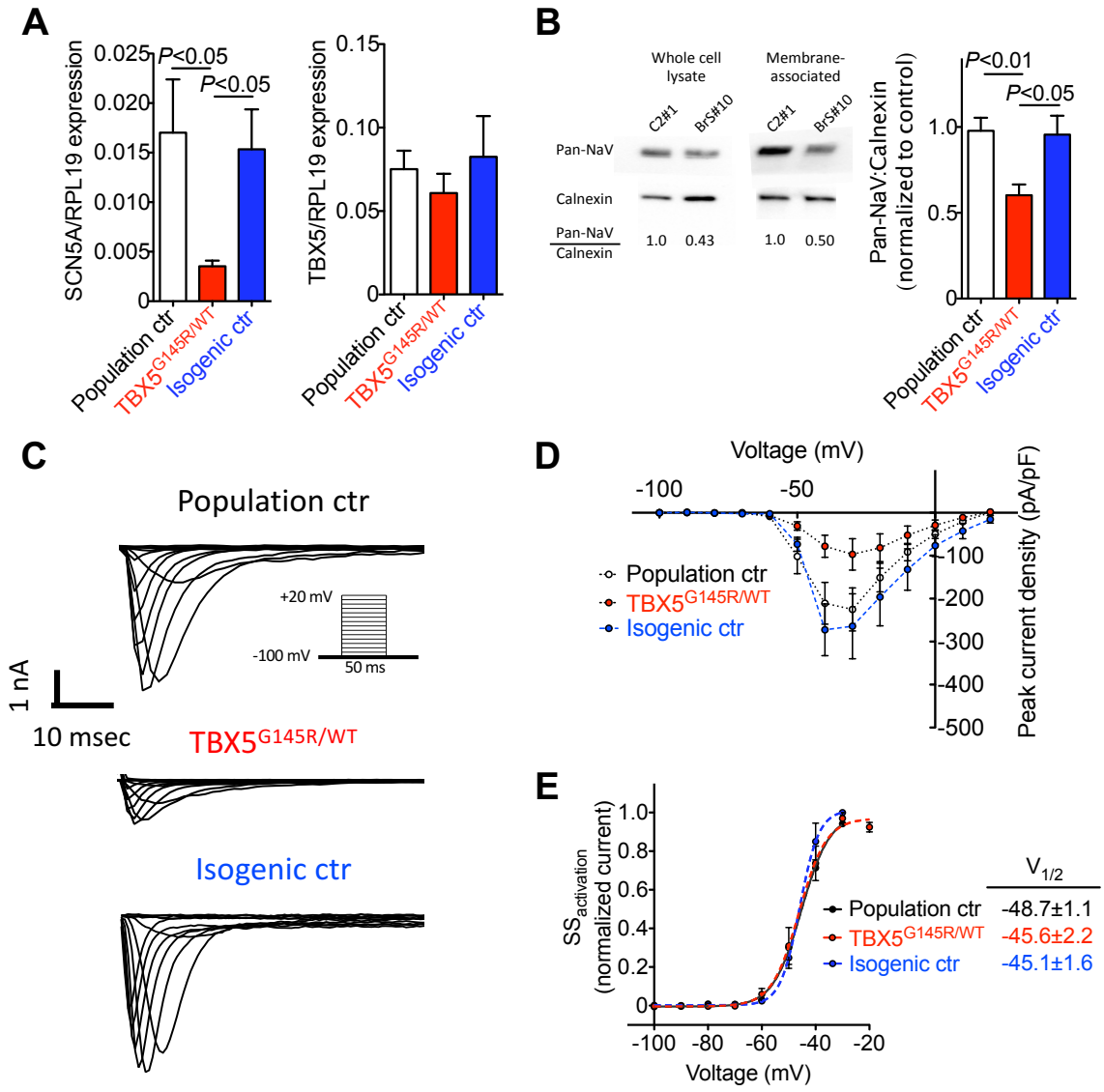

Figure 25. BrS iPSC-CM have reduced sodium channel expression and current density. (**A**) TBX G145R iPSCs have reduced mRNA levels of SCN5A normalized to RPL19 transcript, and this is corrected by Cas9-mediated correction of the mutation. (**B**) Western blot analysis of membrane-associated sodium channel demonstrates TBX5-G145 variant causes reduced protein expression. (**C**) Representative whole cell voltage clamp recordings at voltage steps from -100 to 20 mV in 10 mV increments. (**D**) BrS iPSC-CMs have decreased sodium current density compared population and isogenic controls. (**E**) Steady-state activation kinetics were unaltered by TBX5-G145R. Ctr = control.

(**Fig 26C** and **26D**).[280] The $I_{Na\text{-}L}$ phenotype is caused by the heterozygous TBX5-G145R variant as it was also abolished with genomic editing of the variant back to the reference sequence.

A published iPSC-CM model of LQT3 recapitulates the cellular LQTS phenotype of prolonged action potential duration (APD) and arrhythmogenic afterdepolarizations.[266] Accordingly, we recorded action potentials in whole-cell current clamp experiments. The presence of TBX5-G145R did not alter resting membrane potential or action potential amplitude (**Fig 27A**), but did prolong time to 90% repolarization (APD_{90}) (**Fig 27B)**.[281] Early afterdepolarizations were observed in $TBX5^{G145R/WT}$ iPSC-CMs (12% of cells) but were not found in any cell studied from either control group or after exposure to 3 μM ranolazine (**Fig 27C**).

In healthy stem cell-derived cardiomyocytes, the APD from beat-to-beat is largely consistent (**Fig 27D**).[282] As demonstrated by superimposing 20 action potentials recorded from a single iPSC-CM, iPSC-CMs containing the *TBX5* variant have significant APD heterogeneity that is completely resolved by pharmacologic blockade of $I_{Na\text{-}L}$ with ranolazine or with genomic correction of TBX5-G145R (**Fig 27D**). Poincaré plots, the duration of one action potential (APD_n) plotted against the APD of the subsequent beat (APD_{n+1}), provide a graphical representation of APD variability and permit quantitative assessment of short term variability (STV), long term variability (LTV), and the area of plotted points for a single cell.[283] STV and LTV terms were similar between population and isogenic controls and significantly increased in $TBX5^{G145R/WT}$ iPSC-CMs (**Table 11**). Block of $I_{Na\text{-}L}$ with ranolazine prevented APD variability in myocytes containing TBX5-G145R supporting late sodium current as a mechanism of APD lability. Other studies have demonstrated that chemical enhancement of $I_{Na\text{-}L}$ with ATX-II or veratridine in canine ventricular cardiomyocytes increased STV and APD_{90}.[284] Our findings

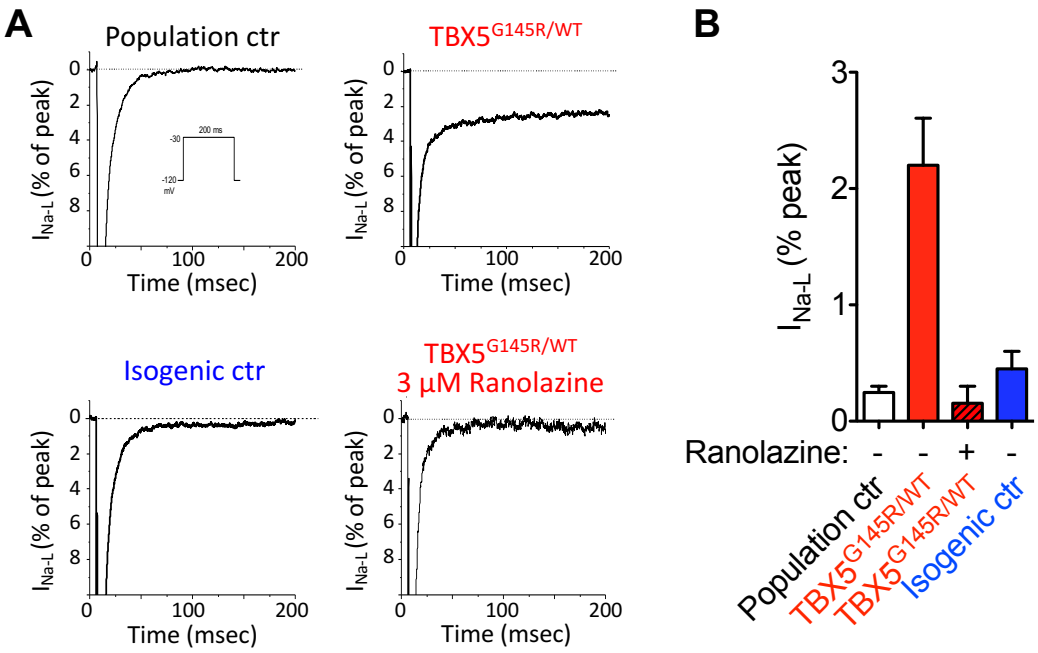

Figure 26. BrS iPSC-CM have increased late sodium current. (**A**) Representative sodium current recordings highlighting late current. (**B**) Increased late current is caused by TBX5 c.G433A and selectively blocked by 3 µM ranolazine (*n*=7-8 per group). Ctr = control. Data collected in collaboration with Tao Yang, PhD.

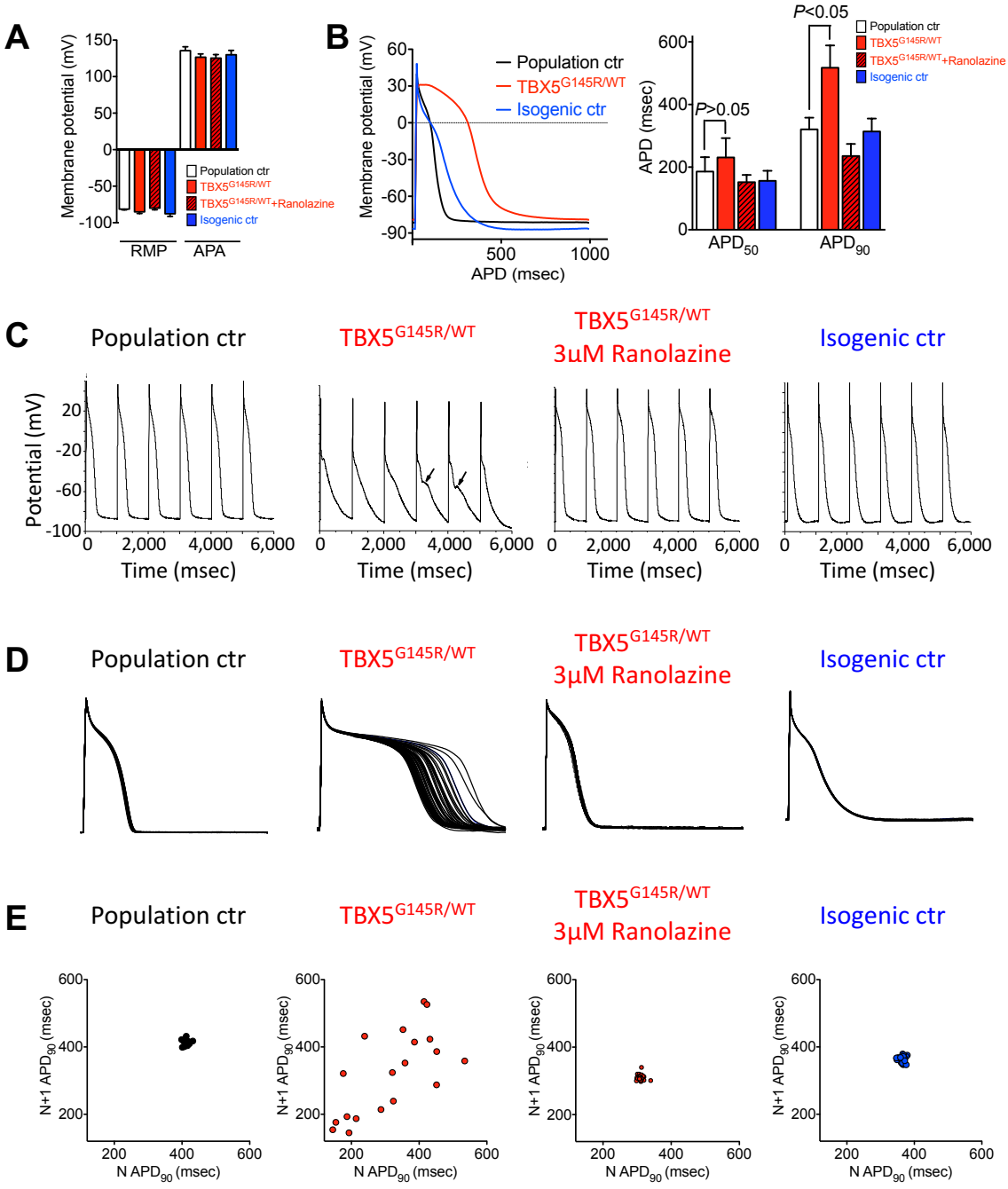

Figure 27. Arrhythmogenic changes in cardiac action potential in TBX5-G145R containing iPSC-CMs. (**A**) Population control, isogenic control, and TBX5$^{G145R/WT}$ iPSC-CMs have similar resting membrane potential (RMP) and action potential amplitude (APA) (**B**) TBX5-G145R containing iPSC-CM have prolonged APD_{90} but not APD_{50}. (**C**) Early afterdepolarizations were observed in TBX5-G145R containing iPSC-CM but not in population or isogenic control cells. (**D**) Superimposed action potentials demonstrate APD variability caused by TBX5-G145R. (**E**) Representative Poincaré plots comparing the APD of each beat (APD_N) to subsequent beat APD (APD_{N+1}). See table 11 for summative data. All recorded action potential were stimulated at 1 Hz. Ctr = control. Data collected in collaboration with Tao Yang, PhD.

provide further evidence that inward sodium current is a driving ionic mechanism of APD variability.

Calcium handling is not impacted by TBX5-G145R

An alternative mechanism of afterdepolarization generation is inappropriate calcium release from the sarcoplasmic reticulum. We used the calcium indicator dye Fura-2AM to interrogate the impact of TBX5-G145R on calcium handling properties of cardiomyocytes. $TBX5^{G145R/WT}$ iPSC-CMs have similar levels of diastolic calcium levels compared to control groups (**Table 12**). When pacing at 0.2 Hz, TBX5 variant containing myocytes were capable of capturing pacing stimuli in 43% of cells studied compared to 78% across multiple control lines analyzed, consistent with descriptions of decreased cardiomyocyte excitability due to reduced sodium current.[285] Of cells that were capable of stimulus capture, the amount of calcium released during each beat, determined by peak height, and kinetics of calcium removal from the cytoplasm was unchanged in $TBX5^{G145R/WT}$ iPSC-CMs (**Fig 28A** and **Table 12**). Total sarcoplasmic reticulum (SR) calcium was evaluated by perfusing 10 mM caffeine over the cell to fully unload the SR. This showed that calcium loading into the SR was not impacted by TBX5-G145R based on peak height after caffeine exposure (**Table 12**). The calcium imaging experiments also highlighted the arrhythmogenic nature of $TBX5^{G145R/WT}$ iPSC-CMs as triggered beats were observed in 8.3% of cells studied during the repolarization phase of the excitation-contraction cycle and at times degenerated into a tachycardic pattern (**Fig 28B**).

Table 11. Poincaré analysis of single iPSC-CM APD.

Group	STV	LTV	STV:LTV	Scatter area ($msec^2$)
Population control	3.21±0.65	4.22±0.82	0.78±0.08	50.85±15.36
$TBX5^{G145R/WT}$	16.42±3.0*	27.93±5.71*	0.71±0.13	1567.0±377.3*
$TBX5^{G145R/WT}$ +ranolazine	2.81±0.78	3.09±1.04	1.0±0.11	45.59±24.37
Isogenic control	8.05±1.83	8.35±1.98	0.97±0.09	276.0±123.4

* $P<0.05$ compared to all other groups studied.

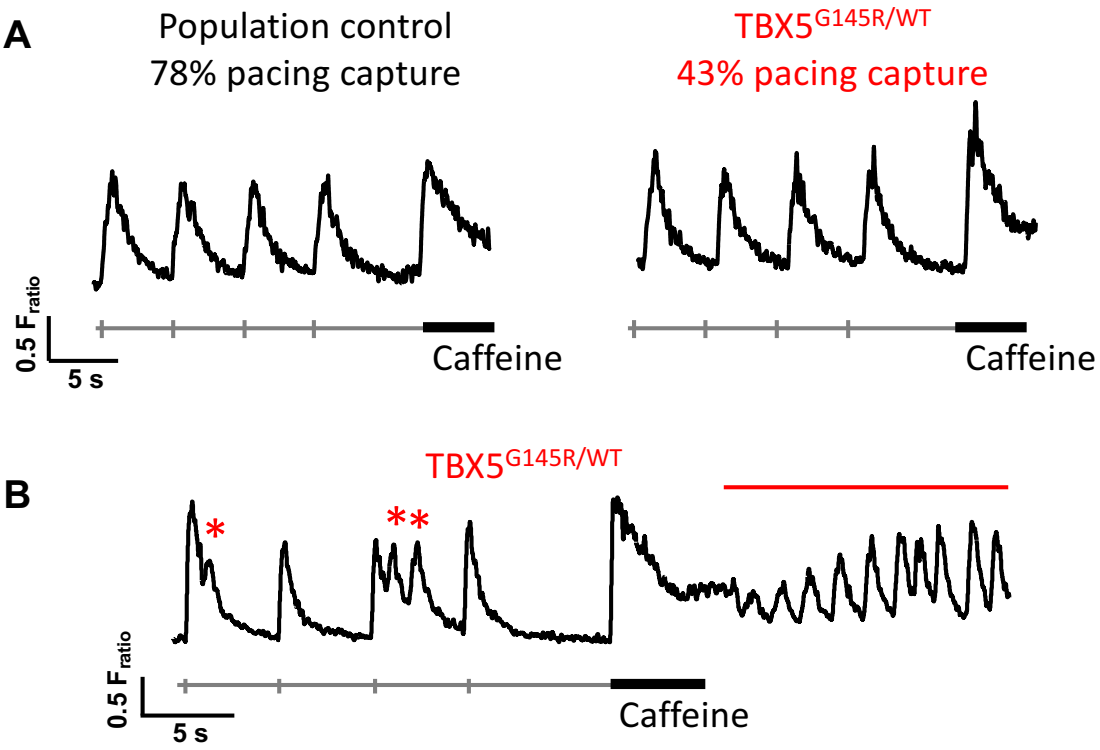

Figure 28. TBX5-G145R iPSC-CMs reduced capture efficiency and arrhythmia activity by calcium evaluation. (**A**) Representative calcium transients of iPSC-CM with 1:1 capture recorded at 0.2Hz pacing rate. See Table 12 for summative data. (**B**) TBX5-G145R containing iPSC-CMs display single (red asterisks) and multiple afterdepolarizations (red line). Data collected in collaboration with Kyunsoo Kim, PhD and Bjorn Knollmann, MD, PhD.

Table 12. Calcium handling properties in TBX5$^{G145R/WT}$ iPSC-CMs.

	Population ctr	TBX5$^{G145R/WT}$	Isogenic ctr
n	30	12	8
Calcium transient height (F_{ratio})	1.19 ± 0.02	1.11 ± 0.10	0.76 ± 0.10
Calcium transient t_{10} (s)	0.21 ± 0.02	0.17 ± 0.2	0.26 ± 0.05
Calcium transient t_{50} (s)	0.95 ± 0.06	0.85 ± 0.7	1.06 ± 0.13
Calcium transient t_{90} (s)	2.60 ± 0.11	2.46 ± 0.15	2.82 ± 0.27
Calcium transient decay rate (s)	1.52 ± 0.11	1.21 ± 0.07	1.55 ± 0.22
SR calcium content (F_{ratio})	1.21 ± 0.08	1.17 ± 0.09	1.46 ± 0.19

Ctr = control

SR = sarcoplasmic reticulum

No significant difference among groups for all parameters. Data analyzed using one-way ANOVA with Bonferroni post-test.

Tissue-level model of TBX5-G145R containing cardiomyocytes exhibit arrhythmogenic features observed in single-cell assays

The arrhythmogenic features of increased I_{Na-L} and APD variability caused by TBX5-G145R were observed in assays evaluating function of single cardiomyocytes. APD variability is reduced in the tissue context of the whole heart or cardiomyocyte monolayers.[286] Therefore, to probe the impact of the single-cell arrhythmogenic phenotype in a tissue context, we assayed the electrical properties of spontaneously beating monolayers of iPSC-CMs using extracellular field potentials (EFPs; Nanion technologies). Endogenous beat rate, beat-to-beat variability, and detection of arrhythmogenic afterdepolarizations can be evaluated using EFP analysis.[287] Population and isogenic controls groups had rapid beat rates of 100 beats/min that occurred at regular intervals (**Fig 29A**). Poincaré plots displayed similar findings to single cell assays of manual patch-clamp experiments as $TBX5^{G145R/WT}$ iPSC-CM monolayers had larger STV and APD variability, both of which were significantly reduced by 3 μM ranolazine (**Fig 29C** and **Table 13**). Additionally, monolayers of $TBX5^{G145R/WT}$ iPSC-CMs also exhibited arrhythmic behaviors of triggered afterdepolarizations (**Fig 29B**). This monolayer assay evaluated the cumulative alteration in electrical behavior in 65,000 iPSC-CMs and dampened the inherent limitation of cell-to-cell heterogeneity frequently described in iPSC-CMs.

Discrete transcriptional changes in TBX5-G145R relative to iPSC-CMs with TBX5 heterozygous deletion

Genomic editing in patient-derived iPSCs provided strong evidence that TBX5-G145R causes reduced sodium channel expression and current in this family. Further, by generating and modifying these lines, we found that TBX5-G145R unexpectedly resulted in arrhythmogenic

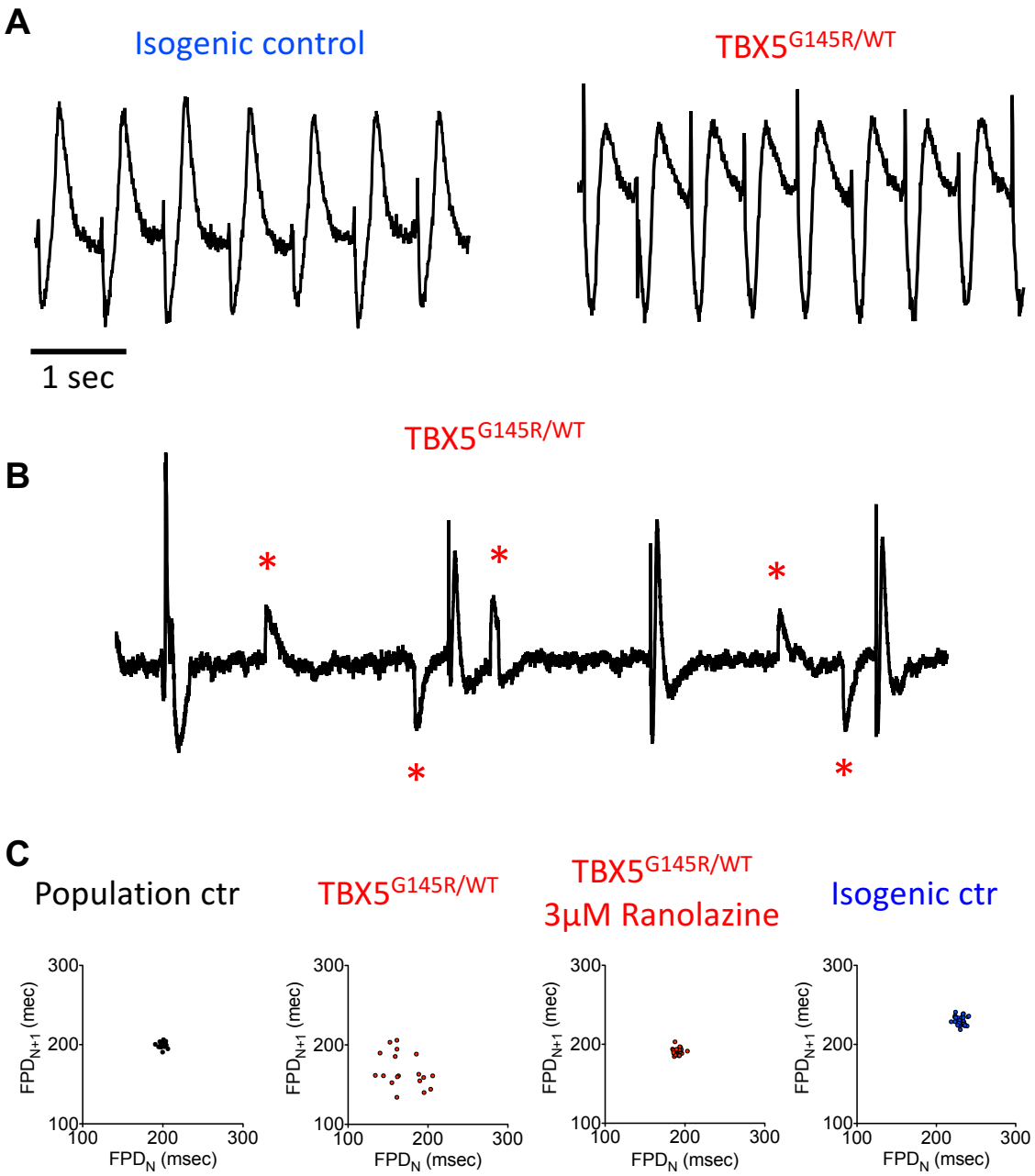

Figure 29. TBX5-G145R containing iPSC-CM monolayers have arrhythmogenic features observed at single-cell level. (**A**) Representative extracellular field potentials recorded from isogenic controls and TBX5$^{G145R/WT}$ iPSC-CM monolayers. (**B**) TBX5$^{G145R/WT}$ iPSC-CM monolayers display afterdepolarizations (red asterisks). (**C**) Representative Poincaré plots comparing the FPD of each beat to the FPD of the subsequent beat. See Table 13 for summative data. All recordings are of spontaneous activity. Data collected in collaboration with Shan Parikh and Bjorn Knollmann, MD, PhD.

Table 13. Poincaré analysis of iPSC-CM monolayer FPD.

Group	STV	LTV	STV:LTV	Scatter area ($msec^2$)
Population control	4.04±0.77	4.40±1.02	0.99±0.06	96.3±46.8
$TBX5^{G145R/WT}$	11.25±2.13*	12.86±2.78*	0.91±0.06	640±229*
$TBX5^{G145R/WT}$ +ranolazine	4.66±0.71	5.29±0.65	0.87±0.73	82.7±22.0
Isogenic control	6.51±0.69	6.04±0.66	1.10±0.06	141±31.6

* $P<0.05$ compared to all other groups studied.

features (increased $I_{Na\text{-}L}$ and APD variability). *TBX5* loss of function variants, mostly nonsense or frameshifting indel mutations that lead to haploinsufficiency, typically cause Holt-Oram syndrome, with severe cardiac and upper limb structural birth defects,[272] but the arrhythmogenic features caused by TBX5-G145R are not described in HOS. One question raised by these findings is why does TBX-G145R, unlike usual HOS variants, lead to a prominent arrhythmia phenotype with a structurally normal heart? One possibility is that the missense variant causes a mild, or perhaps even subclinical, manifestation of Holt-Oram syndrome (*e.g.* the thenar abnormality seen in **Fig 21D**) and overt Brugada syndrome compared to other *TBX5* variants that cause more typical HOS presentations. This hypothesis would predict that the transcriptional consequences of the TBX5-G145R variant diverge from those with a more typical HOS variant.

RNA transcription in a cell is highly regulated and genetic variation that alters transcription factor function can have a large impact on the transcriptome. To compare the transcriptional consequences of TBX5-G145R to a more typical HOS variant, we took advantage of the error prone mode of double-stranded DNA break repair, non-homologous end joining (NHEJ)[288] to generate TBX5 heterozygous knockout lines. We transiently expressed Cas9 and a gRNA targeting exon 5 of *TBX5* without a repair template in $2X10^6$ iPSCs. We sequenced and identified three clones containing unique heterozygous frameshifting indels in isogenic controls ($TBX5^{-/WT}$; **Fig 30A-C**). The three clones have either a deletion of 16-bp, a deletion of 22-bp, or an insertion of 1-bp. These $TBX5^{-/WT}$ lines change the amino acid sequence between position 144 and 148 with all clones having a resultant premature stop codon between amino acid 166 and 182 (**Fig 31**). A similar one base pair deletion has been described in HOS altering the amino acid sequence beginning at position 138 and a premature stop codon at position 148.[289] We have generated the first HOS iPSC-CM model allowing us to compare changes in transcription in the

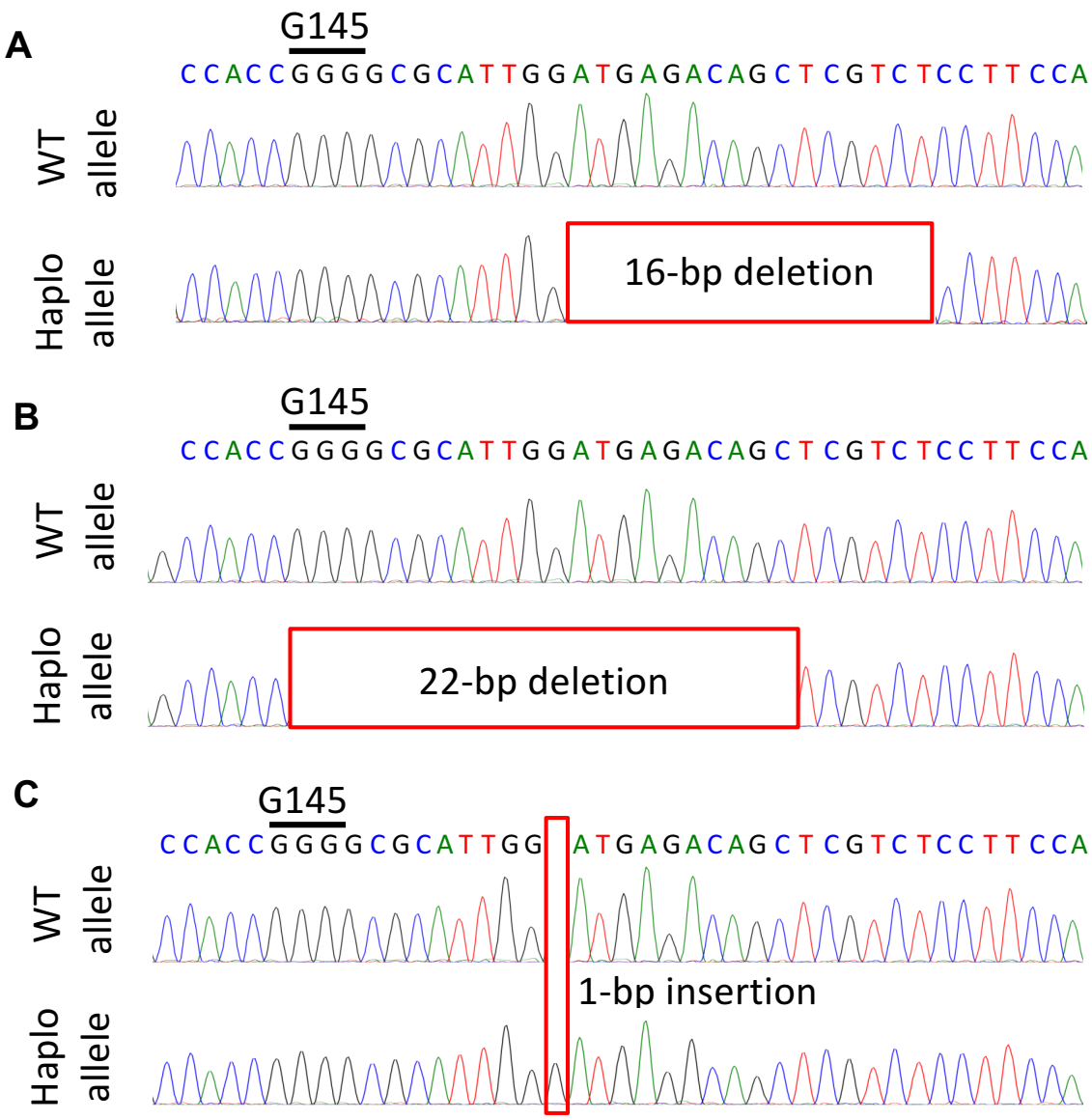

Figure 30. iPSC model of Holt-Oram syndrome. (**A**) Allele-specific sequencing of frame-shifting heterozygous 16-bp deletion. (**B**) Allele-specific sequencing of frame-shifting heterozygous 22-bp deletion. (**C**) Allele-specific sequencing of frame-shifting heterozygous 1-bp insertion.

Figure 31. Predicted amino acid sequence in TBX5 heterozygous deletion model.

G145R missense variant found in BrS compared to TBX5 heterozygous knockout.

In mice, homozygous germline deletion of *Tbx5* is embryonic lethal.[143] Through the generation of the iPSC lines with heterozygous deletion of *TBX5*, we also created lines with homozygous indels in the gene. It was our observation that homozygous indels in *TBX5* render human iPSCs incapable of differentiation into cardiomyocytes. This is in contrast to a recent report using a mouse ESC-CM model possessing a homozygous deletion of Tbx5.[290] As an additional comparison group, we also generated lines that are homozygous for the missense variant ($TBX5^{G145R/G145R}$) using the same HDR targeting approach that created isogenic controls (**Fig 24**). Surprisingly, all $TBX5^{G145R/G145R}$ lines created were capable of differentiation into cardiomyocytes, supporting the findings of biochemical assays that TBX5-G145R is a partial loss of function variant (**Fig 22**).

To determine the transcriptional effects of TBX5 variation in iPSC-CMs, we performed RNA-sequencing on population controls, isogenic controls, $TBX5^{G145R/WT}$ (heterozygotes), $TBX5^{G145R/G145R}$ (homozygotes), and $TBX5^{-/WT}$ cell lines. We isolated RNA from 2-4 replicates per group and generated ribo-depleted Illumina sequencing libraries to generate 46-66 million reads per sample. A standard Bowtie/Tophat/Cufflinks read mapping and differential expression pipeline identified genes that were differentially expressed between samples. $TBX5^{-/WT}$ iPSC-CMs had substantially altered gene expression to the other samples with an average of 266 genes differentially expressed when compared any other group studied (Range 180-400; **Fig 32A**). All other pairwise group comparisons had between 52-96 genes differentially expressed, again, supporting the biochemical evidence that TBX5-G145R is a partial loss of function variant. Unsupervised hierarchical clustering verified that $TBX5^{-/WT}$ lines have distinct expression patterns compared to all other groups (**Fig 32B**). TBX5-G145R seemed to result in discrete

transcriptional changes as TBX5$^{G145R/G145R}$ iPSC-CMs clones cluster together and fall under the same branch as the heterozygous variant containing myocytes, isogenic controls, and population controls (**Fig 32B**). Of the 51 genes differentially expressed between TBX5$^{G145R/WT}$ and isogenic controls, 31 were also differentially expressed when comparing isogenic controls and TBX5$^{-/WT}$ (**Fig 32C**). An additional 189 non-overlapping genes are also differentially expressed between comparing isogenic controls and TBX5$^{-/WT}$.

A heatmap displaying the top 50 significantly upregulated and downregulated genes in TBX5$^{-/WT}$ compared to isogenic controls (sorted by fold change of genes with $P<0.00015$) indicated that all other lines studied are highly dissimilar to iPSC-CMs with a complete loss of one *TBX5* allele (**Fig 33A**). We generated a heatmap of expression changes in BrS-associated genes, including only genes with defined functional mechanisms,[291] to interrogate the effect of TBX5 variation on expression of these genes. The heatmap shows that *SCN5A* expression is commonly reduced in myocytes with any type of *TBX5* variation, consistent with the qRT-PCR data presented in Figure 23. All other genes rarely associated with BrS genes have similar expression in all groups, including *TBX5* (**Fig 33B**).

To investigate the extent of genome wide transcriptional changes that occur in iPSC-CMs generated from a BrS patient containing heterozygous TBX5-G145R compared to the Cas9-mediated generated isogenic controls, we generated a volcano plot (**Fig 33C**). Plotting the fold-change between these groups against the significance of differential expression shows modest differences in expression profiles. The genes that show a significant difference in expression level in this plot likely underlie the reduced sodium channel expression and current observed in this variant. As presented in **Figure 25**, TBX5-G145R caused reduced sodium channel expression and the electrophysiologic signature of BrS, reduced sodium current influx. Since

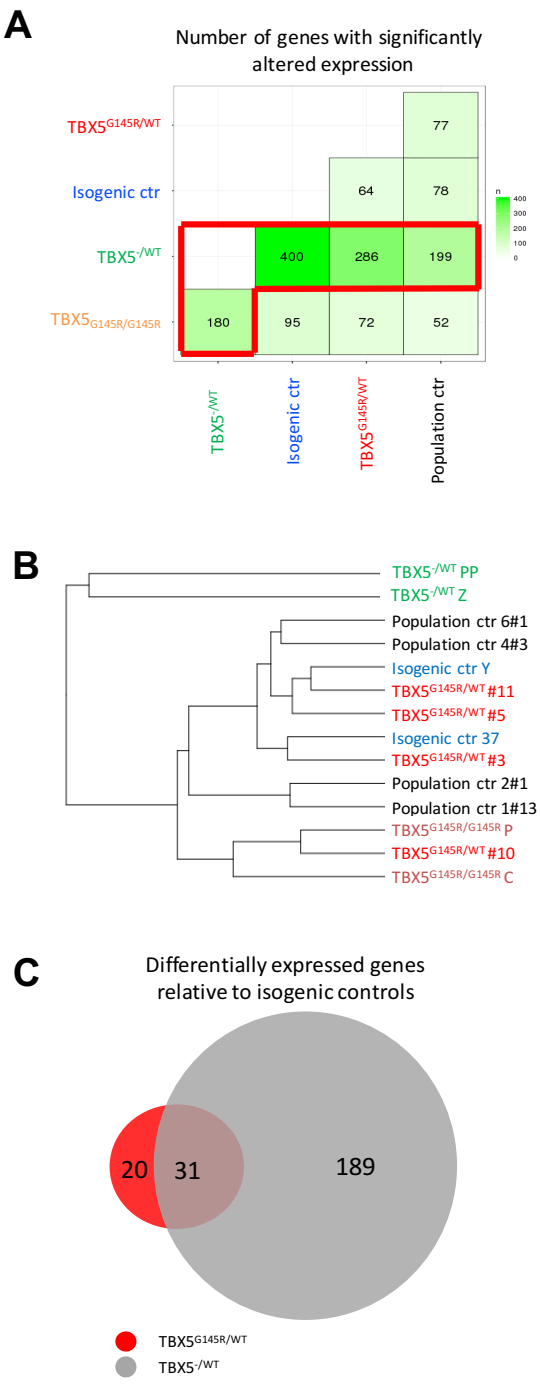

Figure 32. RNA sequencing analysis. (**A**) Pairwise display of number of genes with significantly altered differential expression (**B**) Unsupervised hierarchical clustering of differentially expression genes. (**C**) Venn diagram of genes differentially expressed in $TBX5^{G145R/WT}$ and $TBX5^{-/WT}$ relative to isogenic control levels.

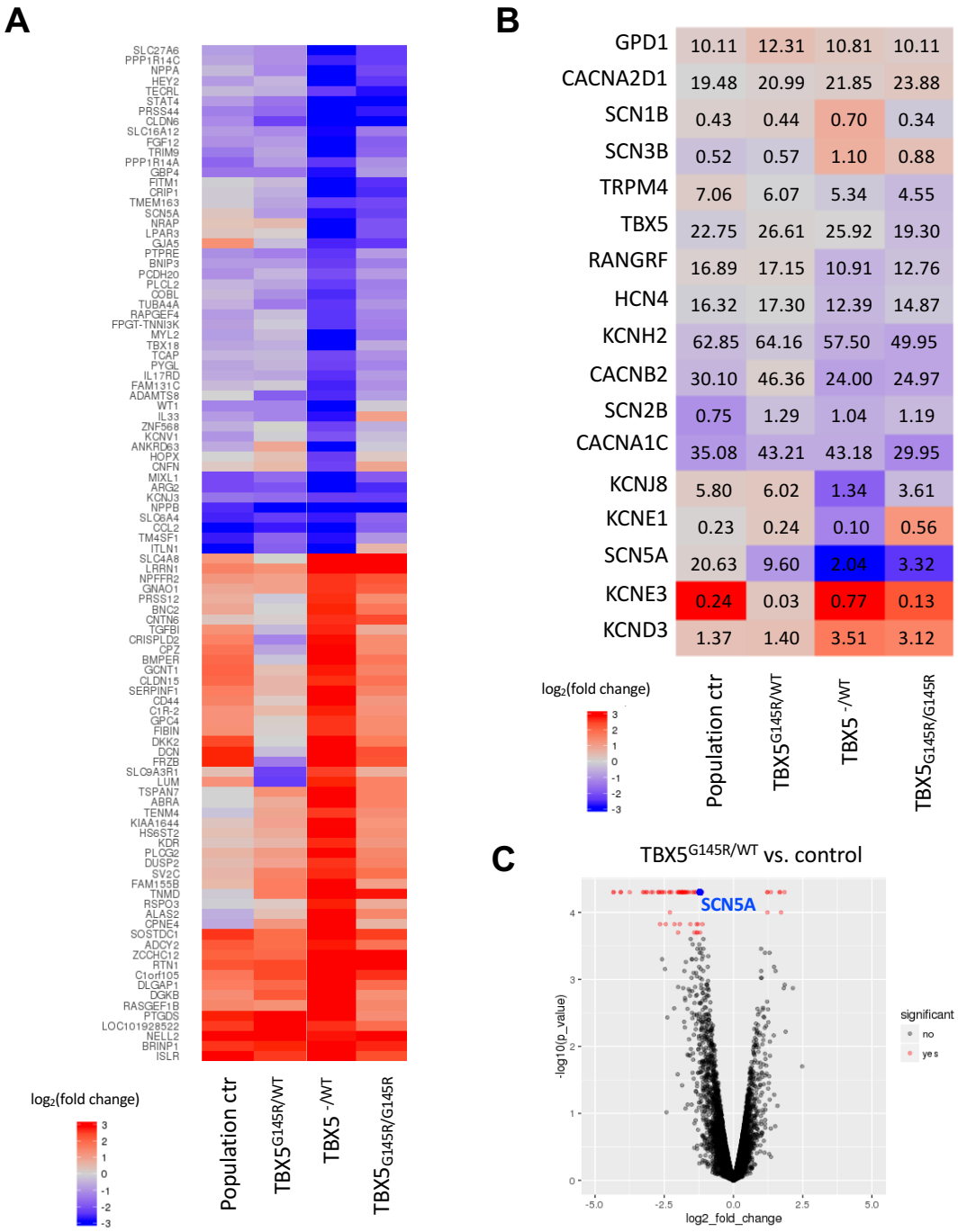

Figure 33. Differentially expressed genes in iPSC-CMs with TBX5 variants. (**A**) Heat map of top 50 upregulated and downregulated genes in TBX5 heterozygous deletions relative to isogenic controls. (**B**) Heat map of relative expression of BrS-associated genes relative to isogenic controls. (**C**) Volcano plot comparing $TBX5^{G145R/WT}$ to isogenic controls.

correction of the TBX5-G145R variant completely rescues the phenotype, we postulate that the arrhythmogenic $I_{Na\text{-}L}$ and APD variability are a result of altered TBX5 transcriptional regulation.

In order to further identify specific genes and pathways underlying the late sodium current, we examined a list of candidate genes in which the encoded protein influences $I_{Na\text{-}L}$ but none were differentially expressed. We then analyzed the list of differentially expressed genes by pathway analysis of gene ontology (GO terms) for biologic processes using PANTHER.[292] When comparing $TBX5^{G145R/WT}$ iPSC-CMs to population and isogenic control myocytes, the list of genes was significantly enriched for the processes of cardiovascular development and regulation of phosphoinositol 3-kinase (PI3K) signaling (**Table 14**). The PI3K signal was driven by reduced expression of genes that encode proteins activating the PI3K pathway (*FLT1*, *DCN*, and *TEK*). Excitingly, our lab and others have recently shown that a reduction in PI3K signaling in cardiomyocytes enhances late sodium current, suggesting that TBX5 regulation of PI3K as a mechanism of the late current in the proband.[293-297] Thus, this unbiased gene ontology approach highlighted a potential role of PI3K signaling on $I_{Na\text{-}L}$ and APD variability that would have remained unappreciated only using candidate gene analyses.

Comparison of differential gene expression between $TBX5^{-/WT}$ and control iPSC-CMs found enrichment for the processes of heart development and response to growth factor signaling (**Table 14**). These findings are consistent with the development on an *in vitro* model of HOS. However, further functional characterization is required to evaluate if the heterozygous knockout lines also contain primary electrophysiologic phenotypes. In contrast, compared to control iPSC-CMs, $TBX5^{G145R/G145R}$ identified the GO terms ion homeostasis and membrane depolarization (**Table 14**). These pathways analyses suggest the gene network regulated by TBX5 that govern heart development is less affected by TBX5-G145R and those that influence cardiac conduction

are equally or perhaps more greatly affected compared to heterozygous *TBX5* deletion. One open question is whether all sites of TBX5 DNA binding are equally altered in $TBX5^{G145R/G145R}$ and $TBX5^{-/WT}$. Future studies that quantitatively compare DNA occupancy between TBX5 variant lines could provide insight into the molecular mechanisms driving the observed transcriptional differences.

Table 14. Gene ontology terms enriched in differentially expressed among pairwise comparisons.

Group1	Group 2	Biologic process	% List	Enrichment	P value
Control	$TBX5^{G145R/WT}$	Regulation of PI3K signaling	4.3	15.23	2.37E-02
Control	$TBX5^{G145R/WT}$	Cardiovascular development	1.5	5.29	1.75E-02
Control	$TBX5^{-/WT}$	Heart development	2.3	5.61	3.52E-02
Control	$TBX5^{-/WT}$	Cardiovascular development	1.7	4.23	4.17E-02
Population ctr	$TBX5^{G145R/G145R}$	Regulation of ventricular membrane depolarization	42.9	>100	6.54E-03
Population ctr	$TBX5^{G145R/G145R}$	Regulation of atrial membrane depolarization	37.5	>100	9.75E-03
Population ctr	$TBX5^{G145R/G145R}$	Regulation of ion homeostasis	3.0	14.75	2.58E-02
Population ctr	$TBX5^{G145R/G145R}$	Cardiac muscle contraction	7.5	36.4	2.33E-03
$TBX5^{G145R/WT}$	$TBX5^{-/WT}$	organ development	1.6	2.68	2.14E-06
$TBX5^{G145R/WT}$	$TBX5^{-/WT}$	mesenchymal cell proliferation	30.8	52.46	1.02E-02
$TBX5^{G145R/WT}$	$TBX5^{-/WT}$	heart morphogenesis	4.2	7.2	4.31E-02
$TBX5^{G145R/WT}$	$TBX5^{-/WT}$	cardiovascular system development	2.6	4.44	8.70E-05
$TBX5^{G145R/WT}$	$TBX5^{-/WT}$	anatomical structure morphogenesis	1.8	3.08	2.40E-06
$TBX5^{G145R/WT}$	$TBX5^{-/WT}$	regulation of cell adhesion	2.5	4.27	9.54E-03
$TBX5^{G145R/WT}$	$TBX5^{-/WT}$	cell migration	2.2	3.79	2.15E-02
$TBX5^{G145R/WT}$	$TBX5^{-/WT}$	tissue development	2.1	3.54	3.71E-06
$TBX5^{G145R/WT}$	$TBX5^{-/WT}$	cell differentiation	1.4	2.37	1.00E-04

All terms biologic processes listed are enriched at statistically significant levels. Control = population controls and isogenic controls.

DISCUSSION

Rare variants in more than 45 genes have been identified in cases of BrS, including *TBX5*, with varying strength of evidence related to causality. Our work addresses the causal role of a *TBX5* variant of previously unknown significance discovered in a patient with BrS. The finding of ~50% decrease in SCN5A expression and sodium current in patient-derived iPSC-CMs validates this cellular model (See **Table 1** in Chapter I), but does not establish causation. Genome editing of patient derived iPSCs reversed these functional defects and thereby established TBX5-G145R as the cause of BrS in this family.

TBX5-G145R is a novel rare variant that is not present in over 130,000 alleles sequenced from more than 65,000 individuals (ExAC database) in which 165 non-synonymous variants (164 missense and a single nonsense; minor allele frequency <0.1% for all) were observed in *TBX5*. Nonsense variants in TBX5 often lead to severe maldevelopment of the heart as part of the constellation of symptoms described in HOS. Rare missense TBX5 variants have been recognized in other forms of heart disease including atrial fibrillation, dilated cardiomyopathy, and hypertrophic cardiomyopathy.[115,141,150] Often, missense variants are evaluated for alterations in DNA binding and transcriptional activation in biochemical assays and heterologous expression systems. However, the extent to which a change in transcription activation from a single TBX5-responsive luciferase assay in non-cardiomyocytes can be applied to pathogenesis remains unestablished.[141] Heterologous expression studies fail to provide insight into the underlying mechanisms as transcription factor (TF) function is dependent upon the correct cellular context, in this case a cardiomyocyte.

Understanding of TF biology is primarily through the study of animal knockout models

that define the global contribution of a particular TF to developmental phenotypes.[298] Heterozygous loss of Tbx5 in mice phenocopies the major features of human HOS: upper limb anomalies, impaired cardiac conduction, and septal defects in the heart.[120,121,274] TBX5 is also critical for homeostatic electrical conduction in the murine heart. Inducible deletion of *Tbx5*, specifically from the conduction system, from the adult mouse heart leads to ventricular tachycardia and disrupted fast conduction through reduced expression of *Scn5a* and *Gja5* (encoding Cx40 a major cardiac connexin in atria and conduction system).[148] Missense variants of Tbx5 have not been studied in mouse models to date. Gain-of-function mutations in TBX5 have been associated with atrial fibrillation.[115,299] TBX5-G125R is a mutation positioned at the TBX5-DNA interface with increased affinity for TBX5 binding sites, presumed because of the attraction of the positively charged arginine to negatively charged DNA, leading to increased promoter activity of *Nppa* and *Gja5* in heterologous assay driving luciferase activity.[115] Gain-of-function variants localized to the transactivation domain of TBX5 (R355C, G376R, S372L, and A428S) increase expression of *Gja5* and *Nppa* without altering expression of structural genes also regulated by TBX5 (α-MCH or MLC-2a).[299] Like mouse models of missense variants in Nkx2.5[300] and ARX,[301] TBX5-R355C has been studied using overexpression in a zebrafish fish model which increases occurrence of atrial fibrillation. TF overexpression leads to an increase in target site occupancy when compared to endogenous levels of TF expression which may confound animal models of missense TF variants overexpression.[302,303]

We provide a human model of missense TF variation studied under expression from the endogenous locus in the appropriate cellular context. Genome editing in patient-derived iPSCs is a scalable approach to test the impact of individual variants of unknown significance within the genetic background of the affected individual. We chose this approach rather than to engineer the

variant into a population control line because of the translation potential of testing the impact of the variant within cardiomyocytes generated from the patient. Other reports have knocked-in missense variants within a defined genetic background when access to the patient was not available. However, the influence of the defined background on cellular function is unknown and may contribute to phenotypic presentation. There are certainly advantages of knocking in variants into a common genetic background when the goal is to directly compare the phenotype of iPSC-CMs due to multiple variants in the same gene, for example our comparison of TBX5-G145R and TBX5 heterozygous knockout.

Compared to $TBX5^{-/WT}$, TBX5-G145R results in discrete alterations in gene expression relevant to the pathogenesis of BrS. Amino acid position 145 of TBX5 is located in the DNA binding domain of the protein but located away from where the protein interfaces with DNA targets. The structural modeling predicts that TBX5-G145R changes the orientation of the amino acids in direct contact with a canonical T-box family binding site within the *NPPA* promoter, consistent with DNA binding assays presented in **Figure 24**. There is some flexibility in transcription factor target sequence and one possible explanation for the discrete expression changes is that our observed reduction in DNA binding is restricted to particular DNA targets. To address this possibility, we proposed ChIP-sequencing experiments in isogenic iPSC-CMs that are either homozygous for wild-type or mutant (G145R) TBX5. We failed to immunoprecipitate endogenous TBX5 using antibodies that were successful in mouse Tbx5-chromatin immunoprecipitation experiments.[290] TBX5-G145R is located near a group of acidic amino acids that are critical for interacting with basic side chains of other transcription factors that work in synergy with TBX5.[126] Probing the effect of missense variants in TBX5 on interactions with other cardiac transcription factors may also provide insight into the

discrete expression changes observed in RNA-sequencing experiments.

The genetic basis of BrS was long presumed to be an autosomal dominant disease with variable penetrance. A GWAS comparing 312 cases of BrS to 1,115 population controls unraveled a strong influence of genetic background on disease risk. Three common variants, one of which marks a variant that disrupts TBX5 binding to a cis-regulatory element of *SCN5A* on chromosome 3, can impart an odds ratio of 21.5 if the individual carries 5 or 6 risk alleles. In the family pedigree presented here a single individual is a *TBX5 cG433A* carrier and currently unaffected by BrS. We genotyped all *TBX5* variant carriers for the common variants associated with BrS to look for a potential influence of these variants on disease penetrance. All carriers in the family carry 4-5 risk alleles (**Table 15**) suggesting currently unappreciated genetic contributions or environmental influences may alter BrS risk. BrS also has an age-related penetrance with the average age at diagnosis of 43 years old which may contribute to the variable penetrance observed in this famly.[304] The unaffected carrier was 17 years of age at time of evaluation. Based on the natural history of BrS and the large effect of TBX5-G145R on *SCN5A* expression in iPSC-CMs, it would be prudent to maintain a screening regimen in this individual.

Unexpectedly, we observed arrhythmogenic features of increased $I_{Na\text{-}L}$ and APD lability in patient-derived iPSC-CMs that is caused by TBX5-G145R. $I_{Na\text{-}L}$ can result from gain-of-function variants in *SCN5A* or altered gating characteristics mediated by auxiliary subunit interactions or post-translational modification (nitrosylation and phosphorylation).[305] The proband carries no coding variants in *SCN5A*, therefore ruling out mutations increasing late current in $Na_V1.5$ as the underlying $I_{Na\text{-}L}$ mechanism. We hypothesized that increased $I_{Na\text{-}L}$ in patient derived iPSC-CMs was due to a transcriptional mechanism because editing the missense *TBX5* variant corrected the phenotype (**Fig 26**). Acute silencing of *SCN2B* in dog ventricular

Table 15. Genotypes of TBX5-G145R carriers for common variants associated with BrS.

	TBX5 c.433G>A	rs6801957		rs11708996		rs9388451	
Ancestral allele	G	G		C		T	
Risk allele	A	T		G		C	
Pt ID		ALLELE 1	ALLELE 2	ALLELE 1	ALLELE 2	ALLELE 1	ALLELE 2
2994 (proband)	G/A	A	A	G	G	T	C
2997 (mother)	G/A	A	A	G	C	T	C
3651 (iPSC donor)	G/A	A	A	G	C	C	C
6614 (noncarrier sibling)	G/G	A	A	G	C	T	C
6615 (carrier sibling)	G/A	A	A	G	C	T	C
MAF (1000 genomes)	0	0.29		0.09		0.41	
OR	N/A	2.55		1.73		1.58	
Gene/biology	missense	*SCN5A* EnhA SNP		*SCN5A* intron 17		*Hey2* SNP	

cardiomyocytes increases $I_{Na\text{-}L}$ while *SCN1B* silencing decreases peak and late I_{Na}, a finding confirmed in an independent heterologous expression experiment.[43,44] We quantified the beta subunit transcripts and they were not differentially expressed in $TBX5^{G145R/WT}$ iPSC-CMs compared to isogenic controls. The nitrosylation and phosphorylation state of $Na_V1.5$ alters the amount of $I_{Na\text{-}L}$ as nitrosylation[306] and phosphorylation by Ca2+/calmodulin-dependent protein kinase II (CaMK)[307] and protein kinase C (PKC)[308] increases $I_{Na\text{-}L}$ while it is reduced by PI3K activity. While expression of the proteins responsible for direct post-translational modification was not affected by the missense *TBX5* variant, pathway analysis unveiled regulators of PI3K activity were downregulated (**Table 14**).[297] Chronic exposure to tyrosine kinase inhibitors or a subset of antiarrhythmic medications inhibit PI3K to increase $I_{Na\text{-}L}$ that can be reversed by intracellular dialysis with 3,4,5-triphosphate (PIP3).[293,295] We found a novel association between TBX5-G145R and decreased expression of PI3K activators. Further work is required to elucidate if the expression changes are a direct result of the *TBX5* variant or other (*e.g.* compensatory) mechanisms.

Experimental models and clinical observations demonstrate that beat-to-beat variability in the duration of the cardiac action potential is a strong predictor of arrhythmia susceptibility.[309] In healthy myocardium, cardiomyocytes are resilient to mild alterations in ionic currents as the heart rate fluctuates based on the activity of an individual. Situations such as genetic variation or medication exposure, where the balance of depolarizing and repolarizing current becomes narrow, small alterations in inward or outward cation current can dramatically (and sometimes on a beat to beat basis) shift the duration of the action potential. Drugs impacting I_{Kr} and I_{Na} have been shown to have a great impact on APD instability.[310] Chemically induced $I_{Na\text{-}L}$ by exposure to either veratridine or ATX-II leads to APD lability in canine ventricular myocytes. The exact

mechanisms of $I_{Na\text{-}L}$ leading to APD lability due to drug exposure or the $TBX5^{G145R/WT}$ iPSC-CMs studied are currently unknown. One possible explanation is variable activation of signaling cascades activated by sodium overload. For example, sodium overload activates the sodium-calcium exchanger leading to increased diastolic calcium. This activates the CaMKII which modifies the behavior of many ion channels, including enhancing $I_{Na\text{-}L}$. Computational modeling predicts beat-to-beat variation in CaMKII signaling occurs and that could be an important modifier of repolarization kinetics.[311] Another potential mechanism of APD variability is the self-perpetuating effect of the diastolic interval on ion channel behavior. The APD restitution curve demonstrates a nonlinear relationship of the diastolic interval influencing the duration of the subsequent action potential. Shortening the diastolic intervals decrease the ionic currents during the plateau phase of the action potential, resulting in a loss of the phase 2 notch generated by I_{to} and a shortening of the APD.[312] A reduction in I_{to}, $I_{Ca\text{-}L}$, and I_{Na} after short diastolic intervals is supported by computational models.[313-316]

This study has multiple translational implications. Based on the reversal of the cellular BrS phenotype of decreased sodium current by genome correction of *TBX5 c.G433A* in patient-derived iPSCs, we have defined the genetic bases of BrS in this study family. Additionally, molecular diagnostics unveiled a previously undiagnosed case of mild HOS. These findings have a direct benefit to the study family by providing the knowledge base required for genetic counseling of the TBX5-G145R carriers within the family. In the development of the iPSC-CM model of BrS, we observed a shared phenotype and anti-arrhythmic response to ranolazine treatment among single cell and monolayer evaluation which accentuates the potential of screening drug response in populations of iPSC-CMs. Monolayers of stem cell-derived cardiomyocytes minimize the limitation of stem cell differentiated cardiomyocytes consisting of

heterogeneous populations of cells.[317] Testing of drug efficacy in patient-specific iPSC-CM monolayers have the potential to guide future clinical decision making based on personalized *in vitro* drug response that can be influenced by the genetic architecture underlying disease. This complements the efforts that have validated iPSC-CM models that evaluate drug toxicity, particularly for arrhythmia risk.[282,318]

CONCLUSION

We have developed a new iPSC-CM model of BrS and applied this model to advance our understanding of TBX5 biology. Generating isogenic controls by genome editing proved TBX5-G145R causes BrS through the mechanism of reduced sodium channel expression. Our findings establish a regulatory role of TBX5 that influences electrical activity in ventricular cardiomyocytes. The missense variant characterized in this report has discrete transcriptional alterations that are unique from haploinsufficiency mechanisms. Unexpectedly, TBX5-G145R causes increased late sodium current leading to action potential duration lability. By studying a missense TBX5 variant in a human cardiomyocyte model, we propose a transcriptional mechanism leading to reduced PI3K signaling and increased arrhythmia risk. Lastly, incorporating molecular diagnostics with strong clinical phenotyping allowed for detection of a subclinical presentation of HOS that may impact future genetic counseling of the presented family.

CHAPTER V

SUMMARY AND FUTURE DIRECTIONS

The vision of precision medicine is to tailor health care in order to optimize treatment for each and every patient. This requires the understanding and integration of genetic, environmental, and lifestyle factors that comprise the individual's risk for developing disease and response to preventative or curative interventions. For precision medicine to reach its full potential, we, as a scientific community, must define these unique disease modifying characteristics with sensitive detection and accurate interpretation. The objective of this body of work was to contribute to the pursuit of precision medicine by advancing the understanding and utilization of genome science for application to inherited heart disease. Through the experiments described in this dissertation, we have advanced the field of molecular cardiology by addressing two important questions:

(1) What types of variants elude detection by genetic testing?

(2) Are variants of unknown significance contributory to disease?

Summary of Chapter II

Some genetic conditions have well-defined genetic architecture which can be explained by variation in just a single or few genes. Therefore, the clinical presentation of such conditions is highly suggestive of variation in a known associated gene. These types of conditions provide a unique opportunity to evaluate the efficacy of broadly used methods in genetic testing for variant identification. A classic example of one such medical condition is cystic fibrosis where the only genetic cause is homozygous or compound heterozygous variation in *CFTR*.[319,320] We utilized an

analogous (in terms of genetic specificity) inherited heart condition called Jervell and Lange-Nielsen syndrome (JLNS), a severe version of the long QT syndrome with congenital deafness. JLNS has only two known genetic causes: homozygous or compound heterozygous mutations in either *KCNQ1* or *KCNE1*. *KCNQ1* encodes the pore forming α subunit and *KCNE1* encodes the auxiliary β subunit of the voltage-gated potassium channel that conducts the slow delayed rectifying potassium current, I_{Ks}. A complete loss of I_{Ks} delays cardiac repolarization and increases risk of developing polymorphic ventricular tachycardia. Genetic testing using next-generation sequencing (NGS) approaches was conducted on the patient with JLNS and returned a single nonsense variant in *KCNQ1*. As described in Chapter II, we tested the hypothesis that the patient possessed a second variant in *KCNQ1* that was not detected by NGS approaches. Using conventional Sanger sequencing methods, we found a complex 52-bp insertion comprised of a partial duplication of exon 15 and a poly-adenine tract, likely a truncated Alu element. Additional filters can be applied to NGS analysis to appropriately identify insertion-type variants that are similar to the one we described.

Future directions for Chapter II

While the cause of long QT syndrome in this patient is well appreciated in loss of I_{Ks}, we still chose to generate and validate induced pluripotent stem cells (iPSCs) for expression of stem cell markers, pluripotency, and a normal karyotype from this individual (**Fig 34A** and **34B**). JLNS has previously been modeled using iPSC-CMs.[259] A striking finding in this report is the severe prolongation of the action potential with a doubling of the APD_{90}. There are multiple rationales for creating this model. While it benefits the field to have a second JLNS model due to different genetic causation, it also provided an internal positive control for detection of APD

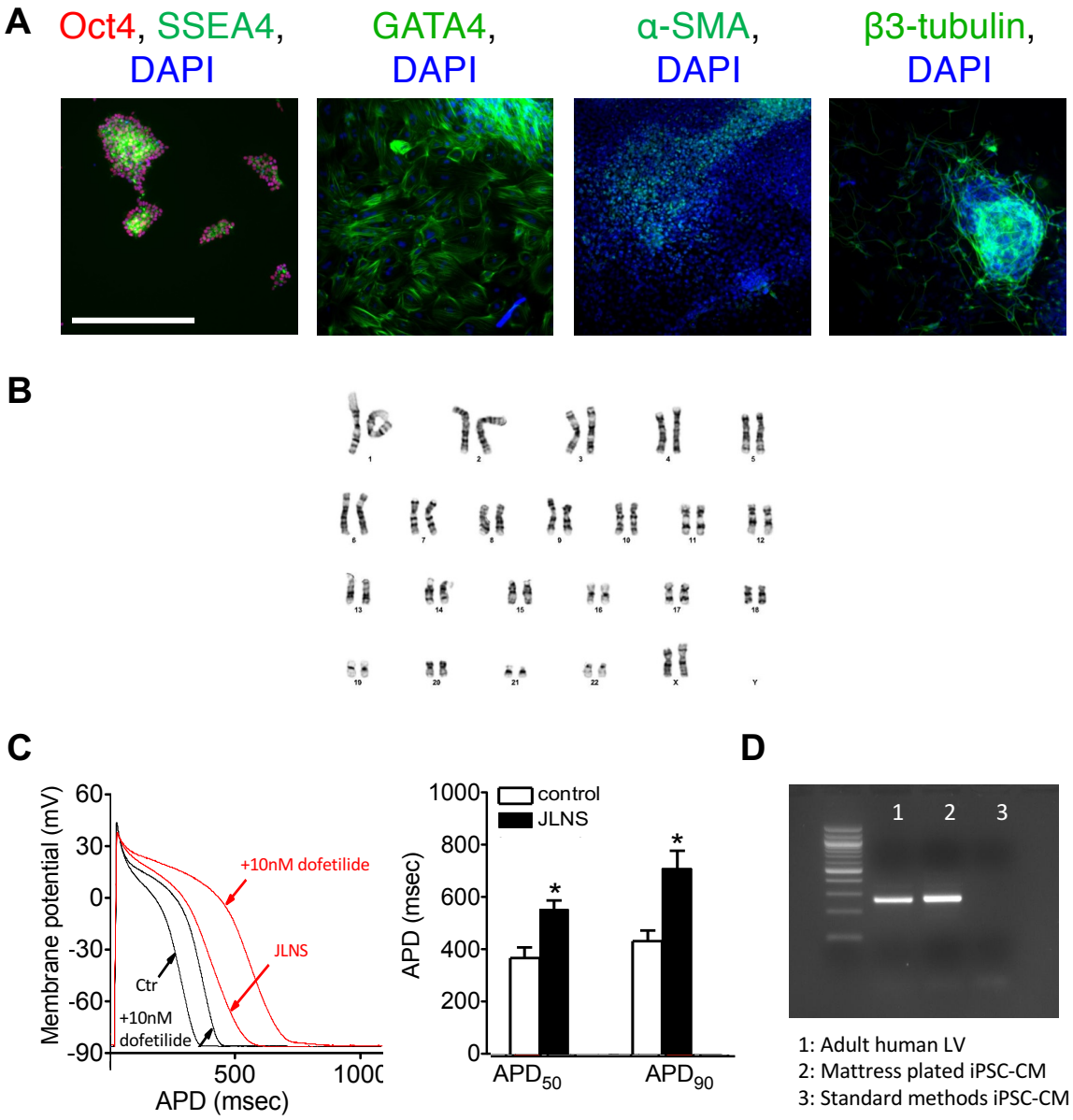

Figure 34. JLNS iPSC-CM model preliminary data. (**A**) JLNS iPSC colonies express stem cell-associated proteins. Embryoid body differentiation to three germ layers demonstrates iPSC pluripotency: endoderm (GATA4), mesoderm (α-SMA), ectoderm (β3-tubulin). Scale bars = 50 microns. (**B**) JLNS iPSC clones maintain a normal karyotype. (**C**) JLNS iPSC-CMs grown using standard 1:200 matrigel plating have prolonged action potential duration (APD) and expected response to dofetilide treatment. (**D**) PCR amplification of KCNQ1 off cDNA template demonstrates low expression when using standard 1:200 matrigel iPSC-CM methodology that is increased by matrigel mattress (undiluted matrigel) plating as previously described[321] that could be used in future patch-clamp experiments to elucidate the mechanisms of KCNQ1 contribution to repolarization beyond I_{Ks} generation. Ctr = population control.

prolongation in iPSC-CMs. We recorded action potentials from population control and JLNS iPSC-CMs and confirmed that complete loss of KCNQ1 causes a severe prolongation of APD_{50} and APD_{90} with further APD prolongation with I_{Kr} blockade by dofetilide (**Fig 34C**). This model also provides an opportunity to learn new KCNQ1 biology. JLNS iPSC-CMs have twice as long action potentials compared to controls even though it is abundant in the literature, and confirmed by our evaluation (**Fig 34D**), that KCNQ1 expression is quite low in iPSC-CMs when using standard plating conditions.[321] We generated cDNA from mRNA isolated from JLNS iPSC-CMs after standard or matrigel mattress[321], a condition that increases expression of many cardiac genes including *KCNQ1*, plating for PCR amplification of *KCNQ1* transcripts. Adult human left ventricle (LV) cDNA was included as a positive control. Amplicons were visible for reactions using cDNA template synthesized from adult LV and mattress treated cells while standard iPSC-CM methods failed to amplify *KCNQ1* transcripts. All samples generated amplicons using primers specific to *GAPDH* to control for the quality of template used in PCR reactions. Based on the very low expression, I hypothesize that KCNQ1 serves other cellular functions in addition to generating I_{Ks}. At the protein level, KCNQ1 is reported to interact with Kv11.1, encoded by *KCNH2* (also known as *HERG*) and may modulate trafficking[322,323] or endocytosis[324] of Kv11.1 channels. iPSC-CMs provide a renewable source of human cardiomyocytes to study the biology of these interactions. Genome modification to alter amino acid sequence or introduce tags for fluorescence resonance energy transfer (FRET) or biochemical assessment of JLNS iPSC-CMs can be used to interrogate the regulatory role of KCNQ1 on other channels at the protein and RNA levels.

During the process of differentiation of JLNS iPSCs into cardiomyocytes, the cells detach from the plate during the Wnt inhibition with IWR-1 step (see methods in chapter IV). This

occurred during every attempted differentiation. The floating cells lacked pyknotic nuclei and membrane blebbing leading me to assess the viability of the floating cells. Using trypan blue exclusion >70% of floating cells were still viable. In order to generate cardiomyocytes, I merged two differentiation protocols: the matrigel sandwich method[325] and the chemical method.[167] I modified the chemical method of differentiation by including 1:200 dilution of matrigel in the media during the first 5 days of differentiation to provide a top layer of extracellular matrix in hopes to keep cells attached to the bottom of the plate. This was very successful producing high yield differentiations with adequate cardiomyocyte purity. These observations may implicate a role of KCNQ1 in interactions with the extracellular matrix early during development. This theory is supported by reports that loss of *KCNQ1* increases metastatic potential of cancerous cells which requires a change in cell-to-cell and cell-to-matrix adhesion.[326] In a mouse model of colon cancer, deletion of *Kcnq1* upregulates expression of pro-proliferative and metastatic genes.[327] Another report describes downregulation of *Kcnq1* or upregulation of *Kcne1* promotes invasive behavior in embryonic stem cells.[328] The observations in the oncology fields support the theory that KCNQ1 and possibly other ion channels serve functions beyond ion conductance.

Summary of Chapter III

A particular challenging aspect of implementing genomic sequencing into clinical practice is accurately assigning a variant as pathogenic or non-contributory to disease. This is difficult when only considering large effect rare variants and becomes overwhelming when attempting to incorporate common variants that comprise an individual's unique genetic background. In Chapter III, I worked in a collaborative effort to evaluate the functional

consequences of a series of rare variants located in or near the selectivity filter of the voltage-gated potassium channel, $K_V2.1$. Prior to my involvement, a clinical effort identified multiple *de novo* variants in a child afflicted with epileptic encephalopathy not carried by either parent. The challenge was to determine variants in which gene caused the child's condition. A missense variant in *KCNB1*, the gene encoding $K_V2.1$, was the top candidate because the variant occurred in a highly conserved region of the protein and this protein contributes to repolarization of a neuron. Therefore, the missense variant identified would likely alter neuronal electric homeostasis. Mice with germline deletion of *Kcnb1* demonstrate increased susceptibility to drug induced seizures but have no change in baseline seizure activity.[253] While species differences may explain why the patient identified had severe epilepsy, it was possible that the identified mutation may have different biophysical properties contributing to the severity of the clinical phenotype.

I performed electrophysiologic characterization of wild-type or mutant $K_V2.1$ in Chinese hamster ovarian (CHO) cells via heterologous expression. This model allows for direct functional testing of $K_V2.1$ without confounding currents since CHO cells do not express endogenous potassium channels. Mutations in the selectivity filter of the pore of $K_V2.1$ altered two major features of channel function. The channels were no longer voltage-gated and lost selectivity. The mutant channels conduct the monovalent cations potassium, sodium, rubidium, and the large cation N-methyl-d-glucamine. Therefore, it is possible that the mutant $K_V2.1$ channels studied not only abolish voltage-gated repolarizing potassium current but directly contribute to hyperexcitability, severe seizure burden, and neuron cell death through conduction of depolarizing I_{Na}.

Future directions for Chapter III

The electrophysiology experiments conducted in Chapter III were done entirely in heterologous expression systems. While this model interrogates the impact of missense variants on ion channel function, insight into the global effect in the relevant cell type, a neuron, or in a whole organism is lacking. A mouse model of the missense *Kcnb1* variant is being generated and characterized by my collaborator and co-author Dr. Jennifer Kearney. The mouse model will compare the seizure burden and response to pro- and anti-epileptic interventions in the mice with the missense variant compared to *Kcnb1* knockout mice. This study will directly test the hypothesis that loss of selectivity results in a gain-of-function mechanism to increase seizure burden and neuronal cell death.

Mouse models of epilepsy provide whole organism evaluation of epilepsy phenotypes and response to therapeutics. It is unrealistic to generate a mouse model for each variant discovered. The discovery of iPSCs (as discussed in Chapter I and IV) provide a renewable source of human neurons. Complex neuron pathology has been modeled using iPSC-neurons, including epilepsy[329] and ALS.[330] The application of genome-editing and advances in 3-dimensional culturing systems will improve the validity and utility of iPSC-neuron epilepsy models.

Summary of Chapter IV

Heterologous expression systems permit relatively high-throughput characterization of mutant proteins from which causation can be inferred. This approach is particularly effective when studying a gene with a strong association to a clinical phenotype. There are examples in

which the dysfunction of a protein can only be detected and the mechanisms elucidated in the appropriate cellular context, for example, SCN5A-D1275N and its disrupted subcellular localization[158] or TBX5-G145R, a cardiac transcription factor.[107] In Chapter IV, we tested the hypothesis that TBX5-G145R caused familial BrS. Through genome editing of patient-derived stem cells, we established the genetic basis, functional mechanisms, and transcriptional mechanisms of BrS in the study family. The TBX5 variant caused decreased sodium current, the electrophysiologic hallmark of BrS.[331] Increased late sodium current and action potential variability were also identified in iPSC-CMs containing the missense *TBX5* variant. These arrhythmogenic features were completely abolished by correction of the variant by CRISPR/Cas9 methodology or treatment with the late sodium current blocker ranolazine.

Relative to the transcriptome of population control and isogenic control iPSC-CMs, the TBX5-G145R variant resulted in modest transcriptional alterations compared to TBX5 heterozygous knockout iPSC-CMs. The genes that were altered by the TBX5-G145R missense variant are important for cardiac conduction and regulation of PI3K signaling. TBX5 heterozygous deletion resulted in global changes in expression of genes associated with cardiac defects in the developmental condition HOS. Through the project described in Chapter IV, we have established TBX5-G145R as a causative variant in familial BrS and expanded the known roles of TBX5 beyond cardiac development to now include human cardiomyocyte homeostasis.

Future directions for Chapter IV

We have established that TBX5-G145R caused BrS in the study family. A remaining question is whether or not this missense variant is sufficient to cause BrS. More specifically, does the

genetic background present in the individuals studied provide the summative risk necessary to cause BrS. The family studied carries many of the common SNVs identified by GWAS to increase BrS risk. The SNVs identified actually mark a region of DNA that contains one functional SNV responsible for this increased risk.[103] Because the functional SNVs of GWAS identified common variants are not known, the genetic background of the study family cannot be modified to test the contribution of genetic background on the phenotype. *TBX5 c.G433A* can alternatively be inserted into population control iPSCs that have been genotyped for the common SNVs associated to BrS to test if TBX5-G145R is sufficient to cause the cellular phenotype we describe (**Table 16**).

TBX5-G145R results in discrete transcriptional changes compared to heterozygous deletion of *TBX5*. I hypothesize that TBX5-G145R has preferential disruption of DNA binding based on the sequence of the DNA target. This hypothesis can be tested by defining the location of TBX5 occupancy within the genome based on the sequence of the DNA target using chromatin-immunoprecipitation sequencing (ChIP-seq) evaluation in isogenic ($TBX5^{WT/WT}$) control and $TBX5^{G145R/G145R}$ iPSC-CMs (**Fig 35**). TBX5 ChIP-seq has only been successfully performed to date in mouse cell lines, originally using overexpression of affinity-tagged Tbx5 in an immortalized mouse cardiomyocyte cell line[332] and recently from endogenous Tbx5 from mouse ESC-derived cardiomyocyte progenitors.[290] We tested multiple commercially available antibodies directed against TBX5, including the antibody successfully applied in endogenous mouse Tbx5-ChIP, by Western blot on nuclear lysate from population control iPSC-CMs without success. Future efforts could test additional commercial antibodies directed against TBX5 for effectiveness in human cardiomyocytes or insertion of affinity tags by homology-directed repair after nuclease targeting of the endogenous TBX5 locus. V5 and biotin tags have been

Table 16. **Genotypes of population control iPSC for common variants associated with BrS.**

	rs6801957		rs11708996		rs9388451		Odds Ratio
Ancestral allele	G		C		T		
Risk allele	T		G		C		
Pt ID	ALLELE 1	ALLELE 2	ALLELE 1	ALLELE 2	ALLELE 1	ALLELE 2	
Population control 1	G	T	G	G	T	C	8.33
Population control 2	G	T	G	C	G	C	4.04
Population control 4	G	T	G	G	C	C	4.04
Population control 6	G	G	G	C	T	C	1.87
MAF (1000 genomes)	0.29		0.09		0.41		
OR	2.55		1.73		1.58		
Gene/biology	*SCN5A* EnhA SNP		*SCN5A* intron 17		*Hey2* SNP		

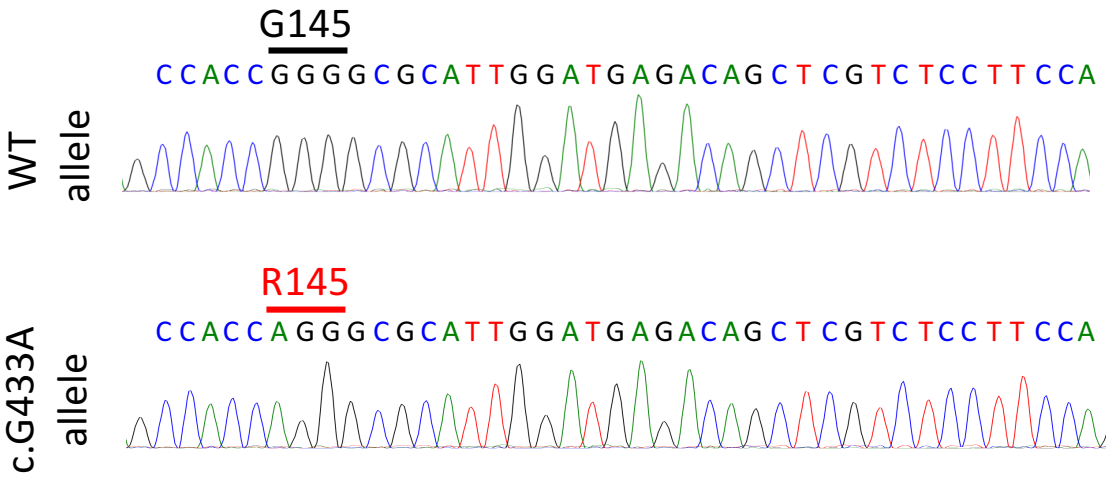

Figure 35. Sanger sequencing of exon 5 of *TBX5*. Chromatogram of Sanger sequencing confirmation of TBX5-G145R homozygous CRISPR/Cas9-mediated edit.

successfully applied to ChIP techniques to overcome the lack of commercially available ChIP-grade antibodies for other transcription factors.[333]

The analysis of RNA-sequencing datasets by gene ontology revealed decreased expression of known PI3K activators as a potential mechanism of late sodium current in iPSC-CMs containing the missense TBX5-G145R variant. Certain tyrosine kinase inhibitors used in the treatment of malignancies result in a common mechanism of reduced PI3K activity and an associated side effect of QT prolongation.[294] The ionic mechanism of increased late sodium current contributes to the prolongation of APD in cardiomyocyte models that can be rescued by intracellular dialysis of PIP3. For example, dofetilide was previously thought to increase risk of arrhythmia onset by potent I_{Kr} block but is it now described to also cause PI3K-mediated increased late sodium current.[293,296] Intracellular dialysis of PIP3 in TBX5$^{G145R/WT}$ iPSC-CM could be tested to prevent late sodium current and APD lability. The activity of PI3K can be indirectly tested by relative quantification of the phosphorylation state of known targets (Akt and S6) by Western blot comparison using phospho-specific antibodies relative to total protein. This would be the first report of a missense variant in a transcription factor altering PI3K activity in cardiomyocytes.

A goal of precision medicine is to tailor therapy based on the underlying genetics. Ongoing efforts are testing the response of genotype specific therapies to treat inherited arrhythmia syndromes. These approaches would directly address underlying mechanisms of disease. Altering transcription of genes affected directly or indirectly may provide another path to the realization of precision medicine. I hypothesize that increasing expression of *TBX5* in TBX5$^{G145R/WT}$ iPSC-CMs to "functional" normal will ameliorate the reduced sodium current, enhanced late sodium current, and APD variability.

CRISPR/Cas9 has been modified to generate RNA-guided synthetic transcription factors by inactivating the nuclease domains of Cas9 and tethering transactivation domains to the C-terminus by a short peptide linker (dCas9-activator).[334-336] To test the expression hypothesis, I began to generate the tools to create a genetically encoded, doxycycline-inducible dCas9-activator (**Fig 36A**). Using HDR after Cas9-induced double strand break, I inserted a Flp recombinase target site and tet repressor system within intron1-2 of PPP1R12C, an area known as a safe harbor site and common target of gene therapy integration (**Fig 36B** and **36C**).[337,338] Transient expression of Flp recombinase in the presence of a donor plasmid containing the dCas9-activator and gRNA expression system will generate stable iPSC lines. This system is modular in that various gRNA can be inserted into the donor plasmid using simple cloning. This approach could also be tested as a proof-of-concept in cell or animal models of other causative non-dominant heterozygous variants.

Final summary

The body of work presented in this dissertation has contributed to the field of molecular cardiology by providing knowledge that can be approach broadly to genetic variant identification and evaluation of variant causality. Specifically, I have identified a class of genetic variation missed by next-generation sequencing-based genetic testing (Chapter II). I have defined the changes in biophysical properties of mutations in $K_V2.1$ that cause severe seizure burden in cases of epileptic encephalopathy (Chapter III). Through genome editing of patient derived induced pluripotent stem cells, I have established a novel genetic cause of the Brugada syndrome, a rare missense variant in *TBX5* (Chapter IV). In studying TBX5-G145R containing stem cell-derived cardiomyocytes, I have implicated a role of TBX5 in regulating expression of upstream regulators of PI3 kinase and when disrupted results in arrhythmogenic increased late sodium current and action potential duration lability. In conclusion, the summation of the presented findings participates in the collective goal of advancing scientific knowledge for translation into clinical practice.

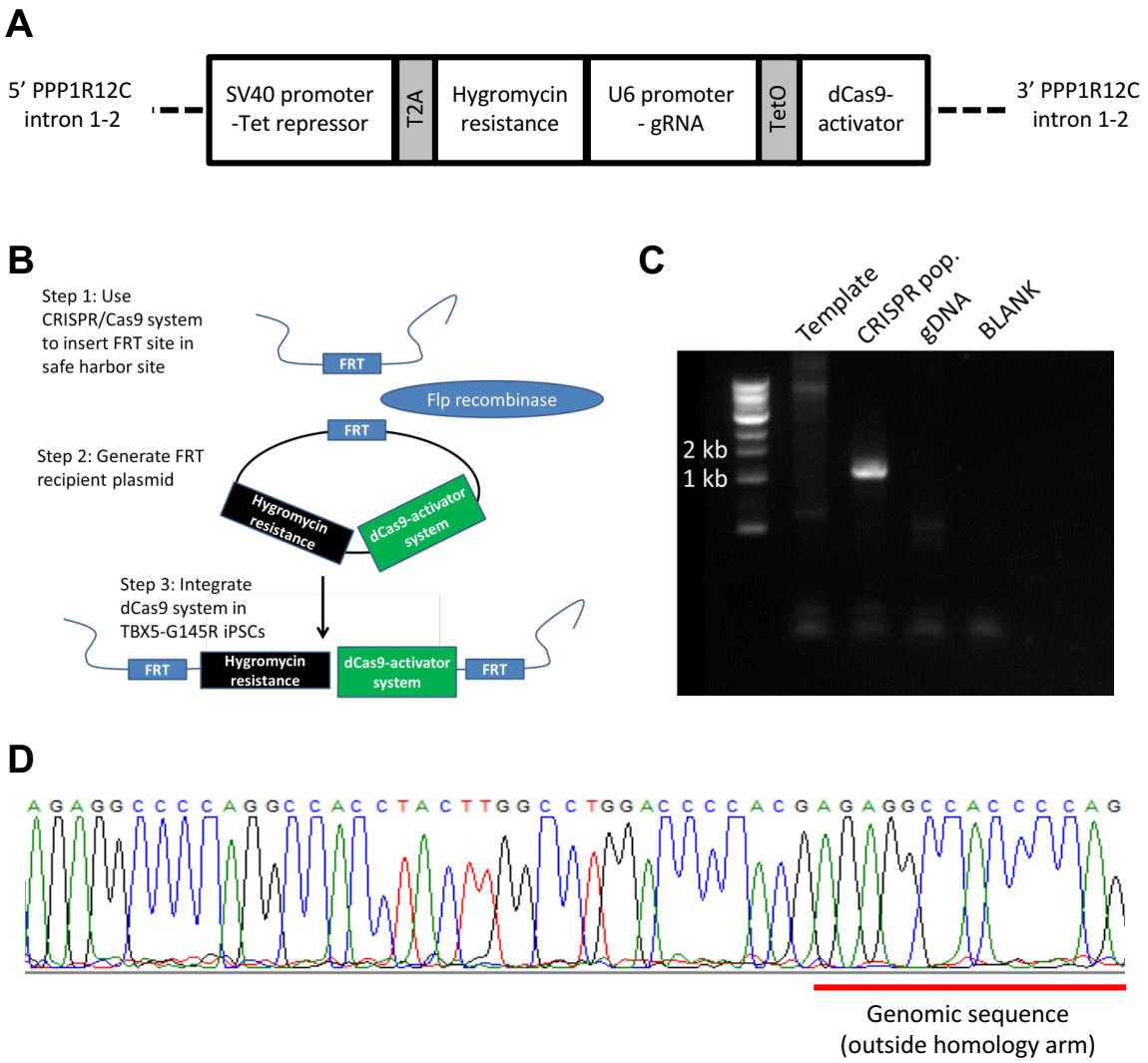

Fig 36. Construction of genetically-encoded doxycycline-inducible dCas9-activator. (**A**) Schematic of genetically encoded doxycycline-inducible expression system in intron 1-2 of *PPP1R12C*. (**B**) Dual CRISPR/Cas9 and Flp recombinase modulate approach. (**C**) PCR reaction with forward primer specific to CRISPR/Cas9-mediated insertion and reverse primer in the genome outside of homologous template. (**D**) Sanger sequencing chromatogram of amplicon depicted in (**D**).

REFERENCES

1. Mollova M, Bersell K, Walsh S, Savla J, Das LT, Park SY, Silberstein LE, Dos Remedios CG, Graham D, Colan S, Kuhn B. Cardiomyocyte proliferation contributes to heart growth in young humans. Proc Natl Acad Sci U S A 2013;110:1446-51.

2. Raju TN. The Nobel chronicles. 1963: Sir Alan Lloyd Hodgkin (1914-98), Sir Andrew Fielding Huxley (b 1917), and Sir John Carew Eccles (1903-97). Lancet 1999;354:263.

3. Hodgkin AL, Huxley AF. Resting and action potentials in single nerve fibres. J Physiol 1945;104:176-95.

4. Neher E. Nobel lecture. Ion channels for communication between and within cells. Neuron 1992;8:605-12.

5. Grant AO. Cardiac ion channels. Circ Arrhythm Electrophysiol 2009;2:185-94.

6. DiFrancesco D. Pacemaker mechanisms in cardiac tissue. Annu Rev Physiol 1993;55:455-72.

7. Accili EA, Proenza C, Baruscotti M, DiFrancesco D. From funny current to HCN channels: 20 years of excitation. News Physiol Sci 2002;17:32-7.

8. Yang N, Horn R. Evidence for voltage-dependent S4 movement in sodium channels. Neuron 1995;15:213-8.

9. Yang N, George AL, Jr., Horn R. Molecular basis of charge movement in voltage-gated sodium channels. Neuron 1996;16:113-22.

10. Yellen G, Jurman ME, Abramson T, MacKinnon R. Mutations affecting internal TEA blockade identify the probable pore-forming region of a K+ channel. Science 1991;251:939-42.

11. West JW, Patton DE, Scheuer T, Wang Y, Goldin AL, Catterall WA. A cluster of hydrophobic amino acid residues required for fast Na(+)-channel inactivation. Proc Natl Acad Sci U S A 1992;89:10910-4.

12. McPhee JC, Ragsdale DS, Scheuer T, Catterall WA. A critical role for the S4-S5 intracellular loop in domain IV of the sodium channel alpha-subunit in fast inactivation. J Biol Chem 1998;273:1121-9.

13. Torkamani A, Bersell K, Jorge BS, Bjork RL, Jr., Friedman JR, Bloss CS, Cohen J, Gupta S, Naidu S, Vanoye CG, George AL, Jr., Kearney JA. De novo KCNB1 mutations in epileptic encephalopathy. Ann Neurol 2014;76:529-40.

14. Shieh CC, Coghlan M, Sullivan JP, Gopalakrishnan M. Potassium channels: molecular defects, diseases, and therapeutic opportunities. Pharmacol Rev 2000;52:557-94.

15. Deschenes I, Tomaselli GF. Modulation of Kv4.3 current by accessory subunits. FEBS Lett 2002;528:183-8.

16. Rosati B, Pan Z, Lypen S, Wang HS, Cohen I, Dixon JE, McKinnon D. Regulation of KChIP2 potassium channel beta subunit gene expression underlies the gradient of transient outward current in canine and human ventricle. J Physiol 2001;533:119-25.

17. Soltysinska E, Olesen SP, Christ T, Wettwer E, Varro A, Grunnet M, Jespersen T. Transmural expression of ion channels and transporters in human nondiseased and end-stage failing hearts. Pflugers Arch 2009;459:11-23.

18. Roden DM. Taking the "idio" out of "idiosyncratic": predicting torsades de pointes. Pacing Clin Electrophysiol 1998;21:1029-34.

19. George AL, Jr. Molecular and genetic basis of sudden cardiac death. J Clin Invest 2013;123:75-83.

20. Cascio WE, Yang H, Muller-Borer BJ, Johnson TA. Ischemia-induced arrhythmia: the role of connexins, gap junctions, and attendant changes in impulse propagation. J Electrocardiol 2005;38:55-9.

21. Pierson JB, Berridge BR, Brooks MB, Dreher K, Koerner J, Schultze AE, Sarazan RD, Valentin JP, Vargas HM, Pettit SD. A public-private consortium advances cardiac safety evaluation: achievements of the HESI Cardiac Safety Technical Committee. J Pharmacol Toxicol Methods 2013;68:7-12.

22. Echt DR, David. Mortality and Morbidity in Patients Receiving Encainide, Flecainide, or Placebo. The New England Journal of Medicine 1991;324:781-8.

23. Moss AJ. Long QT Syndrome. Jama 2003;289:2041-4.

24. Schwartz PJ, Stramba-Badiale M, Crotti L, Pedrazzini M, Besana A, Bosi G, Gabbarini F, Goulene K, Insolia R, Mannarino S, Mosca F, Nespoli L, Rimini A, Rosati E, Salice P, Spazzolini C. Prevalence of the congenital long-QT syndrome. Circulation 2009;120:1761-7.

25. Goldenberg I, Zareba W, Moss AJ. Long QT Syndrome. Curr Probl Cardiol 2008;33:629-94.

26. Passman R, Kadish A. Polymorphic ventricular tachycardia, long Q-T syndrome, and torsades de pointes. Med Clin North Am 2001;85:321-41.

27. Schwartz PJ, Priori SG, Spazzolini C, Moss AJ, Vincent GM, Napolitano C, Denjoy I, Guicheney P, Breithardt G, Keating MT, Towbin JA, Beggs AH, Brink P, Wilde AA, Toivonen L, Zareba W, Robinson JL, Timothy KW, Corfield V, Wattanasirichaigoon D, Corbett C, Haverkamp W, Schulze-Bahr E, Lehmann MH, Schwartz K, Coumel P, Bloise R. Genotype-phenotype correlation in the long-QT syndrome: gene-specific triggers for life-threatening arrhythmias. Circulation 2001;103:89-95.

28. Moss AJ, Schwartz PJ, Crampton RS, Tzivoni D, Locati EH, MacCluer J, Hall WJ, Weitkamp L, Vincent GM, Garson A, Jr., et al. The long QT syndrome. Prospective longitudinal study of 328 families. Circulation 1991;84:1136-44.

29. Zipes DP, Camm AJ, Borggrefe M, Buxton AE, Chaitman B, Fromer M, Gregoratos G, Klein G, Moss AJ, Myerburg RJ, Priori SG, Quinones MA, Roden DM, Silka MJ, Tracy C, Smith SC, Jr., Jacobs AK, Adams CD, Antman EM, Anderson JL, Hunt SA, Halperin JL, Nishimura R, Ornato JP, Page RL, Riegel B, Priori SG, Blanc JJ, Budaj A, Camm AJ, Dean V, Deckers JW, Despres C, Dickstein K, Lekakis J, McGregor K, Metra M, Morais J, Osterspey A, Tamargo JL, Zamorano JL. ACC/AHA/ESC 2006 guidelines for management of patients with ventricular arrhythmias and the prevention of sudden cardiac death: a report of the American College of Cardiology/American Heart Association Task Force and the European Society of Cardiology Committee for Practice Guidelines (Writing Committee to Develop Guidelines for Management of Patients With Ventricular Arrhythmias and the Prevention of Sudden Cardiac Death). J Am Coll Cardiol 2006;48:e247-346.

30. Chockalingam P, Crotti L, Girardengo G, Johnson JN, Harris KM, van der Heijden JF, Hauer RN, Beckmann BM, Spazzolini C, Rordorf R, Rydberg A, Clur SA, Fischer M, van den Heuvel F, Kaab S, Blom NA, Ackerman MJ, Schwartz PJ, Wilde AA. Not all beta-blockers are equal in the management of long QT syndrome types 1 and 2: higher recurrence of events under metoprolol. J Am Coll Cardiol 2012;60:2092-9.

31. Khan IA. Clinical and therapeutic aspects of congenital and acquired long QT syndrome. Am J Med 2002;112:58-66.

32. Priori SG, Wilde AA, Horie M, Cho Y, Behr ER, Berul C, Blom N, Brugada J, Chiang CE, Huikuri H, Kannankeril P, Krahn A, Leenhardt A, Moss A, Schwartz PJ, Shimizu W, Tomaselli G, Tracy C. HRS/EHRA/APHRS expert consensus statement on the diagnosis and management of patients with inherited primary arrhythmia syndromes: document endorsed by HRS, EHRA, and APHRS in May 2013 and by ACCF, AHA, PACES, and AEPC in June 2013. Heart Rhythm 2013;10:1932-63.

33. Spears DA, Gollob MH. Genetics of inherited primary arrhythmia disorders. Appl Clin Genet 2015;8:215-33.

34. Schwartz PJ, Ackerman MJ, George AL, Jr., Wilde AA. Impact of genetics on the clinical management of channelopathies. J Am Coll Cardiol 2013;62:169-80.

35. Keating M, Dunn C, Atkinson D, Timothy K, Vincent GM, Leppert M. Consistent linkage of the long-QT syndrome to the Harvey ras-1 locus on chromosome 11. Am J Hum Genet 1991;49:1335-9.

36. Peroz D, Rodriguez N, Choveau F, Baro I, Merot J, Loussouarn G. Kv7.1 (KCNQ1) properties and channelopathies. J Physiol 2008;586:1785-9.

37. Bezzina CR, Lahrouchi N, Priori SG. Genetics of sudden cardiac death. Circ Res 2015;116:1919-36.

38. Schulze-Bahr E, Wang Q, Wedekind H, Haverkamp W, Chen Q, Sun Y, Rubie C, Hordt M, Towbin JA, Borggrefe M, Assmann G, Qu X, Somberg JC, Breithardt G, Oberti C, Funke H. KCNE1 mutations cause jervell and Lange-Nielsen syndrome. Nat Genet 1997;17:267-8.

39. Splawski I, Shen J, Timothy KW, Lehmann MH, Priori S, Robinson JL, Moss AJ, Schwartz PJ, Towbin JA, Vincent GM, Keating MT. Spectrum of mutations in long-QT syndrome genes. KVLQT1, HERG, SCN5A, KCNE1, and KCNE2. Circulation 2000;102:1178-85.

40. Giudicessi JR, Ackerman MJ. Prevalence and potential genetic determinants of sensorineural deafness in KCNQ1 homozygosity and compound heterozygosity. Circ Cardiovasc Genet 2013;6:193-200.

41. Tester DJ, Will ML, Haglund CM, Ackerman MJ. Compendium of cardiac channel mutations in 541 consecutive unrelated patients referred for long QT syndrome genetic testing. Heart Rhythm 2005;2:507-17.

42. Zimmer T, Surber R. SCN5A channelopathies--an update on mutations and mechanisms. Prog Biophys Mol Biol 2008;98:120-36.

43. Mishra S, Undrovinas NA, Maltsev VA, Reznikov V, Sabbah HN, Undrovinas A. Post-transcriptional silencing of SCN1B and SCN2B genes modulates late sodium current in cardiac myocytes from normal dogs and dogs with chronic heart failure. Am J Physiol Heart Circ Physiol 2011;301:H1596-605.

44. Maltsev VA, Kyle JW, Undrovinas A. Late Na+ current produced by human cardiac Na+ channel isoform Nav1.5 is modulated by its beta1 subunit. J Physiol Sci 2009;59:217-25.

45. Lin X, O'Malley H, Chen C, Auerbach D, Foster M, Shekhar A, Zhang M, Coetzee W, Jalife J, Fishman GI, Isom L, Delmar M. Scn1b deletion leads to increased tetrodotoxin-sensitive sodium current, altered intracellular calcium homeostasis and arrhythmias in murine hearts. J Physiol 2015;593:1389-407.

46. Kapplinger JD, Giudicessi JR, Ye D, Tester DJ, Callis TE, Valdivia CR, Makielski JC, Wilde AA, Ackerman MJ. Enhanced Classification of Brugada Syndrome-Associated and Long-QT Syndrome-Associated Genetic Variants in the SCN5A-Encoded Na(v)1.5 Cardiac Sodium Channel. Circ Cardiovasc Genet 2015;8:582-95.

47. Moss AJ, Robinson JL, Gessman L, Gillespie R, Zareba W, Schwartz PJ, Vincent GM, Benhorin J, Heilbron EL, Towbin JA, Priori SG, Napolitano C, Zhang L, Medina A, Andrews ML, Timothy K. Comparison of clinical and genetic variables of cardiac events associated with loud noise versus swimming among subjects with the long QT syndrome. Am J Cardiol 1999;84:876-9.

48. Shimizu W, Antzelevitch C. Differential effects of beta-adrenergic agonists and antagonists in LQT1, LQT2 and LQT3 models of the long QT syndrome. J Am Coll Cardiol 2000;35:778-86.

49. Ruan Y, Liu N, Bloise R, Napolitano C, Priori SG. Gating properties of SCN5A mutations and the response to mexiletine in long-QT syndrome type 3 patients. Circulation 2007;116:1137-44.

50. Kehl HG, Haverkamp W, Rellensmann G, Yelbuz TM, Krasemann T, Vogt J, Schulze-Bahr E. Images in cardiovascular medicine. Life-threatening neonatal arrhythmia: successful treatment and confirmation of clinically suspected extreme long QT-syndrome-3. Circulation 2004;109:e205-6.

51. Moss AJ, Zareba W, Schwarz KQ, Rosero S, McNitt S, Robinson JL. Ranolazine shortens repolarization in patients with sustained inward sodium current due to type-3 long-QT syndrome. J Cardiovasc Electrophysiol 2008;19:1289-93.

52. Brugada P, Brugada J. Right bundle branch block, persistent ST segment elevation and sudden cardiac death: a distinct clinical and electrocardiographic syndrome. A multicenter report. J Am Coll Cardiol 1992;20:1391-6.

53. Wilde AA, Antzelevitch C, Borggrefe M, Brugada J, Brugada R, Brugada P, Corrado D, Hauer RN, Kass RS, Nademanee K, Priori SG, Towbin JA. Proposed diagnostic criteria for the Brugada syndrome: consensus report. Circulation 2002;106:2514-9.

54. Brugada J, Brugada R, Brugada P. Right bundle-branch block and ST-segment elevation in leads V1 through V3: a marker for sudden death in patients without demonstrable structural heart disease. Circulation 1998;97:457-60.

55. Belhassen B, Glick A, Viskin S. Efficacy of quinidine in high-risk patients with Brugada syndrome. Circulation 2004;110:1731-7.

56. Ashino S, Watanabe I, Kofune M, Nagashima K, Ohkubo K, Okumura Y, Mano H, Nakai T, Kunimoto S, Kasamaki Y, Hirayama A. Effects of Quinidine on the Action Potential Duration Restitution Property in the Right Ventricular Outflow Tract in Patients With Brugada Syndrome. Circulation Journal 2011;75:2080-6.

57. Wolpert C, Echternach C, Veltmann C, Antzelevitch C, Thomas GP, Spehl S, Streitner F, Kuschyk J, Schimpf R, Haase KK, Borggrefe M. Intravenous drug challenge using flecainide and ajmaline in patients with Brugada syndrome. Heart Rhythm 2005;2:254-60.

58. Keller DI, Rougier JS, Kucera JP, Benammar N, Fressart V, Guicheney P, Madle A, Fromer M, Schlapfer J, Abriel H. Brugada syndrome and fever: genetic and molecular characterization of patients carrying SCN5A mutations. Cardiovasc Res 2005;67:510-9.

59. Eckardt L, Probst V, Smits JP, Bahr ES, Wolpert C, Schimpf R, Wichter T, Boisseau P, Heinecke A, Breithardt G, Borggrefe M, LeMarec H, Bocker D, Wilde AA. Long-term prognosis of individuals with right precordial ST-segment-elevation Brugada syndrome. Circulation 2005;111:257-63.

60. Priori SG, Napolitano C, Gasparini M, Pappone C, Della Bella P, Giordano U, Bloise R, Giustetto C, De Nardis R, Grillo M, Ronchetti E, Faggiano G, Nastoli J. Natural history of Brugada syndrome: insights for risk stratification and management. Circulation 2002;105:1342-7.

61. Postema PG, Wolpert C, Amin AS, Probst V, Borggrefe M, Roden DM, Priori SG, Tan HL, Hiraoka M, Brugada J, Wilde AA. Drugs and Brugada syndrome patients: review of the literature, recommendations, and an up-to-date website (http://www.brugadadrugs.org/). Heart Rhythm 2009;6:1335-41.

62. Yan GX, Antzelevitch C. Cellular basis for the Brugada syndrome and other mechanisms of arrhythmogenesis associated with ST-segment elevation. Circulation 1999;100:1660-6.

63. Antzelevitch C. J wave syndromes: molecular and cellular mechanisms. J Electrocardiol 2013;46:510-8.

64. Postema PG, van Dessel PF, Kors JA, Linnenbank AC, van Herpen G, Ritsema van Eck HJ, van Geloven N, de Bakker JM, Wilde AA, Tan HL. Local depolarization abnormalities are the dominant pathophysiologic mechanism for type 1 electrocardiogram in brugada syndrome a study of electrocardiograms, vectorcardiograms, and body surface potential maps during ajmaline provocation. J Am Coll Cardiol 2010;55:789-97.

65. Frustaci A, Priori SG, Pieroni M, Chimenti C, Napolitano C, Rivolta I, Sanna T, Bellocci F, Russo MA. Cardiac histological substrate in patients with clinical phenotype of Brugada syndrome. Circulation 2005;112:3680-7.

66. Probst V, Veltmann C, Eckardt L, Meregalli PG, Gaita F, Tan HL, Babuty D, Sacher F, Giustetto C, Schulze-Bahr E, Borggrefe M, Haissaguerre M, Mabo P, Le Marec H, Wolpert C, Wilde AA. Long-term prognosis of patients diagnosed with Brugada syndrome: Results from the FINGER Brugada Syndrome Registry. Circulation 2010;121:635-43.

67. Nishii N, Nagase S, Morita H, Kusano KF, Namba T, Miura D, Miyaji K, Hiramatsu S, Tada T, Murakami M, Watanabe A, Banba K, Sakai Y, Nakamura K, Oka T, Ohe T. Abnormal restitution property of action potential duration and conduction delay in Brugada syndrome: both repolarization and depolarization abnormalities. Europace 2010;12:544-52.

68. Nielsen MW, Holst AG, Olesen SP, Olesen MS. The genetic component of Brugada syndrome. Front Physiol 2013;4:179.

69. Hoshi M, Du XX, Shinlapawittayatorn K, Liu H, Chai S, Wan X, Ficker E, Deschenes I. Brugada syndrome disease phenotype explained in apparently benign sodium channel mutations. Circ Cardiovasc Genet 2014;7:123-31.

70. Kyndt F, Probst V, Potet F, Demolombe S, Chevallier JC, Baro I, Moisan JP, Boisseau P, Schott JJ, Escande D, Le Marec H. Novel SCN5A Mutation Leading Either to Isolated Cardiac Conduction Defect or Brugada Syndrome in a Large French Family. Circulation 2001;104:3081-6.

71. Todd SJ, Campbell MJ, Roden DM, Kannankeril PJ. Novel Brugada SCN5A mutation causing sudden death in children. Heart Rhythm 2005;2:540-3.

72. Smits PE, L; Probst, V; Bezzina, CR; Schulze-Bahr, E. Genotype-Phenotype Relationship in Brugada Syndrome: Electrocardiographic Features Differentiate SCN5A-Related Patients From Non–SCN5A-Related Patients. J Am Coll Cardiol 2002;40.

73. Martin CA, Zhang Y, Grace AA, Huang CL. In vivo studies of Scn5a+/- mice modeling Brugada syndrome demonstrate both conduction and repolarization abnormalities. J Electrocardiol 2010;43:433-9.

74. Papadatos GA, Wallerstein PM, Head CE, Ratcliff R, Brady PA, Benndorf K, Saumarez RC, Trezise AE, Huang CL, Vandenberg JI, Colledge WH, Grace AA. Slowed conduction and ventricular tachycardia after targeted disruption of the cardiac sodium channel gene Scn5a. Proc Natl Acad Sci U S A 2002;99:6210-5.

75. Chen Q, Kirsch GE, Zhang D, Brugada R, Brugada J, Brugada P, Potenza D, Moya A, Borggrefe M, Breithardt G, Ortiz-Lopez R, Wang Z, Antzelevitch C, O'Brien RE, Schulze-Bahr E, Keating MT, Towbin JA, Wang Q. Genetic basis and molecular mechanism for idiopathic ventricular fibrillation. Nature 1998;392:293-6.

76. London B, Michalec M, Mehdi H, Zhu X, Kerchner L, Sanyal S, Viswanathan PC, Pfahnl AE, Shang LL, Madhusudanan M, Baty CJ, Lagana S, Aleong R, Gutmann R, Ackerman MJ, McNamara DM, Weiss R, Dudley SC, Jr. Mutation in glycerol-3-phosphate dehydrogenase 1 like gene (GPD1-L) decreases cardiac Na+ current and causes inherited arrhythmias. Circulation 2007;116:2260-8.

77. Antzelevitch C, Pollevick GD, Cordeiro JM, Casis O, Sanguinetti MC, Aizawa Y, Guerchicoff A, Pfeiffer R, Oliva A, Wollnik B, Gelber P, Bonaros EP, Jr., Burashnikov E, Wu Y, Sargent JD, Schickel S, Oberheiden R, Bhatia A, Hsu LF, Haissaguerre M, Schimpf R, Borggrefe M, Wolpert C. Loss-of-function mutations in the cardiac calcium channel underlie a new clinical entity characterized by ST-segment elevation, short QT intervals, and sudden cardiac death. Circulation 2007;115:442-9.

78. Burashnikov E, Pfeiffer R, Barajas-Martinez H, Delpon E, Hu D, Desai M, Borggrefe M, Haissaguerre M, Kanter R, Pollevick GD, Guerchicoff A, Laino R, Marieb M, Nademanee K, Nam GB, Robles R, Schimpf R, Stapleton DD, Viskin S, Winters S, Wolpert C, Zimmern S, Veltmann C, Antzelevitch C. Mutations in the cardiac L-type calcium channel associated with inherited J-wave syndromes and sudden cardiac death. Heart Rhythm 2010;7:1872-82.

79. Crotti L, Marcou CA, Tester DJ, Castelletti S, Giudicessi JR, Torchio M, Medeiros-Domingo A, Simone S, Will ML, Dagradi F, Schwartz PJ, Ackerman MJ. Spectrum and prevalence of mutations involving BrS1- through BrS12-susceptibility genes in a cohort of unrelated patients referred for Brugada syndrome genetic testing: implications for genetic testing. J Am Coll Cardiol 2012;60:1410-8.

80. Watanabe H, Koopmann TT, Le Scouarnec S, Yang T, Ingram CR, Schott JJ, Demolombe S, Probst V, Anselme F, Escande D, Wiesfeld AC, Pfeufer A, Kaab S, Wichmann HE, Hasdemir C, Aizawa Y, Wilde AA, Roden DM, Bezzina CR. Sodium channel beta1 subunit mutations associated with Brugada syndrome and cardiac conduction disease in humans. J Clin Invest 2008;118:2260-8.

81. Holst AG, Saber S, Houshmand M, Zaklyazminskaya EV, Wang Y, Jensen HK, Refsgaard L, Haunso S, Svendsen JH, Olesen MS, Tfelt-Hansen J. Sodium current and potassium transient outward current genes in Brugada syndrome: screening and bioinformatics. Can J Cardiol 2012;28:196-200.

82. Delpon E, Cordeiro JM, Nunez L, Thomsen PE, Guerchicoff A, Pollevick GD, Wu Y, Kanters JK, Larsen CT, Hofman-Bang J, Burashnikov E, Christiansen M, Antzelevitch C.

Functional effects of KCNE3 mutation and its role in the development of Brugada syndrome. Circ Arrhythm Electrophysiol 2008;1:209-18.

83. Hu D, Barajas-Martinez H, Burashnikov E, Springer M, Wu Y, Varro A, Pfeiffer R, Koopmann TT, Cordeiro JM, Guerchicoff A, Pollevick GD, Antzelevitch C. A mutation in the beta 3 subunit of the cardiac sodium channel associated with Brugada ECG phenotype. Circ Cardiovasc Genet 2009;2:270-8.

84. Verkerk AO, Wilders R, Schulze-Bahr E, Beekman L, Bhuiyan ZA, Bertrand J, Eckardt L, Lin D, Borggrefe M, Breithardt G, Mannens MM, Tan HL, Wilde AA, Bezzina CR. Role of sequence variations in the human ether-a-go-go-related gene (HERG, KCNH2) in the Brugada syndrome. Cardiovasc Res 2005;68:441-53.

85. Medeiros-Domingo A, Tan BH, Crotti L, Tester DJ, Eckhardt L, Cuoretti A, Kroboth SL, Song C, Zhou Q, Kopp D, Schwartz PJ, Makielski JC, Ackerman MJ. Gain-of-function mutation S422L in the KCNJ8-encoded cardiac K(ATP) channel Kir6.1 as a pathogenic substrate for J-wave syndromes. Heart Rhythm 2010;7:1466-71.

86. Kattygnarath D, Maugenre S, Neyroud N, Balse E, Ichai C, Denjoy I, Dilanian G, Martins RP, Fressart V, Berthet M, Schott JJ, Leenhardt A, Probst V, Le Marec H, Hainque B, Coulombe A, Hatem SN, Guicheney P. MOG1: a new susceptibility gene for Brugada syndrome. Circ Cardiovasc Genet 2011;4:261-8.

87. Ohno S, Zankov DP, Ding WG, Itoh H, Makiyama T, Doi T, Shizuta S, Hattori T, Miyamoto A, Naiki N, Hancox JC, Matsuura H, Horie M. KCNE5 (KCNE1L) variants are novel modulators of Brugada syndrome and idiopathic ventricular fibrillation. Circ Arrhythm Electrophysiol 2011;4:352-61.

88. Giudicessi JR, Ye D, Tester DJ, Crotti L, Mugione A, Nesterenko VV, Albertson RM, Antzelevitch C, Schwartz PJ, Ackerman MJ. Transient outward current (I(to)) gain-of-function mutations in the KCND3-encoded Kv4.3 potassium channel and Brugada syndrome. Heart Rhythm 2011;8:1024-32.

89. Ishikawa T, Sato A, Marcou CA, Tester DJ, Ackerman MJ, Crotti L, Schwartz PJ, On YK, Park JE, Nakamura K, Hiraoka M, Nakazawa K, Sakurada H, Arimura T, Makita N, Kimura A. A novel disease gene for Brugada syndrome: sarcolemmal membrane-associated protein gene mutations impair intracellular trafficking of hNav1.5. Circ Arrhythm Electrophysiol 2012;5:1098-107.

90. Liu H, Chatel S, Simard C, Syam N, Salle L, Probst V, Morel J, Millat G, Lopez M, Abriel H, Schott JJ, Guinamard R, Bouvagnet P. Molecular genetics and functional anomalies in a series of 248 Brugada cases with 11 mutations in the TRPM4 channel. PLoS one 2013;8:e54131.

91. Riuro H, Beltran-Alvarez P, Tarradas A, Selga E, Campuzano O, Verges M, Pagans S, Iglesias A, Brugada J, Brugada P, Vazquez FM, Perez GJ, Scornik FS, Brugada R. A missense mutation in the sodium channel beta2 subunit reveals SCN2B as a new candidate gene for Brugada syndrome. Hum Mutat 2013;34:961-6.

92. Wang Q, Curran ME, Splawski I, Burn TC, Millholland JM, VanRaay TJ, Shen J, Timothy KW, Vincent GM, de Jager T, Schwartz PJ, Toubin JA, Moss AJ, Atkinson DL, Landes GM, Connors TD, Keating MT. Positional cloning of a novel potassium channel gene: KVLQT1 mutations cause cardiac arrhythmias. Nat Genet 1996;12:17-23.

93. Finishing the euchromatic sequence of the human genome. Nature 2004;431:931-45.

94. Hanson B, Tuna N, Bouchard T, Heston L, Eckert E, Lykken D, Segal N, Rich S. Genetic factors in the electrocardiogram and heart rate of twins reared apart and together. Am J Cardiol 1989;63:606-9.

95. Havlik RJ, Garrison RJ, Fabsitz R, Feinleib M. Variability of heart rate, P-R, QRS and Q-T durations in twins. J Electrocardiol 1980;13:45-8.

96. Russell MW, Law I, Sholinsky P, Fabsitz RR. Heritability of ECG measurements in adult male twins. J Electrocardiol 1998;30 Suppl:64-8.

97. Mutikainen S, Ortega-Alonso A, Alen M, Kaprio J, Karjalainen J, Rantanen T, Kujala UM. Genetic influences on resting electrocardiographic variables in older women: a twin study. Ann Noninvasive Electrocardiol 2009;14:57-64.

98. Arking DE, Pfeufer A, Post W, Kao WH, Newton-Cheh C, Ikeda M, West K, Kashuk C, Akyol M, Perz S, Jalilzadeh S, Illig T, Gieger C, Guo CY, Larson MG, Wichmann HE, Marban E, O'Donnell CJ, Hirschhorn JN, Kaab S, Spooner PM, Meitinger T, Chakravarti A. A common genetic variant in the NOS1 regulator NOS1AP modulates cardiac repolarization. Nat Genet 2006;38:644-51.

99. Pfeufer A, Sanna S, Arking DE, Muller M, Gateva V, Fuchsberger C, Ehret GB, Orru M, Pattaro C, Kottgen A, Perz S, Usala G, Barbalic M, Li M, Putz B, Scuteri A, Prineas RJ, Sinner MF, Gieger C, Najjar SS, Kao WH, Muhleisen TW, Dei M, Happle C, Mohlenkamp S, Crisponi L, Erbel R, Jockel KH, Naitza S, Steinbeck G, Marroni F, Hicks AA, Lakatta E, Muller-Myhsok B, Pramstaller PP, Wichmann HE, Schlessinger D, Boerwinkle E, Meitinger T, Uda M, Coresh J, Kaab S, Abecasis GR, Chakravarti A. Common variants at ten loci modulate the QT interval duration in the QTSCD Study. Nat Genet 2009;41:407-14.

100. Newton-Cheh C, Eijgelsheim M, Rice KM, de Bakker PI, Yin X, Estrada K, Bis JC, Marciante K, Rivadeneira F, Noseworthy PA, Sotoodehnia N, Smith NL, Rotter JI, Kors JA, Witteman JC, Hofman A, Heckbert SR, O'Donnell CJ, Uitterlinden AG, Psaty BM, Lumley T,

Larson MG, Stricker BH. Common variants at ten loci influence QT interval duration in the QTGEN Study. Nat Genet 2009;41:399-406.

101. Manolio TA, Collins FS, Cox NJ, Goldstein DB, Hindorff LA, Hunter DJ, McCarthy MI, Ramos EM, Cardon LR, Chakravarti A, Cho JH, Guttmacher AE, Kong A, Kruglyak L, Mardis E, Rotimi CN, Slatkin M, Valle D, Whittemore AS, Boehnke M, Clark AG, Eichler EE, Gibson G, Haines JL, Mackay TF, McCarroll SA, Visscher PM. Finding the missing heritability of complex diseases. Nature 2009;461:747-53.

102. Arking DE, Pulit SL, Crotti L, van der Harst P, Munroe PB, Koopmann TT, Sotoodehnia N, Rossin EJ, Morley M, Wang X, Johnson AD, Lundby A, Gudbjartsson DF, Noseworthy PA, Eijgelsheim M, Bradford Y, Tarasov KV, Dorr M, Muller-Nurasyid M, Lahtinen AM, Nolte IM, Smith AV, Bis JC, Isaacs A, Newhouse SJ, Evans DS, Post WS, Waggott D, Lyytikainen LP, Hicks AA, Eisele L, Ellinghaus D, Hayward C, Navarro P, Ulivi S, Tanaka T, Tester DJ, Chatel S, Gustafsson S, Kumari M, Morris RW, Naluai AT, Padmanabhan S, Kluttig A, Strohmer B, Panayiotou AG, Torres M, Knoflach M, Hubacek JA, Slowikowski K, Raychaudhuri S, Kumar RD, Harris TB, Launer LJ, Shuldiner AR, Alonso A, Bader JS, Ehret G, Huang H, Kao WH, Strait JB, Macfarlane PW, Brown M, Caulfield MJ, Samani NJ, Kronenberg F, Willeit J, Smith JG, Greiser KH, Meyer Zu Schwabedissen H, Werdan K, Carella M, Zelante L, Heckbert SR, Psaty BM, Rotter JI, Kolcic I, Polasek O, Wright AF, Griffin M, Daly MJ, Arnar DO, Holm H, Thorsteinsdottir U, Denny JC, Roden DM, Zuvich RL, Emilsson V, Plump AS, Larson MG, O'Donnell CJ, Yin X, Bobbo M, D'Adamo AP, Iorio A, Sinagra G, Carracedo A, Cummings SR, Nalls MA, Jula A, Kontula KK, Marjamaa A, Oikarinen L, Perola M, Porthan K, Erbel R, Hoffmann P, Jockel KH, Kalsch H, Nothen MM, den Hoed M, Loos RJ, Thelle DS, Gieger C, Meitinger T, Perz S, Peters A, Prucha H, Sinner MF, Waldenberger M, de Boer RA, Franke L, van der Vleuten PA, Beckmann BM, Martens E, Bardai A, Hofman N, Wilde AA, Behr ER, Dalageorgou C, Giudicessi JR, Medeiros-Domingo A, Barc J, Kyndt F, Probst V, Ghidoni A, Insolia R, Hamilton RM, Scherer SW, Brandimarto J, Margulies K, Moravec CE, del Greco MF, Fuchsberger C, O'Connell JR, Lee WK, Watt GC, Campbell H, Wild SH, El Mokhtari NE, Frey N, Asselbergs FW, Mateo Leach I, Navis G, van den Berg MP, van Veldhuisen DJ, Kellis M, Krijthe BP, Franco OH, Hofman A, Kors JA, Uitterlinden AG, Witteman JC, Kedenko L, Lamina C, Oostra BA, Abecasis GR, Lakatta EG, Mulas A, Orru M, Schlessinger D, Uda M, Markus MR, Volker U, Snieder H, Spector TD, Arnlov J, Lind L, Sundstrom J, Syvanen AC, Kivimaki M, Kahonen M, Mononen N, Raitakari OT, Viikari JS, Adamkova V, Kiechl S, Brion M, Nicolaides AN, Paulweber B, Haerting J, Dominiczak AF, Nyberg F, Whincup PH, Hingorani AD, Schott JJ, Bezzina CR, Ingelsson E, Ferrucci L, Gasparini P, Wilson JF, Rudan I, Franke A, Muhleisen TW, Pramstaller PP, Lehtimaki TJ, Paterson AD, Parsa A, Liu Y, van Duijn CM, Siscovick DS, Gudnason V, Jamshidi Y, Salomaa V, Felix SB, Sanna S, Ritchie MD, Stricker BH, Stefansson K, Boyer LA, Cappola TP, Olsen JV, Lage K, Schwartz PJ, Kaab S, Chakravarti A, Ackerman MJ, Pfeufer A, de Bakker PI, Newton-Cheh C. Genetic association study of QT interval highlights role for calcium signaling pathways in myocardial repolarization. Nat Genet 2014;46:826-36.

103. Bezzina CR, Barc J, Mizusawa Y, Remme CA, Gourraud JB, Simonet F, Verkerk AO, Schwartz PJ, Crotti L, Dagradi F, Guicheney P, Fressart V, Leenhardt A, Antzelevitch C, Bartkowiak S, Borggrefe M, Schimpf R, Schulze-Bahr E, Zumhagen S, Behr ER, Bastiaenen R,

Tfelt-Hansen J, Olesen MS, Kaab S, Beckmann BM, Weeke P, Watanabe H, Endo N, Minamino T, Horie M, Ohno S, Hasegawa K, Makita N, Nogami A, Shimizu W, Aiba T, Froguel P, Balkau B, Lantieri O, Torchio M, Wiese C, Weber D, Wolswinkel R, Coronel R, Boukens BJ, Bezieau S, Charpentier E, Chatel S, Despres A, Gros F, Kyndt F, Lecointe S, Lindenbaum P, Portero V, Violleau J, Gessler M, Tan HL, Roden DM, Christoffels VM, Le Marec H, Wilde AA, Probst V, Schott JJ, Dina C, Redon R. Common variants at SCN5A-SCN10A and HEY2 are associated with Brugada syndrome, a rare disease with high risk of sudden cardiac death. Nat Genet 2013;45:1044-9.

104. Hartman ME, Liu Y, Zhu WZ, Chien WM, Weldy CS, Fishman GI, Laflamme MA, Chin MT. Myocardial deletion of transcription factor CHF1/Hey2 results in altered myocyte action potential and mild conduction system expansion but does not alter conduction system function or promote spontaneous arrhythmias. FASEB J 2014;28:3007-15.

105. Holm H, Gudbjartsson DF, Arnar DO, Thorleifsson G, Thorgeirsson G, Stefansdottir H, Gudjonsson SA, Jonasdottir A, Mathiesen EB, Njolstad I, Nyrnes A, Wilsgaard T, Hald EM, Hveem K, Stoltenberg C, Lochen ML, Kong A, Thorsteinsdottir U, Stefansson K. Several common variants modulate heart rate, PR interval and QRS duration. Nat Genet 2010;42:117-22.

106. Johnson AD, Handsaker RE, Pulit SL, Nizzari MM, O'Donnell CJ, de Bakker PI. SNAP: a web-based tool for identification and annotation of proxy SNPs using HapMap. Bioinformatics 2008;24:2938-9.

107. Behr ER, Savio-Galimberti E, Barc J, Holst AG, Petropoulou E, Prins BP, Jabbari J, Torchio M, Berthet M, Mizusawa Y, Yang T, Nannenberg EA, Dagradi F, Weeke P, Bastiaenan R, Ackerman MJ, Haunso S, Leenhardt A, Kaab S, Probst V, Redon R, Sharma S, Wilde A, Tfelt-Hansen J, Schwartz P, Roden DM, Bezzina CR, Olesen M, Darbar D, Guicheney P, Crotti L, Consortium UK, Jamshidi Y. Role of common and rare variants in SCN10A: results from the Brugada syndrome QRS locus gene discovery collaborative study. Cardiovasc Res 2015;106:520-9.

108. Park DS, Fishman GI. Nav-igating through a complex landscape: SCN10A and cardiac conduction. J Clin Invest 2014;124:1460-2.

109. van den Boogaard M, Smemo S, Burnicka-Turek O, Arnolds DE, van de Werken HJ, Klous P, McKean D, Muehlschlegel JD, Moosmann J, Toka O, Yang XH, Koopmann TT, Adriaens ME, Bezzina CR, de Laat W, Seidman C, Seidman JG, Christoffels VM, Nobrega MA, Barnett P, Moskowitz IP. A common genetic variant within SCN10A modulates cardiac SCN5A expression. J Clin Invest 2014;124:1844-52.

110. Probst V, Wilde AA, Barc J, Sacher F, Babuty D, Mabo P, Mansourati J, Le Scouarnec S, Kyndt F, Le Caignec C, Guicheney P, Gouas L, Albuisson J, Meregalli PG, Le Marec H, Tan HL, Schott JJ. SCN5A mutations and the role of genetic background in the pathophysiology of Brugada syndrome. Circ Cardiovasc Genet 2009;2:552-7.

111. Park JK, Martin LJ, Zhang X, Jegga AG, Benson DW. Genetic variants in SCN5A promoter are associated with arrhythmia phenotype severity in patients with heterozygous loss-of-function mutation. Heart Rhythm 2012;9:1090-6.

112. Yang P, Koopmann TT, Pfeufer A, Jalilzadeh S, Schulze-Bahr E, Kaab S, Wilde AA, Roden DM, Bezzina CR. Polymorphisms in the cardiac sodium channel promoter displaying variant in vitro expression activity. Eur J Hum Genet 2008;16:350-7.

113. Bezzina CR, Shimizu W, Yang P, Koopmann TT, Tanck MW, Miyamoto Y, Kamakura S, Roden DM, Wilde AA. Common sodium channel promoter haplotype in asian subjects underlies variability in cardiac conduction. Circulation 2006;113:338-44.

114. Sotoodehnia N, Isaacs A, de Bakker PI, Dorr M, Newton-Cheh C, Nolte IM, van der Harst P, Muller M, Eijgelsheim M, Alonso A, Hicks AA, Padmanabhan S, Hayward C, Smith AV, Polasek O, Giovannone S, Fu J, Magnani JW, Marciante KD, Pfeufer A, Gharib SA, Teumer A, Li M, Bis JC, Rivadeneira F, Aspelund T, Kottgen A, Johnson T, Rice K, Sie MP, Wang YA, Klopp N, Fuchsberger C, Wild SH, Mateo Leach I, Estrada K, Volker U, Wright AF, Asselbergs FW, Qu J, Chakravarti A, Sinner MF, Kors JA, Petersmann A, Harris TB, Soliman EZ, Munroe PB, Psaty BM, Oostra BA, Cupples LA, Perz S, de Boer RA, Uitterlinden AG, Volzke H, Spector TD, Liu FY, Boerwinkle E, Dominiczak AF, Rotter JI, van Herpen G, Levy D, Wichmann HE, van Gilst WH, Witteman JC, Kroemer HK, Kao WH, Heckbert SR, Meitinger T, Hofman A, Campbell H, Folsom AR, van Veldhuisen DJ, Schwienbacher C, O'Donnell CJ, Volpato CB, Caulfield MJ, Connell JM, Launer L, Lu X, Franke L, Fehrmann RS, te Meerman G, Groen HJ, Weersma RK, van den Berg LH, Wijmenga C, Ophoff RA, Navis G, Rudan I, Snieder H, Wilson JF, Pramstaller PP, Siscovick DS, Wang TJ, Gudnason V, van Duijn CM, Felix SB, Fishman GI, Jamshidi Y, Stricker BH, Samani NJ, Kaab S, Arking DE. Common variants in 22 loci are associated with QRS duration and cardiac ventricular conduction. Nat Genet 2010;42:1068-76.

115. Postma AV, van de Meerakker JB, Mathijssen IB, Barnett P, Christoffels VM, Ilgun A, Lam J, Wilde AA, Lekanne Deprez RH, Moorman AF. A gain-of-function TBX5 mutation is associated with atypical Holt-Oram syndrome and paroxysmal atrial fibrillation. Circ Res 2008;102:1433-42.

116. Yang YQ, Wang MY, Zhang XL, Tan HW, Shi HF, Jiang WF, Wang XH, Fang WY, Liu X. GATA4 loss-of-function mutations in familial atrial fibrillation. Clin Chim Acta 2011;412:1825-30.

117. Jiang JQ, Shen FF, Fang WY, Liu X, Yang YQ. Novel GATA4 mutations in lone atrial fibrillation. Int J Mol Med 2011;28:1025-32.

118. Wang ZC, Ji WH, Ruan CW, Liu XY, Qiu XB, Yuan F, Li RG, Xu YJ, Liu X, Huang RT, Xue S, Yang YQ. Prevalence and Spectrum of TBX5 Mutation in Patients with Lone Atrial Fibrillation. Int J Med Sci 2016;13:60-7.

119. Boldt LH, Posch MG, Perrot A, Polotzki M, Rolf S, Parwani AS, Huemer M, Wutzler A, Ozcelik C, Haverkamp W. Mutational analysis of the PITX2 and NKX2-5 genes in patients with idiopathic atrial fibrillation. Int J Cardiol 2010;145:316-7.

120. Basson CT, Huang T, Lin RC, Bachinsky DR, Weremowicz S, Vaglio A, Bruzzone R, Quadrelli R, Lerone M, Romeo G, Silengo M, Pereira A, Krieger J, Mesquita SF, Kamisago M, Morton CC, Pierpont ME, Muller CW, Seidman JG, Seidman CE. Different TBX5 interactions in heart and limb defined by Holt-Oram syndrome mutations. Proc Natl Acad Sci U S A 1999;96:2919-24.

121. Al-Qattan MM, Abou Al-Shaar H. Molecular basis of the clinical features of Holt-Oram syndrome resulting from missense and extended protein mutations of the TBX5 gene as well as TBX5 intragenic duplications. Gene 2015;560:129-36.

122. Ghosh TK, Packham EA, Bonser AJ, Robinson TE, Cross SJ, Brook JD. Characterization of the TBX5 binding site and analysis of mutations that cause Holt-Oram syndrome. Hum Mol Genet 2001;10:1983-94.

123. van den Boogaard M, Wong LY, Tessadori F, Bakker ML, Dreizehnter LK, Wakker V, Bezzina CR, t Hoen PA, Bakkers J, Barnett P, Christoffels VM. Genetic variation in T-box binding element functionally affects SCN5A/SCN10A enhancer. J Clin Invest 2012;122:2519-30.

124. Pradhan L, Gopal S, Li S, Ashur S, Suryanarayanan S, Kasahara H, Nam HJ. Intermolecular Interactions of Cardiac Transcription Factors NKX2.5 and TBX5. Biochemistry 2016;55:1702-10.

125. Boogerd CJ, Dooijes D, Ilgun A, Mathijssen IB, Hordijk R, van de Laar IM, Rump P, Veenstra-Knol HE, Moorman AF, Barnett P, Postma AV. Functional analysis of novel TBX5 T-box mutations associated with Holt-Oram syndrome. Cardiovasc Res 2010;88:130-9.

126. Stirnimann CU, Ptchelkine D, Grimm C, Muller CW. Structural basis of TBX5-DNA recognition: the T-box domain in its DNA-bound and -unbound form. J Mol Biol 2010;400:71-81.

127. Mori AD, Zhu Y, Vahora I, Nieman B, Koshiba-Takeuchi K, Davidson L, Pizard A, Seidman JG, Seidman CE, Chen XJ, Henkelman RM, Bruneau BG. Tbx5-dependent rheostatic control of cardiac gene expression and morphogenesis. Dev Biol 2006;297:566-86.

128. Sun G, Lewis LE, Huang X, Nguyen Q, Price C, Huang T. TBX5, a gene mutated in Holt-Oram syndrome, is regulated through a GC box and T-box binding elements (TBEs). J Cell Biochem 2004;92:189-99.

129. Latronico MV, Condorelli G. MicroRNAs and cardiac pathology. Nat Rev Cardiol 2009;6:419-29.

130. Wang F, Yang XY, Zhao JY, Yu LW, Zhang P, Duan WY, Chong M, Gui YH. miR-10a and miR-10b target the 3'-untranslated region of TBX5 to repress its expression. Pediatr Cardiol 2014;35:1072-9.

131. Jeong HS, Jung ES, Sim YJ, Kim SJ, Jang JW, Hong KS, Lee WY, Chung HM, Park KT, Jung YS, Kim CH, Kim KS. Fbxo25 controls Tbx5 and Nkx2-5 transcriptional activity to regulate cardiomyocyte development. Biochim Biophys Acta 2015;1849:709-21.

132. Collavoli A, Hatcher CJ, He J, Okin D, Deo R, Basson CT. TBX5 nuclear localization is mediated by dual cooperative intramolecular signals. J Mol Cell Cardiol 2003;35:1191-5.

133. Zaragoza MV, Lewis LE, Sun G, Wang E, Li L, Said-Salman I, Feucht L, Huang T. Identification of the TBX5 transactivating domain and the nuclear localization signal. Gene 2004;330:9-18.

134. Kulisz A, Simon HG. An evolutionarily conserved nuclear export signal facilitates cytoplasmic localization of the Tbx5 transcription factor. Mol Cell Biol 2008;28:1553-64.

135. Lewandowski SL, Janardhan HP, Smee KM, Bachman M, Sun Z, Lazar MA, Trivedi CM. Histone deacetylase 3 modulates Tbx5 activity to regulate early cardiogenesis. Hum Mol Genet 2014;23:3801-9.

136. Herrmann F, Bundschu K, Kuhl SJ, Kuhl M. Tbx5 overexpression favors a first heart field lineage in murine embryonic stem cells and in Xenopus laevis embryos. Dev Dyn 2011;240:2634-45.

137. Hiroi YK, Sumiya; Komuro, Issei. Tbx5 associates with Nkx2.5 and synergistically promotes cardiomyocyte differentiation. Nature 2001;28.

138. Ghosh TK, Song FF, Packham EA, Buxton S, Robinson TE, Ronksley J, Self T, Bonser AJ, Brook JD. Physical interaction between TBX5 and MEF2C is required for early heart development. Mol Cell Biol 2009;29:2205-18.

139. Wang CC, D; Wang, Q; Wang, D. Synergistic Activation of Cardiac Genes by Myocardin and Tbx5. PLoS one 2011;6.

140. Linhares VL, Almeida NA, Menezes DC, Elliott DA, Lai D, Beyer EC, Campos de Carvalho AC, Costa MW. Transcriptional regulation of the murine Connexin40 promoter by cardiac factors Nkx2-5, GATA4 and Tbx5. Cardiovasc Res 2004;64:402-11.

141. Zhou W, Zhao L, Jiang JQ, Jiang WF, Yang YQ, Qiu XB. A novel TBX5 loss-of-function mutation associated with sporadic dilated cardiomyopathy. Int J Mol Med 2015;36:282-8.

142. Yue MS, Plavicki JS, Li XY, Peterson RE, Heideman W. A co-culture assay of embryonic zebrafish hearts to assess migration of epicardial cells in vitro. BMC Dev Biol 2015;15:50.

143. Bruneau BG, Nemer G, Schmitt JP, Charron F, Robitaille L, Caron S, Conner DA, Gessler M, Nemer M, Seidman CE, Seidman JG. A murine model of Holt-Oram syndrome defines roles of the T-box transcription factor Tbx5 in cardiogenesis and disease. Cell 2001;106:709-21.

144. Moskowitz IP, Pizard A, Patel VV, Bruneau BG, Kim JB, Kupershmidt S, Roden D, Berul CI, Seidman CE, Seidman JG. The T-Box transcription factor Tbx5 is required for the patterning and maturation of the murine cardiac conduction system. Development 2004;131:4107-16.

145. Moskowitz IP, Kim JB, Moore ML, Wolf CM, Peterson MA, Shendure J, Nobrega MA, Yokota Y, Berul C, Izumo S, Seidman JG, Seidman CE. A molecular pathway including Id2, Tbx5, and Nkx2-5 required for cardiac conduction system development. Cell 2007;129:1365-76.

146. Nadeaua MG, Romain O. ; Laforest, Brigitte ; Yamaka, Abir; Lefebvrea, Chantal; Beauregard, Janie; Paradis, Pierre; Bruneaud, Benoit G. ; Andelfinger, Gregor; Nemer, Mona. An endocardial pathway involving Tbx5, Gata4, and Nos3 required for atrial septum formation. Proc Natl Acad Sci U S A 2010;107.

147. Hatcher CJ, Goldstein MM, Mah CS, Delia CS, Basson CT. Identification and localization of TBX5 transcription factor during human cardiac morphogenesis. Dev Dyn 2000;219:90-5.

148. Arnolds DE, Liu F, Fahrenbach JP, Kim GH, Schillinger KJ, Smemo S, McNally EM, Nobrega MA, Patel VV, Moskowitz IP. TBX5 drives Scn5a expression to regulate cardiac conduction system function. J Clin Invest 2012;122:2509-18.

149. Hata Y, Kinoshita K, Mizumaki K, Yamaguchi Y, Hirono K, Ichida F, Takasaki A, Mori H, Nishida N. Postmortem genetic analysis of sudden unexplained death syndrome under 50 years of age: A next-generation sequencing study. Heart Rhythm 2016;13:1544-51.

150. Zhang XL, Qiu XB, Yuan F, Wang J, Zhao CM, Li RG, Xu L, Xu YJ, Shi HY, Hou XM, Qu XK, Xu YW, Yang YQ. TBX5 loss-of-function mutation contributes to familial dilated cardiomyopathy. Biochem Biophys Res Commun 2015;459:166-71.

151. Tarazon E, Rosello-Lleti E, Rivera M, Ortega A, Molina-Navarro MM, Trivino JC, Lago F, Gonzalez-Juanatey JR, Orosa P, Montero JA, Salvador A, Portoles M. RNA sequencing analysis and atrial natriuretic peptide production in patients with dilated and ischemic cardiomyopathy. PLoS one 2014;9:e90157.

152. Hodgson-Zingman DM, Karst ML, Zingman LV, Heublein DM, Darbar D, Herron KJ, Ballew JD, de Andrade M, Burnett JC, Jr., Olson TM. Atrial natriuretic peptide frameshift mutation in familial atrial fibrillation. N Engl J Med 2008;359:158-65.

153. Bendl J, Stourac J, Salanda O, Pavelka A, Wieben ED, Zendulka J, Brezovsky J, Damborsky J. PredictSNP: robust and accurate consensus classifier for prediction of disease-related mutations. PloS Computational Biology 2014;10.

154. Kircher M, Witten DM, Jain P, O'Roak BJ, Cooper GM, Shendure J. A general framework for estimating the relative pathogenicity of human genetic variants. Nat Genet 2014;46:310-5.

155. Richards S, Aziz N, Bale S, Bick D, Das S, Gastier-Foster J, Grody WW, Hegde M, Lyon E, Spector E, Voelkerding K, Rehm HL. Standards and guidelines for the interpretation of sequence variants: a joint consensus recommendation of the American College of Medical Genetics and Genomics and the Association for Molecular Pathology. Genet Med 2015;17:405-24.

156. Van Driest SL, Wells QS, Stallings S, Bush WS, Gordon A, Nickerson DA, Kim JH, Crosslin DR, Jarvik GP, Carrell DS, Ralston JD, Larson EB, Bielinski SJ, Olson JE, Ye Z, Kullo IJ, Abul-Husn NS, Scott SA, Bottinger E, Almoguera B, Connolly J, Chiavacci R, Hakonarson H, Rasmussen-Torvik LJ, Pan V, Persell SD, Smith M, Chisholm RL, Kitchner TE, He MM, Brilliant MH, Wallace JR, Doheny KF, Shoemaker MB, Li R, Manolio TA, Callis TE, Macaya D, Williams MS, Carey D, Kapplinger JD, Ackerman MJ, Ritchie MD, Denny JC, Roden DM. Association of Arrhythmia-Related Genetic Variants With Phenotypes Documented in Electronic Medical Records. Jama 2016;315:47-57.

157. Noda M, Shimizu S, Tanabe T, Takai T, Kayano T, Ikeda T, Takahashi H, Nakayama H, Kanaoka Y, Minamino N, et al. Primary structure of Electrophorus electricus sodium channel deduced from cDNA sequence. Nature 1984;312:121-7.

158. Watanabe H, Yang T, Stroud DM, Lowe JS, Harris L, Atack TC, Wang DW, Hipkens SB, Leake B, Hall L, Kupershmidt S, Chopra N, Magnuson MA, Tanabe N, Knollmann BC, George AL, Jr., Roden DM. Striking In vivo phenotype of a disease-associated human SCN5A mutation producing minimal changes in vitro. Circulation 2011;124:1001-11.

159. Martin GR. Isolation of a pluripotent cell line from early mouse embryos cultured in medium conditioned by teratocarcinoma stem cells. Proc Natl Acad Sci U S A 1981;78:7634-8.

160. Thomson JA, Itskovitz-Eldor J, Shapiro SS, Waknitz MA, Swiergiel JJ, Marshall VS, Jones JM. Embryonic stem cell lines derived from human blastocysts. Science 1998;282:1145-7.

161. Condic ML, Rao M. Alternative sources of pluripotent stem cells: ethical and scientific issues revisited. Stem Cells Dev 2010;19:1121-9.

162. Takahashi K, Yamanaka S. Induction of pluripotent stem cells from mouse embryonic and adult fibroblast cultures by defined factors. Cell 2006;126:663-76.

163. Takahashi K, Tanabe K, Ohnuki M, Narita M, Ichisaka T, Tomoda K, Yamanaka S. Induction of pluripotent stem cells from adult human fibroblasts by defined factors. Cell 2007;131:861-72.

164. Raab S, Klingenstein M, Liebau S, Linta L. A Comparative View on Human Somatic Cell Sources for iPSC Generation. Stem Cells Int 2014;2014:768391.

165. Dowey SN, Huang X, Chou BK, Ye Z, Cheng L. Generation of integration-free human induced pluripotent stem cells from postnatal blood mononuclear cells by plasmid vector expression. Nat Protoc 2012;7:2013-21.

166. Zhang J, Wilson GF, Soerens AG, Koonce CH, Yu J, Palecek SP, Thomson JA, Kamp TJ. Functional cardiomyocytes derived from human induced pluripotent stem cells. Circ Res 2009;104:e30-41.

167. Burridge PW, Matsa E, Shukla P, Lin ZC, Churko JM, Ebert AD, Lan F, Diecke S, Huber B, Mordwinkin NM, Plews JR, Abilez OJ, Cui B, Gold JD, Wu JC. Chemically defined generation of human cardiomyocytes. Nat Methods 2014;11:855-60.

168. Hoekstra M, Mummery CL, Wilde AA, Bezzina CR, Verkerk AO. Induced pluripotent stem cell derived cardiomyocytes as models for cardiac arrhythmias. Front Physiol 2012;3:346.

169. Tse HF, Ho JC, Choi SW, Lee YK, Butler AW, Ng KM, Siu CW, Simpson MA, Lai WH, Chan YC, Au KW, Zhang J, Lay KW, Esteban MA, Nicholls JM, Colman A, Sham PC. Patient-specific induced-pluripotent stem cells-derived cardiomyocytes recapitulate the pathogenic phenotypes of dilated cardiomyopathy due to a novel DES mutation identified by whole exome sequencing. Hum Mol Genet 2013;22:1395-403.

170. Moretti AM, M; Welling, A; Laugwitz, K. Patient-Specific Induced Pluripotent Stem-Cell Models for Long-QT Syndrome. New England Journal of Medicine 2010.

171. Itzhaki I, Maizels L, Huber I, Zwi-Dantsis L, Caspi O, Winterstern A, Feldman O, Gepstein A, Arbel G, Hammerman H, Boulos M, Gepstein L. Modelling the long QT syndrome with induced pluripotent stem cells. Nature 2011;471:225-9.

172. Fatima A, Kaifeng S, Dittmann S, Xu G, Gupta MK, Linke M, Zechner U, Nguemo F, Milting H, Farr M, Hescheler J, Saric T. The disease-specific phenotype in cardiomyocytes derived from induced pluripotent stem cells of two long QT syndrome type 3 patients. PLoS one 2013;8:e83005.

173. Kim YG, Cha J, Chandrasegaran S. Hybrid restriction enzymes: zinc finger fusions to Fok I cleavage domain. Proc Natl Acad Sci U S A 1996;93:1156-60.

174. Kim HJ, Lee HJ, Kim H, Cho SW, Kim JS. Targeted genome editing in human cells with zinc finger nucleases constructed via modular assembly. Genome Res 2009;19:1279-88.

175. Cermak T, Doyle EL, Christian M, Wang L, Zhang Y, Schmidt C, Baller JA, Somia NV, Bogdanove AJ, Voytas DF. Efficient design and assembly of custom TALEN and other TAL effector-based constructs for DNA targeting. Nucleic Acids Res 2011;39:e82.

176. Zetsche B, Gootenberg JS, Abudayyeh OO, Slaymaker IM, Makarova KS, Essletzbichler P, Volz SE, Joung J, van der Oost J, Regev A, Koonin EV, Zhang F. Cpf1 is a single RNA-guided endonuclease of a class 2 CRISPR-Cas system. Cell 2015;163:759-71.

177. Bibikova M, Golic M, Golic KG, Carroll D. Targeted chromosomal cleavage and mutagenesis in Drosophila using zinc-finger nucleases. Genetics 2002;161:1169-75.

178. Urnov FD, Miller JC, Lee YL, Beausejour CM, Rock JM, Augustus S, Jamieson AC, Porteus MH, Gregory PD, Holmes MC. Highly efficient endogenous human gene correction using designed zinc-finger nucleases. Nature 2005;435:646-51.

179. Soldner F, Laganiere J, Cheng AW, Hockemeyer D, Gao Q, Alagappan R, Khurana V, Golbe LI, Myers RH, Lindquist S, Zhang L, Guschin D, Fong LK, Vu BJ, Meng X, Urnov FD, Rebar EJ, Gregory PD, Zhang HS, Jaenisch R. Generation of isogenic pluripotent stem cells differing exclusively at two early onset Parkinson point mutations. Cell 2011;146:318-31.

180. Bellin M, Mummery CL. Inherited heart disease: what can we expect from the second decade of human iPS cells research? FEBS Lett 2016.

181. Tennessen JA, Bigham AW, O'Connor TD, Fu W, Kenny EE, Gravel S, McGee S, Do R, Liu X, Jun G, Kang HM, Jordan D, Leal SM, Gabriel S, Rieder MJ, Abecasis G, Altshuler D, Nickerson DA, Boerwinkle E, Sunyaev S, Bustamante CD, Bamshad MJ, Akey JM. Evolution and functional impact of rare coding variation from deep sequencing of human exomes. Science 2012;337:64-9.

182. Daber R, Sukhadia S, Morrissette JJ. Understanding the limitations of next generation sequencing informatics, an approach to clinical pipeline validation using artificial data sets. Cancer Genet 2013;206:441-8.

183. Chu C, Zhang J, Wu Y. GINDEL: accurate genotype calling of insertions and deletions from low coverage population sequence reads. PLoS one 2014;9:e113324.

184. Hasan MS, Wu X, Zhang L. Performance evaluation of indel calling tools using real short-read data. Hum Genomics 2015;9:20.

185. Chiang CE, Roden DM. The long QT syndromes: genetic basis and clinical implications. J Am Coll Cardiol 2000;36:1-12.

186. Huang L, Bitner-Glindzicz M, Tranebjaerg L, Tinker A. A spectrum of functional effects for disease causing mutations in the Jervell and Lange-Nielsen syndrome. Cardiovasc Res 2001;51:670-80.

187. Wei J, Fish FA, Myerburg RJ, Roden DM, George AL, Jr. Novel KCNQ1 mutations associated with recessive and dominant congenital long QT syndromes: evidence for variable hearing phenotype associated with R518X. Hum Mutat 2000;15:387-8.

188. Friedmann I, Fraser GR, Froggatt P. Pathology of the ear in the cardioauditory syndrome of Jervell and Lange-Nielsen (recessive deafness with electrocardiographic abnormalities). J Laryngol Otol 1966;80:451-70.

189. Jervell A, Lange-Nielsen F. Congenital deaf-mutism, functional heart disease with prolongation of the Q-T interval and sudden death. Am Heart J 1957;54:59-68.

190. Schwartz PJ, Spazzolini C, Crotti L, Bathen J, Amlie JP, Timothy K, Shkolnikova M, Berul CI, Bitner-Glindzicz M, Toivonen L, Horie M, Schulze-Bahr E, Denjoy I. The Jervell and Lange-Nielsen syndrome: natural history, molecular basis, and clinical outcome. Circulation 2006;113:783-90.

191. Kapa S, Tester DJ, Salisbury BA, Harris-Kerr C, Pungliya MS, Alders M, Wilde AA, Ackerman MJ. Genetic testing for long-QT syndrome: distinguishing pathogenic mutations from benign variants. Circulation 2009;120:1752-60.

192. Giudicessi JR, Ackerman MJ. Determinants of incomplete penetrance and variable expressivity in heritable cardiac arrhythmia syndromes. Transl Res 2013;161:1-14.

193. Wilson AJ, Quinn KV, Graves FM, Bitner-Glindzicz M, Tinker A. Abnormal KCNQ1 trafficking influences disease pathogenesis in hereditary long QT syndromes (LQT1). Cardiovasc Res 2005;67:476-86.

194. Kanki H, Kupershmidt S, Yang T, Wells S, Roden DM. A structural requirement for processing the cardiac K+ channel KCNQ1. J Biol Chem 2004;279:33976-83.

195. Tyson J, Tranebjaerg L, McEntagart M, Larsen LA, Christiansen M, Whiteford ML, Bathen J, Aslaksen B, Sorland SJ, Lund O, Pembrey ME, Malcolm S, Bitner-Glindzicz M. Mutational spectrum in the cardioauditory syndrome of Jervell and Lange-Nielsen. Hum Genet 2000;107:499-503.

196. Harmer SC, Mohal JS, Royal AA, McKenna WJ, Lambiase PD, Tinker A. Cellular mechanisms underlying the increased disease severity seen for patients with long QT syndrome caused by compound mutations in KCNQ1. Biochem J 2014;462:133-42.

197. Tranebjaerg L, Bathen J, Tyson J, Bitner-Glindzicz M. Jervell and Lange-Nielsen syndrome: a Norwegian perspective. Am J Med Genet 1999;89:137-46.

198. Zehelein J, Kathoefer S, Khalil M, Alter M, Thomas D, Brockmeier K, Ulmer HE, Katus HA, Koenen M. Skipping of Exon 1 in the KCNQ1 gene causes Jervell and Lange-Nielsen syndrome. J Biol Chem 2006;281:35397-403.

199. Campuzano O, Sarquella-Brugada G, Mademont-Soler I, Allegue C, Cesar S, Ferrer-Costa C, Coll M, Mates J, Iglesias A, Brugada J, Brugada R. Identification of Genetic Alterations, as Causative Genetic Defects in Long QT Syndrome, Using Next Generation Sequencing Technology. PLoS one 2014;9:e114894.

200. Ye K, Schulz MH, Long Q, Apweiler R, Ning Z. Pindel: a pattern growth approach to detect break points of large deletions and medium sized insertions from paired-end short reads. Bioinformatics 2009;25:2865-71.

201. Warden CD, Adamson AW, Neuhausen SL, Wu X. Detailed comparison of two popular variant calling packages for exome and targeted exon studies. PeerJ 2014;2:e600.

202. McKenna A, Hanna M, Banks E, Sivachenko A, Cibulskis K, Kernytsky A, Garimella K, Altshuler D, Gabriel S, Daly M, DePristo MA. The Genome Analysis Toolkit: a MapReduce framework for analyzing next-generation DNA sequencing data. Genome Res 2010;20:1297-303.

203. Ghoneim DH, Myers JR, Tuttle E, Paciorkowski AR. Comparison of insertion/deletion calling algorithms on human next-generation sequencing data. BMC Res Notes 2014;7:864.

204. Jiang Y, Wang Y, Brudno M. PRISM: pair-read informed split-read mapping for base-pair level detection of insertion, deletion and structural variants. Bioinformatics 2012;28:2576-83.

205. Qi J, Zhao F. inGAP-sv: a novel scheme to identify and visualize structural variation from paired end mapping data. Nucleic Acids Res 2011;39:W567-75.

206. Strauss BS. Frameshift mutation, microsatellites and mismatch repair. Mutat Res 1999;437:195-203.

207. Jurka J. Sequence patterns indicate an enzymatic involvement in integration of mammalian retroposons. Proc Natl Acad Sci U S A 1997;94:1872-7.

208. Cost GJ, Boeke JD. Targeting of human retrotransposon integration is directed by the specificity of the L1 endonuclease for regions of unusual DNA structure. Biochemistry 1998;37:18081-93.

209. Chen JM, Masson E, Macek M, Jr., Raguenes O, Piskackova T, Fercot B, Fila L, Cooper DN, Audrezet MP, Ferec C. Detection of two Alu insertions in the CFTR gene. J Cyst Fibros 2008;7:37-43.

210. Chen JM, Ferec C, Cooper DN. Mechanism of Alu integration into the human genome. Genomic Med 2007;1:9-17.

211. Batzer MA, Deininger PL. Alu repeats and human genomic diversity. Nat Rev Genet 2002;3:370-9.

212. Deininger PL, Batzer MA. Alu repeats and human disease. Mol Genet Metab 1999;67:183-93.

213. Wallace MR, Andersen LB, Saulino AM, Gregory PE, Glover TW, Collins FS. A de novo Alu insertion results in neurofibromatosis type 1. Nature 1991;353:864-6.

214. Hancks DC, Kazazian HH, Jr. Active human retrotransposons: variation and disease. Curr Opin Genet Dev 2012;22:191-203.

215. Wimmer K, Callens T, Wernstedt A, Messiaen L. The NF1 gene contains hotspots for L1 endonuclease-dependent de novo insertion. PLoS Genet 2011;7:e1002371.

216. Thung DT, de Ligt J, Vissers LE, Steehouwer M, Kroon M, de Vries P, Slagboom EP, Ye K, Veltman JA, Hehir-Kwa JY. Mobster: accurate detection of mobile element insertions in next generation sequencing data. Genome Biol 2014;15:488.

217. Berg AT, Berkovic SF, Brodie MJ, Buchhalter J, Cross JH, van Emde Boas W, Engel J, French J, Glauser TA, Mathern GW, Moshe SL, Nordli D, Plouin P, Scheffer IE. Revised terminology and concepts for organization of seizures and epilepsies: report of the ILAE Commission on Classification and Terminology, 2005-2009. Epilepsia 2010;51:676-85.

218. Berg AT, Loddenkemper T, Baca CB. Diagnostic delays in children with early onset epilepsy: impact, reasons, and opportunities to improve care. Epilepsia 2014;55:123-32.

219. Brunklaus A, Dorris L, Ellis R, Reavey E, Lee E, Forbes G, Appleton R, Cross JH, Ferrie C, Hughes I, Jollands A, King MD, Livingston J, Lynch B, Philip S, Scheffer IE, Williams R, Zuberi SM. The clinical utility of an SCN1A genetic diagnosis in infantile-onset epilepsy. Dev Med Child Neurol 2013;55:154-61.

220. Hirose S, Scheffer IE, Marini C, De Jonghe P, Andermann E, Goldman AM, Kauffman M, Tan NC, Lowenstein DH, Sisodiya SM, Ottman R, Berkovic SF. SCN1A testing for epilepsy: application in clinical practice. Epilepsia 2013;54:946-52.

221. Allen AS, Berkovic SF, Cossette P, Delanty N, Dlugos D, Eichler EE, Epstein MP, Glauser T, Goldstein DB, Han Y, Heinzen EL, Hitomi Y, Howell KB, Johnson MR, Kuzniecky R, Lowenstein DH, Lu YF, Madou MR, Marson AG, Mefford HC, Esmaeeli Nieh S, O'Brien TJ, Ottman R, Petrovski S, Poduri A, Ruzzo EK, Scheffer IE, Sherr EH, Yuskaitis CJ, Abou-Khalil B, Alldredge BK, Bautista JF, Berkovic SF, Boro A, Cascino GD, Consalvo D, Crumrine P, Devinsky O, Dlugos D, Epstein MP, Fiol M, Fountain NB, French J, Friedman D, Geller EB, Glauser T, Glynn S, Haut SR, Hayward J, Helmers SL, Joshi S, Kanner A, Kirsch HE, Knowlton RC, Kossoff EH, Kuperman R, Kuzniecky R, Lowenstein DH, McGuire SM, Motika PV, Novotny EJ, Ottman R, Paolicchi JM, Parent JM, Park K, Poduri A, Scheffer IE, Shellhaas RA, Sherr EH, Shih JJ, Singh R, Sirven J, Smith MC, Sullivan J, Lin Thio L, Venkat A, Vining EP, Von Allmen GK, Weisenberg JL, Widdess-Walsh P, Winawer MR. De novo mutations in epileptic encephalopathies. Nature 2013;501:217-21.

222. Carvill GL, Heavin SB, Yendle SC, McMahon JM, O'Roak BJ, Cook J, Khan A, Dorschner MO, Weaver M, Calvert S, Malone S, Wallace G, Stanley T, Bye AM, Bleasel A, Howell KB, Kivity S, Mackay MT, Rodriguez-Casero V, Webster R, Korczyn A, Afawi Z, Zelnick N, Lerman-Sagie T, Lev D, Moller RS, Gill D, Andrade DM, Freeman JL, Sadleir LG, Shendure J, Berkovic SF, Scheffer IE, Mefford HC. Targeted resequencing in epileptic encephalopathies identifies de novo mutations in CHD2 and SYNGAP1. Nat Genet 2013;45:825-30.

223. O'Brien JE, Meisler MH. Sodium channel SCN8A (Nav1.6): properties and de novo mutations in epileptic encephalopathy and intellectual disability. Front Genet 2013;4:213.

224. Nava C, Dalle C, Rastetter A, Striano P, de Kovel CG, Nabbout R, Cances C, Ville D, Brilstra EH, Gobbi G, Raffo E, Bouteiller D, Marie Y, Trouillard O, Robbiano A, Keren B, Agher D, Roze E, Lesage S, Nicolas A, Brice A, Baulac M, Vogt C, El Hajj N, Schneider E, Suls A, Weckhuysen S, Gormley P, Lehesjoki AE, De Jonghe P, Helbig I, Baulac S, Zara F, Koeleman BP, Haaf T, LeGuern E, Depienne C. De novo mutations in HCN1 cause early infantile epileptic encephalopathy. Nat Genet 2014;46:640-5.

225. Veeramah KR, Johnstone L, Karafet TM, Wolf D, Sprissler R, Salogiannis J, Barth-Maron A, Greenberg ME, Stuhlmann T, Weinert S, Jentsch TJ, Pazzi M, Restifo LL, Talwar D, Erickson RP, Hammer MF. Exome sequencing reveals new causal mutations in children with epileptic encephalopathies. Epilepsia 2013;54:1270-81.

226. O'Roak BJ, Vives L, Girirajan S, Karakoc E, Krumm N, Coe BP, Levy R, Ko A, Lee C, Smith JD, Turner EH, Stanaway IB, Vernot B, Malig M, Baker C, Reilly B, Akey JM, Borenstein E, Rieder MJ, Nickerson DA, Bernier R, Shendure J, Eichler EE. Sporadic autism exomes reveal a highly interconnected protein network of de novo mutations. Nature 2012;485:246-50.

227. Rauch A, Wieczorek D, Graf E, Wieland T, Endele S, Schwarzmayr T, Albrecht B, Bartholdi D, Beygo J, Di Donato N, Dufke A, Cremer K, Hempel M, Horn D, Hoyer J, Joset P, Ropke A, Moog U, Riess A, Thiel CT, Tzschach A, Wiesener A, Wohlleber E, Zweier C, Ekici AB, Zink AM, Rump A, Meisinger C, Grallert H, Sticht H, Schenck A, Engels H, Rappold G, Schrock E, Wieacker P, Riess O, Meitinger T, Reis A, Strom TM. Range of genetic mutations associated with severe non-syndromic sporadic intellectual disability: an exome sequencing study. Lancet 2012;380:1674-82.

228. Sanders SJ, Murtha MT, Gupta AR, Murdoch JD, Raubeson MJ, Willsey AJ, Ercan-Sencicek AG, DiLullo NM, Parikshak NN, Stein JL, Walker MF, Ober GT, Teran NA, Song Y, El-Fishawy P, Murtha RC, Choi M, Overton JD, Bjornson RD, Carriero NJ, Meyer KA, Bilguvar K, Mane SM, Sestan N, Lifton RP, Gunel M, Roeder K, Geschwind DH, Devlin B, State MW. De novo mutations revealed by whole-exome sequencing are strongly associated with autism. Nature 2012;485:237-41.

229. Abou-Khalil B, Alldredge B, Bautista J, Berkovic S, Bluvstein J, Boro A, Cascino G, Consalvo D, Cristofaro S, Crumrine P, Devinsky O, Dlugos D, Epstein M, Fahlstrom R, Fiol M, Fountain N, Fox K, French J, Freyer Karn C, Friedman D, Geller E, Glauser T, Glynn S, Haas K, Haut S, Hayward J, Helmers S, Joshi S, Kanner A, Kirsch H, Knowlton R, Kossoff E, Kuperman R, Kuzniecky R, Lowenstein D, McGuire S, Motika P, Nesbitt G, Novotny E, Ottman R, Paolicchi J, Parent J, Park K, Poduri A, Risch N, Sadleir L, Scheffer I, Shellhaas R, Sherr E, Shih JJ, Shinnar S, Singh R, Sirven J, Smith M, Sullivan J, Thio LL, Venkat A, Vining E, von Allmen G, Weisenberg J, Widdess-Walsh P, Winawer M. The epilepsy phenome/genome project. Clin Trials 2013;10:568-86.

230. Li H, Durbin R. Fast and accurate long-read alignment with Burrows-Wheeler transform. Bioinformatics 2010;26:589-95.

231. DePristo MA, Banks E, Poplin R, Garimella KV, Maguire JR, Hartl C, Philippakis AA, del Angel G, Rivas MA, Hanna M, McKenna A, Fennell TJ, Kernytsky AM, Sivachenko AY, Cibulskis K, Gabriel SB, Altshuler D, Daly MJ. A framework for variation discovery and genotyping using next-generation DNA sequencing data. Nat Genet 2011;43:491-8.

232. Van der Auwera GA, Carneiro MO, Hartl C, Poplin R, Del Angel G, Levy-Moonshine A, Jordan T, Shakir K, Roazen D, Thibault J, Banks E, Garimella KV, Altshuler D, Gabriel S, DePristo MA. From FastQ data to high confidence variant calls: the Genome Analysis Toolkit best practices pipeline. Curr Protoc Bioinformatics 2013;43:11.0.1-33.

233. Abyzov A, Urban AE, Snyder M, Gerstein M. CNVnator: an approach to discover, genotype, and characterize typical and atypical CNVs from family and population genome sequencing. Genome Res 2011;21:974-84.

234. Chen YZ, Friedman JR, Chen DH, Chan GC, Bloss CS, Hisama FM, Topol SE, Carson AR, Pham PH, Bonkowski ES, Scott ER, Lee JK, Zhang G, Oliveira G, Xu J, Scott-Van Zeeland AA, Chen Q, Levy S, Topol EJ, Storm D, Swanson PD, Bird TD, Schork NJ, Raskind WH, Torkamani A. Gain-of-function ADCY5 mutations in familial dyskinesia with facial myokymia. Ann Neurol 2014;75:542-9.

235. Altshuler DM, Gibbs RA, Peltonen L, Altshuler DM, Gibbs RA, Peltonen L, Dermitzakis E, Schaffner SF, Yu F, Peltonen L, Dermitzakis E, Bonnen PE, Altshuler DM, Gibbs RA, de Bakker PI, Deloukas P, Gabriel SB, Gwilliam R, Hunt S, Inouye M, Jia X, Palotie A, Parkin M, Whittaker P, Yu F, Chang K, Hawes A, Lewis LR, Ren Y, Wheeler D, Gibbs RA, Muzny DM, Barnes C, Darvishi K, Hurles M, Korn JM, Kristiansson K, Lee C, McCarrol SA, Nemesh J, Dermitzakis E, Keinan A, Montgomery SB, Pollack S, Price AL, Soranzo N, Bonnen PE, Gibbs RA, Gonzaga-Jauregui C, Keinan A, Price AL, Yu F, Anttila V, Brodeur W, Daly MJ, Leslie S, McVean G, Moutsianas L, Nguyen H, Schaffner SF, Zhang Q, Ghori MJ, McGinnis R, McLaren W, Pollack S, Price AL, Schaffner SF, Takeuchi F, Grossman SR, Shlyakhter I, Hostetter EB, Sabeti PC, Adebamowo CA, Foster MW, Gordon DR, Licinio J, Manca MC, Marshall PA, Matsuda I, Ngare D, Wang VO, Reddy D, Rotimi CN, Royal CD, Sharp RR, Zeng C, Brooks LD, McEwen JE. Integrating common and rare genetic variation in diverse human populations. Nature 2010;467:52-8.

236. Abecasis GR, Auton A, Brooks LD, DePristo MA, Durbin RM, Handsaker RE, Kang HM, Marth GT, McVean GA. An integrated map of genetic variation from 1,092 human genomes. Nature 2012;491:56-65.

237. Bailey JA, Gu Z, Clark RA, Reinert K, Samonte RV, Schwartz S, Adams MD, Myers EW, Li PW, Eichler EE. Recent segmental duplications in the human genome. Science 2002;297:1003-7.

238. O'Roak BJ, Vives L, Fu W, Egertson JD, Stanaway IB, Phelps IG, Carvill G, Kumar A, Lee C, Ankenman K, Munson J, Hiatt JB, Turner EH, Levy R, O'Day DR, Krumm N, Coe BP, Martin BK, Borenstein E, Nickerson DA, Mefford HC, Doherty D, Akey JM, Bernier R, Eichler EE, Shendure J. Multiplex targeted sequencing identifies recurrently mutated genes in autism spectrum disorders. Science 2012;338:1619-22.

239. Jorge BS, Campbell CM, Miller AR, Rutter ED, Gurnett CA, Vanoye CG, George AL, Jr., Kearney JA. Voltage-gated potassium channel KCNV2 (Kv8.2) contributes to epilepsy susceptibility. Proc Natl Acad Sci U S A 2011;108:5443-8.

240. Hille B. Ionic channels: molecular pores of excitable membranes. Harvey Lect 1986;82:47-69.

241. Sievers F, Wilm A, Dineen D, Gibson TJ, Karplus K, Li W, Lopez R, McWilliam H, Remmert M, Soding J, Thompson JD, Higgins DG. Fast, scalable generation of high-quality protein multiple sequence alignments using Clustal Omega. Mol Syst Biol 2011;7:539.

242. Long SB, Tao X, Campbell EB, MacKinnon R. Atomic structure of a voltage-dependent K+ channel in a lipid membrane-like environment. Nature 2007;450:376-82.

243. Consiglio JF, Andalib P, Korn SJ. Influence of pore residues on permeation properties in the Kv2.1 potassium channel. Evidence for a selective functional interaction of K+ with the outer vestibule. J Gen Physiol 2003;121:111-24.

244. Choi M, Scholl UI, Yue P, Bjorklund P, Zhao B, Nelson-Williams C, Ji W, Cho Y, Patel A, Men CJ, Lolis E, Wisgerhof MV, Geller DS, Mane S, Hellman P, Westin G, Akerstrom G, Wang W, Carling T, Lifton RP. K+ channel mutations in adrenal aldosterone-producing adenomas and hereditary hypertension. Science 2011;331:768-72.

245. Dibb KM, Rose T, Makary SY, Claydon TW, Enkvetchakul D, Leach R, Nichols CG, Boyett MR. Molecular basis of ion selectivity, block, and rectification of the inward rectifier Kir3.1/Kir3.4 K(+) channel. J Biol Chem 2003;278:49537-48.

246. Heginbotham L, Lu Z, Abramson T, MacKinnon R. Mutations in the K+ channel signature sequence. Biophys J 1994;66:1061-7.

247. Navarro B, Kennedy ME, Velimirovic B, Bhat D, Peterson AS, Clapham DE. Nonselective and G betagamma-insensitive weaver K+ channels. Science 1996;272:1950-3.

248. Du J, Haak LL, Phillips-Tansey E, Russell JT, McBain CJ. Frequency-dependent regulation of rat hippocampal somato-dendritic excitability by the K+ channel subunit Kv2.1. J Physiol 2000;522 Pt 1:19-31.

249. Guan D, Tkatch T, Surmeier DJ, Armstrong WE, Foehring RC. Kv2 subunits underlie slowly inactivating potassium current in rat neocortical pyramidal neurons. J Physiol 2007;581:941-60.

250. Guan D, Horton LR, Armstrong WE, Foehring RC. Postnatal development of A-type and Kv1- and Kv2-mediated potassium channel currents in neocortical pyramidal neurons. J Neurophysiol 2011;105:2976-88.

251. Guan D, Armstrong WE, Foehring RC. Kv2 channels regulate firing rate in pyramidal neurons from rat sensorimotor cortex. J Physiol 2013;591:4807-25.

252. Liu PW, Bean BP. Kv2 channel regulation of action potential repolarization and firing patterns in superior cervical ganglion neurons and hippocampal CA1 pyramidal neurons. J Neurosci 2014;34:4991-5002.

253. Speca DJ, Ogata G, Mandikian D, Bishop HI, Wiler SW, Eum K, Wenzel HJ, Doisy ET, Matt L, Campi KL, Golub MS, Nerbonne JM, Hell JW, Trainor BC, Sack JT, Schwartzkroin PA, Trimmer JS. Deletion of the Kv2.1 delayed rectifier potassium channel leads to neuronal and behavioral hyperexcitability. Genes Brain Behav 2014;13:394-408.

254. Orhan G, Bock M, Schepers D, Ilina EI, Reichel SN, Loffler H, Jezutkovic N, Weckhuysen S, Mandelstam S, Suls A, Danker T, Guenther E, Scheffer IE, De Jonghe P, Lerche H, Maljevic S. Dominant-negative effects of KCNQ2 mutations are associated with epileptic encephalopathy. Ann Neurol 2014;75:382-94.

255. Brugada J, Brugada R, Brugada P. Right Bundle-Branch Block and ST-Segment Elevation in Leads V1 Through V3 : A Marker for Sudden Death in Patients Without Demonstrable Structural Heart Disease. Circulation 1998;97:457-60.

256. Boczek NJ, Ye D, Jin F, Tester DJ, Huseby A, Bos JM, Johnson AJ, Kanter R, Ackerman MJ. Identification and Functional Characterization of a Novel CACNA1C-Mediated Cardiac Disorder Characterized by Prolonged QT Intervals With Hypertrophic Cardiomyopathy, Congenital Heart Defects, and Sudden Cardiac Death. Circ Arrhythm Electrophysiol 2015;8:1122-32.

257. Novak A, Barad L, Lorber A, Gherghiceanu M, Reiter I, Eisen B, Eldor L, Itskovitz-Eldor J, Eldar M, Arad M, Binah O. Functional abnormalities in iPSC-derived cardiomyocytes generated from CPVT1 and CPVT2 patients carrying ryanodine or calsequestrin mutations. J Cell Mol Med 2015;19:2006-18.

258. Mehta A, Sequiera GL, Ramachandra CJ, Sudibyo Y, Chung Y, Sheng J, Wong KY, Tan TH, Wong P, Liew R, Shim W. Re-trafficking of hERG reverses long QT syndrome 2 phenotype in human iPS-derived cardiomyocytes. Cardiovasc Res 2014;102:497-506.

259. Zhang M, D'Aniello C, Verkerk AO, Wrobel E, Frank S, Ward-van Oostwaard D, Piccini I, Freund C, Rao J, Seebohm G, Atsma DE, Schulze-Bahr E, Mummery CL, Greber B, Bellin M. Recessive cardiac phenotypes in induced pluripotent stem cell models of Jervell and Lange-Nielsen syndrome: disease mechanisms and pharmacological rescue. Proc Natl Acad Sci U S A 2014;111:E5383-92.

260. Lahti AL, Kujala VJ, Chapman H, Koivisto AP, Pekkanen-Mattila M, Kerkela E, Hyttinen J, Kontula K, Swan H, Conklin BR, Yamanaka S, Silvennoinen O, Aalto-Setala K. Model for long QT syndrome type 2 using human iPS cells demonstrates arrhythmogenic characteristics in cell culture. Dis Model Mech 2012;5:220-30.

261. Ma D, Wei H, Zhao Y, Lu J, Li G, Sahib NB, Tan TH, Wong KY, Shim W, Wong P, Cook SA, Liew R. Modeling type 3 long QT syndrome with cardiomyocytes derived from patient-specific induced pluripotent stem cells. Int J Cardiol 2013;168:5277-86.

262. Moretti A, Bellin M, Welling A, Jung CB, Lam JT, Bott-Flugel L, Dorn T, Goedel A, Hohnke C, Hofmann F, Seyfarth M, Sinnecker D, Schomig A, Laugwitz KL. Patient-specific induced pluripotent stem-cell models for long-QT syndrome. N Engl J Med 2010;363:1397-409.

263. Malan D, Friedrichs S, Fleischmann BK, Sasse P. Cardiomyocytes obtained from induced pluripotent stem cells with long-QT syndrome 3 recapitulate typical disease-specific features in vitro. Circ Res 2011;109:841-7.

264. Gibson JK, Yue Y, Bronson J, Palmer C, Numann R. Human stem cell-derived cardiomyocytes detect drug-mediated changes in action potentials and ion currents. J Pharmacol Toxicol Methods 2014;70:255-67.

265. Wang Y, Liang P, Lan F, Wu H, Lisowski L, Gu M, Hu S, Kay MA, Urnov FD, Shinnawi R, Gold JD, Gepstein L, Wu JC. Genome editing of isogenic human induced pluripotent stem cells recapitulates long QT phenotype for drug testing. J Am Coll Cardiol 2014;64:451-9.

266. Davis RP, Casini S, van den Berg CW, Hoekstra M, Remme CA, Dambrot C, Salvatori D, Oostwaard DW, Wilde AA, Bezzina CR, Verkerk AO, Freund C, Mummery CL. Cardiomyocytes derived from pluripotent stem cells recapitulate electrophysiological characteristics of an overlap syndrome of cardiac sodium channel disease. Circulation 2012;125:3079-91.

267. Bellin M, Casini S, Davis RP, D'Aniello C, Haas J, Ward-van Oostwaard D, Tertoolen LG, Jung CB, Elliott DA, Welling A, Laugwitz KL, Moretti A, Mummery CL. Isogenic human pluripotent stem cell pairs reveal the role of a KCNH2 mutation in long-QT syndrome. EMBO J 2013;32:3161-75.

268. Karakikes I, Stillitano F, Nonnenmacher M, Tzimas C, Sanoudou D, Termglinchan V, Kong CW, Rushing S, Hansen J, Ceholski D, Kolokathis F, Kremastinos D, Katoulis A, Ren L, Cohen N, Gho JM, Tsiapras D, Vink A, Wu JC, Asselbergs FW, Li RA, Hulot JS, Kranias EG, Hajjar RJ. Correction of human phospholamban R14del mutation associated with cardiomyopathy using targeted nucleases and combination therapy. Nat Commun 2015;6:6955.

269. Ran FA, Hsu PD, Wright J, Agarwala V, Scott DA, Zhang F. Genome engineering using the CRISPR-Cas9 system. Nat Protoc 2013;8:2281-308.

270. Karmakar CK, Khandoker AH, Voss A, Palaniswami M. Sensitivity of temporal heart rate variability in Poincare plot to changes in parasympathetic nervous system activity. Biomed Eng Online 2011;10:17.

271. Fan C, Duhagon MA, Oberti C, Chen S, Hiroi Y, Komuro I, Duhagon PI, Canessa R, Wang Q. Novel TBX5 mutations and molecular mechanism for Holt-Oram syndrome. J Med Genet 2003;40.

272. McDermott DA, Bressan MC, He J, Lee JS, Aftimos S, Brueckner M, Gilbert F, Graham GE, Hannibal MC, Innis JW, Pierpont ME, Raas-Rothschild A, Shanske AL, Smith WE, Spencer RH, St John-Sutton MG, van Maldergem L, Waggoner DJ, Weber M, Basson CT. TBX5 genetic testing validates strict clinical criteria for Holt-Oram syndrome. Pediatr Res 2005;58:981-6.

273. Spranger S, Ulmer H, Troger J, Jansen O, Graf J, Meinck HM, Spranger M. Muscular involvement in the Holt-Oram syndrome. J Med Genet 1997;34:978-81.

274. Fan C, Liu M, Wang Q. Functional analysis of TBX5 missense mutations associated with Holt-Oram syndrome. J Biol Chem 2003;278:8780-5.

275. Barrangou R, Fremaux C, Deveau H, Richards M, Boyaval P, Moineau S, Romero DA, Horvath P. CRISPR provides acquired resistance against viruses in prokaryotes. Science 2007;315:1709-12.

276. Sternberg SH, Redding S, Jinek M, Greene EC, Doudna JA. DNA interrogation by the CRISPR RNA-guided endonuclease Cas9. Nature 2014;507:62-7.

277. Sternberg SH, LaFrance B, Kaplan M, Doudna JA. Conformational control of DNA target cleavage by CRISPR-Cas9. Nature 2015;527:110-3.

278. Makita N, Behr E, Shimizu W, Horie M, Sunami A, Crotti L, Schulze-Bahr E, Fukuhara S, Mochizuki N, Makiyama T, Itoh H, Christiansen M, McKeown P, Miyamoto K, Kamakura S, Tsutsui H, Schwartz PJ, George AL, Jr., Roden DM. The E1784K mutation in SCN5A is associated with mixed clinical phenotype of type 3 long QT syndrome. J Clin Invest 2008;118:2219-29.

279. Hummel YM, Wilde AA, Voors AA, Bugatti S, Hillege HL, van den Berg MP. Ventricular dysfunction in a family with long QT syndrome type 3. Europace 2013;15:1516-21.

280. Sokolov S, Peters CH, Rajamani S, Ruben PC. Proton-dependent inhibition of the cardiac sodium channel Nav1.5 by ranolazine. Front Pharmacol 2013;4:78.

281. Lowe JS, Stroud DM, Yang T, Hall L, Atack TC, Roden DM. Increased late sodium current contributes to long QT-related arrhythmia susceptibility in female mice. Cardiovasc Res 2012;95:300-7.

282. Kaneko T, Nomura F, Hamada T, Abe Y, Takamori H, Sakakura T, Takasuna K, Sanbuissho A, Hyllner J, Sartipy P, Yasuda K. On-chip in vitro cell-network pre-clinical cardiac

toxicity using spatiotemporal human cardiomyocyte measurement on a chip. Sci Rep 2014;4:4670.

283. Kamen PW, Tonkin AM. Application of the Poincare plot to heart rate variability: a new measure of functional status in heart failure. Aust N Z J Med 1995;25:18-26.

284. Szentandrassy N, Kistamas K, Hegyi B, Horvath B, Ruzsnavszky F, Vaczi K, Magyar J, Banyasz T, Varro A, Nanasi PP. Contribution of ion currents to beat-to-beat variability of action potential duration in canine ventricular myocytes. Pflugers Arch 2015;467:1431-43.

285. Koesters A, Engisch KL, Rich MM. Decreased cardiac excitability secondary to reduction of sodium current may be a significant contributor to reduced contractility in a rat model of sepsis. Crit Care 2014;18:R54.

286. Pueyo E, Corrias A, Virag L, Jost N, Szel T, Varro A, Szentandrassy N, Nanasi PP, Burrage K, Rodriguez B. A multiscale investigation of repolarization variability and its role in cardiac arrhythmogenesis. Biophys J 2011;101:2892-902.

287. Doerr L, Thomas U, Guinot DR, Bot CT, Stoelzle-Feix S, Beckler M, George M, Fertig N. New easy-to-use hybrid system for extracellular potential and impedance recordings. J Lab Autom 2015;20:175-88.

288. Pardo B, Gomez-Gonzalez B, Aguilera A. DNA repair in mammalian cells: DNA double-strand break repair: how to fix a broken relationship. Cell Mol Life Sci 2009;66:1039-56.

289. Yang J, Hu D, Xia J, Yang Y, Ying B, Hu J, Zhou X. Three novel TBX5 mutations in Chinese patients with Holt-Oram syndrome. Am J Med Genet 2000;92:237-40.

290. Luna-Zurita L, Stirnimann CU, Glatt S, Kaynak BL, Thomas S, Baudin F, Samee MA, He D, Small EM, Mileikovsky M, Nagy A, Holloway AK, Pollard KS, Muller CW, Bruneau BG. Complex Interdependence Regulates Heterotypic Transcription Factor Distribution and Coordinates Cardiogenesis. Cell 2016;164:999-1014.

291. Gourraud JB, Barc J, Thollet A, Le Scouarnec S, Le Marec H, Schott JJ, Redon R, Probst V. The Brugada Syndrome: A Rare Arrhythmia Disorder with Complex Inheritance. Front Cardiovasc Med 2016;3:9.

292. Mi H, Muruganujan A, Casagrande JT, Thomas PD. Large-scale gene function analysis with the PANTHER classification system. Nat Protoc 2013;8:1551-66.

293. Yang T, Chun YW, Stroud DM, Mosley JD, Knollmann BC, Hong C, Roden DM. Screening for acute IKr block is insufficient to detect torsades de pointes liability: role of late sodium current. Circulation 2014;130:224-34.

294. Lu Z, Wu CY, Jiang YP, Ballou LM, Clausen C, Cohen IS, Lin RZ. Suppression of phosphoinositide 3-kinase signaling and alteration of multiple ion currents in drug-induced long QT syndrome. Sci Transl Med 2012;4:131ra50.

295. Lu Z, Jiang YP, Wu CY, Ballou LM, Liu S, Carpenter ES, Rosen MR, Cohen IS, Lin RZ. Increased persistent sodium current due to decreased PI3K signaling contributes to QT prolongation in the diabetic heart. Diabetes 2013;62:4257-65.

296. Qiu XS, Chauveau S, Anyukhovsky EP, Rahim T, Jiang YP, Harleton E, Feinmark SJ, Lin RZ, Coronel R, Janse MJ, Opthof T, Rosen TS, Cohen IS, Rosen MR. Increased Late Sodium Current Contributes to the Electrophysiological Effects of Chronic, but Not Acute, Dofetilide Administration. Circ Arrhythm Electrophysiol 2016;9:e003655.

297. Ballou LM, Lin RZ, Cohen IS. Control of cardiac repolarization by phosphoinositide 3-kinase signaling to ion channels. Circ Res 2015;116:127-37.

298. Jamsai D, Clark BJ, Smith SJ, Whittle B, Goodnow CC, Ormandy CJ, O'Bryan MK. A missense mutation in the transcription factor ETV5 leads to sterility, increased embryonic and perinatal death, postnatal growth restriction, renal asymmetry and polydactyly in the mouse. PLoS one 2013;8:e77311.

299. Ma JF, Yang F, Mahida SN, Zhao L, Chen X, Zhang ML, Sun Z, Yao Y, Zhang YX, Zheng GY, Dong J, Feng MJ, Zhang R, Sun J, Li S, Wang QS, Cao H, Benjamin EJ, Ellinor PT, Li YG, Tian XL. TBX5 mutations contribute to early-onset atrial fibrillation in Chinese and Caucasians. Cardiovasc Res 2016;109:442-50.

300. Chowdhury R, Ashraf H, Melanson M, Tanada Y, Nguyen M, Silberbach M, Wakimoto H, Benson DW, Anderson RH, Kasahara H. Mouse Model of Human Congenital Heart Disease: Progressive Atrioventricular Block Induced by a Heterozygous Nkx2-5 Homeodomain Missense Mutation. Circ Arrhythm Electrophysiol 2015;8:1255-64.

301. Shoubridge C, Tan MH, Seiboth G, Gecz J. ARX homeodomain mutations abolish DNA binding and lead to a loss of transcriptional repression. Hum Mol Genet 2012;21:1639-47.

302. Deniaud E, Baguet J, Chalard R, Blanquier B, Brinza L, Meunier J, Michallet MC, Laugraud A, Ah-Soon C, Wierinckx A, Castellazzi M, Lachuer J, Gautier C, Marvel J, Leverrier Y. Overexpression of transcription factor Sp1 leads to gene expression perturbations and cell cycle inhibition. PLoS one 2009;4:e7035.

303. Yao Z, Fong AP, Cao Y, Ruzzo WL, Gentleman RC, Tapscott SJ. Comparison of endogenous and overexpressed MyoD shows enhanced binding of physiologically bound sites. Skelet Muscle 2013;3:8.

304. Peters CH, Abdelsayed M, Ruben PC. Triggers for arrhythmogenesis in the Brugada and long QT 3 syndromes. Prog Biophys Mol Biol 2016;120:77-88.

305. Wilde AA, Brugada R. Phenotypical manifestations of mutations in the genes encoding subunits of the cardiac sodium channel. Circ Res 2011;108:884-97.

306. Ahern GP, Hsu SF, Klyachko VA, Jackson MB. Induction of persistent sodium current by exogenous and endogenous nitric oxide. J Biol Chem 2000;275:28810-5.

307. Wagner S, Dybkova N, Rasenack EC, Jacobshagen C, Fabritz L, Kirchhof P, Maier SK, Zhang T, Hasenfuss G, Brown JH, Bers DM, Maier LS. Ca2+/calmodulin-dependent protein kinase II regulates cardiac Na+ channels. J Clin Invest 2006;116:3127-38.

308. Qu Y, Rogers JC, Tanada TN, Catterall WA, Scheuer T. Phosphorylation of S1505 in the cardiac Na+ channel inactivation gate is required for modulation by protein kinase C. J Gen Physiol 1996;108:375-9.

309. Hinterseer M, Beckmann BM, Thomsen MB, Pfeufer A, Ulbrich M, Sinner MF, Perz S, Wichmann HE, Lengyel C, Schimpf R, Maier SK, Varro A, Vos MA, Steinbeck G, Kaab S. Usefulness of short-term variability of QT intervals as a predictor for electrical remodeling and proarrhythmia in patients with nonischemic heart failure. Am J Cardiol 2010;106:216-20.

310. Heijman J, Zaza A, Johnson DM, Rudy Y, Peeters RL, Volders PG, Westra RL. Determinants of beat-to-beat variability of repolarization duration in the canine ventricular myocyte: a computational analysis. PLoS Comput Biol 2013;9:e1003202.

311. Iribe G, Kohl P, Noble D. Modulatory effect of calmodulin-dependent kinase II (CaMKII) on sarcoplasmic reticulum Ca2+ handling and interval-force relations: a modelling study. Philos Trans A Math Phys Eng Sci 2006;364:1107-33.

312. Hiraoka M, Kawano S. Mechanism of increased amplitude and duration of the plateau with sudden shortening of diastolic intervals in rabbit ventricular cells. Circ Res 1987;60:14-26.

313. Wu R, Patwardhan A. Restitution of action potential duration during sequential changes in diastolic intervals shows multimodal behavior. Circ Res 2004;94:634-41.

314. Mahajan A, Sato D, Shiferaw Y, Baher A, Xie LH, Peralta R, Olcese R, Garfinkel A, Qu Z, Weiss JN. Modifying L-type calcium current kinetics: consequences for cardiac excitation and arrhythmia dynamics. Biophys J 2008;94:411-23.

315. Goldhaber JI, Xie LH, Duong T, Motter C, Khuu K, Weiss JN. Action potential duration restitution and alternans in rabbit ventricular myocytes: the key role of intracellular calcium cycling. Circ Res 2005;96:459-66.

316. Ujhelyi MR, Creazzo TL. Action potentials that mimic fibrillation activate sodium current. J Mol Cell Cardiol 1999;31:1673-84.

317. Sinnecker D, Goedel A, Laugwitz KL, Moretti A. Induced pluripotent stem cell-derived cardiomyocytes: a versatile tool for arrhythmia research. Circ Res 2013;112:961-8.

318. Liang P, Lan F, Lee AS, Gong T, Sanchez-Freire V, Wang Y, Diecke S, Sallam K, Knowles JW, Wang PJ, Nguyen PK, Bers DM, Robbins RC, Wu JC. Drug screening using a library of human induced pluripotent stem cell-derived cardiomyocytes reveals disease-specific patterns of cardiotoxicity. Circulation 2013;127:1677-91.

319. Sosnay PR, Raraigh KS, Gibson RL. Molecular Genetics of Cystic Fibrosis Transmembrane Conductance Regulator: Genotype and Phenotype. Pediatr Clin North Am 2016;63:585-98.

320. Trujillano D, Weiss ME, Koster J, Papachristos EB, Werber M, Kandaswamy KK, Marais A, Eichler S, Creed J, Baysal E, Jaber IY, Mehaney DA, Farra C, Rolfs A. Validation of a semiconductor next-generation sequencing assay for the clinical genetic screening of CFTR. Mol Genet Genomic Med 2015;3:396-403.

321. Feaster TK, Cadar AG, Wang L, Williams CH, Chun YW, Hempel JE, Bloodworth N, Merryman WD, Lim CC, Wu JC, Knollmann BC, Hong CC. Matrigel Mattress: A Method for the Generation of Single Contracting Human-Induced Pluripotent Stem Cell-Derived Cardiomyocytes. Circ Res 2015;117:995-1000.

322. Hayashi K, Shuai W, Sakamoto Y, Higashida H, Yamagishi M, Kupershmidt S. Trafficking-competent KCNQ1 variably influences the function of HERG long QT alleles. Heart Rhythm 2010;7:973-80.

323. Ren XQ, Liu GX, Organ-Darling LE, Zheng R, Roder K, Jindal HK, Centracchio J, McDonald TV, Koren G. Pore mutants of HERG and KvLQT1 downregulate the reciprocal currents in stable cell lines. Am J Physiol Heart Circ Physiol 2010;299:H1525-34.

324. Guo J, Wang T, Yang T, Xu J, Li W, Fridman MD, Fisher JT, Zhang S. Interaction between the cardiac rapidly (IKr) and slowly (IKs) activating delayed rectifier potassium channels revealed by low K+-induced hERG endocytic degradation. J Biol Chem 2011;286:34664-74.

325. Zhang J, Klos M, Wilson GF, Herman AM, Lian X, Raval KK, Barron MR, Hou L, Soerens AG, Yu J, Palecek SP, Lyons GE, Thomson JA, Herron TJ, Jalife J, Kamp TJ. Extracellular matrix promotes highly efficient cardiac differentiation of human pluripotent stem cells: the matrix sandwich method. Circ Res 2012;111:1125-36.

326. Cavallaro U, Christofori G. Cell adhesion and signalling by cadherins and Ig-CAMs in cancer. Nat Rev Cancer 2004;4:118-32.

327. Than BL, Goos JA, Sarver AL, O'Sullivan MG, Rod A, Starr TK, Fijneman RJ, Meijer GA, Zhao L, Zhang Y, Largaespada DA, Scott PM, Cormier RT. The role of KCNQ1 in mouse and human gastrointestinal cancers. Oncogene 2014;33:3861-8.

328. Morokuma J, Blackiston D, Adams DS, Seebohm G, Trimmer B, Levin M. Modulation of potassium channel function confers a hyperproliferative invasive phenotype on embryonic stem cells. Proc Natl Acad Sci U S A 2008;105:16608-13.

329. Parent JM, Anderson SA. Reprogramming patient-derived cells to study the epilepsies. Nat Neurosci 2015;18:360-6.

330. Chen H, Qian K, Du Z, Cao J, Petersen A, Liu H, Blackbourn LWt, Huang CL, Errigo A, Yin Y, Lu J, Ayala M, Zhang SC. Modeling ALS with iPSCs reveals that mutant SOD1 misregulates neurofilament balance in motor neurons. Cell Stem Cell 2014;14:796-809.

331. Kapplinger JD, Tester DJ, Alders M, Benito B, Berthet M, Brugada J, Brugada P, Fressart V, Guerchicoff A, Harris-Kerr C, Kamakura S, Kyndt F, Koopmann TT, Miyamoto Y, Pfeiffer R, Pollevick GD, Probst V, Zumhagen S, Vatta M, Towbin JA, Shimizu W, Schulze-Bahr E, Antzelevitch C, Salisbury BA, Guicheney P, Wilde AA, Brugada R, Schott JJ, Ackerman MJ. An international compendium of mutations in the SCN5A-encoded cardiac sodium channel in patients referred for Brugada syndrome genetic testing. Heart Rhythm 2010;7:33-46.

332. He A, Kong SW, Ma Q, Pu WT. Co-occupancy by multiple cardiac transcription factors identifies transcriptional enhancers active in heart. Proc Natl Acad Sci U S A 2011;108:5632-7.

333. Mazzoni EO, Mahony S, Iacovino M, Morrison CA, Mountoufaris G, Closser M, Whyte WA, Young RA, Kyba M, Gifford DK, Wichterle H. Embryonic stem cell-based mapping of developmental transcriptional programs. Nat Methods 2011;8:1056-8.

334. Maeder ML, Linder SJ, Cascio VM, Fu Y, Ho QH, Joung JK. CRISPR RNA-guided activation of endogenous human genes. Nat Methods 2013;10:977-9.

335. Perez-Pinera P, Kocak DD, Vockley CM, Adler AF, Kabadi AM, Polstein LR, Thakore PI, Glass KA, Ousterout DG, Leong KW, Guilak F, Crawford GE, Reddy TE, Gersbach CA. RNA-guided gene activation by CRISPR-Cas9-based transcription factors. Nat Methods 2013;10:973-6.

336. Gilbert LA, Larson MH, Morsut L, Liu Z, Brar GA, Torres SE, Stern-Ginossar N, Brandman O, Whitehead EH, Doudna JA, Lim WA, Weissman JS, Qi LS. CRISPR-mediated modular RNA-guided regulation of transcription in eukaryotes. Cell 2013;154:442-51.

337. Luo Y, Rao M, Zou J. Generation of GFP Reporter Human Induced Pluripotent Stem Cells Using AAVS1 Safe Harbor Transcription Activator-Like Effector Nuclease. Curr Protoc Stem Cell Biol 2014;29:5a.7.1-18.

338. Wang Y, Zhang WY, Hu S, Lan F, Lee AS, Huber B, Lisowski L, Liang P, Huang M, de Almeida PE, Won JH, Sun N, Robbins RC, Kay MA, Urnov FD, Wu JC. Genome editing of human embryonic stem cells and induced pluripotent stem cells with zinc finger nucleases for cellular imaging. Circ Res 2012;111:1494-503.